

RESERVOIR HETEROGENEITY, SEDIMENTOLOGY, AND DIAGENESIS OF
ORDOVICIAN BEDİNAN FORMATION, SOUTHERN DİYARBAKIR BASIN,
SE TURKEY: PALEO GEOGRAPHIC IMPLICATIONS

A THESIS SUBMITTED TO
THE GRADUATE SCHOOL OF NATURAL AND APPLIED SCIENCES
OF
MIDDLE EAST TECHNICAL UNIVERSITY

BY

GÖKAY YILDIZ

IN PARTIAL FULFILLMENT OF THE REQUIREMENTS
FOR
THE DEGREE OF MASTER OF SCIENCE
IN
GEOLOGICAL ENGINEERING

MAY 2019

Approval of the thesis:

**RESERVOIR HETEROGENEITY, SEDIMENTOLOGY, AND DIAGENESIS
OF ORDOVICIAN BEDİNAN FORMATION, SOUTHERN DİYARBAKIR
BASIN, SE TURKEY: PALEOGEOGRAPHIC IMPLICATIONS**

submitted by **GÖKAY YILDIZ** in partial fulfillment of the requirements for the degree of **Master of Science in Geological Engineering Department, Middle East Technical University** by,

Prof. Dr. Halil Kalıpçılar
Dean, Graduate School of **Natural and Applied Sciences**

Prof. Dr. Erdin Bozkurt
Head of Department, **Geological Engineering**

Prof. Dr. İsmail Ömer Yılmaz
Supervisor, **Geological Engineering, METU**

Examining Committee Members:

Prof. Dr. Erdoğan Tekin
Geological Engineering, Ankara University

Prof. Dr. İsmail Ömer Yılmaz
Geological Engineering, METU

Prof. Dr. Turhan Ayyıldız
Geological Engineering, Ankara University

Assoc. Prof. Dr. Kaan Sayıt
Geological Engineering, METU

Assist. Prof. Dr. Ulaş Avşar
Geological Engineering, METU

Date: 29.05.2019

I hereby declare that all information in this document has been obtained and presented in accordance with academic rules and ethical conduct. I also declare that, as required by these rules and conduct, I have fully cited and referenced all material and results that are not original to this work.

Name, Surname: Gökay Yıldız

Signature:

ABSTRACT

RESERVOIR HETEROGENEITY, SEDIMENTOLOGY, AND DIAGENESIS OF ORDOVICIAN BEDINAN FORMATION, SOUTHERN DİYARBAKIR BASIN, SE TURKEY: PALEOGEOGRAPHIC IMPLICATIONS

Yıldız, Gökay
Master of Science, Geological Engineering
Supervisor: Prof. Dr. İsmail Ömer Yılmaz

May 2019, 195 pages

Recent high-quality oil discoveries in SE Turkey, specifically Diyarbakır Basin from the Ordovician aged Bedinan Formation sandstone reservoir levels have introduced many questions. The fact that variable hydrocarbon production rates in the studied wells oblige us to delineate internal framework of the sandstone levels and to find the answer for the reason of the reservoir heterogeneity which will be a proxy to find convenient well stimulation methods in order to increase hydrocarbon recovery.

In this study, Gazzi-Dickinson method of point counting on thin sections, X-ray computed tomography imaging technique, semi-quantitative X-ray diffraction (XRD) bulk powder mineral analysis, seismic lines, wireline log data, and available well data were used to understand the depositional environment, the paleogeography during the geological evaluation, the mineral framework and the provenance of the levels of interest. Additionally, petrophysical log interpretation via Petrel software together with regional stratigraphy and correlation studies were carried out to explain the reason and scale of the reservoir heterogeneity.

As a consequence of the studies, it is seen that the subarkose to quartz arenitic sandstone levels of the Bedinan Formation were deposited between the lower and

upper shoreface of an ice-distal glaciomarine depositional environment. Additionally, the origin of sandstones are related to igneous and cratonic sources.

The most important result of this study on the reservoir heterogeneity of this sandstone levels of uppermost Bedinan Formation is that besides the depositional facies, structural features and compaction, particularly diagenetic clay coating minerals (illite, kaolinite and illite/smectite mixed clay layer) together with quartz and carbonate cements have exerted great control on the reservoir quality in meters scale, which results in variable hydrocarbon production rate.

Keywords: Reservoir Heterogeneity, Eodiagenesis, Mesodiagenesis, Diyarbakır Basin, Illitization, Mixed Clay Layer

ÖZ

GÜNEYDOĞU ANADOLU BÖLGESİ, GÜNEY DİYARBAKIR BASENİNDE ORDOVİSİYEN BEDİNAN FORMASYONU REZERVUAR HETEROJENLİĞİ, SEDİMENTOLOJİSİ VE DİYAJENEZİ: PALEOCOĞRAFİK ÇIKARIMLAR

Yıldız, Gökay
Yüksek Lisans, Jeoloji Mühendisliği
Tez Danışmanı: Prof. Dr. İsmail Ömer Yılmaz

Mayıs 2019, 195 sayfa

Güneydoğu Anadolu bölgesinde, Diyarbakır Baseninde Ordovisiyen yaşlı Bedinan Formasyonu kumtaşı rezervuar seviyelerinden gerçekleştirilen yüksek kaliteli petrol üretimi beraberinde bir çok soruyu getirmiştir. Bu seviyelerden gerçekleştirilen değişken hidrokarbon üretimi, rezervuarı oluşturan çatı elemanlarının ortaya çıkarılmasına ve hidrokarbon kurtarımını artırmaya yönelik yeni kuyu canlandırma yöntemleri geliştirmek için rezervuar heterojenliğinin nedenlerini araştırmaya zorlamıştır.

Bu çalışmada, Bedinan Formasyonu en üst rezervuar seviyelerinin çökelim ortamı, paleocoğrafyası, köken ve çatı elemanlarını belirlemeye yönelik olarak; ince kesitler üzerinde nokta sayım (Gazzi-Dickinson metodu), sismik hatlar, log ve kuyu verileri, X-ray Computed Tomography görüntüleme tekniği ve X-ışını kırınım (XRD) yöntemi kullanılmıştır. Ek olarak, rezervuar heterojenliğini ve skalasını açıklamak için bölgesel stratigrafik veriler, kuyu korelasyonları ve özellikle Petrel yazılımı kullanılarak petrofizik log yorumlamaları yapılmıştır.

Bu çalışmanın sonucuna göre, subarkoz-kuvars arenitik kumtaşı seviyeleri buzul ilerisinde, alt kıyı önü ile üst kıyı önü arasında çökelmiş ve kıtasal kökenlidir. Bunun

yanı sıra, alıřılan kumtařı rezervuar seviyelerinin ana kaynak kayasının magmatik kayalar olduđu anlařılmıřtır.

Bu alıřmanın Bedinan Formasyonu kumtařı rezervuar seviyeleri heterojenliđi üzerine en önemli ve asıl sonucu ise, ökelim fasiyesi, yapısal elementleri ve kompaksiyon dıřında, kuvars ve karbonat imentosu ile birlikte özellikle matriksi oluřturan diyajenetik kil minerallerinin (illite, kaolinit ve illit-smektit karıřık kil tabakası) rezervuar kalitesini metre öleđinde etkilediđi, ve bunun da hidrokarbon üretim ve kurtarım farklılıklarına neden olduđudur.

Anahtar Kelimeler: Rezervuar Heterojenliđi, Eodiyajenez, Mesodiyajenez, Diyarbakır Baseni, İllitleřme, Karıřık Kil Tabakası

To My Family

ACKNOWLEDGEMENTS

I would like to express my gratitude to my supervisor Prof. Dr. İsmail Ömer Yılmaz for his advice, recommendations, criticism and encouragements during all stage of my study.

Many thanks are due to Çalık Petrol Arama Üretim Sanayi ve Ticaret A.Ş management and exploration team for their endless support and permitting me to use the data and the related materials.

Appreciativeness and special thanks are extended to my dear family for their unending support throughout my life.

I would like to thank to laboratory technician Mr. Orhan Karaman who prepared the thin sections in Geological Engineering Department laboratory of Middle East Technical University.

Finally, many thanks are due to the owner of my heart, my wife Miss. Hatice Kılıç Yıldız, for being with me whenever I need and for her patience and encouragement.

TABLE OF CONTENTS

ABSTRACT	v
ÖZ	vii
ACKNOWLEDGEMENTS	x
TABLE OF CONTENTS	xi
LIST OF TABLES	xiv
LIST OF FIGURES	xvi
CHAPTERS	
1. INTRODUCTION	1
1.1. Purpose and Scope.....	1
1.2. Location of the Study Area.....	2
1.3. Data and Methods of Study	3
1.4. Previous Works	11
2. GEOLOGICAL SETTING	19
2.1. Stratigraphy	33
2.1.1. Derik Group (Precambrian-Cambrian)	33
2.1.2. Habur Group (Ordovician).....	34
2.1.3. Diyarbakır Group (Silurian-Devonian).....	35
2.1.4. Tanin Group (Late Permian).....	36
2.1.5. Çığlı Group (Early Triassic)	37
2.1.6. Mardin Group (Aptian-Campanian)	40
2.1.7. Adıyaman Group (Campanian).....	41
2.1.8. Şırnak Group (Campanian-Paleocene)	41

2.1.9. Midyat Group (Eocene-Oligocene)	42
2.1.10. Şelmo Formation (Late Miocene- Early Pliocene).....	42
3. LITHOSTRATIGRAPHY.....	45
3.1. Bedinan Formation Members.....	48
3.1.1. Bedinan-I.....	48
3.1.2. Bedinan-II.....	48
3.1.3. Bedinan-III	49
3.1.4. Bedinan IV	50
4. SEDIMENTOLOGY	53
4.1. Facies Analysis	55
4.1.1. Sandstone Facies	55
4.1.1.1. Provenance Interpretation	70
4.1.2. Shale Facies	78
4.1.3. Marl Facies	79
4.2. Porosity Measurement and X-ray Computed Tomography	80
4.3. Depositional Environment	87
5. PALEOGEOGRAPHY	97
5.1. Late Ordovician Paleogeography.....	97
6. RESERVOIR HETEROGENEITY.....	107
6.1. Statistical Measurements for Reservoir Heterogeneity.....	117
6.1.1. Coefficient of Variation.....	117
7. CLAY TYPING BASED ON PETROPHYSICAL METHODS.....	121
8. X-RAY DIFFRACTION BULK POWDER ANALYSIS	127
8.1. Clay Typing based on XRD Analysis	135

8.2. Comparison of Petrophysical and XRD Methods for Clay Typing	138
9. DIAGENESIS	141
9.1. Clay Coating Mineral Associations and Their Origin	142
9.1.1. Regional Correlation	149
9.2. Diagenetic Quartz Cementation	150
9.3. Diagenetic Carbonate Cementation	155
9.4. The Impact of Diagenesis on the Reservoir Quality	157
10. DISCUSSION	161
11. CONCLUSION	165
REFERENCES	169

LIST OF TABLES

TABLES

Table 1: The minerological composition of the uppermost Bedinan Formation 2 nd sandstone level penetrated in A well, Core-1.....	62
Table 2: The minerological composition of the uppermost Bedinan Formation 1 st sandstone level penetrated in B well, Core-1.....	62
Table 3: The minerological composition of the uppermost Bedinan Formation 2 nd sandstone level penetrated in B well, Core-2.....	63
Table 4: The minerological composition of the uppermost Bedinan Formation 1 st sandstone level penetrated in F well, Core-1.....	63
Table 5: The minerological composition of the uppermost Bedinan Formation 1 st sandstone level penetrated in F well, Core-2.....	64
Table 6: The lithological description of each cutting samples collected from the 1 st and the 2 nd sandstone levels of uppermost Bedinan Formation in A and F wells.....	65
Table 7: Major Provenance type with tectonic settings and related sand composition. Modified from Dickinson (1985).....	71
Table 8: The maximum diameter and volume calculation list for each pore spaces of the selected cube.....	87
Table 9: Ripple Index and Ripple Symmetry Index Measurement on the Ripple Marks identified on the cores.....	89
Table 10: Vertical and horizontal porosity variation in the 1 st and 2 nd sandstone levels penetrated in A, B, C, D, E and F wells.....	109
Table 11: Vertical and horizontal permeability variation in the 1 st and 2 nd sandstone levels penetrated in A, B, C, D, E and F wells.....	110
Table 12: Vertical and horizontal water saturation variation in the 1 st and 2 nd sandstone reservoir levels penetrated in A, B, C, D, E and F wells.....	111

Table 13: Statistical measurements for the heterogeneity index of the studied sandstone levels.....	118
Table 14: Statistical measurements for the heterogeneity index of the sandstone levels penetrated in each studied well.	120
Table 15: Density range of clay minerals (Tottens et al., 2002).....	121
Table 16: The framework minerals in accordance with X-ray diffraction bulk powder analysis.....	127

LIST OF FIGURES

FIGURES

- Figure 1: Location map of the study area. The rectangle shows the zoomed area. 2
- Figure 2: Extention map of Lower Paleozoic units; Ordovician aged Bedinan Formation and Silurian aged Dadaş Formation. The area where Dadaş Formation exist is so-called Diyarbakır Basin. Hachures shows the area where the related formations exist (modified from Aydemir (2012)). 3
- Figure 3: The location map of the studied wells, namely, A, B, C, D, E and F wells. 6
- Figure 4: The core sample of the uppermost Bedinan Formation, 1st sandstone level from F well is used to determine pore type, volume, size and porosity via Nikon's XT H 225 X-ray computed tomography scanner..... 8
- Figure 5: X-ray computed tomography working principle..... 9
- Figure 6: The geological map (constructed by geology team of Çalık Petrol) of the area of interest embedded on the Google Earth image. 19
- Figure 7: The location of the study area over 1/500.000 scaled geological map of southeastern Turkey (modified from Perinçek et al. (1991) and the geological map compiled by Necati Turhan, Veli Balcı and Yılmaz Günay (TPAO)). 20
- Figure 8: Correlation chart of the Precambrian to the Permian formations from the previous studies. In this study, the formation names, their groups and ages were adapted from Yılmaz and Duran (1997) and Çoruh et al. (1997) . 27
- Figure 9: Correlation chart of the Early Triassic to the Early Campanian formations from the previous studies. In this study, the formation names, their groups and ages were adapted from Yılmaz and Duran (1997) and Çoruh et al. (1997). 30
- Figure 10: Correlation chart of the Middle Campanian to the Early Pliocene formations from the previous studies. In this study, the formation names,

their groups and ages were adapted from Yılmaz and Duran (1997) and Çoruh et al. (1997).	32
Figure 11: North-South geological cross section from Hazro high to Mardin high passing on D-1, D-2, D-3, D-4, D-5, A, D-6, D-7 and D-8 wells. The wells data, surface geology map (1/500.000 scaled) and topography profile (Google Earth) were used for revealing the cross section. The well data from Çalık Petrol Arama Üretim San. Tic. A.Ş. database.	38
Figure 12: Generalized stratigraphic columnar section of the study area (modified from Yılmaz and Duran (1997)).....	39
Figure 13: The compiled chronostratigraphic chart for the middle-upper Ordovician to Silurian units of Saudi Arabia, Iran (Zagros), Iraq, SE Turkey, Morocco, Syria, Algeria, Libya, Jordan and Oman, compiled from Çoruh et al., 1997; Alsharhan and Nairn, 1997; Le Heron and Howard, 2010; Ghiennie et al., 2010; Le Hérissé et al., 2015; Craigie et al., 2016; Saberi et al., 2016; Oktay and Wellman, 2019.....	46
Figure 14: The compiled chronostratigraphic studies for the lower Paleozoic sequence of Diyarbakır Basin, Southeastern Turkey.....	47
Figure 15: The vertical stratigraphic columnar section of the Middle-Late Ordovician aged Bedinan Formation and the studied interval with gamma ray readings in Diyarbakır Region.	51
Figure 16: The intervals of the full diameter cores and the cutting samples of uppermost Bedinan Formation levels of interest for the thin section investigation and the point counting method. Scale: Each minor tick in MD column: 1m. The well log data is obtained from Çalık Petrol database.	54
Figure 17: Photomicrograph of the sandstone with patchy dolomite cement, the core-1, the 1 st sandstone level of the uppermost Bedinan Formation, F well. Dol: Dolomite.....	58
Figure 18: Photomicrograph of the 1 st sandstone level of the uppermost Bedinan Formation with quartz overgrowth, the core-1, F well.	59

Figure 19: Photomicrographs (a: cross-polarized light, b: plane-polarized light) of the 2 nd sandstone level of the uppermost Bedinan Formation with quartz overgrowth (core-1, A well).	60
Figure 20: Photomicrograph of the 1 st sandstone level of the uppermost Bedinan Formation with muscovites, the core-1, F well.	61
Figure 21: The relative percentage of each facies identified from the cutting samples collected from the 1 st and 2 nd sandstone levels of uppermost Bedinan Formation in A and F wells.	66
Figure 22: Sandstone classification after Pettijohn (1975).	67
Figure 23 : Ternary plots of the studied core samples of the 1 st and the 2 nd sandstone levels of the uppermost Bedinan Formation.	68
Figure 24: The photomicrograph of quartz arenitic the 1 st sandstone level (core-2) of F well, Plane polarized light. Scale is indicated with a white bar.	69
Figure 25: The photomicrograph of quartz arenitic the 1 st sandstone level (core-1) of F well, Plane polarized light. Scale is indicated with a white bar.	69
Figure 26: Provenance types of sandstones having different quartz, feldspar and lithic fragment ratio. Qt: quartz, F: Feldspar, L: Lithic fragment (Dickinson 1985).	71
Figure 27: The diagram exhibits the plan view of Stable Craton provenance (Dickinson and Suczek 1979).	72
Figure 28: The diagram exhibit the plan view of Basement Uplift provenance (Dickinson and Suczek, 1979).	73
Figure 29: The diagram exhibits the plan view of Recycled Orogen provenance (Dickinson and Suczek, 1979).	73
Figure 30: The diagram exhibits the plan view of Magmatic Arc provenance (Dickinson and Suczek, 1979).	74
Figure 31: The diagram shows the provenance of the uppermost Bedinan Formation 1 st and 2 nd sandstone levels.	76
Figure 32: Monocrystalline quartz observed in the photomicrograph of the 1 st sandstone level, the core-1, F well. Qm: Monocrystalline quartz.	77

Figure 33: The photomicrograph of the core-1, the 1 st sandstone level of the uppermost Bedinan Formation, F well, polycrystalline quartz with straight boundary.	77
Figure 34: Photomicrograph (a: Cross-polarized light, b: Plane-polarized light) of the sandstone with shale laminae displays silt size quartz grains with muscovites in the core-2, the 1 st sandstone level of the uppermost Bedinan Formation, F well.	78
Figure 35: The photomicrograph of the marl lithofacies, the cutting sample-1 of the 2 nd sandstone level of the uppermost Bedinan Formation, F well.	79
Figure 36: The radiographic view (side views) of the studied core of F well 1 st sandstone level in different dimensions.	81
Figure 37: 2 dimensional cross sectional slices and pore spaces generated by X-ray attenuation method of the core sample of the 1 st sandstone level of F well. Red arrow points on the porespace. Bright white patches are carbonate cement (calcite or dolomite).....	82
Figure 38: 3 dimensional view of the core sample of the 1 st sandstone level of F well by using VG studio max high-end technological software system.	82
Figure 39: The region of interest for measuring pore shape size and volume distribution, created by X-ray computed tomography high-end technology.	83
Figure 40: 3 dimensional view of the region of interest and colored pore spaces shape, intensity and size.	84
Figure 41: The volumetric calculation via CT for each pore of the selected cube. ...	85
Figure 42: The diagram shows the volumetric calculation versus maximum diameter variation through each detected pore of the core sample (F well, the 1 st sandstone level of the uppermost Bedinan Formation, x axis: volume, y axis: diameter).....	86
Figure 43: Ripple index and Ripple symmetry index values plotted on the chart with regard to six measurable ripple marks observed on the cores of the	

uppermost Bedinan Formation sandstone reservoir levels adapted from Tanner (1967).	91
Figure 44: Sedimentary structures observed in the cores of the 1 st and the 2 nd sandstone levels of the uppermost Bedinan Formation. A: trough cross bedding, b: planar wedge-shaped cross bedding with moderate bioturbation, c: lenticular bedding with bioturbation, d: sand-mud parallel lamination with moderate bioturbation, e: planar sigmoidal cross bedding and parallel lamination.	93
Figure 45: The GR log reading shows left boxcar GR trend of the upper shoreface to lower shoreface in the 1 st and 2 nd sandstone levels and right boxcar GR trend of offshore transition to offshore shale dominant interlayers (shale-1 and shale-2) of the uppermost Bedinan Formation. Scale: each minor tick space in SSTVD column= 1m. Distance between wells: no scale...	94
Figure 46: Depositional environment model for the uppermost Bedinan Formation, the 1 st and the 2 nd sandstone levels and shale interlayers (shale-1 and shale-2).	95
Figure 47: Late Ordovician (Hirnantian) paleogeographic map of Gondwana and relative position of Arabian plate and the study area. Adapted from Scotese (2014) and Torsvik and Cocks (2013).	101
Figure 48: Paleozoic global temperature curve and the temperature at which the uppermost Bedinan Formation deposited (Scotese, 2015).	102
Figure 49: Regional sea level change studies for the Ordovician (Munnecke et al., 2010). The red rectangle is time interval when the studied levels deposited.	102
Figure 50: Relative thickness variation of the Early Silurian aged Basal Tanezzouft Formation due to paleodepressions attributed with ice activity (Lüning et al., 1999)..	103
Figure 51: E-W seismic line across the northern side of the study area. Parallel seismic reflections of the Silurian organic rich Dadaş Formation and the Bedinan	

Formation clastic levels denies subaerial exposure and glacial activity. The seismic data is obtained from Çalık Petrol database.....	104
Figure 52: The correlation of the “Hot Shale” level of the Silurian aged Dadaş Formation in the studied wells (A, B, C, D, E and F). Each minor tick in SSTVD column corresponds to 1 meter. The wireline log data from Çalık Petrol database.....	105
Figure 53: The uppermost Bedinan Formation 1 st and 2 nd sandstone reservoir levels are correlable which is justified by GR and Sonic wireline log readings. This fact denies the ice activity on the levels of interest. Scale: each minor tick space in MD column= 1m. The well logs data is obtained from Çalık Petrol database.....	106
Figure 54: Micrometers to hundreds of meters scaled reservoir heterogeneity types with various extend constitutes as a function of depositional facies and diagenetic evaluation (Morad et al., 2010).....	108
Figure 55: Vertical and horizontal permeability variation and correlation through the 1 st and the 2 nd sandstone levels of the uppermost Bedinan Formation in A, B, C, D, E and F wells (permeability log in logarithmic scale, minor ticks in MD corresponds to 5 meters). Distance between the wells: no scale.	112
Figure 56: Vertical and horizontal porosity variation and correlation through the 1 st and the 2 nd sandstone levels of the uppermost Bedinan Formation in A, B, C, D, E and F wells (minor ticks in MD column corresponds to 5 meters). Distance between the wells: no scale. The wireline log data from Çalık Petrol database.....	113
Figure 57: Vertical and horizontal water saturation variation and correlation through the 1 st and the 2 nd sandstone levels of the uppermost Bedinan Formation in A, B, C, D, E and F wells (minor ticks in MD column corresponds to 5 meters). Distance between the wells: no scale. The wireline log data from Çalık Petrol database.....	114

Figure 58: Vertical and horizontal porosity, permeability and water saturation variation and correlation through the 1st and the 2nd sandstone levels of the uppermost Bedinan Formation in B, E and F wells located in different prospects (minor ticks in SSTVD column corresponds to 5 meters). Distance between the wells: no scale. The wireline log data from Çalık Petrol database. 115

Figure 59: 3D property (permeability, water saturation) modelling of the trapped area where A, B, C wells drilled..... 116

Figure 60: Permeability distribution in the uppermost Bedinan Formation penetrated in A, B, C, D, E and F wells (x axis: permeability, y axis: percentage of permeability distribution). 118

Figure 61: Permeability distribution in the uppermost Bedinan Formation in each well (x axis: permeability, y axis: percentage of permeability distribution). 119

Figure 62: Types of the clay coating minerals forming matrix of the sandstone levels of the uppermost Bedinan Formation based on Thorium and Potassium concentration cross plot for D well..... 123

Figure 63: Type of the clay coating minerals forming matrix of the sandstone levels of the uppermost Bedinan Formation based on Potassium concentration and Photoelectric factor cross plot for D well. 124

Figure 64: Besides depositional environment, Thorium/Potassium & Thorium/Uranium cross plot is useful tool to determine type of clay and used for determination of the clay coating minerals occupying matrix of the uppermost Bedinan Formation sandstone levels (D well). 125

Figure 65: The raw (a) and interpreted (b) bulk powder XRD diffractograms of the sample of the 2nd sandstone level (A well). 128

Figure 66: The pie diagram of mineral abundance of the sample (the 2nd sandstone level, A well)..... 129

Figure 67: The raw (a) and interpreted (b) bulk powder XRD diffractograms of the sample of 1st sandstone level (B well). 130

Figure 68: The pie digram of the mineral abundance of the sample (the 1 st sandstone level, B well).	131
Figure 69: The raw (a) and interpreted (b) bulk powder XRD diffractograms of the sample of 2 nd sandstone level (B well).....	132
Figure 70: The pie diagram of the mineral abundance of the sample (the 2 nd sandstone level, B well).	133
Figure 71: The raw (a) and interpreted (b) bulk powder XRD diffractograms of the sample of the 1 st sandstone level (F well).	134
Figure 72: The pie diagram of the mineral abundance of the sample (the 1 st sandstone level, F well).....	135
Figure 73: The interpreted clay mineral XRD diffractograms of the sample of the 2 nd sandstone level (A well).....	136
Figure 74: The interpreted clay mineral XRD diffractograms of the samples of the 1 st and 2 nd sandstone levels (B well).	137
Figure 75: The interpreted clay mineral XRD diffractograms of the sample of the 1 st sandstone level (F well).....	138
Figure 76: Depth depended variation of relative ratio and amount of illite/smectite, quartz, kaolinite, chlorite and potassium feldspar through progressive temperature increment, modified from Hower et al., (1976).	146
Figure 77: Hydrocarbon generation, diagenesis, source rock maturity (vitrinite reflectance) and relative ration of mixed-layer illite/smectite relationship. Figure and data summarized from Kübler and Jaboyedoff (2000), Jiang (2012).	149
Figure 78: SEM image of the most common clay coating minerals of the siltstone levels of the Halevikdere Formation exposed in Mardin-Derik-Kızıltepe area. a: illite (I) plates. b: Kaolinite (K) minerals. c: Mixed layer illite-smectite (I-S). d: illite, kaolinite and euhedral feldspars (Tetiker et al., 2015).....	150

Figure 79: Photomicrograph of the quartz overgrowth developed around tightly packed fine grained quartz of the 1st sandstone level (Core-2) of the uppermost Bedinan Formation in F well. 151

Figure 80: Photomicrograph of solution of fine grained quartz edges (F well, the 1st sandstone level, the core-2) by compaction related pressure solution.. 152

Figure 81: The contact of the grains has subjected to dissolution leading to the penetration one grain by another (F well, 1st sandstone level, Core-2).152

Figure 82: Relative variation of the quartz cement and rest of other cements in accordance with the type of rock. Based on QFL (Quartz-Feldspar-Lithic fragment) relative ratio, the uppermost Bedinan Formation sandstone levels are subarkose to quartz arenite (Worden and Morad, 2000). 155

Figure 83: The photomicrography of isolated (patchy-shaped)dolomite cement in the 1st sandstone level of the uppermost Bedinan Formation (core-2) in F well. 156

Figure 84: The experimental study through the impact of clay coating minerals on porosity and permeability of the Chang 7 sandstone reservoir levels (Ordos Basin) (Liu et al., 2016). 160

CHAPTER 1

INTRODUCTION

1.1. Purpose and Scope

The subsurface of SE Turkey, northern margin of the Arabian Plate, is rather complex due to the impacts of both tectonism and relative sea level changes. Despite the complexity of the structures and variation in facies distribution due to variable paleobathymetry during deposition of each sequence in SE Turkey, the new enhanced well stimulation methods enable to increase hydrocarbon recovery and fluid flow from reservoir levels with heterogeneity problem, unexpected fluid flow barriers. The Ordovician aged uppermost Bedinan Formation sandstone reservoir levels are good examples for formations having reservoir heterogeneity problem.

In some wells drilled in Diyarbakır basin, oil production has been performed from the uppermost Bedinan Formation sandstone levels, while the others could produce only low levels of oil or could not produce it at all due to the reservoir heterogeneity problem.

The purpose of this study is to find an answer to the reason of the reservoir heterogeneity of the sandstone levels, which could enable us to develop proper enhanced oil recovery programs.

The study covers sedimentary petrography, X-ray computed tomography, XRD analysis, petrophysical interpretations to understand the following issues;

- Depositional environment
- Sedimentological properties
- Determination of porosity types, texture and fabric
- Clay typing

➤ Diagenetic evaluation of the formation

1.2. Location of the Study Area

The study area, which includes 6 wells (A, B, C, D, E and F), lies between Mardin and Diyarbakir provinces and covers approximately 600 km² area. More precisely, the location of the study area is confined by latitudes 37°37'26.00"N- 37°43'51.00"N and longitudes 40°39'15.00"E- 40°29'59.97"E (Figure 1).

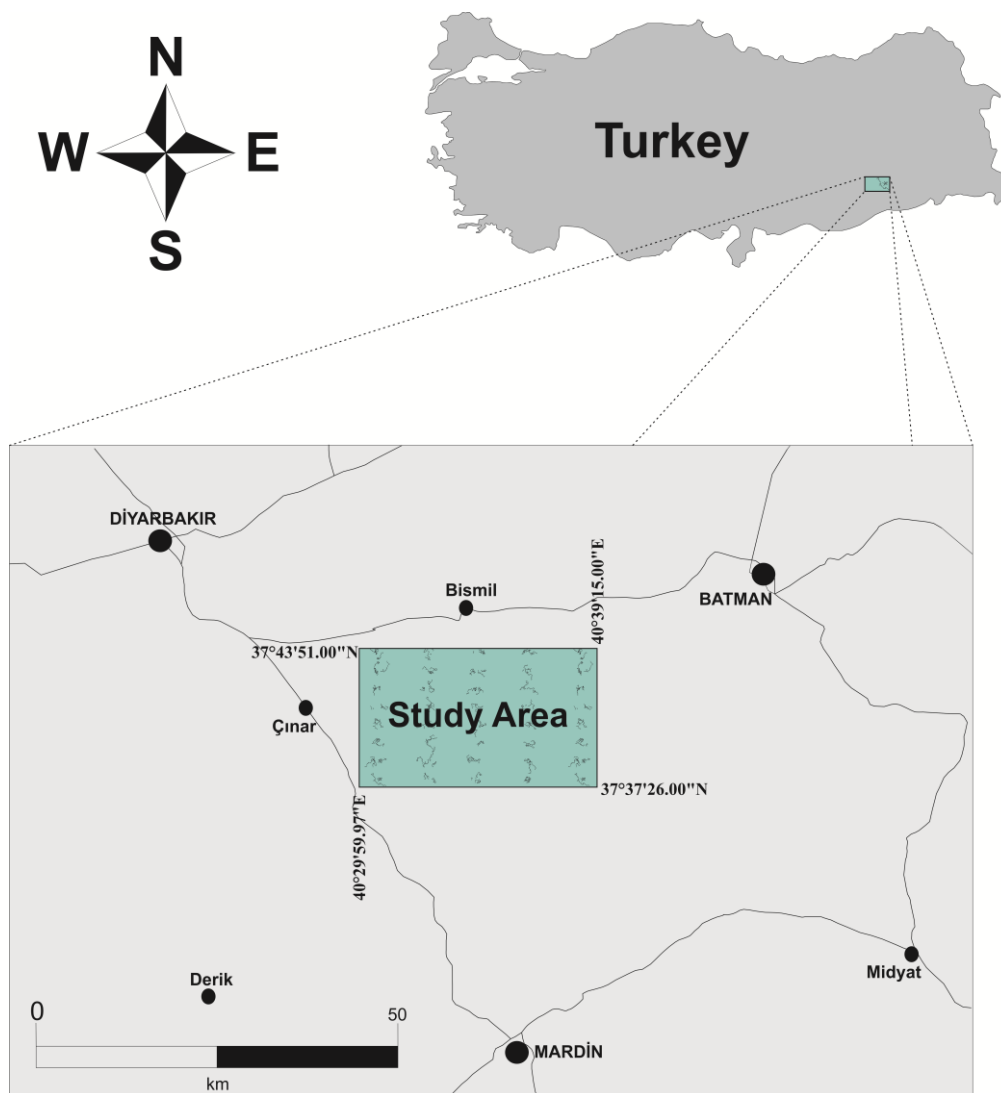


Figure 1: Location map of the study area. The rectangle shows the zoomed area.

Geologically, the study area located southern part of the Diyarbakır Basin (Figure 2) can be a pioneer site to find answer for reservoir heterogeneity problems for the rest of the upper Ordovician sandstone reservoir levels of the basin.

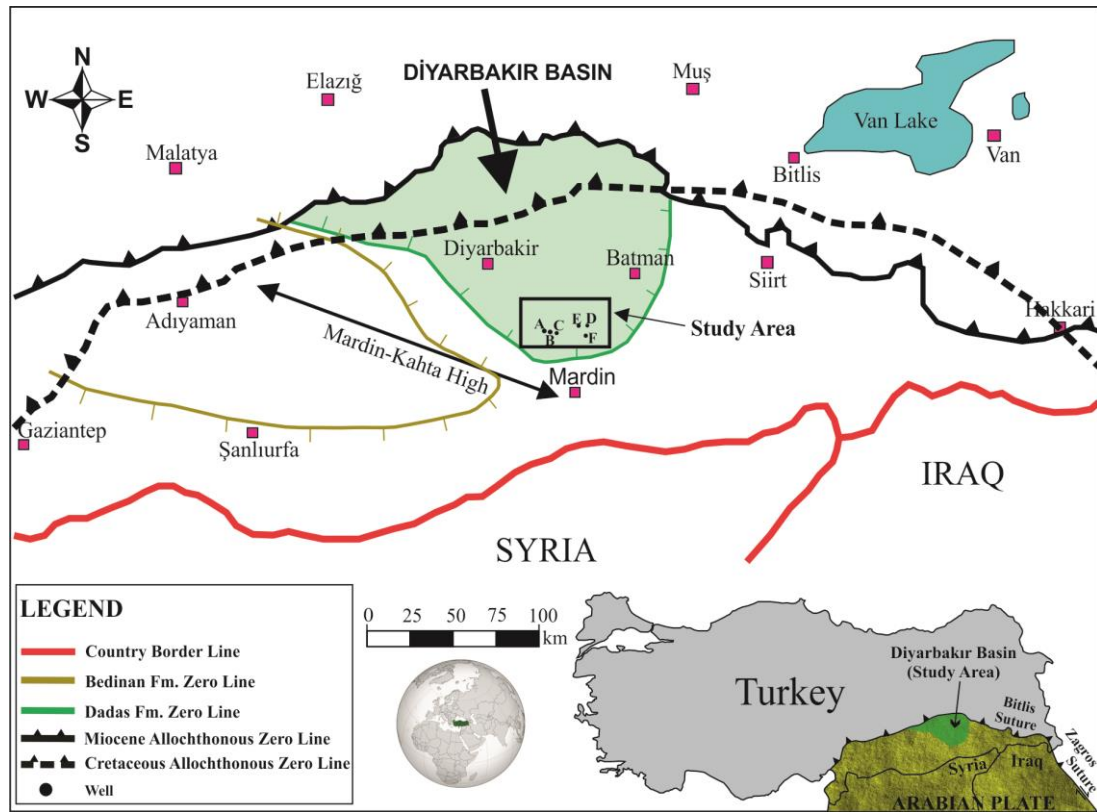


Figure 2: Extention map of Lower Paleozoic units; Ordovician aged Bedinan Formation and Silurian aged Dadaş Formation. The area where Dadaş Formation exist is so-called Diyarbakır Basin. Hachures shows the area where the related formations exist (modified from Aydemir (2012)).

1.3 Data and Methods of Study

Reservoir heterogeneity refers to relative variation in porosity, permeability and capillary pressure due to depositional facies, type and amount of matrix content, provenance, rate of deposition, the degree of compaction (mechanical and chemical),

diagenetic impact, the time of oil emplacement, paleo-climate, structural deformations (fracturing, fault e.t.), thermal history of basin (Worden and Morad, 2000; Worden and Barclay, 2003; Ajdukiewicz and Lander, 2010; Morad et al., 2010; Al-Laboun et al., 2014; Worden et al., 2018). The heterogeneity of the reservoirs is responsible for variation in volume, hydrocarbon recovery from the reservoir and fluid flow rate (Morad et al., 2010).

The study is carried out in three phases following the stages of;

- 1) Data collection and literature survey.
- 2) Fieldwork and laboratory work (petrography, X-ray microCT, XRD analysis).
- 3) Software analyses, observations and evaluation of outcomes.

The data consists of;

- 1) Digital (ASCII and LAS files) wireline log data (Spectral Gamma Ray, Sonic, Photoelectric factor from Çalık Petrol database).
- 2) Petrophysical interpretations (porosity, permeability and water saturation).
- 3) Hydrocarbon production performance (daily oil production rates) of 6 wells (Figure 3) (A, B, C, D, E and F).
- 4) 15 cores (vertical full-diameter cores, 2 5/8 inches in diameter, 5-10 cm in length) and 4 cutting samples (5 cores and 4 cutting samples for petrographic analysis, 5 cores for the depositional environment interpretation, 1 core for X-ray CT measurement and 4 cores for XRD analysis) from 4 wells (A, B, D and F).
- 5) 1 seismic profile for paleogeographic re-construction.
- 6) Regional well side geology observations (cutting sample analysis under microscope and correlation of the facies between the studied wells).

All available resources and reports regarding the Bedinan Formation reservoir levels and other relevant studies on reservoir heterogeneity were compiled and analyzed comprehensively.

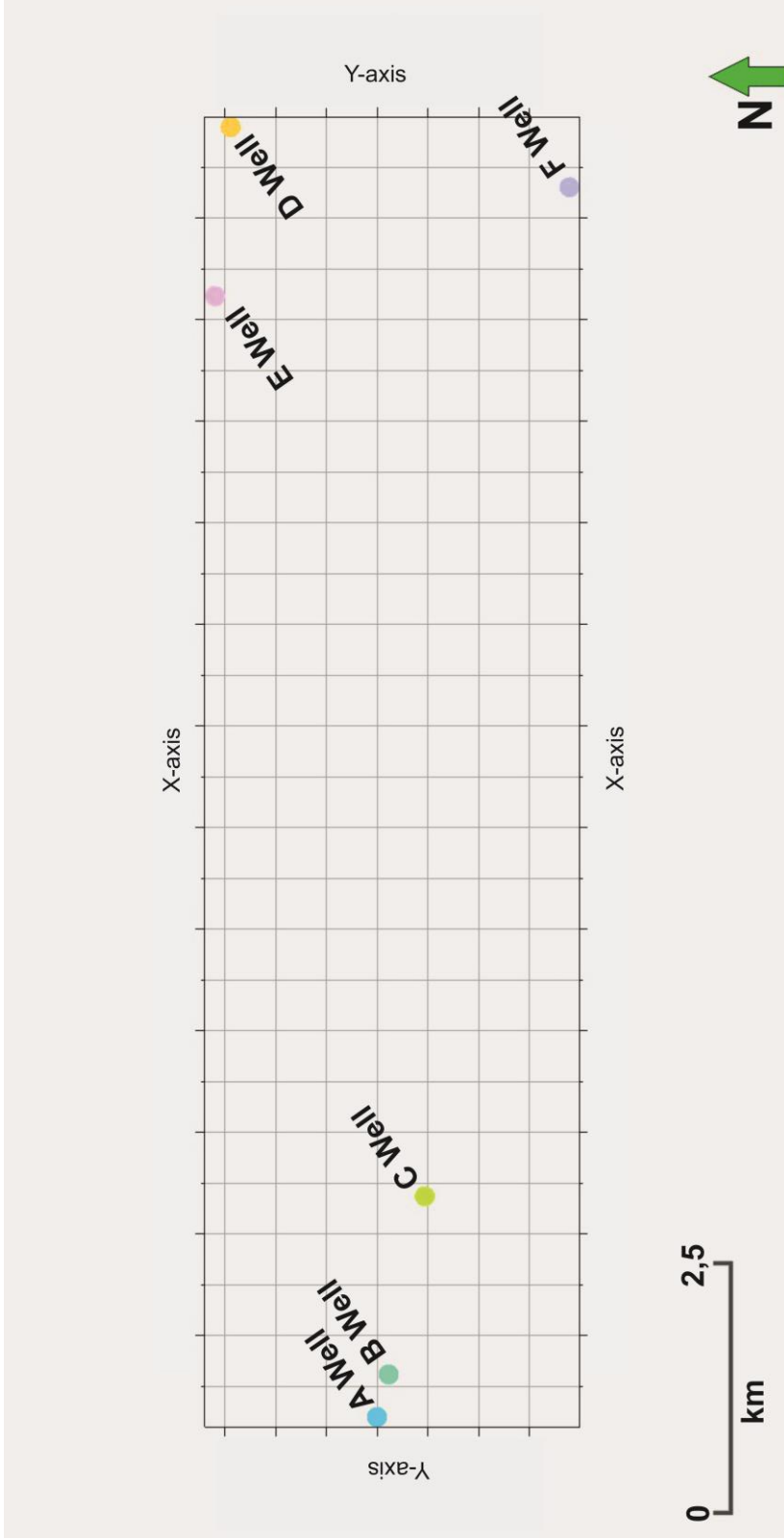


Figure 3: The location map of the studied wells, namely, A, B, C, D, E and F wells.

3D petrophysical models, wireline log, facies, water saturation, porosity and permeability correlations and modeling, and particularly reservoir matrix evaluation for the Bedinan Formation reservoir levels of interest between the studied wells are constructed using Petrel E&P Software Platform, Version 2017.1 of Schlumberger Company. The workflow for the 3D modelling was started with importing seismic depth map of the Bedinan Formation and wireline log data in ASCII format to Petrel software system. The geological elements including key horizons and faults were picked on seismic profiles with the aid of borehole information. The depths to the surface determined in seismic profiles were adjusted by using real formation tops data. And then, structural framework was determined by using fault modelling, pillar gridding and generation of the faulted horizons. Finally, porosity, permeability and water saturation distributions throughout the trapped area were obtained by the reservoir modelling by utilizing appropriate simulation methods (Gaussian, Kriging), variograms and trends.

X-ray computed tomography (CT) imaging was used to determine porosity, 3D volumetric and diametrical dimensions of pore spaces and type of porosity in the reservoir levels (Figure 4). This technique reveals the internal features of the interested opaque objects. It was originally used for medical care but later on, developed and becoming widely used for geoscientific studies especially to measure porosity, size and volume of each pore and penetration of injected fluids (Mees et al., 2003).

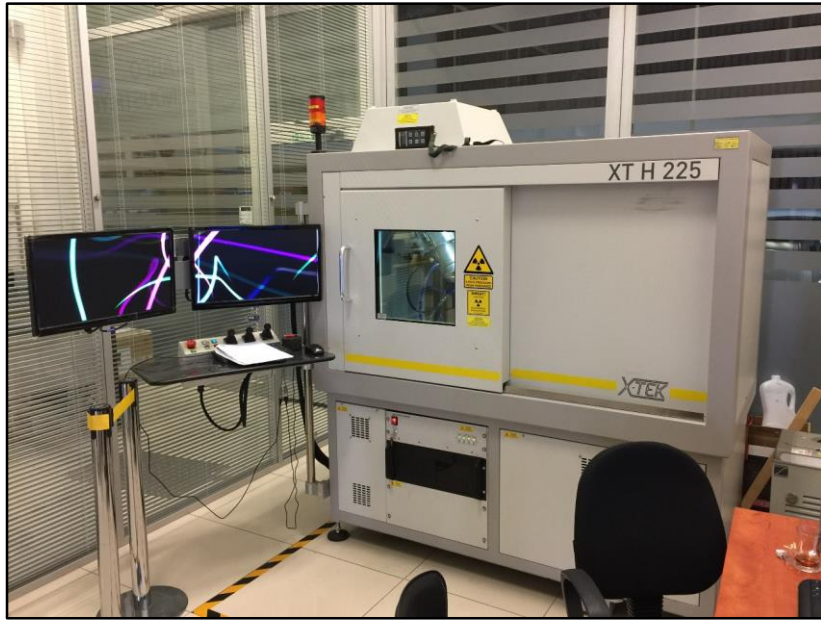


Figure 4: The core sample of the uppermost Bedinan Formation, 1st sandstone level from F well is used to determine pore type, volume, size and porosity via Nikon's XT H 225 X-ray computed tomography scanner.

X-ray tomography measurement is based on 2D radiographs from different angle around the studied sample to create 3D image from the projection. The 2D radiographs are constituted by x-ray beams from X-ray source passing on the studied opaque sample and visualization of attenuated x-ray on the detector. The x-ray attenuation is resulted from X-ray absorption, in other words, photoelectric absorption or compton scattering. X-ray attenuation measurements around the studied core in 360 degree yield 2-dimensional cross sectional images (Taud et al., 2005). 3-dimensional cube or image can be generated by stacking / interpolation of 2-dimensional images (Akin and Kavscek, 2014) (Figure 5).

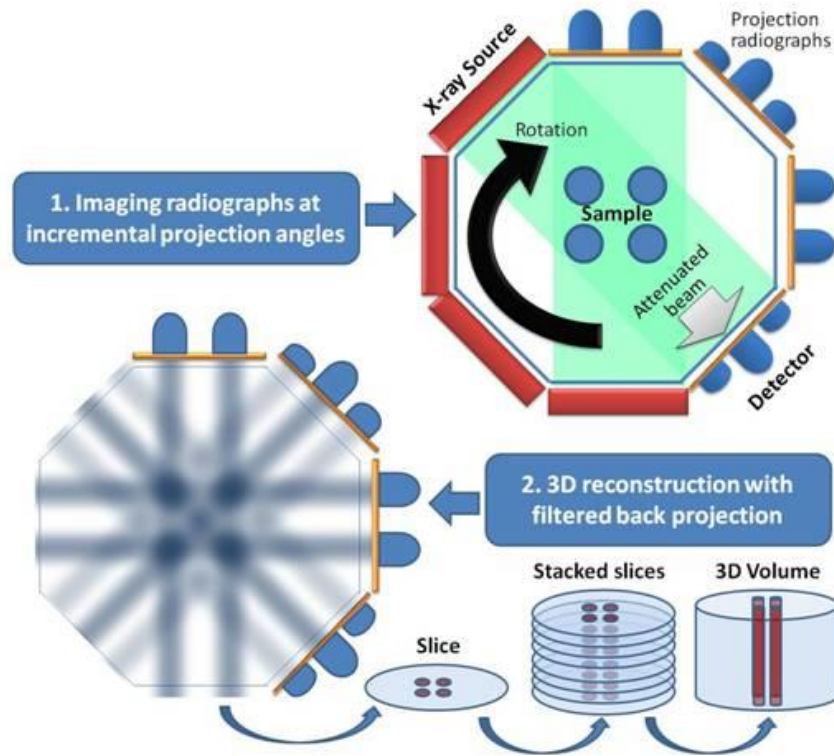


Figure 5: X-ray computed tomography working principle.

CT imaging was applied to the core sample of the first sandstone level penetrated in F well by using Nikon XT H 225 industrial CT scanner. The technical specifications of the scanner are as follows;

- 225kV / 225 W Reflection target source
- Varian 4030 Flat Panel
- 5-axis fully programmable part manipulator
- Minimum spot size of 3 μm .

Scan conditions;

- 90 kV
- 175 μA
- 500 ms Exposure.

The core sample used for the CT scanning was selected from an interval almost without any shale laminas.

A total number of 30 thin sections from 5 full-diameter cores and 4 cutting samples of the uppermost Bedinan Formation collected from 3 wells (A, B and F) were examined under microscope. Gazzi-Dickinson method of point counting measurements (Dickinson, 1970; Ingersoll et al., 1984) by using James Swift brand mechanical stage mounted on the microscope were carried out to explore mineral framework of the studied intervals, relative ratio of quartz, feldspar and rock fragment for classifying the sandstone and provenance study (with quartz type). Approximately 2500-2600 points were counted in the selected thin sections. Alizarin red test was carried out to discriminate between calcite and dolomite.

The sedimentary structures and their geometries with the corresponding gamma ray readings of 5 cores were used to understand the depositional environment and paleogeography of the studied levels. The dimensionless parameters such as ripple index (the ratio between two adjacent crests spacing and horizontal distance between crest and trough) and ripple symmetry index (the ratio between one crest to trough along the gentler slope and the crest to next trough along the steeper slope) (Tanner, 1967) of the ripples recognized in the full diameter cores were plotted on the chart suggested by Tanner (1967). In addition, the sedimentary structures (cross bedding etc.) recognized in the cores and their formation conditions were used to understand the depositional environment with the aid of gamma ray log reading trends (Siddiqui et al., 2013).

Spectral gamma ray and photoelectric factor wireline log data (ASCII and LAS files) of D well were uploaded to Petrel Software System to differentiate the type of clay minerals constituting the matrix of the sandstone levels. The charts (Thorium (ppm) – Potassium (%), Thorium (ppm) – Pefz, Thorium(ppm) / Potassium(%) – Thorium (ppm) / Uranium (ppm)) suggested by Schlumberger (2009) were used to specify the type of clay minerals in the sandstone levels studied.

The semi-quantitative X-ray diffraction (XRD) bulk powder mineral analysis on 4 core samples collected the studied levels (penetrated in A, B and F wells) were carried out to identify the mineral framework and particularly to determine type of the clay matrix. XRD analysis were performed in Turkish Petroleum Corporation by the use of a Rigaku D/MAX-2200 Ultima⁺/PC diffractometer under the following conditions;

- Scan range: 5- 70°
- Scan speed: 1 °/s
- X-ray tube: Cu (kV: 40kV mA: 30mA)
- Voltage: 40 kV
- Current: 20 mA
- Wavelength: (CuK α) 1.54059 Angström
- Software: MDI Jade 7.0

Sample preparation;

- Powdering a piece of the core sample by Retsch RS-200 grinding equipment
- Mounting of the powders on glass for XRD bulk powder analyses.

The X-ray diffractograms were evaluated according to Inorganic Crystal Structure Database (ICSD) of International Center for Diffraction Data (ICCD).

1.4 Previous Works

The main objective of the study is to find an answer for reservoir heterogeneity of the sandstone levels followed by the variety of hydrocarbon production performance. With regard to this fact; lithofacies, sedimentology and depositional environment of the levels are substantial to delineate the reservoir heterogeneity maps.

The Paleozoic stratigraphy has been studied by several authors since 1950's for different aspects, especially for hydrocarbon researches.

After hydrocarbon discoveries in the Bedinan Formation subarkose sandstone reservoir levels in the southern side of Diyarbakır Basin, the reservoir has become very popular for Paleozoic petroleum system of SE Turkey.

The formation is described for the first time by Cobb (1957c) in Mardin-Bedinan region with cropping out successions. Cobb's study was followed by the studies performed by Blakslee et al. (1960), Durkee (1961), Kellogg (1961); Stratum (1963), Koaster (1963), Schmidt (1964; 1966), TPAO (1966), N.V. Turkse Shell (1966), Dean (1979a; 1979b), Ala and Moss (1979), Monod and Dean (1980), Dean et al. (1981), Amaco (1985), Dean and Monod (1985), Dean et al. (1993), Bozdogan et al. (1987; 1994; 1995).

This chapter provides a brief summary regarding the published regional and relevant studies, which has been used to investigate the reservoir heterogeneity of the uppermost Bedinan Formation in chronological order.

The regional published studies related to the Bedinan Formation are listed below in chronological order.

Kellogg (1960c) spent significant efforts to sort out the Paleozoic level of SE Turkey. Based on his study performed on the Paleozoic outcrops in Mardin Derik area, the Bedinan Formation comprises in ascending order 500 meters shale, siltstone and 120 meters fine grained sandstone levels. He is the first one stated that the uppermost Bedinan Formation sandstone levels can be good hydrocarbon reservoir.

Dean (1967; 1975) worked on the outcrop of Bedinan Formation in Mardin-Derik area. He argued that the fossil assemblage, especially trilobites in clastic levels of the uppermost part of Bedinan Formation is not younger than Caradocian age (Late Ordovician).

Demirtaşlı (1974) performed an exhaustive study on the Paleozoic level of Turkey-Iran and Pakistan to make a correlation. The author argued that, based on fossils assemblage, especially trilobites in the Bedinan Formation shale levels, the unit deposited in the Middle Ordovician, and can be correlated with Shirgest and Mila Formations in Iran and the upper level of Habur Group in Iraq.

Bozdogan et al. (1987; 1994; 1995; 1996) carried out a comprehensive study to clarify depositional environment, distribution, hydrocarbon source, reservoir characteristics, paleogeographic evaluation and tectonic history of Paleozoic autochthonous units of SE Turkey. He argued that the Bedinan Formation might be informally divided into four members in accordance with the depositional environment, lithology and wireline log responses; comprises predominantly sandstone, siltstone and shale lithology and showing regressive character especially in the upper clastic levels in response to global cooling. Lanvirnian-Ashgillian age (Middle-Late Ordovician) is assigned to the Bedinan Formation clastic units based on the fossils found in the mentioned formation.

Perinçek (1990) dealt with the stratigraphic units of Hakkari province and surrounding area located at the border of Turkey-Iraq. He tried to determine contacts and lithostratigraphic properties of the exposed strata including the Middle-Late Ordovician aged Bedinan Formation. He argued that the upper part of Habur Group named by Wetzel (1959) in Iraq might be equivalent to the uppermost Bedinan Formation, after the age of uppermost Bedinan Formation is assigned as Ashgillian in accordance with fossils assemblage like *Calymenesun* sp, *Dindymene* sp, *Dionide* sp, *Duftonia* sp, *Hammatocnemis* sp, *Otarion* sp, *Prionocheilus* sp, and *Remopleurides* sp, trilobites.

Stemans et al. (1996) recorded well-preserved palynomorphs consisting of cryptospores and miospores in samples of Ordovician (Bedinan Formation) and Silurian (Dadaş Formation) units. Different from the old studies, the age of the uppermost part of Bedinan Formation was assigned as Hirnantion in accordance with late biozone documented with the cores taken from the well that is located northern part of Diyarbakır basin.

Besides the old studies related with the age assignment for the Ordovician units regarded macrofossils such as trilobites and graptolites; Paris et al. (2007) studied on samples collected from the surface and subsurface in Taurus range, Hakkari and Mardin-Derik area that is based on microfossils chitinozoans and acritarchs. The study indicates that the Bedinan Formation is deposited in the time range from Darriwilian (Middle Ordovician) to Late Katian (Late Ordovician).

Bozkaya and Kozlu (2011) examined the clay minerals of the upper Paleozoic-lower Mesozoic clastic units. They claimed that the clay mineral association such as illite/illite-smectite, glauconite in Paleozoic-lower Mesozoic sequence in Hazro area formed during diagenesis rather than detrital inputs.

Tetiker et al. (2015) carried out a study on the samples collected from the Precambrian and lower Paleozoic levels in Mardin-Derik-Kızıltepe area. SEM (Scanning electron microscopy) and XRD (X-ray diffractometry) method are applied on the samples to determine mineral composition of the interested formations. The study is performed on the shale and siltstone levels of the Bedinan Formation rather than the sandstone levels. Based on the study results, the Ordovician aged Bedinan Formation, especially shale and siltstone levels are composed of predominantly phyllosilicates in order of

abundance by kaolinite, illite, chlorite, I-S (mixed layered clay, illite-smectite), smectite minerals.

The studies related to the reservoir heterogeneity of sandstones can be listed as below in chronological order.

Hower et al. (1976) introduced the mechanism of burial metamorphism of argillaceous sediments. He claimed that based on x-ray diffraction analyses results performed on the samples taken from the Oligocene-Miocene sediments of Gulf Coast of the United States from 1.250m to 5.500m, a significant change in the mineralogical composition (clay coating minerals, quartz cements, carbonate cements) is observed in the rocks from 2.000 m to 3.700 m with burial depth accompanied with increasing temperature.

Hurst and Irwin (1982) proved that porewater chemistry exerts great control on diagenetic alteration in sandstone reservoir levels. They emphasized that the hydraulic head variation in basins control mineral composition of clay matrix of sandstones.

Chang (1986) emphasized the impact of burial diagenesis to dioctahedral and trioctahedral smectite clay minerals in the Cretaceous offshore sediments of Brazilian offshore sediments of Potiguar, Ceara, and Ilha de Santana basins. With regard to the results of the study, the percentage of illite shows progressive increment in response to rising temperature with depth and expense of dioctahedral smectite clay minerals. However, it is observed that the trioctahedral smectite clay mineral in sandstone, nevertheless, transformed to mixed clay layer chlorite/saponite with the progressive rising of temperature with burial depth.

Worden and Morad (2000) investigated the origin of quartz cement and controls on its distribution. With regard to the study, the controlling factors for quartz cementation are temperature, effective stress, clay coating minerals along grain interface and emplacement of oil. They have accentuated that the transitional reactions among clay coating mineral such as illitization of smectite as a response of rising temperature with depth, dissolution of feldspars, pressure solution, and adjacent mud-rock constitute the main source of the silica.

Worden and Barclay (2003) studied on the Upper Jurassic Magnus turbiditic sandstone levels having the higher concentration of illite and potassium in the oil zone in comparison with water saturated zone. They noticed that the potassium transportation capacity of oil saturated zone by either diffusion or advection is lesser than water saturated zone; therefore, illitization proceed can be expected more in oil saturated zone rather than water zone due to the more available potassium in formation fluid.

McKinley et al. (2003) contextualised smectite occurrence and their behavior during diagenesis. They stated that smectite clay minerals form as a function of not only the depositional environment but also diagenetic factors such as bioturbation, mechanical infiltration and soft-sediment deformation. Smectite clay minerals are mostly carried into deeper water in marine environment due to the fact that these minerals are finer grained than the other clay minerals. Smectite holding considerable amount of structural water induces to overpressuring as a consequence of in situ generation of water during the clay transformation reactions.

Martín-Martín et al. (2006) worked through the kaolin minerals in Permo-Trias sandstone levels of SE Iberian basin. The variation of kaolin mineral in amount

throughout the basin extent was attributed to illitization of kaolin clay minerals in relation to maximum burial temperature.

Lahann (1980) stated that transformation reactions among clay coating mineral in elevated temperature and presence of available potassium and aluminum cause releasing of considerable amount of water and silica which resulted in movement of hydrocarbon and sedimentary cement.

Morad et al. (2010) accentuated the role of depositional fades and sequence stratigraphy on the heterogeneity of sandstone reservoir rocks. He claimed that grain coating clays formed during eodiagenesis (early diagenesis) and mesodiagenesis (late diagenesis) such as kaolinite, illite, chlorite, which in turn, affect the permeability and porosity of the sandstone formations; additionally, the place of sandstone level in system tracts plays a very important role for reservoir quality.

Rahman and McCann (2011) aimed to shed light on the diagenetic impact on Miocene Surma Group sandstone reservoir levels. They stated that the origin of quartz cement is the function of pressure solution, transformation reaction among clay coating minerals and dissolution of K-feldspar, and the syntaxial quartz overgrowth around detrital quartz grains denotes the mesodiagenetic stage. Furthermore, mesodiagenetic illite clay minerals form around the temperature of 90-130 C° with the presence of high available potassium in pore water.

Creoz et al. (2011) studied on the reactivity of mixed clay layer of illite-smectite in the different range of ph values from 3 to 8.5 at 80 °C and 0.1 M NaCl solution. Based on the results of the study, the acidic condition increases the illitization of the initial clay mineral.

Al-Ramadan (2014) straightened out the illite- smectite transition and its effect on reservoir quality of Permian aged Unayzah Formation in Saudi Arabia. He stated that while the transformation of smectite to illite in response to increasing depth accompanied by rising temperature causes to the preservation of pore volume, the reaction resulted in deterioration of permeability of the sandstone reservoir level. Even though the study is not related with Bedinan Formation, reservoir heterogeneity problem in targeted formation is essentially similar with reservoir quality problem of Ordovician age Bedinan Formation; therefore the study constitutes the most important milestone to solve reservoir quality and heterogeneity problem in Bedinan Formation. This study is different from the studies above mentioned and the first study on reservoir heterogeneity of the Bedinan Formation sandstone reservoir levels in the region.

CHAPTER 2

GEOLOGICAL SETTING

The study area situated in Diyarbakır and Mardin provinces covered by the Late Miocene-Early Pliocene aged fluvial Şelmo Formation in northern side and the Eocene to Oligocene aged Midyat Group carbonates in the southern side (Figure 6, 7). The oldest unit exposed along the southern side of the study area is the Early Eocene to Early Oligocene aged Hoya Formation carbonates. The Germik (the Middle Eocene-Oligocene) and Şelmo Formations (the Late Miocene-Early Pliocene) crop along the middle and northern parts of the study area.

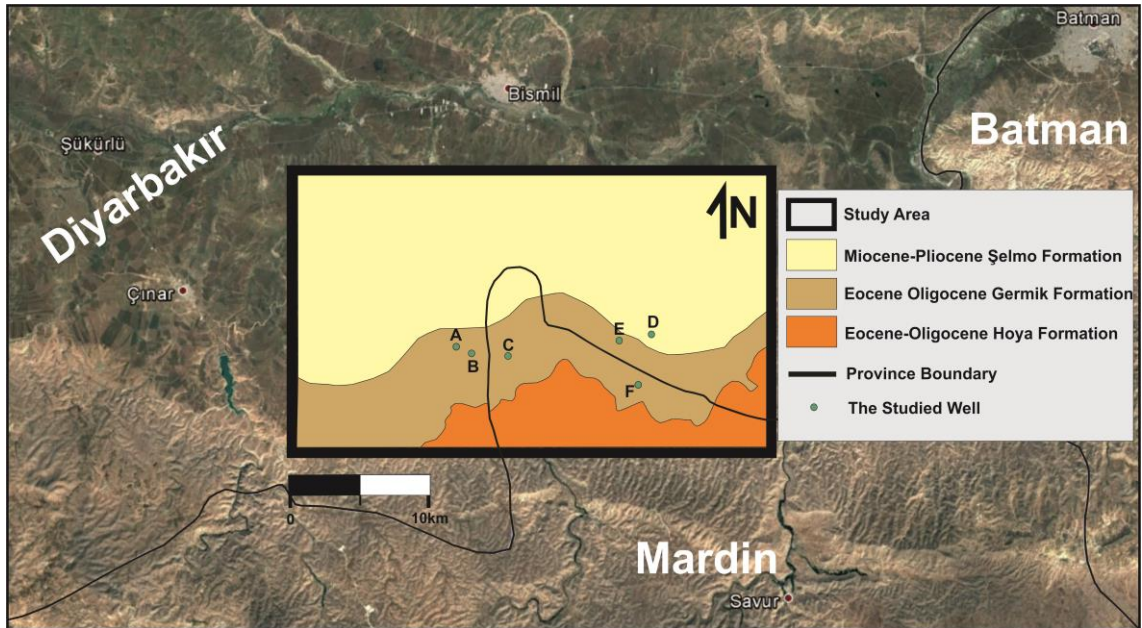


Figure 6: The geological map (constructed by geology team of Çalık Petrol) of the area of interest embedded on the Google Earth image.

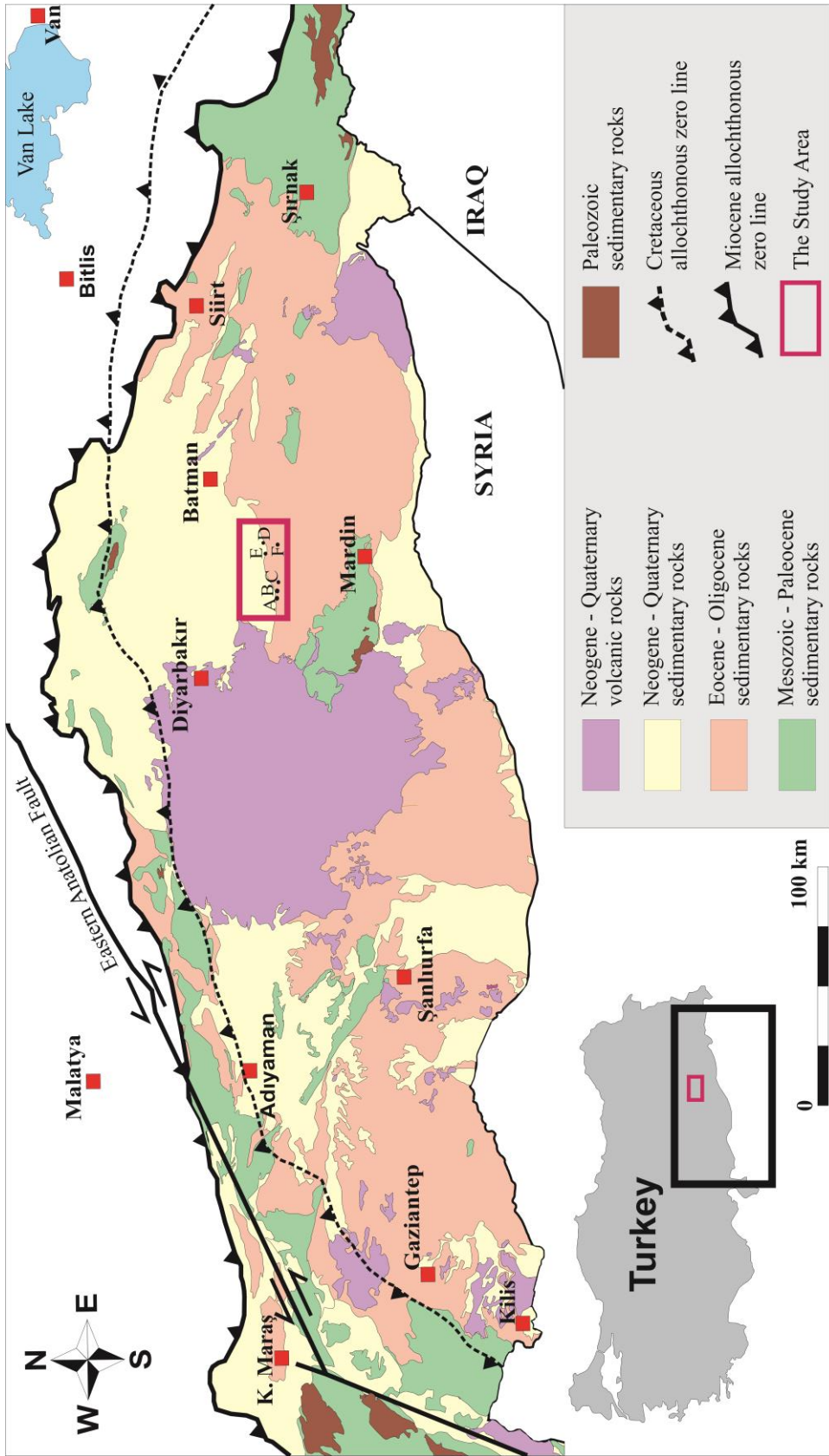


Figure 7: The location of the study area over 1/500,000 scaled geological map of southeastern Turkey (modified from Perinçek et al. (1991) and the geological map compiled by Necati Turhan, Veli Balcı and Yılmaz Günay (TPAO)).

The subsurface of the study area is rather complex, and revealed by the borehole data and the outcrop studies. The Telbesmi Formation constitutes the basement rock and is the oldest member of the Derik Group (Çoruh et al., 1997; Yılmaz and Duran, 1997) in the study area. The type locality of the Telbesmi Formation is Telbesmi village, located 40 km west of Mardin city. This formation was firstly described as a level within “Telbesmi Series” by Moses (1934) (Figure 8). The formation consists of andesite, agglomerate and volcanic breccia at the bottom, and red colored sandstone and shale intercalation, andesite towards the top (Kellogg, 1960c; Schmidt, 1964; Ala and Moss, 1979; Güven et al., 1991; Bozdoğan et al., 1994; Yılmaz and Duran, 1997; Göncüoğlu and Kozlu, 2000).

The Precambrian aged Telbesmi Formation is unconformably overlain by the Early Cambrian aged Sadan Formation (Figure 8) which belongs to the Derik Group (Çoruh et al., 1997; Yılmaz and Duran, 1997). The type locality of Sadan Formation is 1 km west of Sadan village, located Derik district of Mardin city. The formation was firstly defined as a level within “Telbesmi Series” by Moses (1934) (Figure 8). Cobb (1957a) used the name of Sadan for the interval first. The formation consists of brick red, pink, wine colored sandstone, pink, wine colored quartzite and red colored shale-siltstone intercalation (Ala and Moss, 1979; Perinçek et al., 1991; Güven et al., 1991; Bozdoğan, 1994; Yılmaz and Duran, 1997).

The Sadan Formation is conformably topped by the Middle Cambrian aged Koruk Formation (Figure 8) which is the member of the Derik Group (Çoruh et al., 1997; Yılmaz and Duran, 1997). The type locality of Koruk Formation is near Koruk village, located 40 km west of Mardin city. The Koruk Formation was firstly described as a level “Telbesmi Series” by Moses (1934). The name of Koruk Formation for the interval was used for the first time by Ketin (1964). The formation is composed of the intercalation of white, light gray colored dolomite and gray colored limestone (Köylüoğlu, 1986; Perinçek et al., 1991; Bozdoğan et al., 1995; Yılmaz and Duran, 1997).

The Koruk Formation conformably underlies the Middle to Late Cambrian aged Sosink Formation (Figure 8) which is the youngest member of the Derik Group (Yılmaz and Duran, 1997; Çoruh et al., 1997). The type locality of Sosink Formation is Koruk valley north of Sosink village, located Derik district of Mardin city. The formation was firstly described as a level within “Telbesmi Series” by Moses (1934) (Figure 8). The name of Sosink Formation for the interval was first used by Cobb (1957a). The formation is composed of gray colored sandstone; gray, greenish gray colored siltstone and greenish gray colored shale at the bottom and reddish brown, beige, dirty green colored sandstone at the top (Ala and Moss, 1979; Tardu et al., 1990; Güven et al., 1991; Bozdoğan et al., 1994; Yılmaz and Duran, 1997).

The Sosink Formation unconformably underlies the Early Ordovician aged Seydişehir Formation which is the oldest member of Habur Group (Yılmaz and Duran 1997; Çoruh et al., 1997). The type locality of Seydişehir Formation is near Seydişehir village of Konya city. This formation was firstly described as “Seydişehir-Schiefer” by Blumenthal (1947) (Figure 8). The formation starts with yellow, greenish colored sandstone; olive green, dark gray colored siltstone and pink, white colored quartzite intercalation at the bottom, and grades to yellow, dirty yellow colored sandstone, yellowish gray sandstone, yellowish gray, green colored shale and brownish gray colored siltstone intercalation towards the top (Tardu et al., 1990; Perinçek et al., 1991; Bozdoğan, 1994; Yılmaz and Duran, 1997).

The Seydişehir Formation is unconformably topped by the Middle-Late Ordovician aged Bedinan Formation (Figure 8) which belongs to the Habur Group (Güven et al., 1991; Perinçek et al., 1991; Bozdoğan et al., 1994; Steemans et al., 1996; Çoruh et al., 1997; Yılmaz and Duran, 1997; Oktay and Wellman, 2019). The type locality of Bedinan Formation is Bedinan village, located 20 km southeast of Derik district of Mardin city. The formation was firstly described as “Bedinan Formation” by Cobb (1957c). The formation starts with greenish gray, dark gray colored shale at the bottom and grades to light gray, yellowish gray colored sandstone and greenish gray shale intercalation towards the top (Kellogg, 1960c; Tuna, 1973; Ala and Moss, 1979;

Köylüođlu, 1986; Tardu et al., 1990; Bozdođan et al., 1987; Bozdođan et al., 1994; Yılmaz and Duran, 1997).

The Bedinan Formation is unconformably overlain by the Early Silurian to Early Devonian aged Dadaş Formation which is the member of the Diyarbakır Group (Çoruh et al., 1997; Yılmaz and Duran 1997; Oktay and Wellman, 2019). The type locality of Dadaş Formation is 2 km east of Dadaş village, located Hazro district of Diyarbakır city. The Dadaş Formation was firstly introduced as ‘‘Dadaş Formation’’ by Kellogg and Kayar (1959; in Kellogg, 1960a) (Figure 8). The formation starts with dark gray, brownish gray colored shale at the bottom, and grades to greenish gray, gray colored shale, gray colored limestone and brownish colored sandstone intercalation towards the top (Yılmaz and Duran, 1997).

The Dadaş Formation is conformably topped by the Early Devonian aged Hazro Formation which belongs to the Diyarbakır Group (Yılmaz and Duran, 1997; Çoruh et al., 1997). The type locality of Hazro Formation is 6 km east of Hazro district of Diyarbakır city. The Hazro Formation was firstly described as ‘‘Hazro sandstone member’’ by Kellogg and Kayar (1959; in Kellogg, 1960a) (Figure 8). The formation starts with dark gray, gray colored sandstone, bluish green colored siltstone and gray, greenish colored marl intercalation, and grades to yellowish beige colored dolomitic limestone and greenish red, red colored marl towards the top (Kellogg, 1960a; Tardu et al., 1990; Perinçek et al., 1991; Güven et al., 1991; Bozdođan et al., 1992; Topdemir, 1992; Yılmaz and Duran, 1997).

The Hazro Formation unconformably underlies the Late Permian aged Gomanibrik Formation which is the member of the Tanin Group (Bozdođan et al., 1987; Perinçek, 1990; Güven et al., 1991; Perinçek et al., 1991; Bozdođan et al., 1994; Yılmaz and Duran, 1997; Çoruh et al., 1997). The type locality of Gomanibrik Formation is gomanibrik village, located 1 km northeast of Hazro district of Diyarbakır city. The Gomanibrik Formation was firstly described as ‘‘Inbrik Formation’’ by Kellogg and Kayar (1959; in Kellogg, 1960a). After Schmidt (1964), the name of Gomanibrik

Formation was used for the interval (Figure 8). The formation starts with dark gray, gray colored, fossiliferous limestones at the bottom and grades to gray colored shale with coal levels and dark gray, black colored clayey limestone levels towards the top (Tardu et al., 1990; Yılmaz and Duran, 1997).

The Gomaniibrik Formation is unconformably overlain by the Early Triassic aged Uludere Formation which is the only representative of the Çığılı Group in the study area (Yılmaz and Duran, 1997; Çoruh et al., 1997). The type locality of Uludere Formation is near Uludere district of Şırnak city. The formation was firstly described as lower levels of “Goyan Formation” by Maxson (1937) (Figure 9). The Uludere Formation consists of purplish red, greenish gray colored shale, and gray, yellow colored limestone intercalation (Perinçek et al., 1991; Güven et al., 1991; Yılmaz and Duran, 1997).

The Uludere Formation is unconformably overlain by the Aptian-Albian aged Areban Formation which is the oldest member of the Mardin Group (Güven et al., 1991; Yılmaz and Duran, 1997; Çoruh et al., 1997). The type locality of Areban Formation is Areban village, situated 16 km southeast of Derik district of Mardin city. The formation was firstly described as ‘Varicolored shale/sandstone member’ within Sabunsuyu Formation by Wilson and Krummenacher (1959). Schmidt (1961) first used the name of Areban Formation for the interval (Figure 9). The Areban Formation is composed of whitish yellow, bluish green, dark yellow colored sandstone and marl intercalations (Güven et al., 1991; Perinçek et al., 1991; Yılmaz and Duran, 1997; Çoruh et al., 1997).

The Areban Formation is conformably overlain by the Albian to Cenomanian aged Sabunsuyu Formation (Figure 9) which belongs to the Mardin Group (Tuna, 1973; Perinçek et al., 1991; Güven et al., 1991; Yılmaz and Duran, 1997; Çoruh et al., 1997). The type locality of Sabunsuyu Formation is Sabunsuyu valley, located east of Kilis city. The formation was firstly described as the lower member of “Mardin limestone formation” by Krausert and Temple (1957). Wilson and Krummenacher (1959) first

used “Sabunsuyu Formation” name for the interval (Figure 9). The Sabunsuyu Formation starts with gray, beige colored dolomite with greenish white colored marl, and continues with gray, light gray colored, thickly bedded dolomite towards the top (Perinçek et al., 1991; Güven et al., 1991; Yılmaz and Duran, 1997).

The Sabunsuyu Formation is unconformably topped by the Cenomanian aged Derdere Formation (Figure 9) which belongs to the Mardin Group (Şengündüz et al., 1990; Güven et al., 1991; Perinçek et al. 1991; Karabulut et al., 1992; Cater and Gillcrist, 1994; Coşkun, 1996; Yılmaz and Duran, 1997; Çoruh et al., 1997; Demirel and Guneri, 2000). The type locality of Derdere Formation is Derdere village, located in Çüngüş district of Diyarbakır city. Handfield et al. (1959) was firstly described the “Derdere Formation” with the name of Derdere (Figure 9). The formation consists of dark gray, brown colored dolomite at the bottom and white colored limestone towards the top (Perinçek, 1990; Güven et al., 1991; Cater and Gillcrist, 1994; Yılmaz and Duran, 1997).

The Derdere Formation unconformably underlies the Late Coniasian to Early Campanian aged Karababa Formation (Figure 9) which belongs to the Mardin Group (Perinçek, 1980; Köylüoğlu, 1988; Perinçek, 1990; Perinçek, 1991; Güven et al., 1991; Yılmaz and Duran, 1997; Demirel and Guneri, 2000). The type locality of Karababa Formation is the southern side of Karababa Mountain, located 32 km south of Adıyaman city. This formation was firstly described by Gossage (1956) as “Karababa limestone” (Figure 9). The formation starts with gray, dark gray, brown colored, clayey, organic-rich limestone with marl interbeds and grades to beige colored, cherty thickly bedded limestone and beige colored thinly-moderately bedded limestone towards the top (Güven et al., 1991; Coşkun, 1996; Yılmaz and Duran, 1997; Demirel and Guneri, 2000).

The Karababa Formation is unconformably overlain by the Middle to Late Campanian aged Beloka Formation (Figure 10) which belongs to the Adıyaman Group (Yılmaz and Duran, 1997; Çoruh et al., 1997). The type locality of Beloka Formation is Beloka

village, located east of Derik district of Mardin city. The interval corresponding to the Beloka Formation was firstly described as a unit within “Massive limestone” by Ten Dam (1954). Schmidt (1964) first used the name of Beloka for the interval as “Beloka limestone/dolomite formation” (Figure 10). The Beloka Formation starts with glauconitic and clayey limestone, and grades to bioclastic limestone towards the top (Schmidt, 1964; Köylüoğlu, 1986; Güven et al., 1991; Yılmaz and Duran, 1997).

This formation is unconformably topped by the Middle Maastrichtian aged Garzan Formation carbonates (Figure 10) (Araç et al., 1990; Güven et al., 1991, Yılmaz and Duran, 1997; Çoruh et al., 1997). The formation belongs to the Şırnak Group (Güven et al., 1991; Yılmaz and Duran, 1997; Çoruh et al., 1997). The type locality of Garzan Formation is the wells drilled Garzan oil field, located east of Batman city. The stratigraphic interval corresponding to the Garzan formation was firstly described as a unit within “Lower Maastrichtian-Campanian” beds by Ten Dam (1953). The name of Garzan was firstly used for the interval from the wells in the Garzan oil field by Kellogg (1960a) (Figure 10). The formation starts with dark beige, beige colored, crystalline limestone at the bottom and grades cream, whitish cream colored limestone towards the top (Kellogg, 1960a; Schmidt 1964; Köylüoğlu, 1986; Güven et al., 1991; Perinçek et al., 1991; Yılmaz and Duran, 1997).

The Middle Maastrichtian to Late Paleocene aged Germav Formation conformably overlies the Garzan Formation (Araç et al., 1990; Güven et al., 1991, Yılmaz and Duran, 1997; Çoruh et al., 1997). The type locality of Germav Formation is Germav village, located 40 km east of Gercüş district of Batman city. This formation was firstly described by Maxson (1936) as “Kermav Formation” in Hermis anticline (Figure 10). The equivalent level of the formation was defined as “greenish shales” by Mason (1930). This formation is pervasive throughout Southeastern Turkey.

Age	Kellogg 1960a,c	Schmidt 1964a	Rigo de Righi and Cortesini 1964	Tuna 1973	Ala and Moss 1979	Köylüoğlu 1986	Perinçek et al. 1991	Bozdoğan et al. 1994	Güven et al. 1991	Yılmaz and Duran 1997
Paleozoic	Late Permian	Inbirik Formation	Inbirik Formation		Inbirik Formation	Gomanibrik Formation	Gomanibrik Formation	Gomanibrik Formation	Gomanibrik Formation	Gomanibrik Formation
	Early Devonian	Eskar Formation	Hazro Formation Lower Levels			Hazro Formation Lower Levels	Hazro Formation	Hazro Formation	Hazro Formation	Hazro Formation
Paleozoic	Silurian	Dadaş Formation	Handof Formation	Bedinan Formation	Handof Formation	Dadaş Formation	Dadaş Formation	Dadaş Formation	Dadaş Formation	Dadaş Formation
	Ordovician	Bedinan Formation	Bedinan Formation + Ordovician-Devonian	Bedinan Formation	Bedinan Formation	Bedinan Formation	Bedinan Formation	Bedinan Formation	Bedinan Formation	Bedinan Formation
Paleozoic		Sosink Formation	Sosink Formation Sandstone/Shale Member	Sosink Formation	Sosink Formation	Sosink Formation	Sosink Formation	Sosink Formation	Sosink Formation	Sosink Formation
	Cambrian	Sadan Dolomites	Sosink Limestone/Dolomite Formation	Koruk Limestone Formation	Sosink Formation Lower Levels	Koruk Formation	Koruk Formation	Koruk Formation	Koruk Formation	Koruk Formation
Paleozoic		Telbesmi Formation	Sadan Formation + Sosink Formation Sandstone Member	Zabuk Formation	Sadan Formation	Sadan Formation + Zabuk Formation	Sadan Formation	Sadan Formation	Sadan Formation	Sadan Formation
	Precambrian	Derik Volcanics	Derik Formation	Sadan Formation	Derik Formation	Telbesmi Formation	Telbesmi Formation	Telbesmi Formation	Telbesmi Formation	Telbesmi Formation

Figure 8: Correlation chart of the Precambrian to the Permian formations from the previous studies. In this study, the formation names, their groups and ages were adapted from Yılmaz and Duran (1997) and Çoruh et al. (1997).

The Germav Formation starts with bluish gray, gray colored, clayey limestone levels and gray colored marl and grades to gray to dark gray colored shale, greenish gray sandstone and green, gray colored marl intercalations (Kellogg, 1960a; Schmidt, 1964; Tuna, 1973; Köylüoğlu, 1986; Perinçek, 1990; Güven et al., 1991; Yılmaz and Duran, 1997).

The Germav Formation is conformably overlain by the Late Maastrichtian to Middle Paleocene aged Sinan Formation (Figure 10) which is the member of Şırnak Group (Güven et al., 1991; Yılmaz and Duran, 1997; Çoruh et al., 1997). The type locality of Sinan Formation is Sinan-1 exploration well, located 20 km northwest of Batman city. The Sinan Formation was firstly introduced by Blakslee et al. (1960) as “Sinan reef” (Figure 10). The formation is composed of thin laminated light beige colored dolomite with white colored anhydrite and gypsum interbeds at the bottom, and light gray, beige colored dolomite towards the top of the formation (Schmidt, 1964; Köylüoğlu, 1986; Yılmaz and Duran, 1997).

The Sinan Formation is conformably topped by the Late Paleocene aged Becirman Formation (Çoruh et al., 1997; Yılmaz and Duran, 1997) which belongs to the Şırnak Group (Figure 10). The type locality of Becirman Formation is Becirman village which is located 20 km northeast of Gercüş district of Batman city. The formation is firstly defined by Schmidt (1935) as “Mardin top limestones”. Maxson (1936) used the name of “Bicirman limestone” for the interval (Figure 10) first. The formation starts with cream colored, clayey limestone at the bottom and grayish white colored marl and greenish gray shale towards the top of formation (Tuna 1973; Güven et al., 1991; Perinçek, 1991; Yılmaz and Duran, 1997).

This formation conformably underlies the Gercüş Formation (Figure 10) which is the oldest member of Midyat Group (Duran et al., 1988; Çoruh et al., 1997; Yılmaz and Duran, 1997). The type locality of the formation is Hermis basin, located close to Gercüş district of Batman city. The formation was firstly defined by Mason (1930) as “Red beds”. Maxson (1936) used the name of Gercüş Formation for the first time

(Figure 10). The formation includes brick red, green colored shale and marl; gray colored sandstone, grayish white colored limestone and pink, light green colored conglomerates (Kellogg, 1960a; Schmidt, 1964; Duran et al., 1988; Perinçek, 1990; Güven et al., 1991; Perinçek et al., 1991; Yılmaz and Duran, 1997).

The Gercüş Formation is unconformably overlain by the Early Eocene to Early Oligocene aged Hoya Formation (Duran et al., 1988; Yılmaz and Duran, 1997; Çoruh et al., 1997) which is member of Midyat Group (Güven et al., 1991, Yılmaz and Duran, 1997; Çoruh et al., 1997). The type locality of the formation is the Hoya village located 2 km southwest of Gercüş district of Diyarbakır city. It is firstly defined as “Nummulites limestone” by Taşman (1930). Perinçek (1978) first used the name of “Hoya Formation” as a member of Midyat Group (Figure 10). The formation starts with thickly bedded, beige colored limestone and grades into light gray colored, chalky dolomite towards the top (Duran et al., 1988; Perinçek, 1990; Yılmaz and Duran, 1997).

The Hoya Formation conformably underlies the Middle Eocene to Oligocene aged Germik Formation (Figure 10) which is the member of Midyat Grup (Duran et al., 1988; Güven et al., 1991; Yılmaz and Duran, 1997; Çoruh et al., 1997). The Germik Formation was firstly described by Bolgi (1961) as “Germik Formation” (Figure 10). The formation consists of beige to gray colored dolomite, reddish brown colored shale and white colored gypsum (Duran et al., 1988; Perinçek et al., 1991; Güven et al., 1991; Yılmaz and Duran, 1997).

The Germik Formation is unconformably topped by the Late Miocene to Early Pliocene aged Şelmo Formation (Yılmaz and Duran, 1997; Çoruh et al., 1997). The type locality of Şelmo Formation is Şelmo village, located southwestern of Sason district of Batman city. The formation is firstly defined by Gossage (1956) as “Adıyaman gravel group”. Bolgi (1961) first used the Şelmo Formation name for the interval (Figure 10). The Şelmo Formation consists of reddish to greenish gray colored siltstone and shale with gypsum intercalation at the bottom and greenish gray, green, reddish brown colored siltstone and sandstone towards the top of the formation (Schmidt, 1964; Ala and Moss, 1979; Perinçek, 1990; Güven et al., 1991; Perinçek et al., 1991; Yılmaz and Duran, 1997; Nazik et al., 2013).

In this study, the formation names, their ages and the group names were complied with the studies Yılmaz and Duran (1997) and Çoruh et al. (1997) which are the latest revised ones.

2.1. Stratigraphy

The stratigraphy of the studied area is lightened with regard to the studied wells data, the surface geology maps and relevant published papers. The N-S geological cross section from Diyarbakır Basin were compiled according to the subsurface borehole data and surface geology maps (Figure 11) to delineate vertical and horizontal variation of the stratigraphy of the area. With regard to borehole and outcrop data, nine stratigraphic groups and 1 Formation are distinguished; namely, in ascending order, Derik Group, Habur Group, Diyarbakır Group, Tanin Group, Çığlı Group, Mardin Group, Şırnak Group, Midyat Group and Şelmo Formation. The detailed description of the sedimentary sequences existing in the study area are explained in the following chapters (Figure 12).

2.1.1. Derik Group (Precambrian-Cambrian)

The formations which belong to Derik Group in the study area are Telbesmi Formation, Sadan Formation, Koruk Formation and Sosink Formation respectively.

Telbesmi Formation giving outcrop in Amanos Mountains, Adıyaman-Gölbaşı and Mardin-Derik area, consists of predominantly volcano sedimentary units such as submarine lavas, red green colored andesite, pillow lavas, spilitic andesite, agglomerate, tuff, shale and sandstone levels (Goncuoglu and Kozlu, 2000; Bozdogan et al., 1994; Yılmaz and Duran, 1997; Tardu et al., 1987). The presence of pillow lava and coastal sandstone and siltstone units within Telbesmi Formation is the indicator of shallow marine environment during the Precambrian time for SE Turkey (Goncuoglu and Kozlu, 2000; Yılmaz and Duran, 1997; Çoruh et al., 1997). The effect of volcanism decrease towards the western side (Adıyaman, Amanos Mountains); therefore, lithologic differences can be seen region to region (Bozdogan et al., 1994, Yılmaz and Duran, 1997). The age of upper sandstone levels of Telbesmi Formation rich in Trilobite fossils and lower volcano sedimentary units was evaluated as

Precambrian (Çoruh et al., 1997; Yılmaz and Duran, 1997). The Early Cambrian aged Sadan Formation unconformably overlies Telbesmi

Formation (Figure 12) (Bozdogan et al., 1994; Tardu et al., 1987; Bozdoğan et al., 1995, Yılmaz and Duran, 1997; Çoruh et al., 1997). The Early Cambrian aged Sadan Formation consisting of predominantly gray-red shales and cross bedded quartzite sandstone levels, deposited under the condition of fluvio-deltaic environment. Based on paleocurrent analyses of Sadan Formation clastic levels, sediment influx was supplied from southern positive area (Bozdogan et al., 1995; Yılmaz and Duran, 1997). The Middle Cambrian aged Koruk Formation comprises the main key horizon for the Paleozoic interval. Dolomite and limestone lithology of Koruk Formation deposited under low energy condition of tidal flat environment which are conformably overlain by the Middle-Late Cambrian aged Sosink Formation having predominantly quartz arenite sandstone, iron-rich shale, siltstone and limestone intercalation (Figure 12) (Bozdogan et al., 1995; Yılmaz and Duran, 1997). The formation deposited in floodplain and wave-dominated environments (Yılmaz and Duran, 1997). The Sosink Formation is unconformably overlain by Seydişehir Formation which belongs to the Habur Group (Figure 12) (Çoruh et al., 1997; Yılmaz and Duran, 1997).

2.1.2. Habur Group (Ordovician)

The Ordovician aged units in ascending order Seydişehir Formation (Early Ordovician) and Bedinan Formation (Middle-Late Ordovician) are so-called Habur Group (Yılmaz and Duran, 1997; Çoruh et al., 1997; Paris et al., 2007; Oktay and Wellman, 2019). The Early Ordovician aged Seydişehir Formation deposited under low energy conditions of near-shore, deltaic environments (Bozdogan et al., 1995; Yılmaz and Duran, 1997), consists of predominantly sandstone, shale and siltstone. While the contact between Seydişehir and underlying Sosink Formation is conformable, the contact of Seydişehir Formation between overlying Bedinan Formation is unconformable and correlative conformable (Güven et al., 1991; Yılmaz and Duran,

1997; Çoruh et al., 1997; Paris et al., 2007). The Middle to Late Ordovician aged Bedinan Formation includes mostly sandstone, shale and siltstone lithologies. Depositional environment of Bedinan Formation is deep marine in the Middle Ordovician and near shore in the Late Ordovician (Bozdogan et al., 1995; Yılmaz and Duran, 1997; Haq and Al-Qahtani, 2005). It shows regressive character based on lithology (Bozdogan et al., 1995) and wireline log (GR, Sonic, Resistivite) responses. During the Late Ordovician time, Arabian Plate entered glaciation episode (Konert et al., 2001; Haq and Al-Qahtani, 2005; Munnecke et al., 2010). Glaciation affected especially western part of the Arabian Plate. Glacial deposits can be observed in the Late Ordovician (Hirnantian) aged units of the western Arabian Plate such as Halevikdere Formation in Taurus region and Mardin-Derik area in Turkey (Monod et al., 2003; Paris et al., 2007; Gienne et al., 2010; Öztürk et al., 2016). However, the uppermost sandstone levels of the Bedinan Formation, instead of glacier deposits, can be easily correlated by using wireline log responses throughout the study area. The Late Ordovician (Hirnantian) short-term climatic trend and its effect on the depositional sequences of the uppermost Bedinan Formation are discussed in detail in the Paleogeography chapter.

2.1.3. Diyarbakır Group (Silurian-Devonian)

In the study area, Diyarbakır group is represented by the lower Silurian – the lower Devonian depositional sequences, Dadaş Formation and Hazro Formation respectively (Yılmaz and Duran, 1997; Çoruh et al., 1997; Oktay and Wellman, 2019). The Early Silurian (Llandovery) to Early Devonian (Lochkovian) aged Dadaş Formation unconformably overlies the Ordovician aged Bedinan Formation and underlies conformably the lower Devonian aged Hazro Formation (Çoruh et al., 1997; Oktay and Wellman, 2019). The Dadaş Formation including shoaling upward depositional sequences in response to relative sea level fall, consists of predominantly gray, dark gray, brownish, dark green colored, organic rich, silty shale with thin sandy

micritic limestone and brownish to beige colored sandstone lithology (Bozdoğan et al., 1987; Bozdoğan et al., 1994; Bozdoğan et al., 1995; Yılmaz and Duran, 1997). The Dadaş Formation is succeeded conformably by the Early Devonian (Lockhovian-Emsian) aged Hazro Formation with the lithology from bottom to top; beige, dark gray cross bedded sandstone, gray, brick red, green colored silty marl and shale, beige to yellowish beige colored tight dolomite, dark beige, brick red, green colored marl (Bozdoğan et al., 1987, Bozdoğan et al., 1995). Tidal flat, deltaic and lagoonal depositional environments are inferred for Hazro Formation (Topdemir, 1992; Yılmaz and Duran, 1997).

2.1.4. Tanin Group (Late Permian)

In Southeastern Turkey, the Late Permian aged sedimentary sequences are so-called Tanin Group (Bozdoğan et al., 1987; Bozdoğan et al., 1994; Bozdoğan et al., 1995; Yılmaz and Duran, 1997). The unique representative of Tanin group in the study area is the Late Permian aged Gomanibrik Formation which thickens from west to east and also is characterised by alternation of extensive successions such as alternation of gray to dark gray colored, sandy fossiliferous, shallow marine limestones with gray colored terrestrial and deltaic coaly shale and reddish yellow colored sandstone (Bozdoğan et al., 1987; Bozdoğan et al., 1994; Bozdoğan et al., 1995; Yılmaz and Duran, 1997). While the boundary between Late Permian aged Gomanibrik Formation and overlying Triassic aged Çığlı Group depositional sequences is concordant in Hakkari Area, it becomes discordant in the study area (Bozdoğan et al., 1995). The lower boundary of the unit is also discordant in response to Hercynian orogenesis which had been very effective on Arabian Plate from Late Devonian to Early Permian (Konert et al., 2001, Haq and Al-Qahtani, 2005).

2.1.5. ıđlı Group (Early Triassic)

Terrestrial, shallow marine deposits (Perinek, 1990; Yılmaz and Duran, 1997), Uludere Formation is representative for ıđlı Group in the study area. The Early Triassic aged Uludere Formation (Yılmaz and Duran, 1997; oruh et al., 1997) consists of predominantly green, red colored, sandy, partly silty shales and marls, and green to purple colored, sandy limestone lithologies. Both upper and lower boundaries of Uludere Formation with Cretaceous Mardin Group and Late Permian aged Gomaniiirik Formation respectively are discordant (Yılmaz and Duran, 1997).

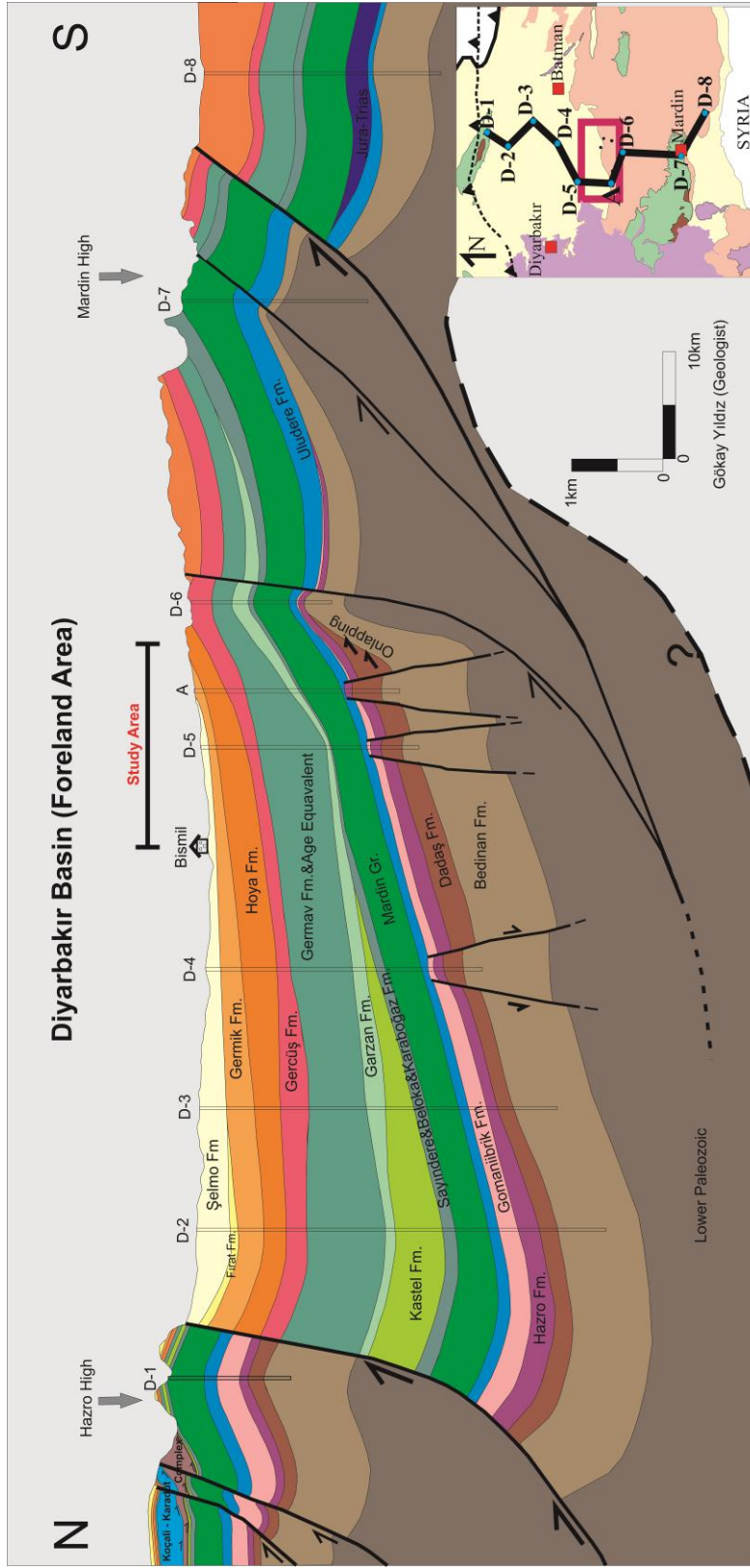


Figure 11: North-South geological cross section from Hazro high to Mardin high passing on D-1, D-2, D-3, D-4, D-5, A, D-6, D-7 and D-8 wells. The wells data, surface geology map (1/500.000 scaled) and topography profile (Google Earth) were used for revealing the cross section. The well data from Çalık Petrol Arama Üretim San. Tic. A.Ş. database.

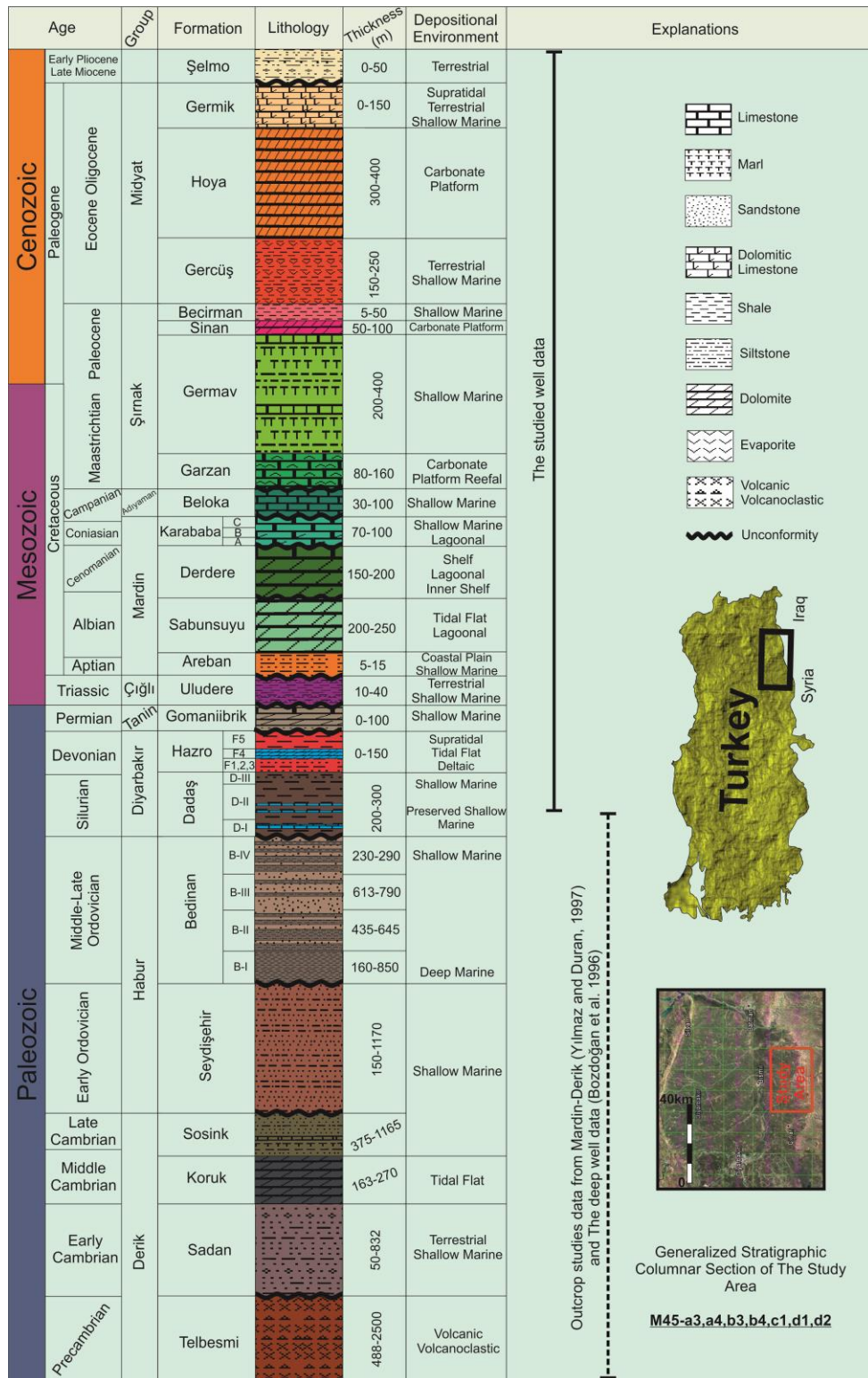


Figure 12: Generalized stratigraphic columnar section of the study area (modified from Yılmaz and Duran (1997)).

2.1.6. Mardin Group (Aptian-Campanian)

Mardin Group carbonates occupy a very extensive area in Southeastern Turkey. Based on sedimentological character, wireline log responses, Mardin Group can be divided into four members, namely in ascending order; Areban Formation, Sabunsuyu Formation, Derdere Formation and Karababa Formation (Coşkun, 1996; Yılmaz and Duran, 1997). The oldest unit of the Mardin Group, the Aptian aged Areban Formation deposited in tidal flat and shallow marine environment which consists of whitish yellow colored sandstone, green shale and argillaceous limestone (Karabulut et al., 1992). The Areban Formation constitutes the base member of Mardin Group and unconformably overlies the Early Triassic aged Uludere Formation in the study area. The unit grades conformably to tidal flat to supratidal carbonates of Sabunsuyu Formation (Karabulut et al., 1992; Demirel and Guneri, 2000). The Albian to Cenomanian aged (Karabulut et al., 1992) Sabunsuyu Formation includes predominantly light gray, brownish gray colored, recrystallized dolostones (Coşkun, 1996, Yılmaz and Duran, 1997). The top of Sabunsuyu Formation is erosional and graded unconformably to Cenomanian aged Derdere Formation. The unit formed in response to transgression during Cenomanian is shoaling upward in character (Karabulut et al., 1992; Demirel and Guneri, 2000). The bottom level of the unit consists of organic rich wackestone to packstone; the upper part of Derdere Formation includes predominantly argillaceous limestone and dolostone (Perinçek, 1990; Cater and Gillcrist, 1994; Coşkun, 1996, Karabulut et al., 1992; Demirel and Guneri, 2000; Şengündüz and Soylu, 1990). The Derdere Formation is overlain by the Late Coniasian to Early Campanian aged Karababa Formation (Köylüoğlu, 1988; Güven et al., 1991; Cater and Gillcrist, 1994; Yılmaz and Duran, 1997; Demirel and Guneri, 2000). Beige to gray colored limestone and dolomitic limestone are the main lithology of Karababa Formation (Yılmaz and Duran, 1997) The lower part of the unit is deposited in deep marine condition. The upper part of the unit is deposited in shallow marine and lagoonal depositional environments (Demirel and Guneri, 2000).

2.1.7. Adıyaman Group (Campanian)

Adıyaman Group represented by the Middle to Late Campanian aged Beloka Formation in the study area. The unit has cream to beige colored, moderate-thick bedded fossiliferous limestone with chert lithology. The Beloka Formation deposited under the control of shallow marine, slope and deep marine environment. The top and bottom boundary of Beloka Formation with the Middle Maastrichtian aged Garzan Formation and Mardin Group respectively in the study area are discordant (Figure 12) (Köylüoğlu, 1988; Perinçek, 1990; Güven et al., 1991; Yılmaz and Duran, 1997).

2.1.8. Şırnak Group (Campanian-Paleocene)

Şırnak Group consists of Garzan Formation, Germav Formation, Sinan Formation and Becirman Formation respectively. Şırnak Group unconformably overlies Adıyaman Group and is overlain by Midyat Group. The Garzan Formation deposited under the control of shallow marine, reefal and shelf edge depositional environments, and comprises cream to white colored, soft, crystalline, partly chalky limestone. The Germav Formation conformably overlies the Garzan Formation (Araç et al., 1990, Yılmaz and Duran, 1997 Çoruh et al., 1997). The unit comprises predominantly dark gray to bluish gray colored shale with marl interbeds (Yılmaz and Duran, 1997). The Late Maastrichtian to Paleocene aged Germav Formation deposited under the control of deep marine and slope (Yılmaz and Duran, 1997). The Late Maastrichtian to middle Paleocene aged Sinan Formation consists of light brownish colored, sucrosic texture, porous dolomite and dolomitic limestone, gray to dark gray colored, silty, slightly calcareous shale and evaporitic levels (Güven et al., 1991; Yılmaz and Duran, 1997). This unit rests conformably on the Germav Formation shale levels (Yılmaz and Duran, 1997; Çoruh et al., 1997). The Sinan Formation is conformably overlain by the Late Paleocene aged Becirman Formation comprising an alternation of pinkish white to beige colored, hard, fairly porous, partly clayey limestone, and green to gray colored, hard shale with a thin cream to gray colored

marl interbeds (Yılmaz and Duran, 1997). The unit is deposited in restricted shallow marine, and conformably overlain by the Gercüş Formation (Yılmaz and Duran, 1997; Çoruh et al., 1997).

2.1.9. Midyat Group (Eocene-Oligocene)

Midyat Group refers to Eocene to Oligocene aged sedimentary sequences of Gercüş Formation, Hoya Formation and Germik Formation in study area. The Early Eocene aged Gercüş Formation rests conformably on Şırnak Group deposits. The unit is composed of terrestrial, fluvial and lagoonal deposits (Çoruh et al., 1997; Yılmaz and Duran, 1997). Gercüş Formation consists of brick to green colored, soft, shale with marl and evaporates (Güven et al., 1991; Yılmaz and Duran, 1997). The Gercüş Formation is conformably covered by the Eocene to Oligocene aged Hoya Formation. The Hoya Formation is composed of white to beige colored, fossiliferous, hard, partly chalky limestone with dolomite and dolomitic limestone (Duran et al., 1988; Perinçek, 1990; Yılmaz and Duran, 1997). Restricted to semi-restricted shallow marine units of Hoya Formation are conformably overlain by the Oligocene aged Germik Formation including evaporitic, shallow marine and regressive sedimentary sequences (Duran et al., 1988; Güven et al., 1991; Yılmaz and Duran, 1997). The Germik Formation consists of the alternation of red colored shales, white colored gypsums and light beige colored dolomites and limestones (Duran et al., 1988; Yılmaz and Duran, 1997).

2.1.10. Şelmo Formation (Late Miocene- Early Pliocene)

The Şelmo Formation includes diverse depositional environments ranging from terrestrial to marine environments such as fluvial, tidal flat and beach environment (Perinçek, 1990; Güven et al., 1991; Yılmaz and Duran, 1997; Nazik et al., 2013). The Late Miocene to Early Pliocene aged Şelmo Formation unconformably overlies the Midyat Group (Yılmaz and Duran, 1997; Çoruh et al., 1997). The unit is composed of

the alternations of green, yellowish colored sandstone, gray colored shale at the bottom greenish gray colored conglomerate towards the top (Yılmaz and Duran, 1997).

CHAPTER 3

LITHOSTRATIGRAPHY

The Bedinan Formation is extensive throughout southeastern Turkey, also co-exists with the Sarah and Qasim Formations in Saudi Arabia and Bahrain, the Khabour Formation in Iraq, the Affendi and Swab Formations in Syria, the Memouniat, Melez Shuqran and Hawaz Formations in Libya, the Tamadjert and Tahouite Formations in Algeria, the Bani and Ktaoua Formations in Morocco, the Ammar, Risha, Tubeiliyat, Dubeidib and Hiswah Formations in Jordan, the Dargaz and the Seyahou Formations in Iran, the Ghudun and the Hasirah and Saih Nihayda Formations in Oman (Figure 13) (Çoruh et al., 1997; Alsharhan and Nairn, 1997; Le Heron and Howard, 2010; Ghienne et al., 2010; Le Hérissé et al., 2015; Craigie et al., 2016; Saberi et al., 2016; Oktay and Wellman, 2019). The Bedinan Formation exposes to surface in Mardin-Derik, Hakkari and Amanous mountain range areas (Bozdoğan et al., 1996; Yılmaz and Duran, 1997; Çoruh et al., 1997; Paris et al., 2007; Giennie et al., 2010). The age of the Bedinan Formation is assigned as the Middle (Late Darriwilian) – Late Ordovician (Hirnantian) (Figure 14) according to the previous studies by using macrofaunas (trilobites, brachiopods, graptolites) and palynological investigations (Chitinozoans and acritarchs) (Stemans et al., 1996, Bozdoğan et al., 1994; Çoruh et al., 1997; Yılmaz and Duran, 1997; Paris et al., 2007; Oktay and Wellman, 2019). The Bedinan Formation is informally divided into four members (Figure 15), namely Bedinan I, Bedinan II, Bedinan III and Bedinan IV, by the use of lithology, stratigraphy and wireline log data (Bozdoğan et al., 1994). A few wells (Güney Sarık-1, Ceylanpınar-1) penetrate the all members of the Bedinan Formation (Bozdoğan et al., 1994; Stemans et al., 1996; Yılmaz and Duran, 1997; Paris et al., 2007; Ghienne et al., 2010). The maximum thickness (1683 m) of the Bedinan Formation is measured in Ceylanpınar-1 well.

Period	Stage & Series	Saudi Arabia	Iran (Zagros)	Iraq	SE. Turkey (Diyarbakir Basin)	Morocco	Syria	Algeria	Libya	Jordan	Oman	
SILURIAN	PRIDOLI	Tawil Fm.				Iriqui Fm.						
	WENLOCK/LUDLOW	Ludfordian							Oued Tifermine Fm.		Kish Sha Fm.	
		Gorstian										
		Homerian										
		Sheinwoodian										
	LLANDOVERY	Telychian	Qalibah Group Qusaiba Fm.	Sarchahan Fm.	Akkas Fm.	Dadaş Fm.	Amsailikh Fm.	Tanf Fm.	Atafaitafa Fm.			Sahmah Fm.
		Aeronian							Oued Imirhou Fm.	Tanezzuft Fm.	Mudawwana Fm.	
		Rhuddanian										
			Uqlah Fm.									
	ORDOVICIAN	Hirnantian	Sarah Fm.	Dargaz Fm.			Ain Delioune Fm. Upper 2nd Bani Fm.		Tanadjert	Memouniat Fm.	Ammar Fm.	
UPPER		Katian									Tubeiliyat Fm.	Hasirah Fm.
		Sandbian	Qasim Fm.	Seyahou Fm.	Khabour Fm.	Bedinan Fm.	Lower 2nd Bani Fm.	Affendi Fm.	Tahouite Fm.	Melez Shuqran Fm.	Dubeidib Fm.	
MIDDLE		Darriwilian				Ktaoua Fm.	Swab Fm.		Hawaz Fm.	Hiswa Fm.	Saih Nihayda Fm.	

Figure 13: The compiled chronostratigraphic chart for the middle-upper Ordovician to Silurian units of Saudi Arabia, Iran (Zagros), Iraq, SE Turkey, Morocco, Syria, Algeria, Libya, Jordan and Oman, compiled from Çoruh et al., 1997; Alsharhan and Nairn, 1997; Le Heron and Howard, 2010; Ghienne et al., 2010; Le Hérisse et al., 2015; Craigie et al., 2016; Saberi et al., 2016; Oktay and Wellman, 2019.

634 m thick Bedinan Formation is measured in Mardin-Derik section from the surface (Yılmaz and Duran, 1997). The lower part of the Bedinan Formation is composed of fossiliferous, dark gray, black colored shales and greenish gray colored siltstones, followed by the intercalation of white, light gray, yellowish colored sandstones and greenish gray, gray colored shales towards the top (Bozdoğan et al., 1994; Bozdoğan et al., 1996; Yılmaz and Duran, 1997). The uppermost sandstone levels of the Bedinan Formation are considered as reservoir rock in which the studied wells (A, B, C, D, E, F) have been producing oil with minor gas. The sandstone levels in Bedinan III member have reservoir rock potential with regard to the porosity measurement in

Güney Sarık-1 well (Bozdoğan et al., 1994). The lower part (Bedinan I) of Bedinan Formation may have source rock potential due to the fact that the shelf is subjected to increased subsidence in accordance with the stratigraphic records of northeastern of Arabian Plate during the Middle Ordovician times that resulted in transgression in the area (Sharland et al., 2001; Haq and Al-Qahtani, 2005; Ghienne et al., 2010).

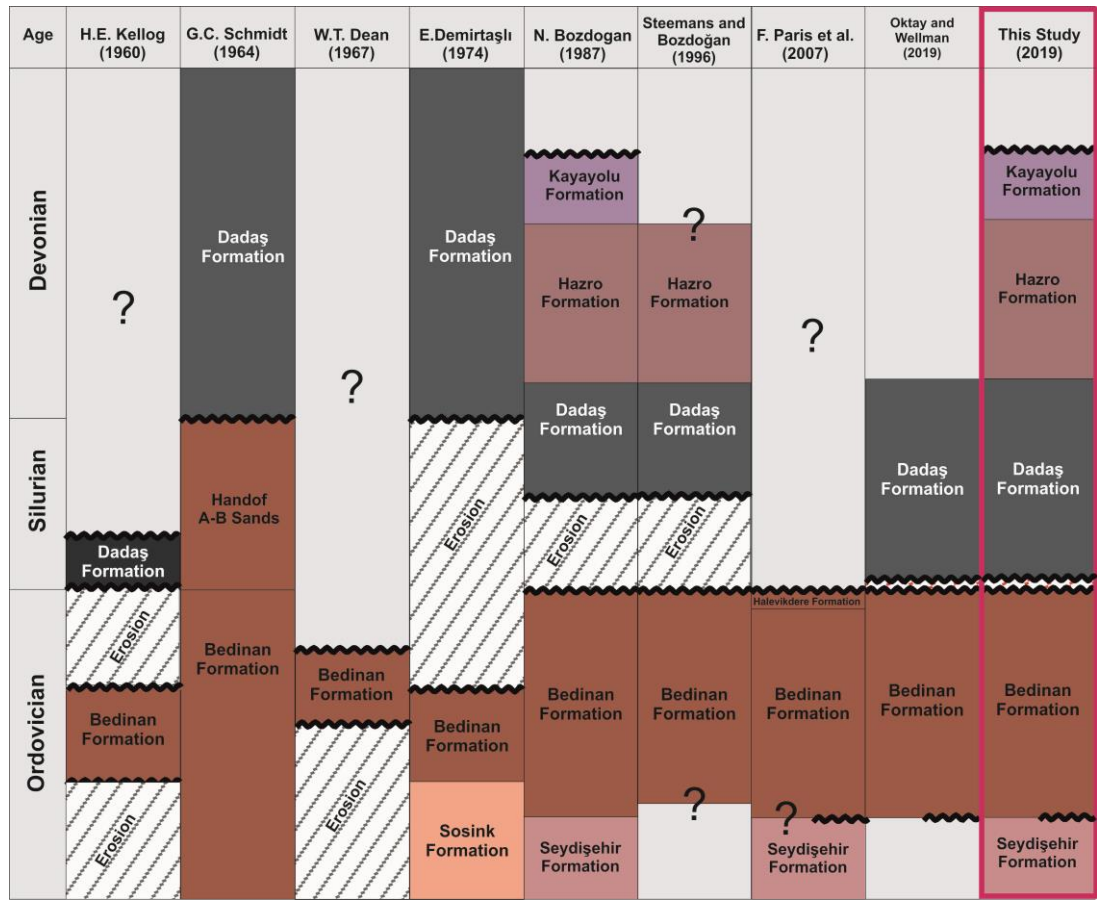


Figure 14: The compiled chronostratigraphic studies for the lower Paleozoic sequence of Diyarbakır Basin, Southeastern Turkey.

3.1. Bedinan Formation Members

3.1.1. Bedinan-I

The lowest member of Bedinan Formation is widely extensive throughout southeastern Turkey in the subsurface (Bozdoğan et al. 1994; Bozdoğan et al. 1996). The age of the Bedinan I member is assigned as the Middle Ordovician (Late Darriwilian) by the presence of the architarcs of *Priscogalea simplex* and *Veryhachium trisulcum* which are the key ones for the Late Darriwilian (Llanvirn), and defined in Akçakale-1, Raman-101/A, Kastel-1, Ceylanpınar-1, Girmeli-1, Hazro-101 and Güney Sarık-1 wells (Çoruh et al., 1997; Bozdoğan et al., 1994). The member is composed of dark gray, black colored, micaceous shales, and deposited in deep marine (Bozdoğan et al., 1994). The thickness of the lowest member of Bedinan Formation ranges from 160 to 850 meters in the subsurface (Bozdoğan et al., 1994). The Bedinan I member covers unconformably (Hakkari-Çukurca section) the Early Ordovician aged Seydişehir Formation (Kellogg, 1960b; Tardu et al., 1987; Bozdoğan et al., 1994; Güven et al., 1991; Yılmaz and Duran, 1997; Çoruh et al., 1997). During the Middle Ordovician times, Northeast Arabian Plate is tectonically unstable leading to the increased subsidence in the area (Sharland et al., 2001; Haq and Al-Qahtani, 2005; Ghienne et al., 2010). The subsidence led to deposition of transgressive strata such as Bedinan I member in SE Turkey. Therefore, the member can be taken into account as a potential source rock for the Paleozoic petroleum system of SE Turkey.

3.1.2. Bedinan-II

The Bedinan II member is extensively observed throughout SE Turkey in the subsurface (Bozdoğan et al., 1994; Bozdoğan et al., 1996). The age of the Bedinan II member is suggested as Late Darriwilian (Llandeilo) by considering some key architarcs species such as *Multilicisphaeridium digitatum*, *Peteinosphaeridium trifurcatum*, *Goniosphaeridium polygonale*, *Ordovicidum elegantulum* and *Aremoricanium rigandae* which are defined in Akçakale-1, Raman-101/A, Hazro-

2/A, Hazro-101, Gercüş-1, Bakük-1 and Güney Sarık-1 wells (Çoruh et al., 1997). The member starts with thin, beige colored shales and grades to gray, dark brownish colored siltstone with pyrite content and high amount of mica towards the top of the member (Bozdoğan et al., 1994). The thickness of the member ranges between 435-645 meters in the subsurface (Bozdoğan et al., 1994). The Bedinan II member deposited under low energy conditions of inner shelf, and is deepening towards the top (Bozdoğan et al., 1994).

3.1.3. Bedinan-III

The member is the most pervasive member of the Bedinan formation throughout SE Turkey (Bozdoğan et al., 1994; Bozdoğan et al., 1996). The Bedinan III member is the best studied interval of the Bedinan Formation not only in the subsurface but also on the surface (Amonous mountain range, Mardin-Derik), also it is the thickest interval of the Bedinan Formation (Bozdoğan et al., 1994). The thickness of the member ranges from 613 to 790 meters in subsurface according to the wells data such as 613 meters in Güney Sarık-1 well (Bozdoğan et al., 1994). The age of the Bedinan III member is envisaged as the Late Ordovician (Caradocian) by consideration of some key well preserved and diversified architarcs for the Caradocian time interval such as *Orthosphaeridium insculptum*, *Dactylofusa spinata*, *Aremoricanium syringosagis*, *Peteinosphaeridium trifurcatum* and *Multiplicisphaeridium bifurcatum* (Bozdoğan et al., 1994; Çoruh et al., 1997; Yılmaz and Duran, 1997). The Bedinan III member which is the shoaling upward sequence of strata consists of predominantly well sorted, fine grained, dolomite cemented and white colored sandstones with subarkose to quartz arenitic character and greenish gray, gray colored shales (Bozdoğan et al., 1994). The Bedinan III member is characterized by the shallow marine, the nearshore deposits (Bozdoğan et al., 1994). The member is the best reservoir level of the Bedinan Formation according to the reservoir quality analyses carried out in Güney Sarık-1 well (Bozdoğan et al., 1994).

3.1.4. Bedinan IV

The uppermost part of Bedinan Formation, so-called the Bedinan IV member, is not pervasive in SE Turkey due to tectonic instability during the Late Ordovician (Bozdoğan et al., 1994; Çoruh et al., 1997; Yılmaz and Duran, 1997). The thickness of the Bedinan IV member ranges between 230 and 290 meters according to the wells' data (Güney Sarıklı-1, Batı Azıklı-1) (Bozdoğan et al., 1994). The maximum thickness of the member is observed as 283 meters in Batı Azıklı-1 well (Bozdoğan et al., 1994). The time interval during which the member deposited is suggested as the Late Ordovician (Late Caradocian-Ashgillian) according to some key well preserved and diversified architarcs assemblages such as *Aremoricanium syringosagis*, *Rugulidium triangulatum*, *Veryhachium trisulcum*, *Multiplicisphaeridium bifurcatum* and *Goniosphaeridium connectum*, and well preserved and diversified organic-walled microfossils (chitinozoans) such as *Fungochitina fungiformis* Eisenack, *Acanthochitina barbata* Eisenack (Bozdoğan and Erten, 1990; Bozdoğan, 1992; Bozdoğan et al., 1994; Çoruh et al., 1997; Yılmaz and Duran, 1997; Paris et al., 2007; Ghienne et al., 2010). This member starts with the alternation of micaceous, non-calcerous, gray to brown colored siltstone and micaceous, subfissile, greenish gray, gray colored shales with pyrite content at the bottom, and grades to predominantly surrounded to rounded, well sorted, very fine to fine grained, off white colored sandstone with pyrite content and silty, micaceous, greenish gray, light gray colored shale and (the studied wells data; Bozdoğan et al., 1996; Paris et al., 2007; Ghienne et al., 2010). The Bedinan IV member is a shoaling upward sequence associated with climate induced regression (Bozdoğan and Erten, 1990; Bozdoğan et al., 1994; Bozdoğan et al., 1996; Lüning et al., 1999; Lüning et al., 2000; Monod et al., 2003; Herrmann et al., 2004; Guiraud et al., 2005; Turner et al., 2005; Haq and Al-Qahtani, 2005; Paris et al., 2007; Haq and Schutter, 2008; Ghienne et al., 2010; Munnecke et al., 2010; Le Heron and Howard, 2010; Torsvik and Cocks, 2013; Masri, 2017). The depositional environment of the Bedinan IV member is interpreted as tidal flat to

CHAPTER 4

SEDIMENTOLOGY

The sedimentological investigation was performed on the vertical full-diameter cores (2 5/8 inches in diameter) and the cutting samples of the uppermost sandstone levels of the Bedinan Formation. 5 full-diameter cores and 4 cutting samples of the 1th and 2nd sandstone reservoir levels of the Bedinan Formation were collected from the studied wells (A, B and F) and, used to statistically measure the all framework components of the sandstone levels by the Gazzi-Dickinson method of point counting (Dickinson, 1970; Ingersoll et al., 1984). The full-diameter cores and the cutting samples are selected from the studied interval (the 1st and 2nd sandstone levels of the uppermost Bedinan Formation), and well-preserved ones from the studied wells (A, B and F). The thin sections are prepared from the selected cores and the cutting samples to elucidate petrographical and mineralogical compositions of each sandstone levels of interest. Figure 16 exhibits the intervals where the full-diameter core and the cutting samples are collected. The name of each interval (1st sandstone level, 2nd sandstone level) is designated according to their alignment from the top of the Bedinan Formation with the aid of the corresponding gamma ray readings.

Besides the full-diameter cores used for petrographic and mineralogical analyses, 6 full-diameter cores (2 full-diameter cores from 1st sandstone level of F well, 2 full-diameter core from 2nd Sandstone level of D well and 2 full-diameter cores from 1st sandstone level and underlying shale dominant interval (shale-1) of B well) are investigated to determine the type of porosity (primary, secondary) by X-ray computed tomography imaging method. These full-diameter cores are also used to interrogate the depositional environment of the levels of interest with recognition of sedimentary structures (cross bedding, ripple marks, the angle of lamination etc...) their geometry, and corresponding gamma ray readings.

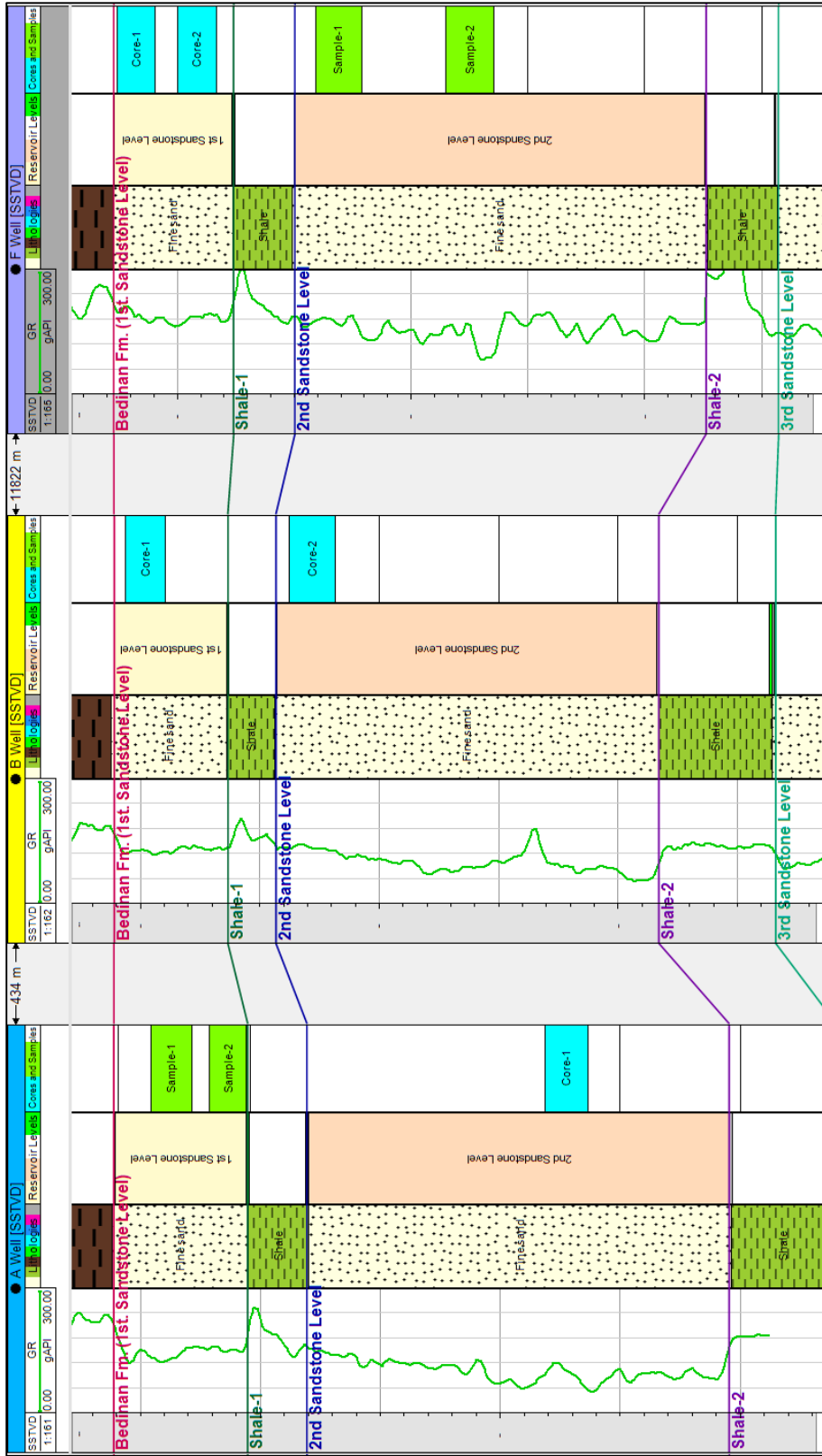


Figure 16: The intervals of the full diameter cores and the cutting samples of uppermost Bedinian Formation levels of interest for the thin section investigation and the point counting method. Scale: Each minor tick in MD column: 1m. The well log data is obtained from Çalk Petrol database.

4.1. Facies Analysis

3 different lithofacies, sandstone, shale and marl are identified from the cores and the cutting samples of the uppermost Bedinan Formation in the studied wells (A, B, F). These facies were identified by sedimentary petrographic analysis (Gazzi-Dickinson method of point counting) performed on the studied intervals (the 1st sandstone levels and 2nd sandstone levels of the uppermost Bedinan Formation). The percentage of component of each facies in selected samples was determined with petrographic analysis. Furthermore, 2400-2600 points were averagely counted from each thin section of cores to make enhanced lithology description.

4.1.1. Sandstone Facies

Sandstone dominant facies were recognized from the studied full-diameter cores and the cutting samples of the uppermost Bedinan Formation reservoir levels. These lithofacies display thinly laminated shale and marl intercalation.

The sandstone facies are generally white to beige in color, subangular to subrounded, fine to very fine grained, very well to well sorted. The studied sandstone intervals is highly porous (intergranular and dissolution). Based on the relative abundance of stable (e.g, quartz) and unstable framework grains (e.g, feldspars), the studied sandstone intervals are compositionally mature. With regard to the relative abundance of clay matrix, the degree of roundness and sorting of the grains, these sandstones are texturally mature. Dolomite (patchy-shaped), calcite (patchy-shaped) and silicate as of overgrowth constitute the big portion of the framework grains as of cementing material.

The clay matrix of the studied full-diameter cores and the cutting samples of the 1st sandstone levels in A well, B well and the 1st and the 2nd sandstone levels in F well are low in percentage, whereas those within the 2nd sandstone levels in A and B wells

and the 1st and the 2nd sandstone levels in D and E well (well side observation) are relatively high in percentage.

The investigations for mineral composition and other constituents such as rock fragment are deemed as of milestone for petrographic analysis. In addition to mineral composition, matrix content also is essential for understanding the reason/reasons lateral and vertical reservoir quality variation.

The studied minerals within the sandstone levels are; quartz, feldspar (plagioclase, microcline), matrix (clay, calcite and dolomite), mica (muscovite, biotite), rock fragments and some accessory minerals (pyrite, iron).

Quartz (SiO_2) is the main fraction of sandstones and constitutes average about 50-60 percent of the framework of the sandstone body (Pettijohn, 1957; Boggs, 2010). The studied sandstone sections in A, B and F wells include 66,87-72,42% quartz grains.

The second most abundant mineral composition of sandstones is feldspar. In spite of the fact that they are somewhat sensitive to destruction as a consequence of some chemical and physical external effects (Pettijohn, 1957; Boggs, 2010), they constitute big fraction of the sandstone body. Plagioclase and microcline (K-Feldspar) are recognized with the percentage of 1,8-3,68% in point counting (modal analysis) of the thin sections.

Rock fragments make up 15-20% of the composition of sandstone in average; however percentage in some samples ranges from zero to more than 95 percent in framework fraction (Pettijohn, 1957; Boggs, 2010). In accordance with the point counting, performed on the thin sections, the percentage of rock fragments in the studied cores ranges between 0,28-0,76 %.

Matrix content fills the interstitial spaces and consists of clay minerals which are smaller than 0.03 mm (Pettijohn, 1957; Boggs, 2010). The most common clay mineral groups which are so-called illite, smectite (montmorillonite), chlorite and kaolinite, can be identified by x-ray diffraction techniques, electron microscopy and other

nonoptical methods such as petrophysical wireline log interpretation (spectral gamma-ray, photoelectric-factor etc.). The studied cores and cutting samples from different levels of A well, B well and F well have variable amount of clay matrix not exceeding 15 percent of the bulk of rock volume. The 2nd sandstone level in A well, the 1st and the 2nd sandstone levels in B well have higher amounts of clay matrix in comparison with the 1st sandstone level in A well, the 1st and the 2nd sandstone levels in F well.

Mineral cement which bound the framework grains either are silicate minerals such as quartz and nonsilicates minerals such as calcite and dolomite. Quartz is also observed as quartz overgrowths. Secondary carbonate cement such as calcite and dolomite hold framework grains together (Pettijohn, 1957; Boggs, 2010). Alizarin red test was applied to the sample of the thin section belongs to the core of 1st sandstone level (F well) to discriminate calcite and dolomite. As a result of the test, calcite taking red color is either not present or slow developing. Secondarily formed carbonate cement's percentage in the studied sandstone levels in A, B and F wells ranges from 5,08% to 9,64% in patchy like form (Figure 17); furthermore, quartz cement (Figure 18, Figure 19) constitutes quite small amount in comparison with nonsilicate cement especially in sandstone levels having low clay matrix content.

Accessory framework minerals constitute few amount (1-2% in average) of the total fraction of sedimentary rock compared to the other major minerals such as quartz, feldspar minerals in sandstone. These minerals consist of pyrite, iron minerals and mica group which exhibit platy habit to be distinguished from other minerals. The most common mica group minerals are muscovite and biotite derived from metamorphic and plutonic igneous source rocks (Pettijohn, 1957; Boggs, 2010). The average percentage of micas in the studied sandstone cores and cutting samples is varying from 1,08 to 3,08 in total framework fraction. Muscovite (Figure 20) is the most common one, compared with other mica group mineral, biotite. Pyrite in cubic shape and amorphous iron minerals were also observed in thin sections of the studied cores and cutting samples of uppermost Bedinan Formation sandstone reservoir levels.

The percentage of pyrite and iron mineral in the studied interval is changing from 0,08 to 0,2.

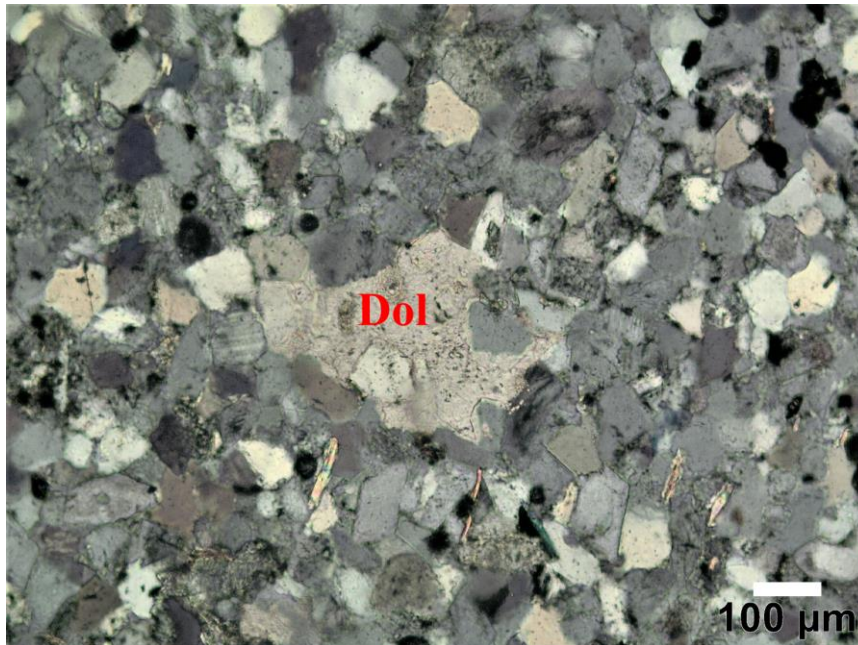


Figure 17: Photomicrograph of the sandstone with patchy dolomite cement, the core-1, the 1st sandstone level of the uppermost Bedinan Formation, F well. Dol: Dolomite.

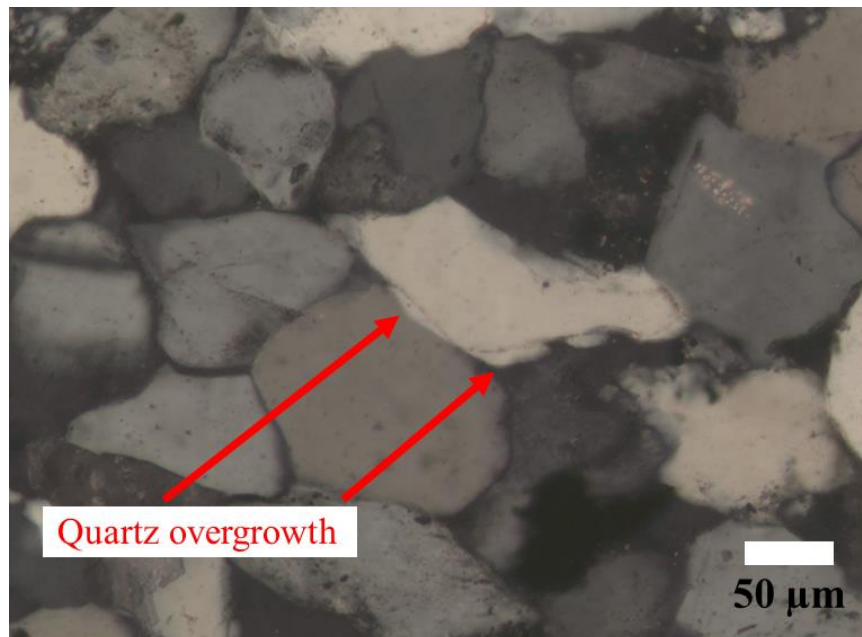


Figure 18: Photomicrograph of the 1st sandstone level of the uppermost Bedinan Formation with quartz overgrowth, the core-1, F well.

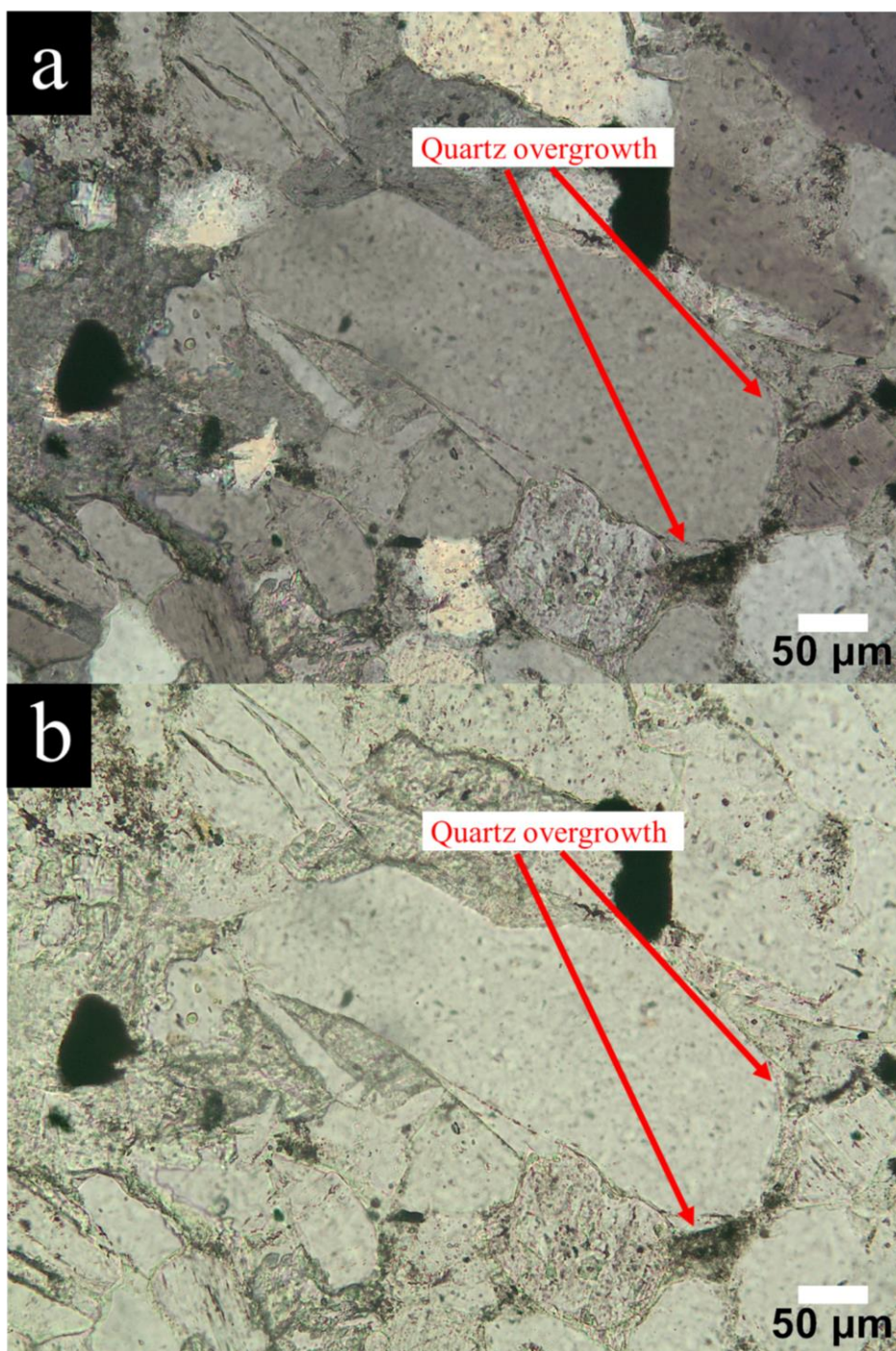


Figure 19: Photomicrographs (a: cross-polarized light, b: plane-polarized light) of the 2nd sandstone level of the uppermost Bedinan Formation with quartz overgrowth (core-1, A well).

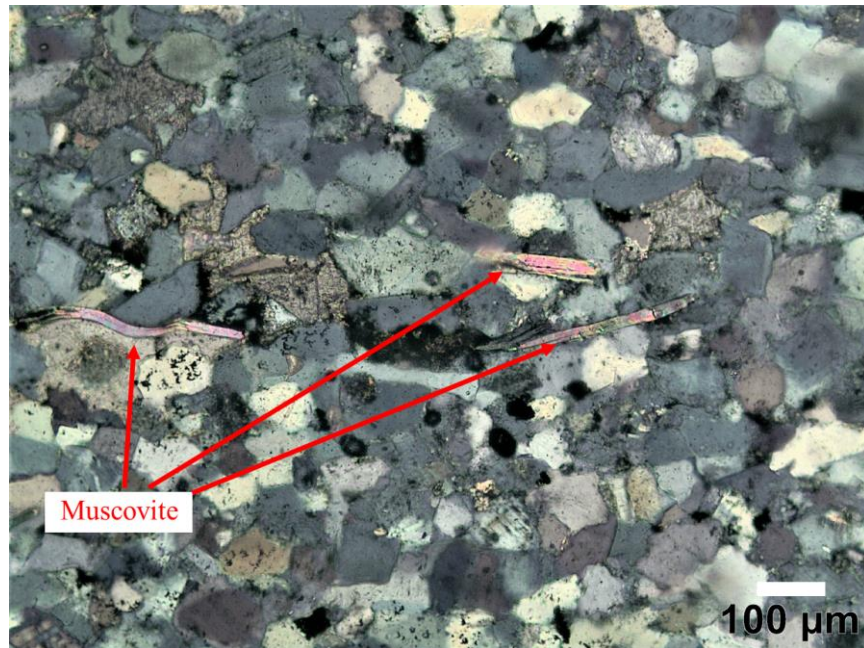


Figure 20: Photomicrograph of the 1st sandstone level of the uppermost Bedinan Formation with muscovites, the core-1, F well.

The F. J. Pettijohn (1975) QFR classification is used in this study to determine the sandstone types and categorize the sandstone levels of interest (Figure 22). The matrix percentage is another constituent playing substantial role for sandstone classification. The sandstone facies with less than 15% matrix is so-called arenite according to Pettijohn (1975) sandstone classification.

The Gazzi-Dickinson method of point counting was fulfilled to classify the studied cores of sandstones (Table 1, 2, 3, 4, 5) and determine their frameworks. The cutting samples collected from the studied sandstone levels of the Bedinan Formation were evaluated based on the point counting (Table 6, Figure 21). 2400-2600 points were counted and plotted on a ternary diagram inferred to Pettijohn 1975 sandstone classification. The types of the studied full-diameter cores of sandstone levels of A, B and F well can be stated ranging from subarkose to quartz arenite (Figure 23, 24, 25).

Table 1: The mineralogical composition of the uppermost Bedinan Formation 2nd sandstone level penetrated in A well, Core-1.

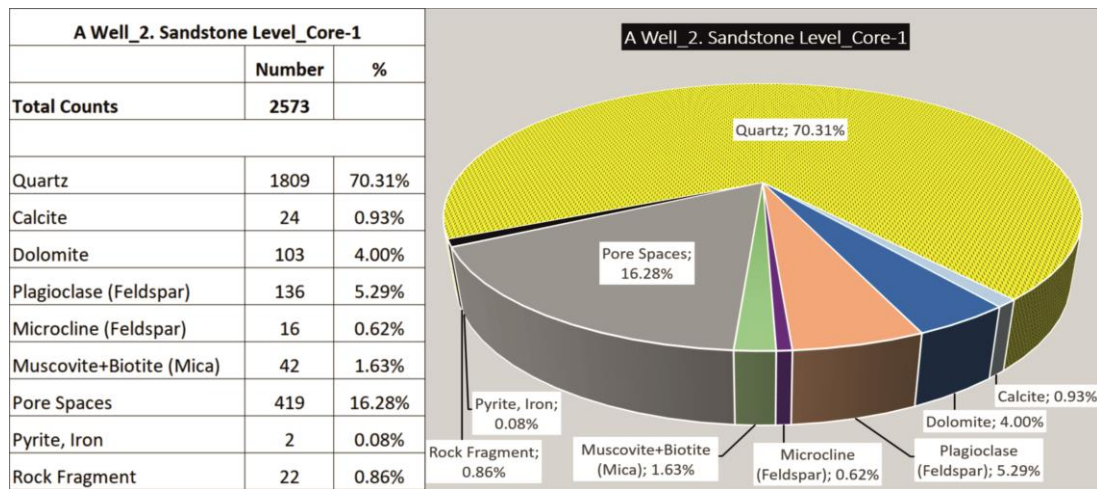


Table 2: The mineralogical composition of the uppermost Bedinan Formation 1st sandstone level penetrated in B well, Core-1.

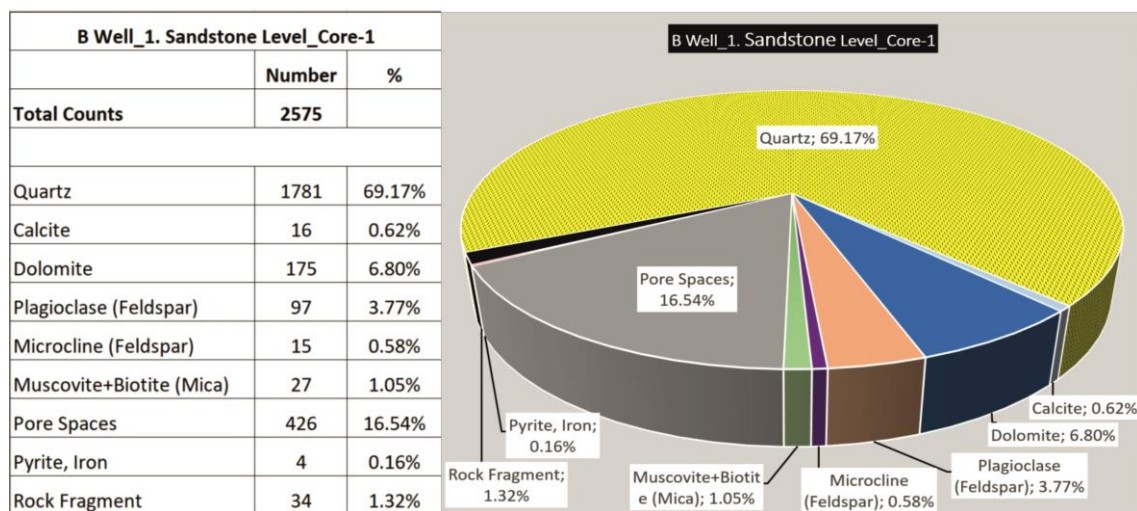


Table 3: The mineralogical composition of the uppermost Bedinan Formation 2nd sandstone level penetrated in B well, Core-2.

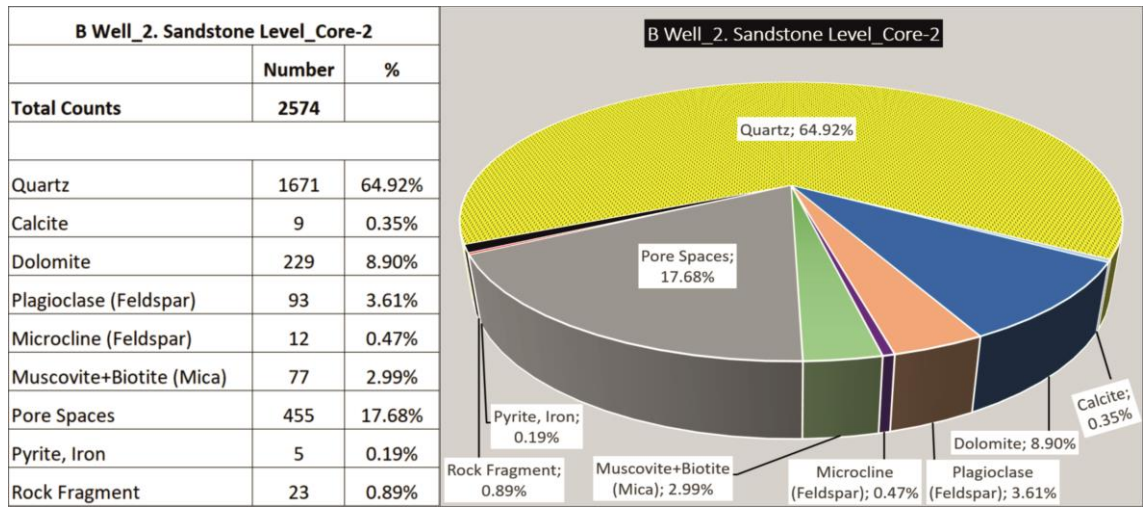


Table 4: The mineralogical composition of the uppermost Bedinan Formation 1st sandstone level penetrated in F well, Core-1.

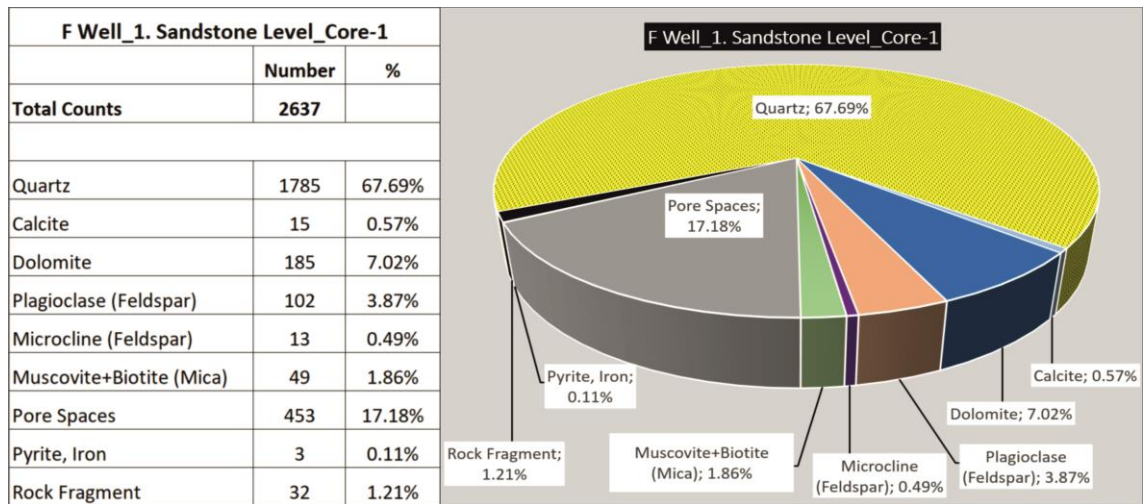


Table 5: The mineralogical composition of the uppermost Bedinan Formation 1st sandstone level penetrated in F well, Core-2.

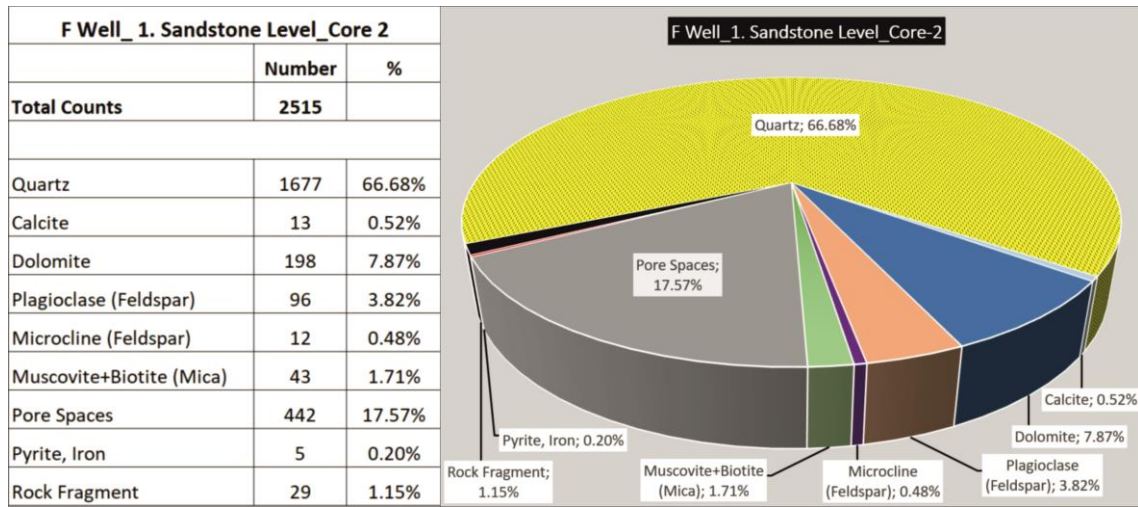


Table 6: The lithological description of each cutting samples collected from the 1st and the 2nd sandstone levels of uppermost Bedinan Formation in A and F wells.

<u>F Well 2nd Sandstone Level (Sample-1)</u>
<u>% 30 Sandstone</u> : Subarkose, very fine to fine grained, subangular-subrounded, muscovite, patchy calcite, oil stain, trace of plagioclase, low amount of clay matrix.
<u>%40 Marl</u> : Partly silty, calcerous, oil stain, partly laminated, dissaminated pyrite, dolomitic
<u>%30 Shale</u> : Silty, patchy calcite, laminated, silty shale laminates, dissaminated pyrite
<u>F Well 2nd Sandstone Level (Sample-2)</u>
<u>%60 Sandstone</u> : Subarkose, very fine to fine grained, subangular-subrounded, muscovite, low amount of patchy calcite, oil stain, trace of plagioclase, low amount of clay matrix.
<u>%20 Marl</u> : Partly silty, calcerous, alternating with siltstone and mudstone, oil stain, partly laminated, dissaminated pyrite, dolomitic
<u>%20 Shale</u> : Silty, patchy calcite, laminated, silty shale laminates, dissaminated pyrite
<u>A Well 1st Sandstone Level (Sample-1)</u>
<u>%70 Sandstone</u> : Subarkose, very fine to fine grained, subangular-subrounded, high amount of patchy calcite and dolomite, oil stain, moderately clayey, plagioclase, muscovite
<u>%20 Marl+Mudstone</u> : Partly silty, dissaminated pyrite, partly laminated, calcerous, dolomitic
<u>%10 Shale</u> : Silty, laminated, dissaminated pyrite, patchy calcite, calcite laminas
<u>A Well 1st Sandstone Level (Sample-2)</u>
<u>%60 Sandstone</u> : Subarkose, very fine to fine grained, subangular-subrounded, high amount of patchy calcite and dolomite, oil stain, moderately clayey, plagioclase, microcline (cross hatching).
<u>%20 Marl+Mudstone</u> : Partly silty, dissaminated pyrite, partly laminated, calcerous, dolomitic
<u>%20 Shale</u> : Alternating with siltstone, Silty, laminated, dissaminated pyrite, patchy calcite, calcite laminas, sandstone pockets

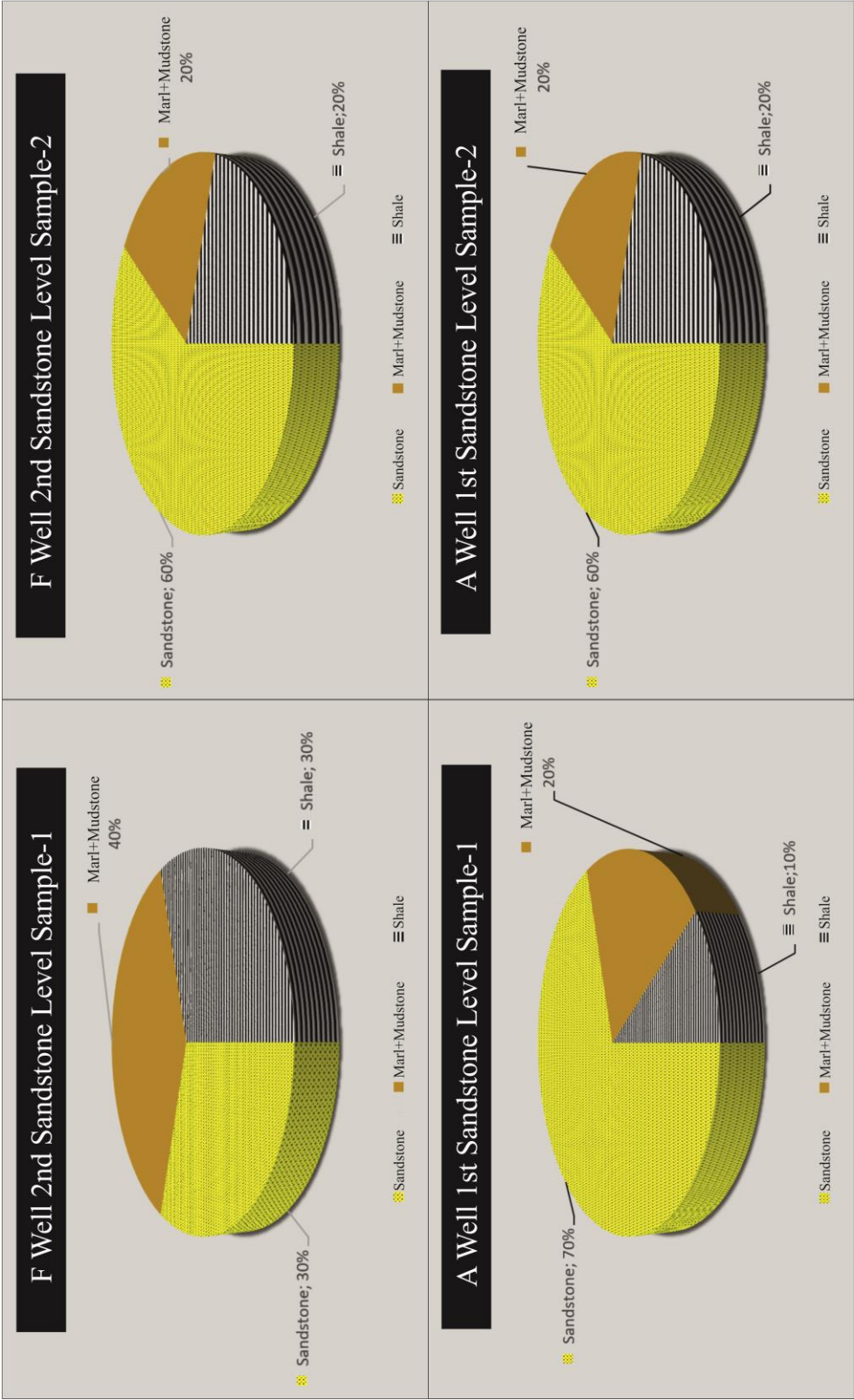


Figure 21: The relative percentage of each facies identified from the cutting samples collected from the 1st and 2nd sandstone levels of uppermost Bedinan Formation in A and F wells.

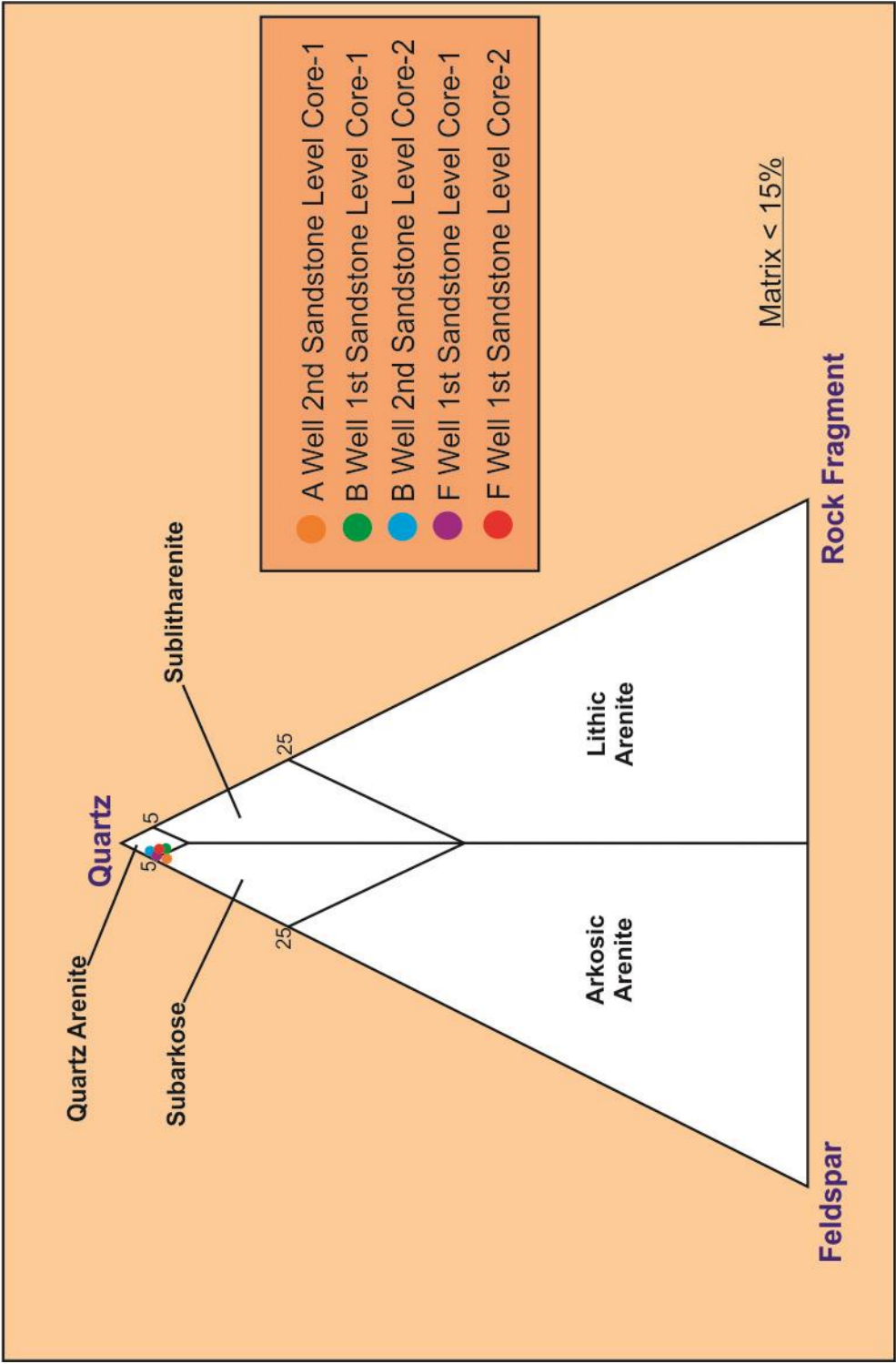


Figure 23 : Ternary plots of the studied core samples of the 1st and the 2nd sandstone levels of the uppermost Bedinan Formation.

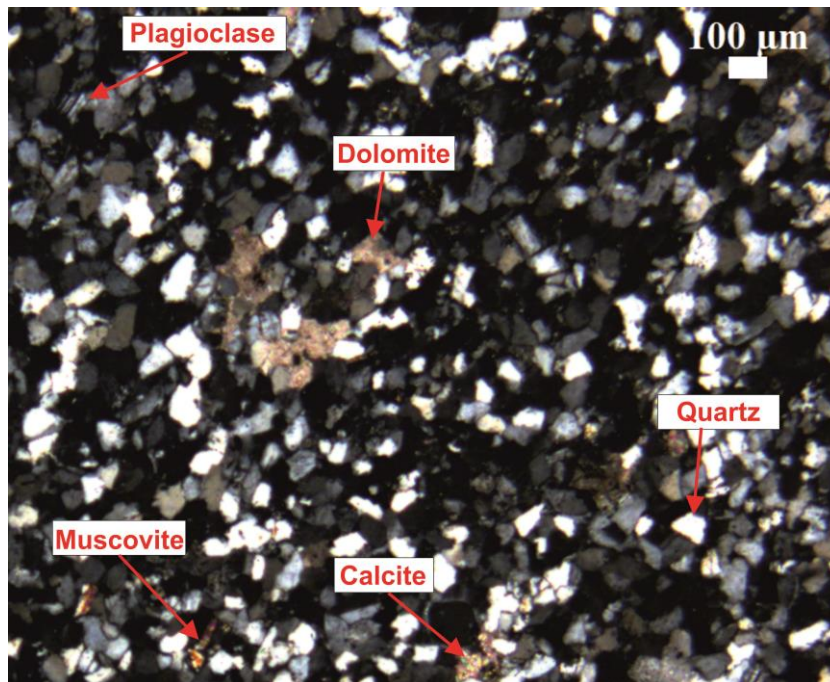


Figure 24: The photomicrograph of quartz arenitic the 1st sandstone level (core-2) of F well, Plane polarized light. Scale is indicated with a white bar.

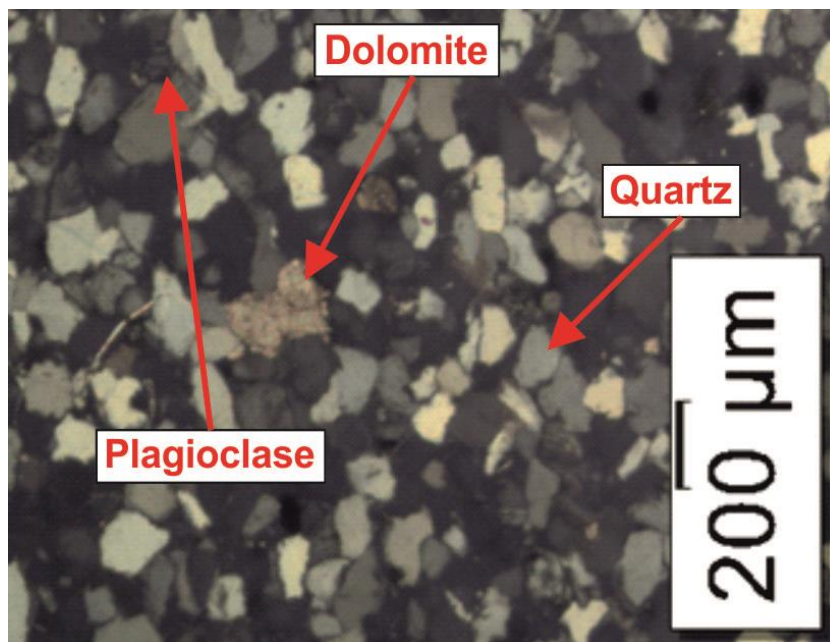


Figure 25: The photomicrograph of quartz arenitic the 1st sandstone level (core-1) of F well, Plane polarized light. Scale is indicated with a white bar.

4.1.1.1. Provenance Interpretation

Apart from the depositional environment, transform mechanism and climate, understanding the origin of the sandstone framework grains carries vital importance to assess reservoir quality for hydrocarbon exploration. Based on recent studies carried out especially by Dickinson (1985), the relative abundance of quartz (monocrystalline, polycrystalline), feldspar (K-feldspar, plagioclase) and rock fragment/lithic fragment (volcanic/metavolcanic rock fragment, sedimentary/metasedimentary rock fragment) constituents is adequate with the aid of some supplementary details to reveal the source area of the sandstone framework grains of interest (Figure 26). The other framework grains such as cement (calcite, dolomite, quartz etc..), accessory minerals (mica groups, stable, and metastable opaque and nonopaque minerals and heavy minerals), and matrix are ignored for the provenance studies. The major provenance types for the sandstones are continental block (stable craton, basement uplift), recycled orogens and magmatic arc (Dickinson and Suczek, 1979; Dickinson, 1985; Boggs, 2010). Table 8 exhibits the provenance types and related tectonic setting and their lithologic derivatives.

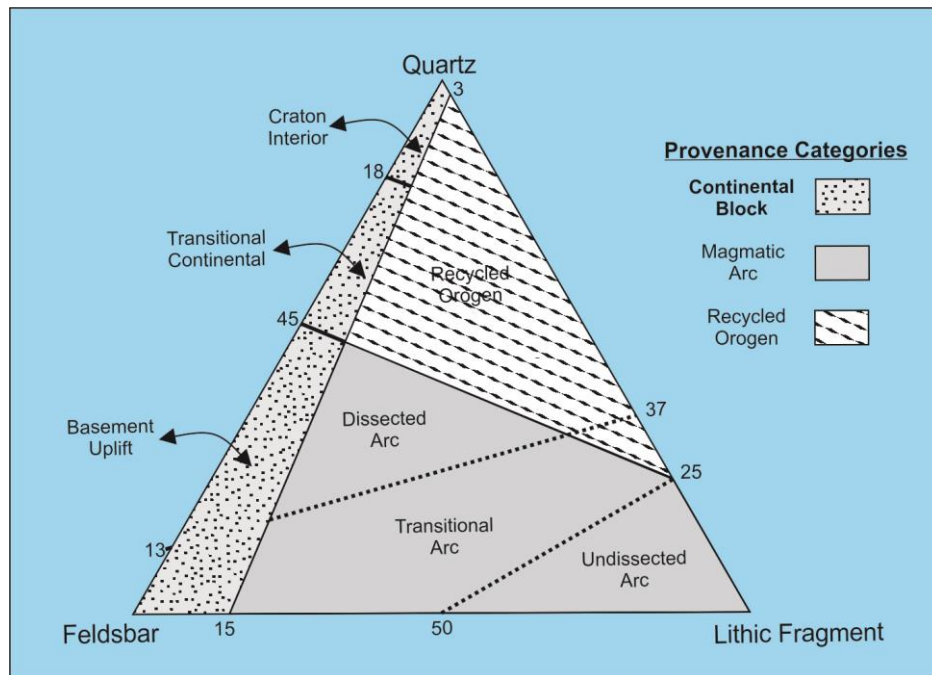


Figure 26: Provenance types of sandstones having different quartz, feldspar and lithic fragment ratio. Qt: quartz, F: Feldspar, L: Lithic fragment (Dickinson 1985).

Table 7: Major Provenance type with tectonic settings and related sand composition. Modified from Dickinson (1985).

Provenance Type	Tectonic Setting	Derivative Sand Composition
Stable craton	Continental interior or passive platform	Quartzose sands with high Q_m/Q_p and K-feldspar/Plagioclase ratios
Basement uplift	Rift shoulder or transform rupture	Quartzofeldspathic sands low in rock fragment with Q_m /Feldspar and K/P ratios
Recycled orogen	Subduction complex or fold-thrust belt	Quartzolithic sands low in F and L_v with variable Q_m/Q_p and Q_p/L_s ratios
Magmatic arc	Island arc or continental arc	Feldspatholithic volcanoclastic sands with high P/K and L_v/L_s ratios

Stable cratons (Figure 27) derived sandstones are sourced from low-lying granite and gneissic exposure and recycling platform sediments (Dickinson and Suczek, 1979; Dickinson, 1985). The sand derived from continental block accumulates either continental interior or passive continental margin or continental flanks of foreland basin (Dickinson, 1985).

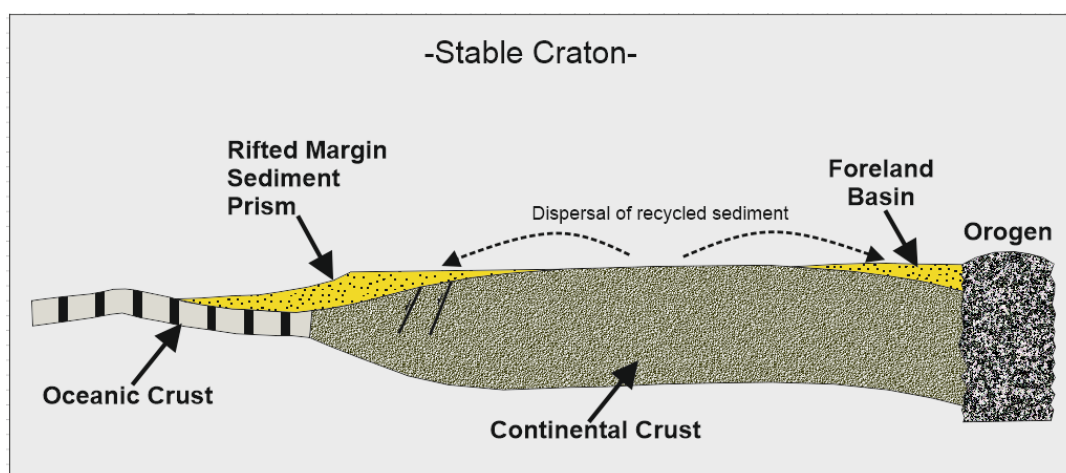


Figure 27: The diagram exhibits the plan view of Stable Craton provenance (Dickinson and Suczek 1979).

Basement uplift (Figure 28) in correspondence to faulting cause to horst-graben system observed in continent interior and pull apart basin. Sands eroded from uplifted area shaded to linear troughs being so-called grabens. Those materials are generally rich in feldspar (arkose) due to the absence of long transportation (Dickinson and Suczek, 1979; Dickinson, 1985).

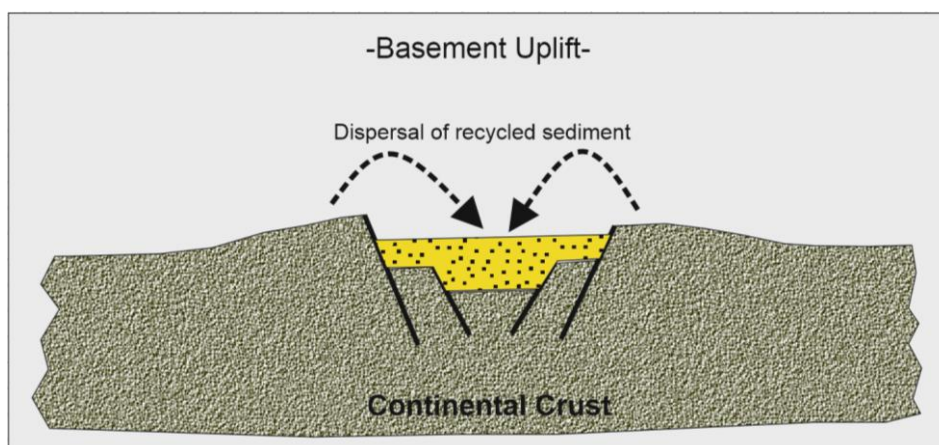


Figure 28: The diagram exhibit the plan view of Basement Uplift provenance (Dickinson and Suczek, 1979).

Recycled orogenic (Figure 29) provenance occurs as a consequence of plate collision; in other words, the collision of the major plates resulted in the uplifting of orogenic belt creates source area for adjacent depression area (Dickinson and Suczek, 1979; Dickinson, 1985; Boggs, 2010). Uplifted sedimentary and metamorphic rocks constitute the main type of the source, thus the framework of the accumulated sands have high amount of sedimentary and metasedimentary rock fragment, moderate quartz and a high ratio of quartz to feldspar (Boggs, 2010).

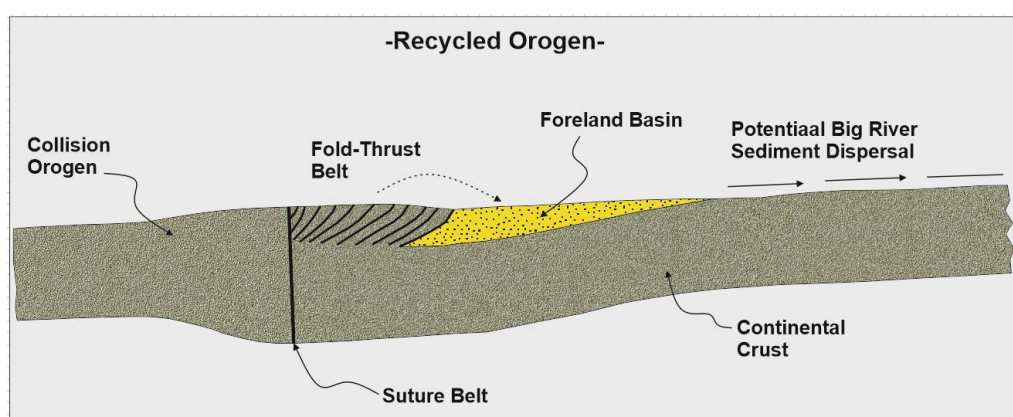


Figure 29: The diagram exhibits the plan view of Recycled Orogen provenance (Dickinson and Suczek, 1979).

Magmatic arc provenance constitutes the source for the sands in the zones of plate convergence. Volcanoclastic materials being rich in volcanic lithic material and plagioclase feldspar, erupted and eroded, from stratovolcanos shed (undissected) in forearc, backarc and even can reach up to foreland basin (Dickinson and Suczek, 1979; Dickinson, 1985; Boggs, 2010). Erosion of volcanoclastic materials causes to exposing of the underlying batholithic root (dissected). The sandstone framework is feeded by dissected volcanic arc, rich in quartz and potassium feldspar which may rise a hesitation for related sandstone framework from other arkosic sandstone constituents produced by another basement uplifts (Dickinson, 1985). Figure 30 exhibits the sandstone sourced by volcanoclastic material and batholithic root and its occurrence system.

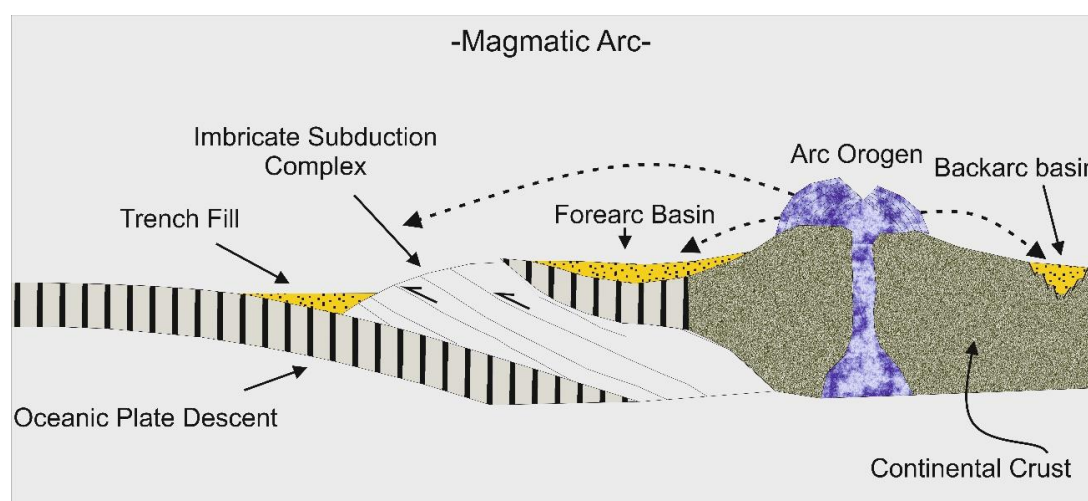


Figure 30: The diagram exhibits the plan view of Magmatic Arc provenance (Dickinson and Suczek, 1979).

The ternary diagram suggested by Dickinson (1979; 1985) is used to clarify the source area of the studied uppermost 1st and 2nd sandstone levels of the uppermost Bedinan Formation. The point counting method is carried out on the thin sections prepared from the full-diameter cores and the cutting samples of both the sandstone levels of

interest of A, B and F wells to determine the relative percentage of quartz, feldspar and lithic fragment (QFL). The suggested framework constituents (QFL) of the full-diameter cores of interest are plotted on the ternary diagram. The tectonic setting of the quartz arenitic to subarkosic sandstone levels of the uppermost Bedinan Formation in A, B and F wells can be assigned as stable craton as a consequence of the interpretation of the triangular diagram that involves a QFL plot (Figure 31).

The rock type which is the source for the studied interval of the sandstones of uppermost Bedinan Formation is tried to be discovered. There are lots of methods to determine rock type constituting the source for the sandstones level of interest. Two of them is; in turn, to reveal whether quartz grains occupying a big portion of the sandstone framework are single crystal (monocrystalline) or formed by the number of crystal in a different orientation (polycrystalline or composite), and crystal boundaries of the polycrystalline quartz are straight or sutured. The monocrystalline quartz or polycrystalline quartz with straight crystal boundary are the clue for igneous source rock; furthermore, polycrystalline quartz with sutured crystal boundary and polycrystalline quartz elongated in the preferred direction (stretched metamorphic quartz) is evidence for metamorphic source rock (Adams et al., 1984). Based on the observation for quartz grains accomplished on thin sections of 1st and 2nd sandstone levels of A, B and F wells, the quartz grains are monocrystalline (Figure 32) with around 85-90 percent and polycrystalline around 10-15 percent in accordance with point counting method. The polycrystalline quartz with different crystal direction boundaries are straight (Figure 33); therefore, the quartz grains constituting a big portion of the sandstone framework of the 1st and 2nd sandstone levels of A, B and F wells eroded and transferred from igneous source rock. The sandstones framework grains of the uppermost Bedinan Formation are most probably derived from the granites of the Late Precambrian Arabian-Nubian Shield.

The Provenance Study for the Uppermost Bedinan Formation Sandstone Levels

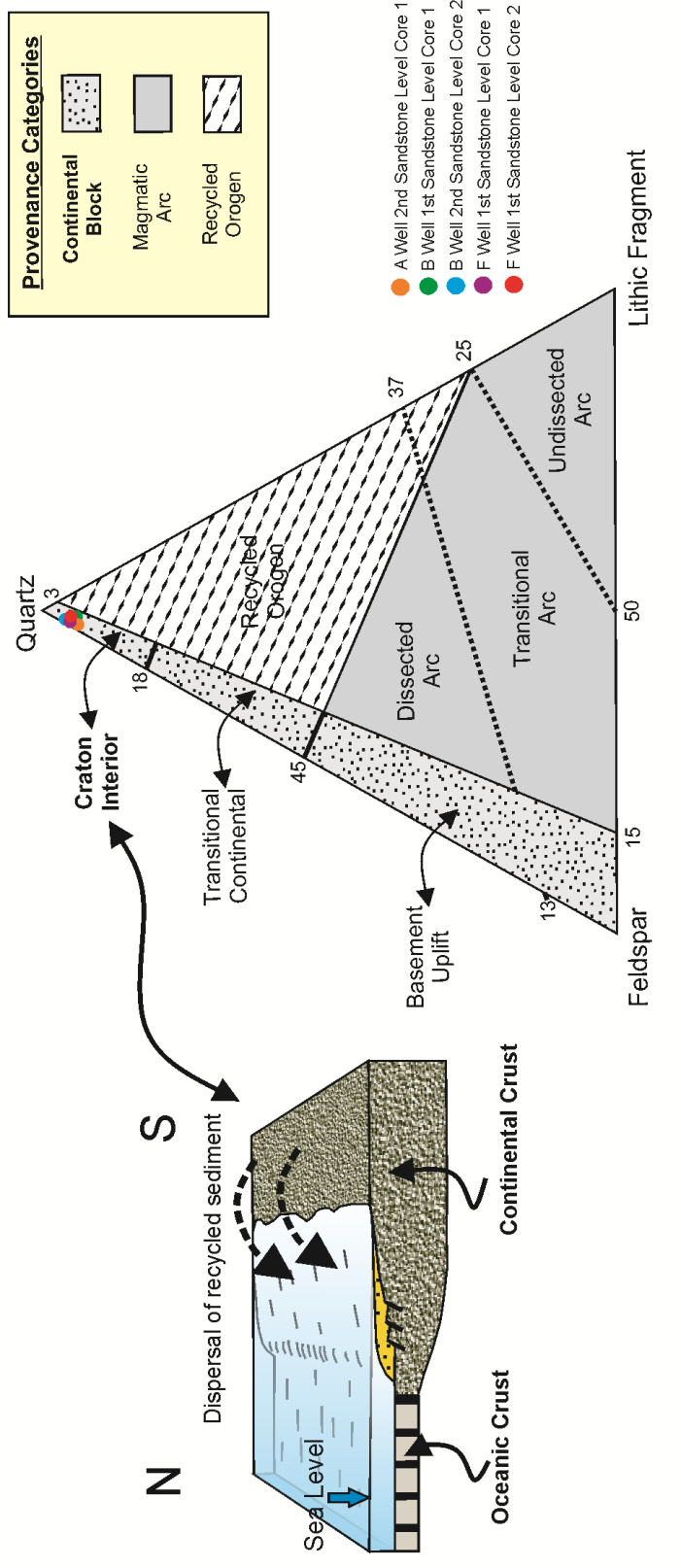


Figure 31: The diagram shows the provenance of the uppermost Bedinan Formation 1st and 2nd sandstone levels.

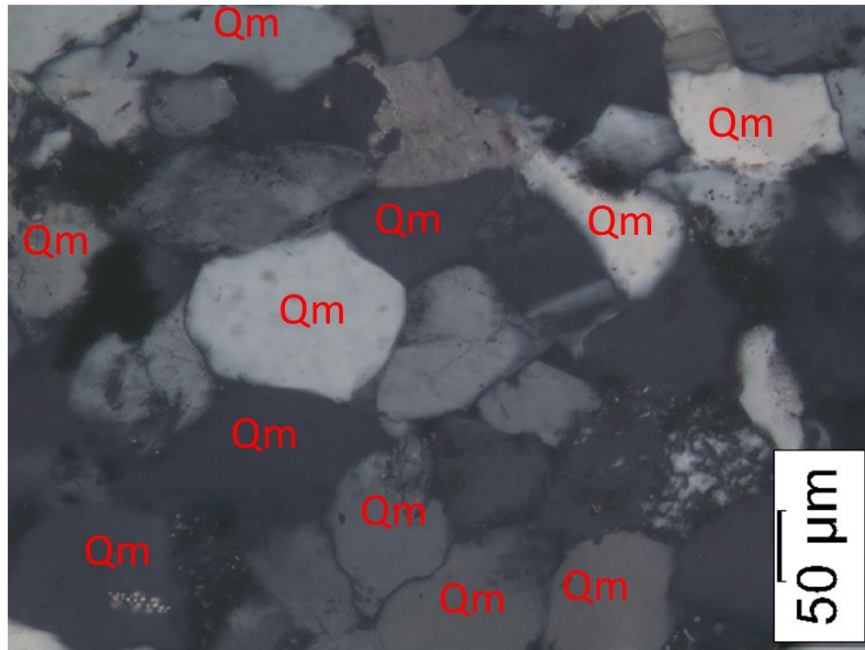


Figure 32: Monocrystalline quartz observed in the photomicrograph of the 1st sandstone level, the core-1, F well. Qm: Monocrystalline quartz.



Figure 33: The photomicrograph of the core-1, the 1st sandstone level of the uppermost Bedinan Formation, F well, polycrystalline quartz with straight boundary.

4.1.2. Shale Facies

The shale facies with laminated texture are observed in the core and the cutting samples collected from A, B and F wells in 1st and 2nd sandstone levels (Figure 34). They include patchy like calcite and dolomite grains, silt size quartz grains, sandstone pockets and some micas aligned parallel to the flakes. Shale facies is dark gray color, includes disseminated pyrite minerals and displays fissility, and presents slightly calcareous composition. The areal percentage of the shale laminae in the core samples is not higher than 5%.

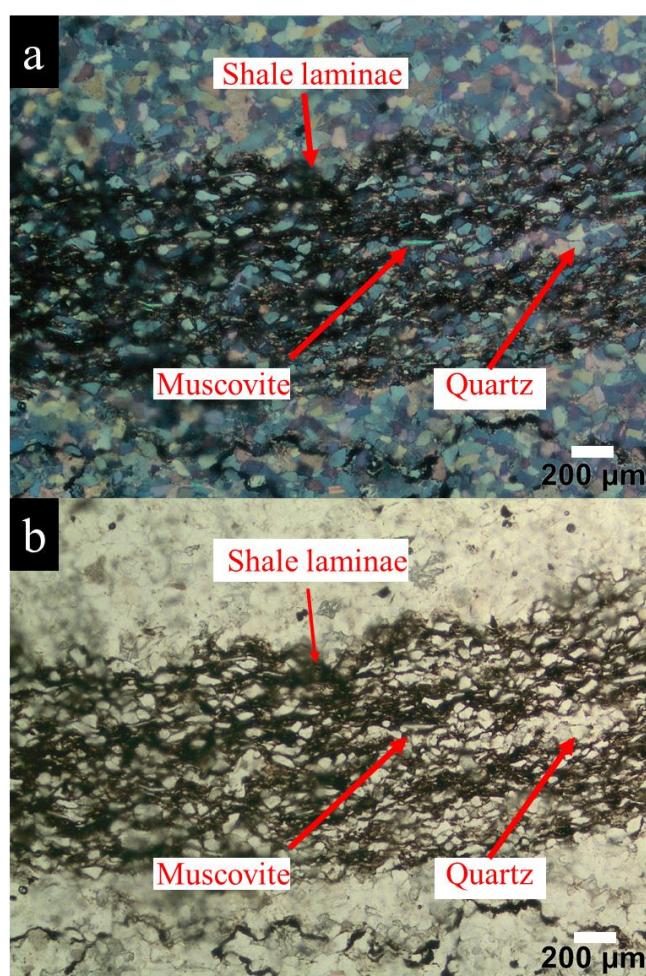


Figure 34: Photomicrograph (a: Cross-polarized light, b: Plane-polarized light) of the sandstone with shale laminae displays silt size quartz grains with muscovites in the core-2, the 1st sandstone level of the uppermost Bedinan Formation, F well.

4.1.3. Marl Facies

Another facies observed especially in the collected sample is marl. In spite of the fact that marl facies constitutes small amount in total rock volume in comparison with the other facies, the presence of the facies plays important role in reservoir quality evaluation and further enhanced reservoir stimulation programme. The marl facies displays partly silty content with disseminated pyrite and mostly dolomite. It has laminated texture (Figure 35).



Figure 35: The photomicrograph of the marl lithofacies, the cutting sample-1 of the 2nd sandstone level of the uppermost Bedinan Formation, F well.

4.2. Porosity Measurement and X-ray Computed Tomography

The percentage of pore spaces in 1st and 2nd sandstone levels of A, B and F wells detected by the point counting method ranges between 16 and 19. Intergranular porosity is the main type of porosity and relatively minor amount of dissolution porosity are detected on thin sections of the studied cutting samples and cores. Additional study for porosity is also carried out by using different non-destructive imaging technique which is so-called X-ray computed tomography (CT)).

X-ray computed tomography measurement method was carried out on the core sample taken from the uppermost Bedinan Formation, from the 1st sandstone level of F well. Around 2000 radiographic photos taken from different angles are used to generate 2-dimensional cross sectional slices (Figure 36, Figure 37). Radiographic viewing from different directions (360 degree) of the core sample of the 1st sandstone level of F well took 24 minutes and digital data is transferred to Vgstudio max high-end software system to visualize and analyse 3 dimensional volume (Figure 38) generated by stacking of lots of 2-dimensional slices.

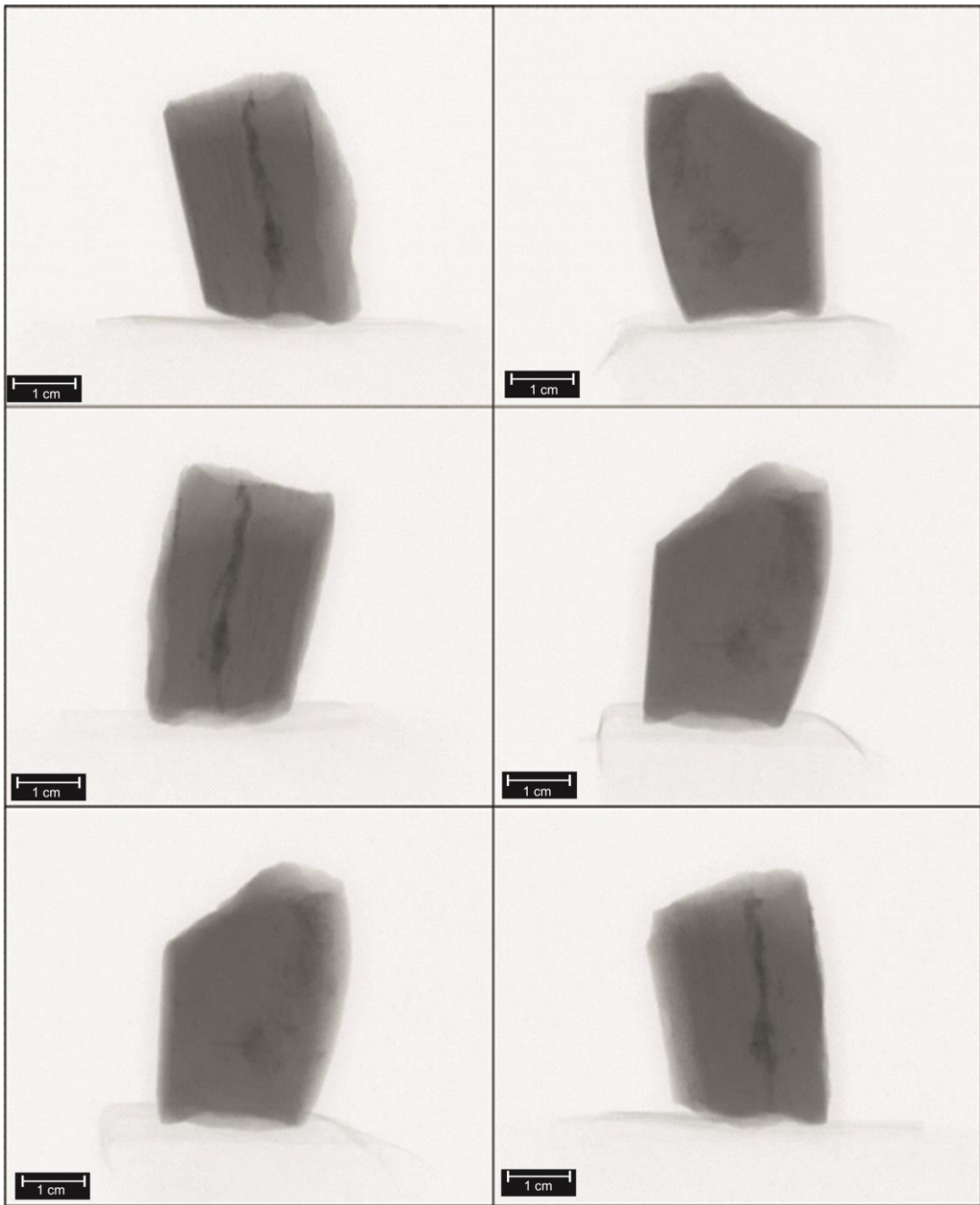


Figure 36: The radiographic view (side views) of the studied core of F well 1st sandstone level in different dimensions.

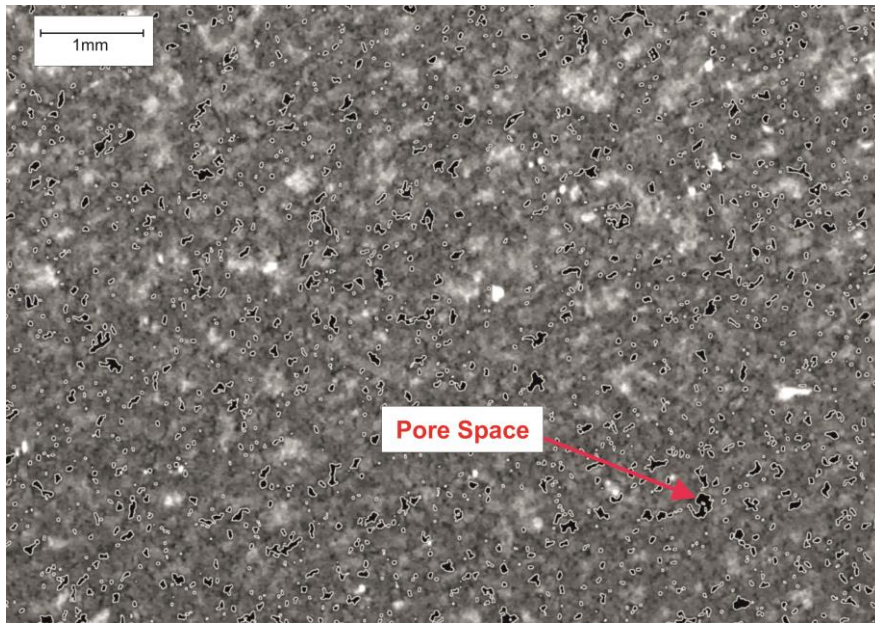


Figure 37: 2 dimensional cross sectional slices and pore spaces generated by X-ray attenuation method of the core sample of the 1st sandstone level of F well. Red arrow points on the porespace. Bright white patches are carbonate cement (calcite or dolomite).

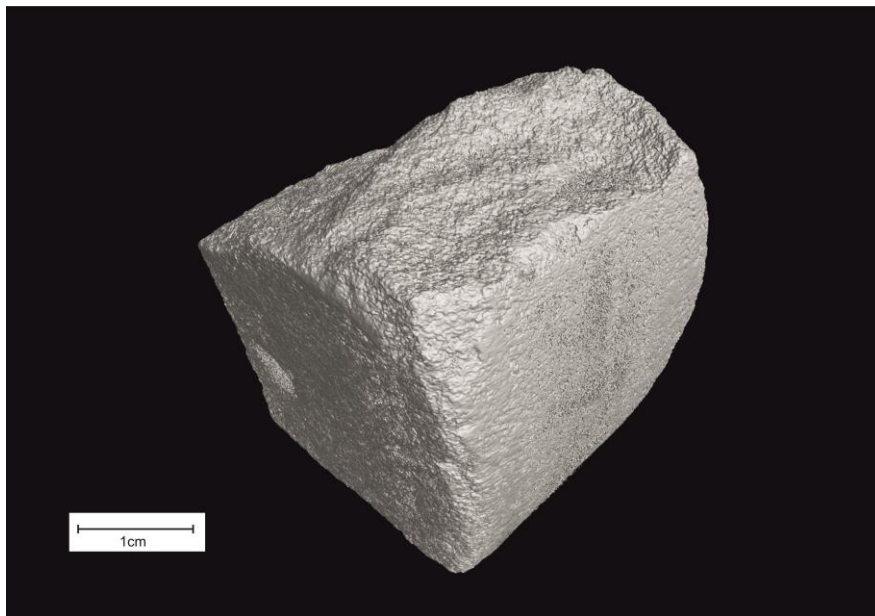


Figure 38: 3 dimensional view of the core sample of the 1st sandstone level of F well by using VG studio max high-end technological software system.

In order to measure and detect pore size and volume of the studied core, a square was drawn randomly to study enhanced pore shape. The surface area of the selected region of interest and the total volume of the cube which generated by appointing z dimension is in turn 19,85 mm² and 6,05 mm³. Figure 39 exhibits the accurate interval of the randomly selected region to make the measurement for pore volumes and their size.

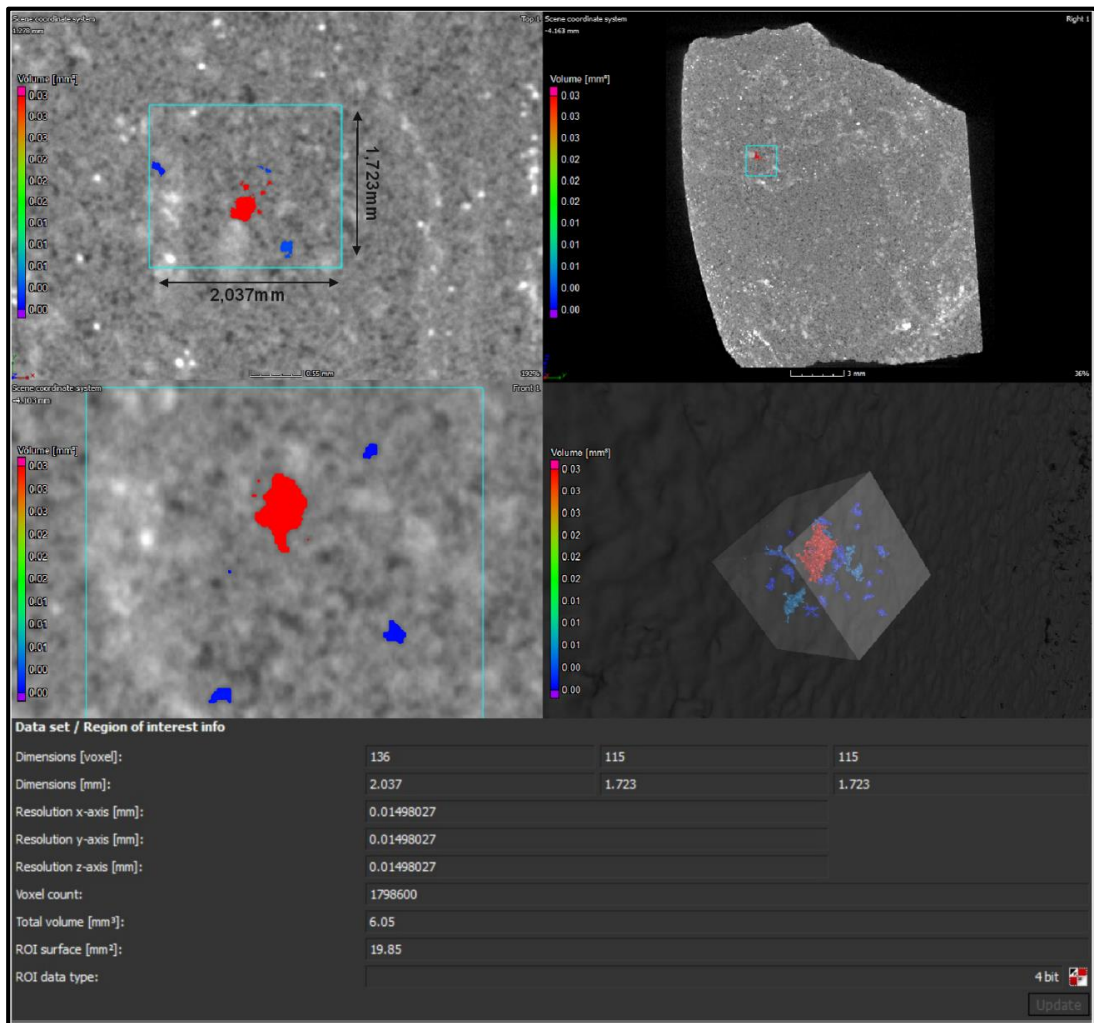


Figure 39: The region of interest for measuring pore shape size and volume distribution, created by X-ray computed tomography high-end technology.

Each pore space is evaluated in terms of its size and volume (Figure 40, Figure 41 and Figure 42). According to the measurement, volume and the maximum diameter of pore spaces have the value between 0,001-0,04 mm³ and 0,095-1,023 mm (Table 7), respectively. Additionally, the measured porosity of the studied interval is 1,2 %.

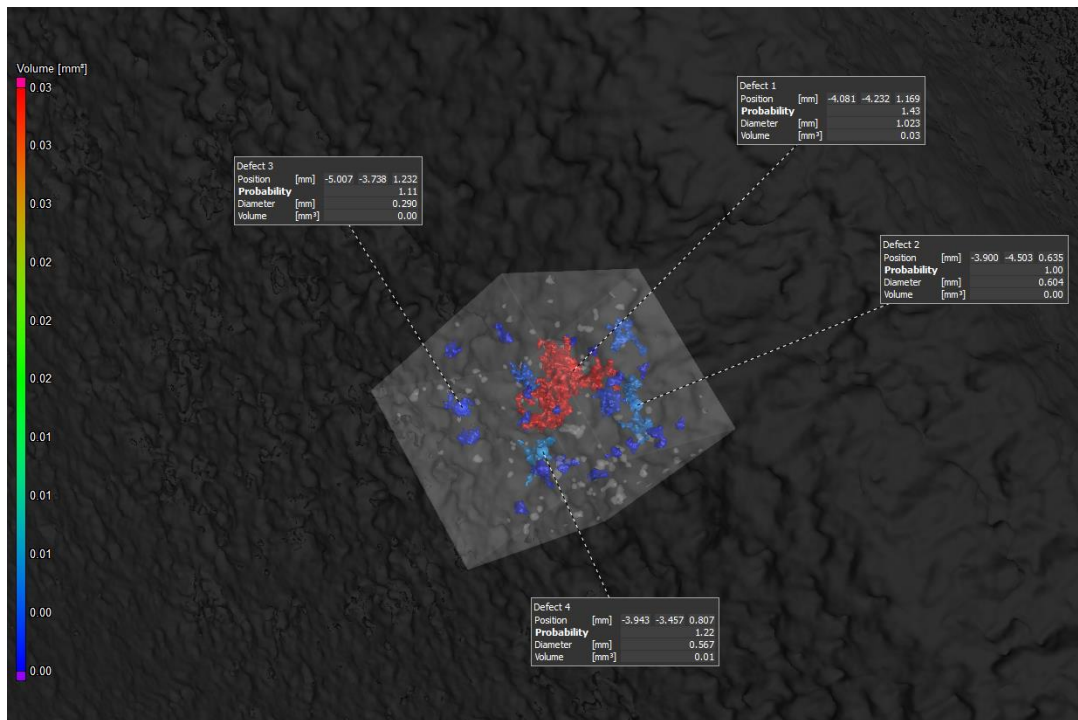


Figure 40: 3 dimensional view of the region of interest and colored pore spaces shape, intensity and size.

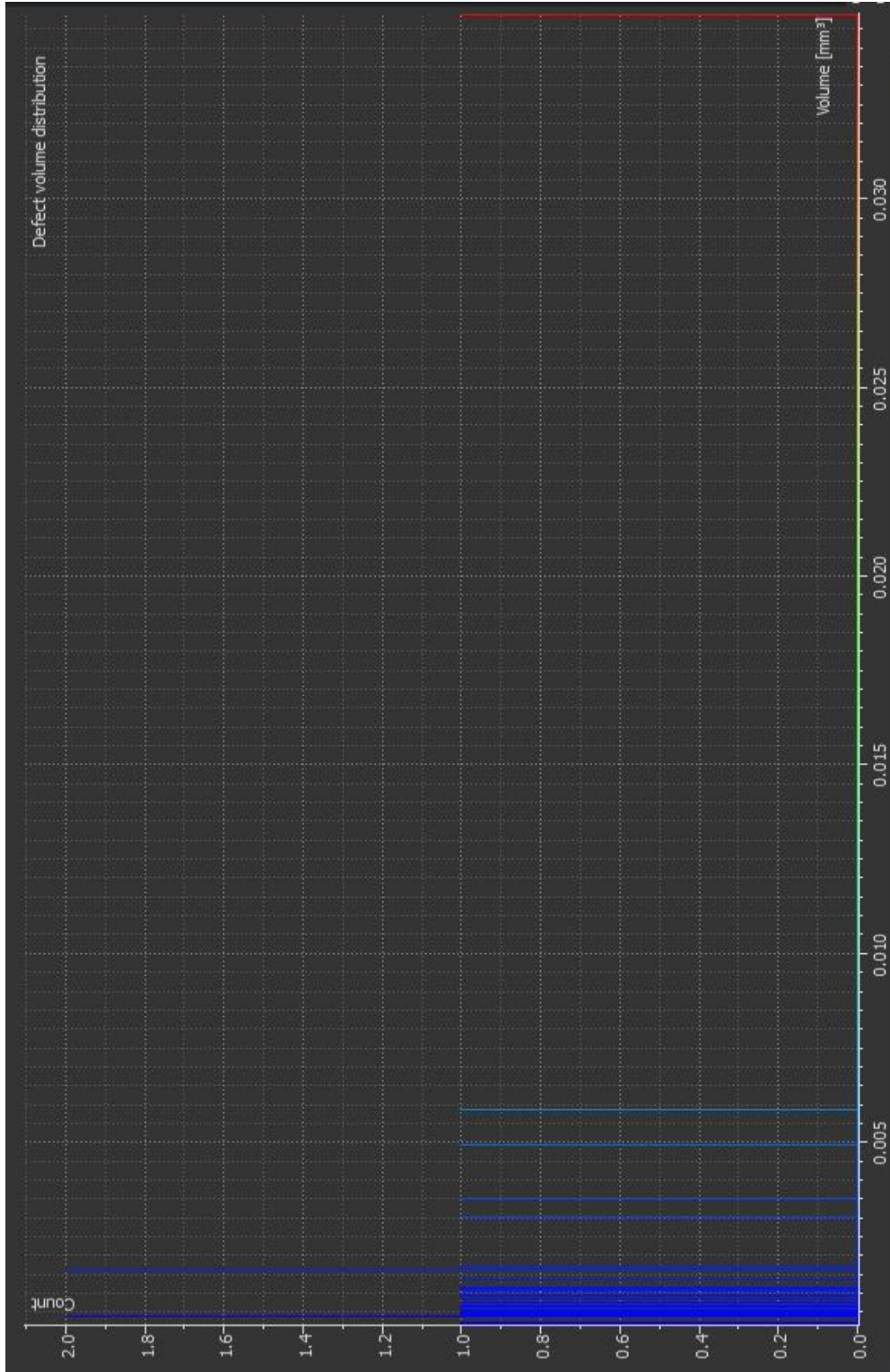


Figure 41: The volumetric calculation via CT for each pore of the selected cube.

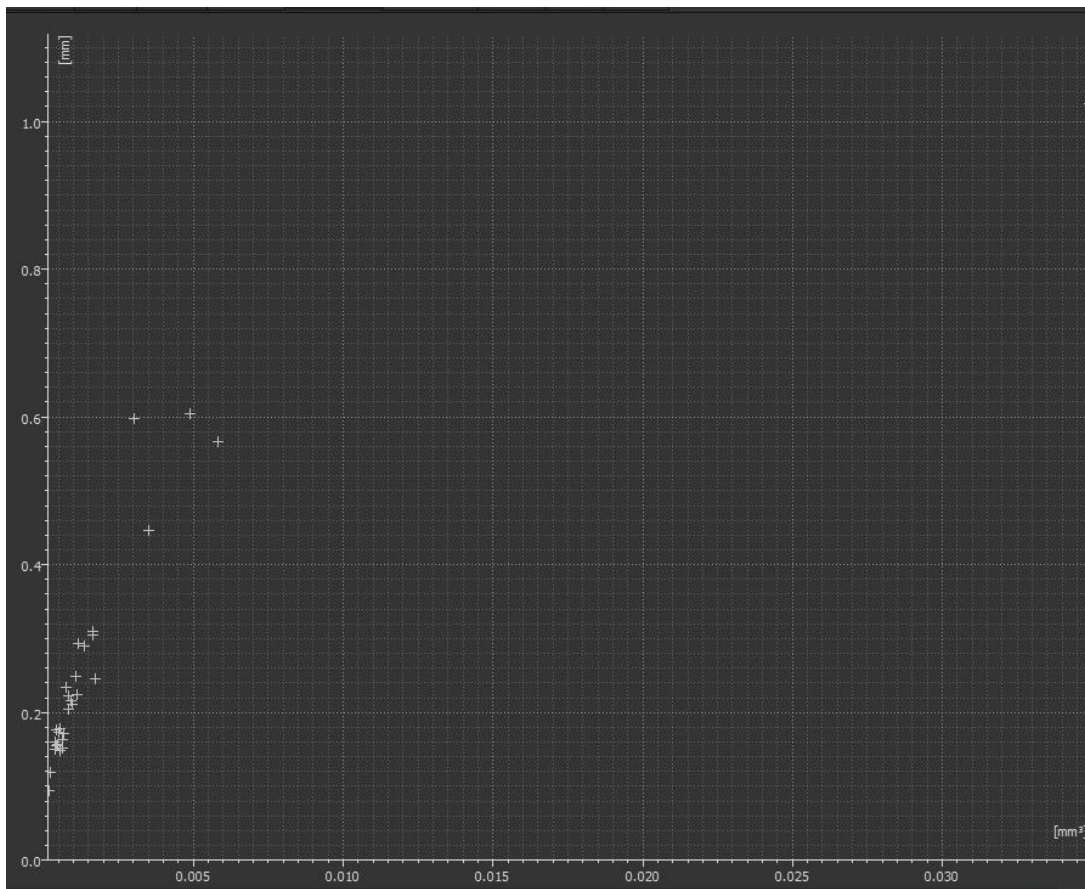


Figure 42: The diagram shows the volumetric calculation versus maximum diameter variation through each detected pore of the core sample (F well, the 1st sandstone level of the uppermost Bedinan Formation, x axis: volume, y axis: diameter).

Table 8: The maximum diameter and volume calculation list for each pore spaces of the selected cube.

Probability	Radius [mm]	Diameter [mm]	Volume [mm ³]
1.43	0.512	1.023	0.03
1.00	0.302	0.604	0.00
1.06	0.299	0.597	0.00
1.22	0.283	0.567	0.01
1.01	0.223	0.446	0.00
1.09	0.155	0.309	0.00
1.11	0.153	0.305	0.00
1.01	0.146	0.293	0.00
1.11	0.145	0.290	0.00
1.00	0.124	0.249	0.00
1.18	0.123	0.246	0.00
1.03	0.117	0.234	0.00
1.16	0.112	0.224	0.00
1.13	0.111	0.223	0.00
1.05	0.108	0.216	0.00
1.18	0.105	0.210	0.00
1.05	0.102	0.204	0.00
1.31	0.089	0.177	0.00
1.07	0.088	0.176	0.00
1.10	0.087	0.173	0.00
1.05	0.086	0.172	0.00
1.31	0.082	0.163	0.00
1.05	0.080	0.161	0.00
1.23	0.078	0.156	0.00
1.11	0.077	0.155	0.00
1.32	0.076	0.151	0.00
1.01	0.075	0.150	0.00
1.15	0.075	0.149	0.00
1.05	0.059	0.119	0.00
1.05	0.047	0.095	0.00

4.3. Depositional Environment

The knowledge of the depositional environment of the uppermost Bedinan Formation sandstone reservoir levels is vital to make a prediction for the reservoir quality thus to apply the most convenient well stimulation methods in order to increase hydrocarbon production and recovery.

Although the presence of pyrite associated with the SO_4^{+2} activity and saline pore water in the sandstone levels of interest proves that the uppermost Bedinan Formation is deposited in shallow marine environment (Morad et al., 2010), in order to make more comprehensive depositional environment interpretation, some sedimentary structures such as ripple marks together with GR readings may give clue regarding the depositional environment of the uppermost Bedinan Formation.

Ripple marks serve as an aid to interrogate the depositional environment of the studied rocks (Tanner, 1967). Ripple mark types have been described from a variety of depositional environment. For instance, very shallow water, tidal flat, wind driven, water current (streams) and deep ocean water currents ripple marks have additional distinctions which are useful to be interpreted (Tanner, 1967). The numerous studies carried out in shallow marine nearshore coastal areas, creeks, wind driven dunes of Florida and creeks of west Texas, Colorado, New Mexico and Utah indicate that ripple mark pattern is particularly one of the most useful in paleogeography construction (Tanner, 1967). The dimensionless well known parameters defined as ripple index and ripple symmetry index are used to determine ripple mark geometry and depositional environment of the studied rock piles. Ripple index is formulated as two adjacent crest spacing (wave-length) divided by the horizontal distance between crest and trough (height). While ripple index, which is equal or less than 15, indicates wave or water current origin; ripple index is equal or more than 17 is particularly clue for swash or wind origin (Tanner, 1967).

The other dimensionless parameter designated as ripple symmetry index to elucidate the depositional environment of the sandstone levels of interest is defined as the ratio of the distance from one crest to trough along gentler slope divided by the crest to next trough along the steeper slope. Ripple symmetry index which is equal or less than 1,5 suggests wave or swash origin. Additionally, ripple symmetry index which is equal or more than 3 introduces wind or water current origins (Tanner 1967).

In spite of the fact that the ripple marks observed in the cores of the studied interval have mostly higher wavelengths (distance between adjacent two crests) than the core diameter (2 5/8 inches), 6 measurements (ripple index, ripple symmetry index) are performed to disclose the depositional environment of the studied intervals. With regard to the ripple index (8-15) and ripple symmetry index (1,8-2,7) measurements (Table 9) performed on the cores of the 1st and the 2nd sandstone levels of uppermost Bedinan Formation, the intervals of interest piled under wave dominated (upper shoreface to lower shoreface) depositional environment condition (Figure 43).

Table 9: Ripple Index and Ripple Symmetry Index Measurement on the Ripple Marks identified on the cores.

	Ripple Index	Ripple Symmetry Index
Ripple Mark-1	15	2,15
Ripple Mark-2	11,2	2,7
Ripple Mark-3	8	2,25
Ripple Mark-4	13,1	2,21
Ripple Mark-5	12,3	1,8
Ripple Mark-6	13,9	2,48

Wave induces downward orbital motion of water body. This motion is effective to half depth of wavelength being so-called wave base (Howell, 2005). While the wave base deepens during the period of winter, the wave base becomes relatively shallower in the summer time.

In wave dominated eustuary which subjected to high wave energy, the shear between water mass and seabed induce a variety of sedimentary structures including ripples, dunes, cross bedding (tabular, trough) and plane beds (Howell, 2005; Vakarelov et al., 2012, Siddiqui et al., 2013; Siddiquiet al., 2017).

In deeper parts, storm dominated waves preclude ripple or dune formation and produce large scale and low angle hummocky cross stratification (Howell, 2005; Charvin et al., 2011; Pemberton et al., 2012; Morsilli and Pomar, 2012; Vakarelov et al., 2012).

The distinctive sedimentary structures identified from the 1st and the 2nd sandstone levels of Bedinan Formation are trough cross bedding, tabular cross bedding, planar wedge shaped cross bedding, sigmoidal cross bedding, parallel mud and sand lamination (Figure 44). Because of the fact that the core sizes are not favorable to identify large scale sedimentary structures like hummocky cross stratification, small scale sedimentary structures were used to make depositional environment interpretation. One of the most prominent sedimentary structures observed in the studied cores with very fine to fine grained sandstone dominant sections are multidirectional trough and tabular (sigmoidal, wedge shaped) cross bedding which are distinctive sedimentary structures for Upper Shoreface lying between breaker zone and low tide mark (Tanner, 1967; Reineck, 1980; Howell, 2005; Charvin et al., 2011; Pemberton et al., 2012; Vakarelov et al., 2012; Siddiqui et al., 2013; Siddiqui et al., 2017).

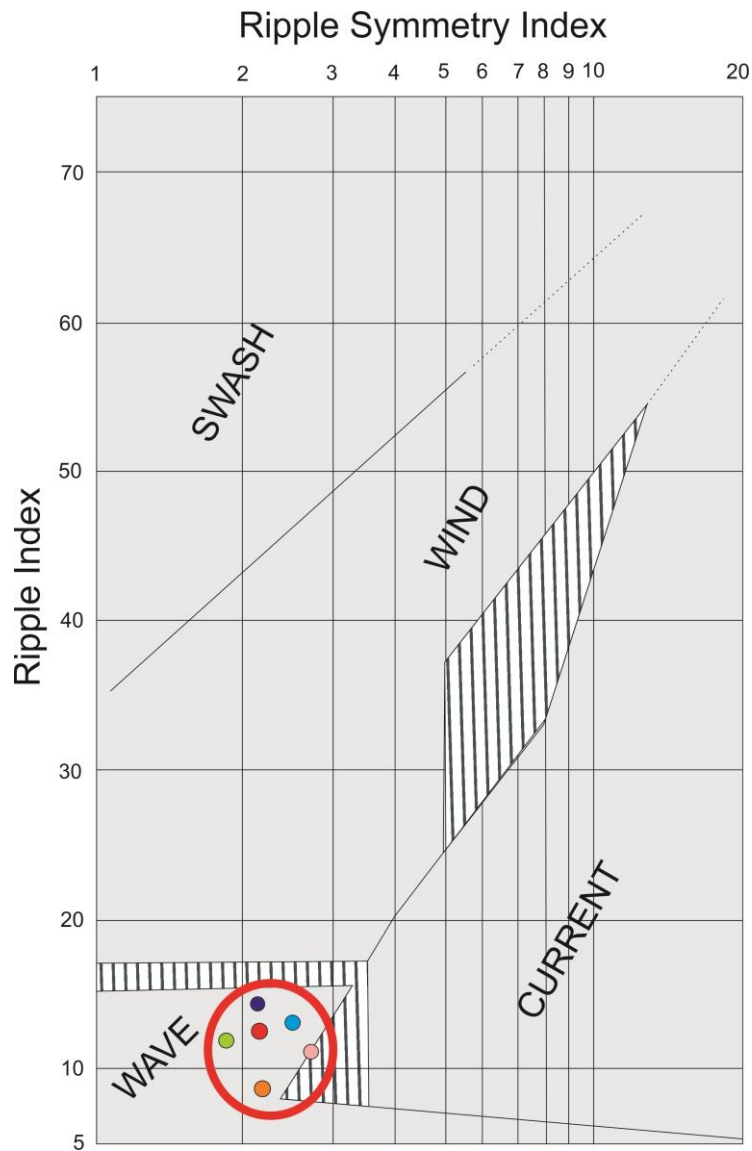


Figure 43: Ripple index and Ripple symmetry index values plotted on the chart with regard to six measurable ripple marks observed on the cores of the uppermost Bedinan Formation sandstone reservoir levels adapted from Tanner (1967).

Parallel laminated sand with thin shale levels (high sand/mud ratio) and sparse bioturbation observed in the cores are the invaluable and commensurate indicator of lower shoreface (dominantly proximal lower shoreface) depositional environment (Reineck, 1980; Charvin et al., 2011; Pemberton et al., 2012).

Besides the sandstone levels, the shale dominant levels between the 1st and the 2nd sandstone levels have also some sedimentary structures to identify depositional environment. Wave to lenticular bedding with some flat lenses showing sparse to moderate bioturbation and low sand/mud ratio are the proxy for offshore transition zone lying between fair weather wave base and storm wave base (Reineck, 1980; Charvin et al., 2011; Vakarelov et al., 2012).

Besides the sedimentary structures and petrographic properties, gamma ray log trend changes with respect to facies distribution may also serve as aid to make reservoir analogy (Siddiqui et al., 2013). This technology gives a clue regarding thickness and geometry of sand body, depositional environment, grain size and lithology. Recent studies indicate that gamma ray trends with left boxcar, right boxcar, funnel shape and irregular shapes with regard to facies distribution are interpreted as wave dominated environment. For instance, sandstone dominated lower shoreface to upper shoreface deposits have left boxcar trend (Siddiqui et al., 2013). Additionally, the right boxcar with sharp boundaries in gamma ray trend is mostly associated with offshore transition to offshore deposits (Siddiqui et al., 2013).

With regard to gamma ray changes in trend throughout the 1st and the 2nd sandstone levels of uppermost Bedinan Formation and shale dominant interbeds, shale dominant levels between the 1st sandstone and 2nd sandstone level and below the 2nd sandstone level are interpreted as deposited in offshore to offshore transition zone (Figure 45) confirming the depositional environment interpretation performed through sedimentary structures.

To sum up, ripple index and ripple symmetry index, sedimentary structures and gamma ray trend evaluation indicate that while the 1st and the 2nd sandstone levels of uppermost Bedinan Formation deposited in lower shoreface to upper shoreface, the shale dominant interval lying between the 1st and the 2nd sandstone levels and below the 2nd sandstone level piled in offshore to offshore transitional environment (Figure 46).

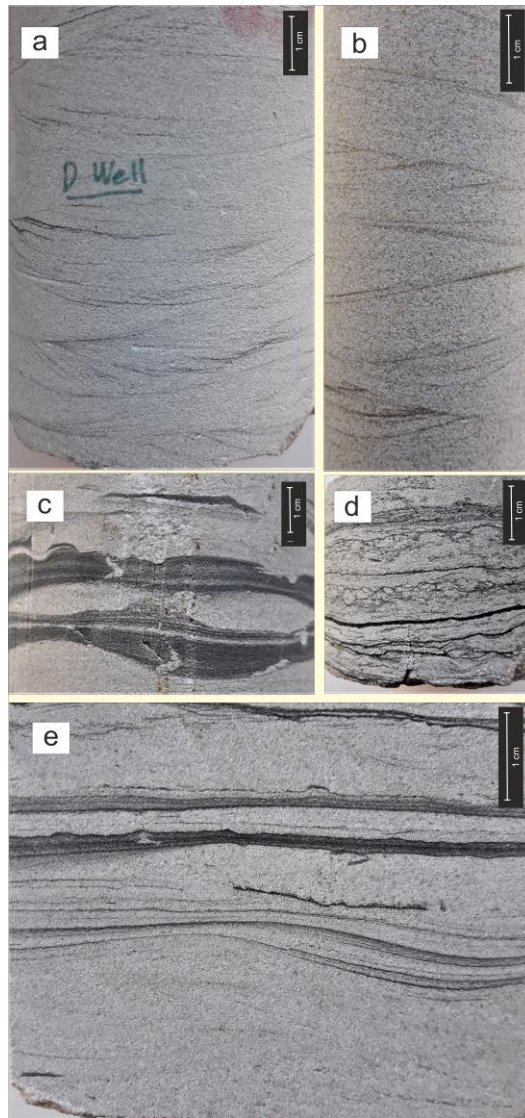


Figure 44: Sedimentary structures observed in the cores of the 1st and the 2nd sandstone levels of the uppermost Bedinan Formation. A: trough cross bedding, b: planar wedge-shaped cross bedding with moderate bioturbation, c: lenticular bedding with bioturbation, d: sand-mud parallel lamination with moderate bioturbation, e: planar sigmoidal cross bedding and parallel lamination.

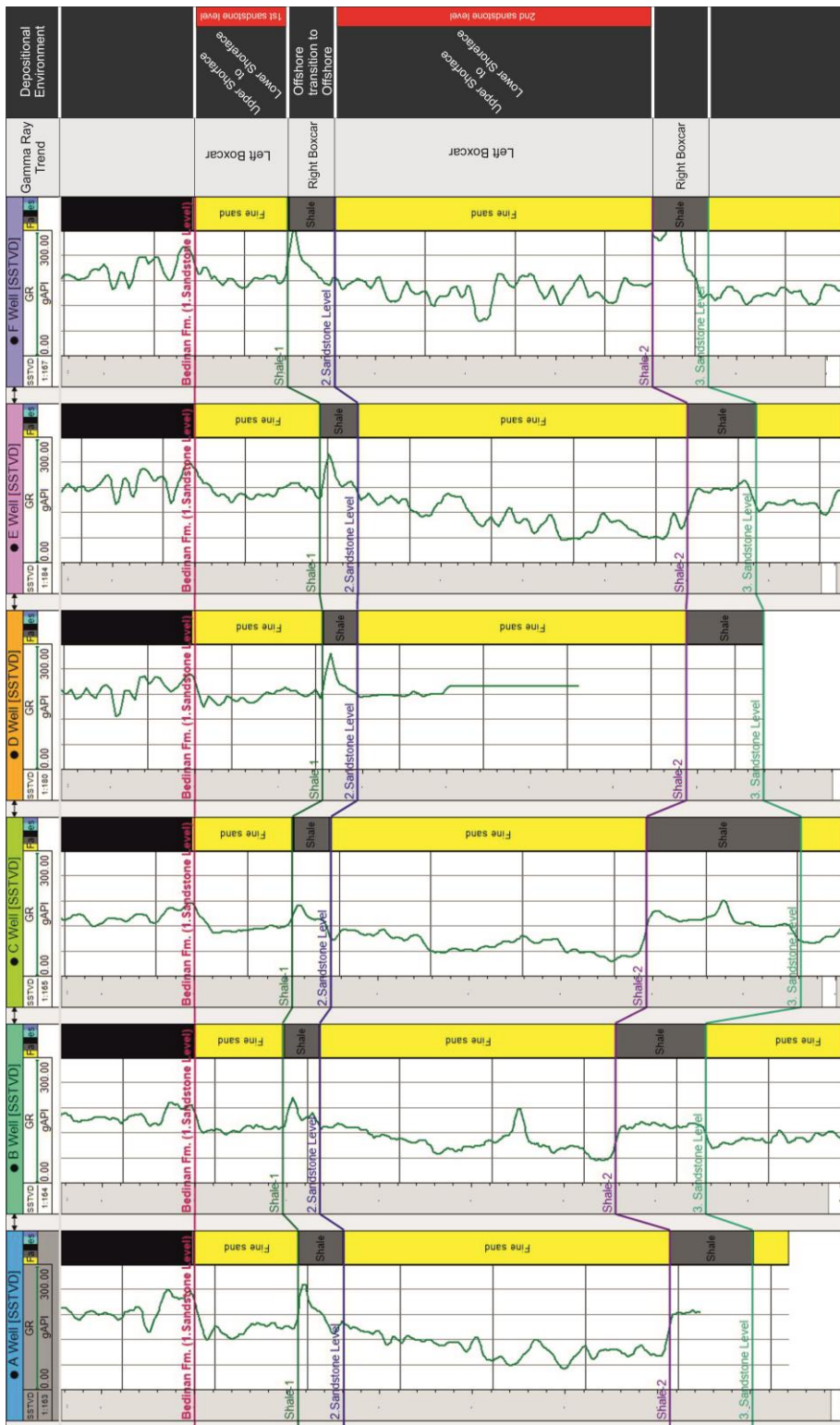


Figure 45: The GR log reading shows left boxcar GR trend of the upper shoreface to lower shoreface in the 1st and 2nd sandstone levels and right boxcar GR trend of offshore transition to onshore shale dominant interlayers (shale-1 and shale-2) of the uppermost Bedinan Formation. Scale: each minor tick space in SSTVD column= 1m. Distance between wells: no scale.

Depositional Environment Model for Ordovician Aged Uppermost Bedinan Formation

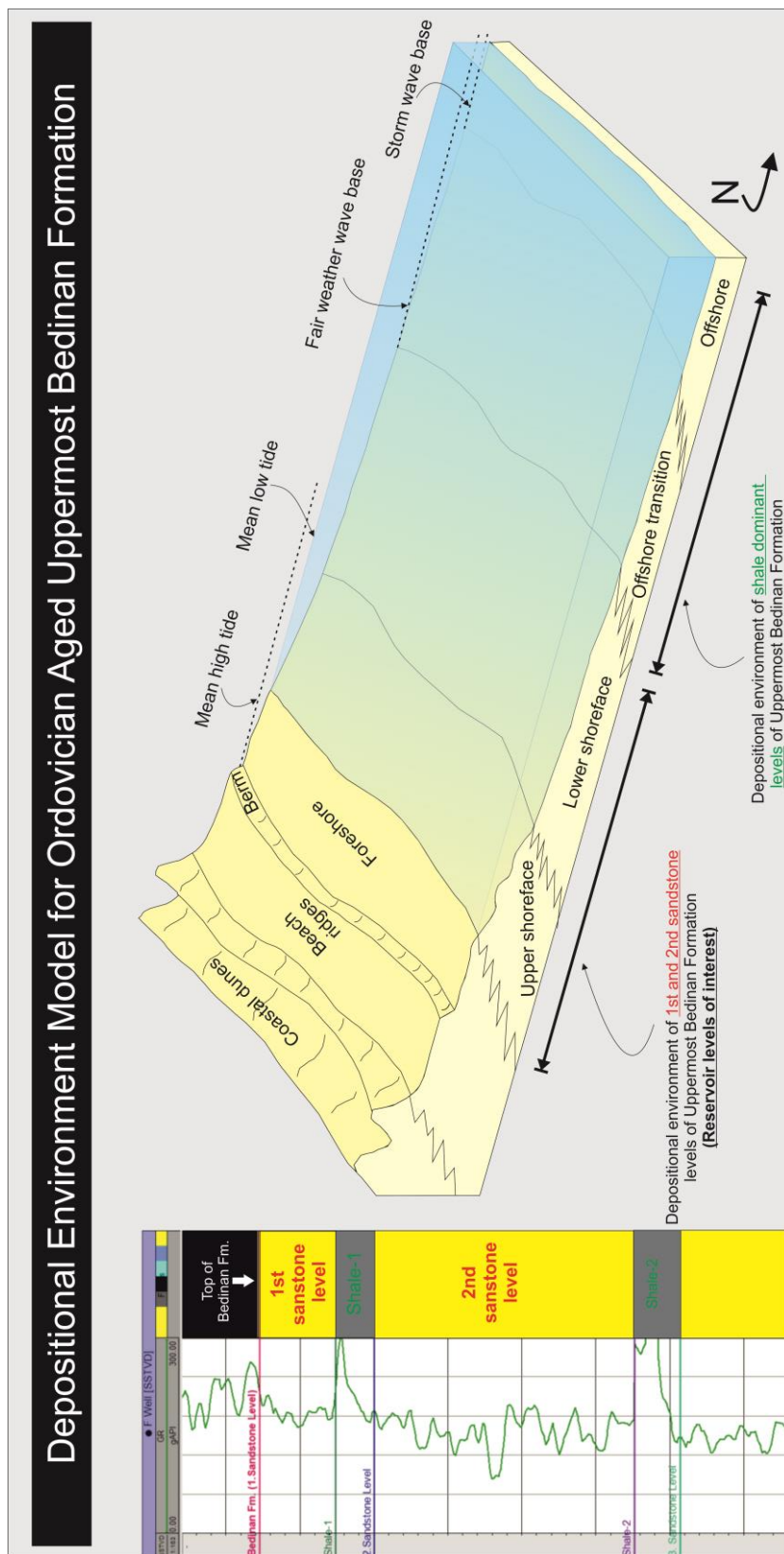


Figure 46: Depositional environment model for the uppermost Bedinan Formation, the 1st and the 2nd sandstone levels and shale interlayers (shale-1 and shale-2).

CHAPTER 5

PALEOGEOGRAPHY

5.1. Late Ordovician Paleogeography

The study area is located the northern periphery of the Arabian Plate that has experienced numerous of tectonic events and also influenced from eustatic sea level change which led to the creation of accommodation space for sedimentary sequences or extensive erosional hiatuses during Phanerozoic (Haq and Al-Qahtani, 2005). During the Paleozoic times, SE Turkey has mostly controlled by eustatic sea level change with the imprints of some big tectonic phenomena such as Variscan orogenesis (Konert et al., 2001).

During Late Ordovician time, when the studied uppermost Bedinan Formation is deposited, Arabian Plate occupies southern high latitudes (Figure 47) and entered glacial episode (Figure 48) which left behind an imprint of glaciation like deeply cut glacial-valleys (Lüning et al 1999; Lüning et al., 2000; Monod et al., 2003; Herrmann et al., 2004; Guiraud et al., 2005; Turner et al., 2005; Haq and Al-Qahtani, 2005; Paris et al., 2007; Ghienne et al., 2007; Haq and Schutter, 2008; Ghienne et al., 2010; Munnecke et al., 2010; Le Heron and Howard, 2010; Laboun, 2010; Masri, 2017; Torsvik and Cocks, 2013; Boulila et al., 2018). Glaciation and global cooling resulted in eustatic sea level fall started in the Middle to the Late Katian and reached its highest level (Figure 49) at Hirnantian (Munnecke et al., 2010). Hirnantian glaciation is responsible for disappearance of %85 marine fauna and stated as second largest mass extinction cause after Permo-Triassic event. The fauna such as Hirnantia brachiopod fauna and the Dalmanitia trilobite fauna which are survived and adapted to cool conditions are very sparse. The great mass extinction during Hirnantian stage has been causally linked to two reasons, namely onset of ice body centered Northern African

margin, and melting of ice sheet close to Silurian-Ordovician boundary (Lüning et al., 2000; Guiraud et al., 2005; Delabroye and Vecoli, 2010; Le Heron and Howard, 2010).

Aparts from latitudinally-controlled faunal and flora provinces (Delabroye and Vecoli, 2010, Munnecke et al., 2010) and glaciogenic sedimentary features such as till, erratics and moraines, another substantial method to reveal climate change during geological evaluation is atmospheric CO₂ level. The enhanced studies indicate that the large CO₂ drawdown in Late Ordovician (Hirnantian) is commonly associated with onset of cooler to glacial condition (Elise Nardin et al., 2011, Lefebvre et al., 2010; Ettensohn, 2010; Pohl et al., 2014).

The region subjected to short-lived (less than 1m. yr.) glacial activity covers large-extended area of Northern Gondwana and lies from Moritania to Turkey (Lüning et al., 1999; Lüning et al., 2000; Monod et al., 2003; Guiraud et al., 2005; Turner et al., 2005; Ghienne et al., 2007; Paris et al., 2007; Le Heron et al., 2006; Delabroye and Vecoli, 2010; Munnecke et al., 2010; Ghienne et al., 2010; Le Heron and Howard, 2010; Laboun, 2010; Torsvik and Cocks, 2013; Saberi et al., 2016; Öztürk et al., 2016; Gürsu et al., 2017; Masri, 2017).

The Hirnantian aged glacio-marine deposits (The Halevikdere Formation) crops in the central Taurus range (Silifke-Ovacık, Akyaka-Anamur, Kemer-Antalya), the eastern Taurus range (Sariz-Kayseri, Tufanbeyli-Adana, Kozan-Adana, Feke-Saimbeyli-Adana), Southeastern Turkey (Kızıltepe-Mardin), and consist of diamictites, lonestones (granules to cobbles) and granitic pebbles (Monod et al., 2003; Paris et al., 2007; Ghienne et al., 2010; Gürsu et al., 2017). The glaciation-related deposits (The Halevikdere Formation) in Mardin region (Bedinan/Yurteri section) are comprehensively defined from the outcrop samples. The Halevikdere Formation in the section starts with the glaciomarine outwash deposits such as crudely bedded conglomeratic sandstone to sandy diamictites, coarse-grained sandstone lenses, quartz pebbles and some boulders (granites, rhyolites), and grades to the distal glaciomarine to offshore shelf deposits including some gravels (0,5-5 meters in diameter), quartz

granules at the bottom, the intercalation of sandstone, siltstone and shale (Paris et al., 2007; Ghienne et al., 2010).

The glaciogenic sediments (The Halevikdere Formation) in the Late Ordovician (Hirnantian) strata are also recognized in the well, Ceylanpınar-1 (Paris et al., 2007; Ghienne et al., 2010). However, it would be difficult to extend the glacial ice sheet to the study area and Diyarbakır basin due to the following possible reasons;

1a-) The isostatic response to ice sheet loading event causes to isostatic downwarping and strong paleorelief in subglacial units (Le Heron et al., 2006; Zieba and Grøver, 2016; Martini et al., 2011; Dietrich et al., 2018). However, the subglacial deformations such as the gravitational load structures in response to ice overriding are not observed in the surface of the Bedinan Formation according to seismic interpretations (Figure 51).

1b-) Diapirism (Sediment diapirs) may occur just after the retreat of ice sheet (Martini et al., 2011). Thus, ice sheet related topographic relief causes to stratigraphic thickness variation for the overlying subsequent units, reflecting the topography of underlying glacial deposits. However; with regard to the seismic interpretation and well to well stratigraphic correlations, almost no sudden change is seen in thickness of overlying basal (hot shale) level of Silurian-Devonian aged Dadaş Formation (Figure 51, Figure 52).

2-) The glacio-fluvial paleovalleys are formed by the ice sculpting in the Late Ordovician units (The Memouniat Formation, The Sarah Formation) of Morocco, Algeria, Libya, Tunisia, Chad, Sudan (Lüning et al., 1999, Turner et al., 2005; Le Heron et al., 2006; Martini et al., 2011), Jordan and Saudi Arabia (Masri, 2017). Therefore, the basal section of the Silurian aged Tanezzuft Formation deposited on paleodepressions (Lüning et al., 1999; Le Heron et al., 2006) (Figure 50) which is responsible for patchy-like stratigraphic distribution and stratigraphic thickness variation of the basal section of Tanezzuft Formation. However, the concordant reflection at the boundary of Bedinan-Dadaş Formations in the east-west seismic line

(Figure 51), and the fact that the uppermost sandstone levels of the Bedinan Formation is easily correlable according to wireline log readings and the well side observations in the wells (A, B, C, D, E, F) of the study area (Figure 53) deny subaerial exposure and subglacial erosion of the platform.

3-) The advance of ice body induces to syn-sedimentary thrust and fold belts in ice-marginal areas (Martini et al., 2011). However, no deformation related with ice bulldozing is present in the Bedinan Formation according to seismic interpretations (Figure 51).

4-) Glacio-related (subglacial, englacial, supraglacial, proglacial) sediments such as till/tillite (Monod et al., 2003; Paris et al., 2007; Ghienne et al., 2010; Martini et al., 2011) are not present in the full-diameter cores and the cutting samples collected from the uppermost Bedinan Formation sandstone levels in the studied wells (A, B, C, D, E, F).

5-) The occurrence of glaciers induces the increment of the salinity in ice distal area. Additionally, the units having direct contact with ice sheet may be expected to include fresh water due to exposure. However, the sandstone reservoir levels of the uppermost Bedinan Formation consist of hypersaline (brine water, ~120.000 ppm) formation water.

The above accentuated items indicate that the uppermost Bedinan Formation does not include the ice-related structures, the deformations and the glaciogenic sediments. Ice distal glaciomarine environment to offshore can be inferred to the depositional environment of the uppermost Bedinan Formation. Some dropstones formed by melting of floating ice sheet may be encountered in more detailed studies for the uppermost part of Bedinan Formation.

Consequently, the reservoir quality variation in the uppermost Bedinan Formation sandstone levels can not be linked to ice-related activity due to the fact that the ice-body did not reach the Diyarbakır Basin during Hirnantian.

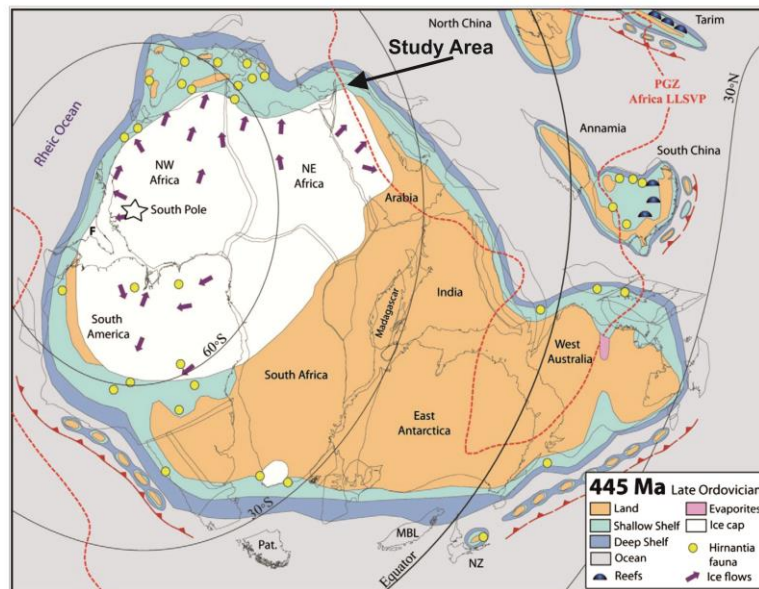
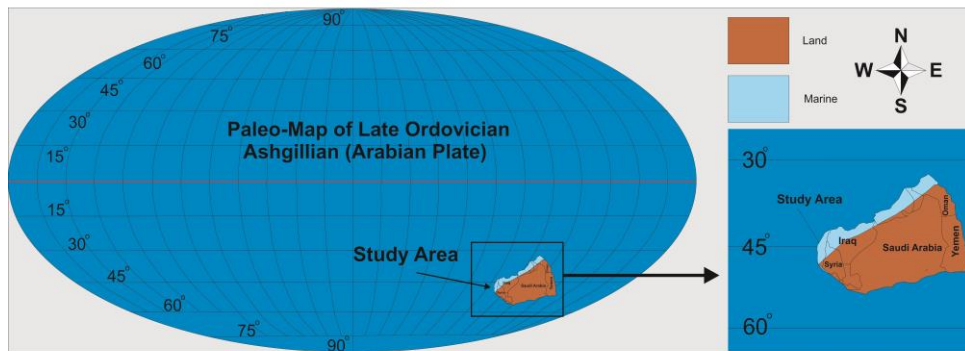
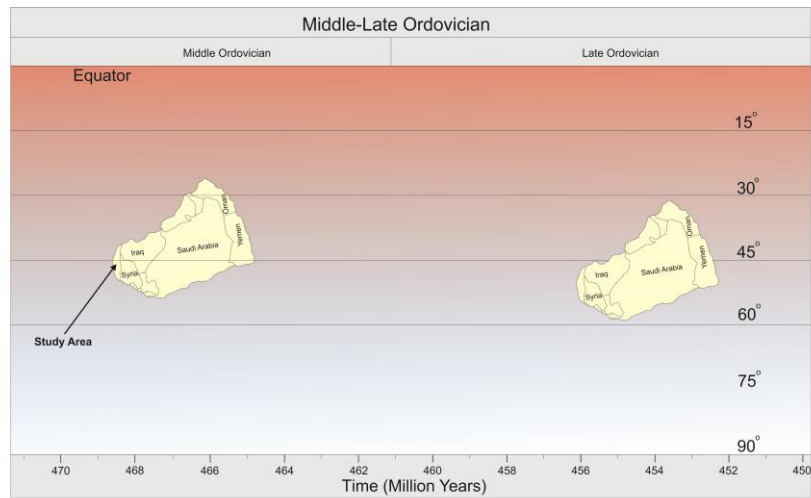


Figure 47: Late Ordovician (Hirnantian) paleogeographic map of Gondwana and relative position of Arabian plate and the study area. Adapted from Scotese (2014) and Torsvik and Cocks (2013).

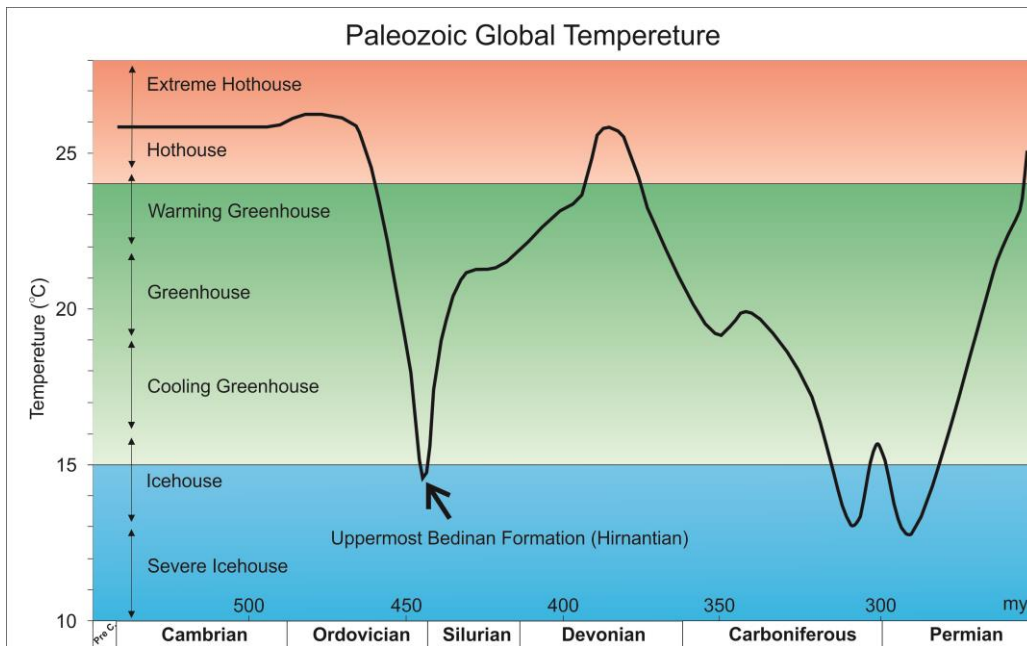


Figure 48: Paleozoic global temperature curve and the temperature at which the uppermost Bedinan Formation deposited (Scotese, 2015).

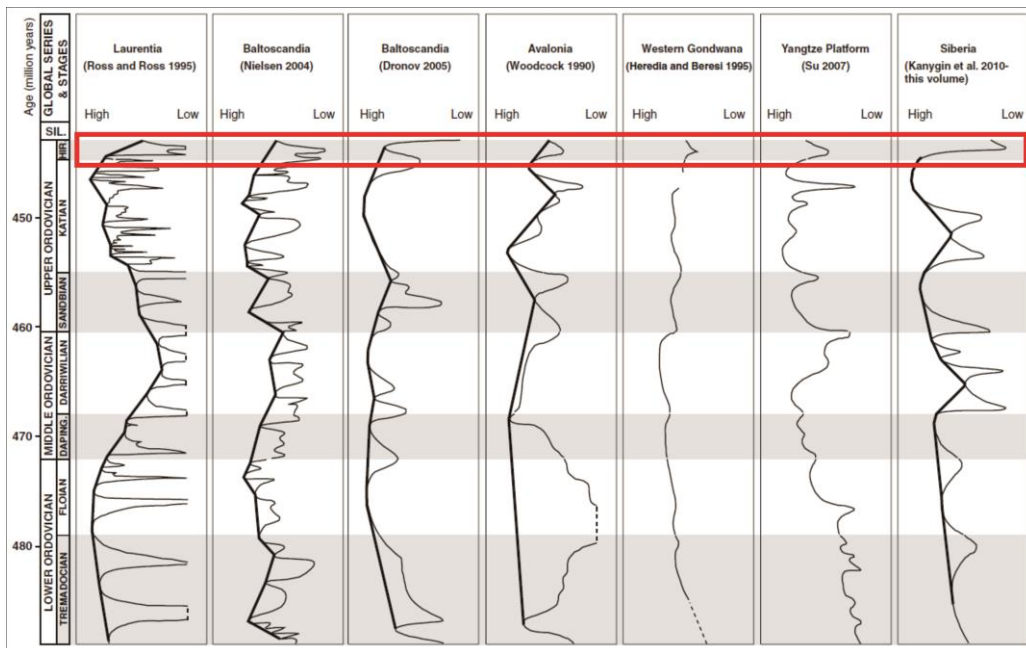


Figure 49: Regional sea level change studies for the Ordovician (Munnecke et al., 2010). The red rectangle is time interval when the studied levels deposited.

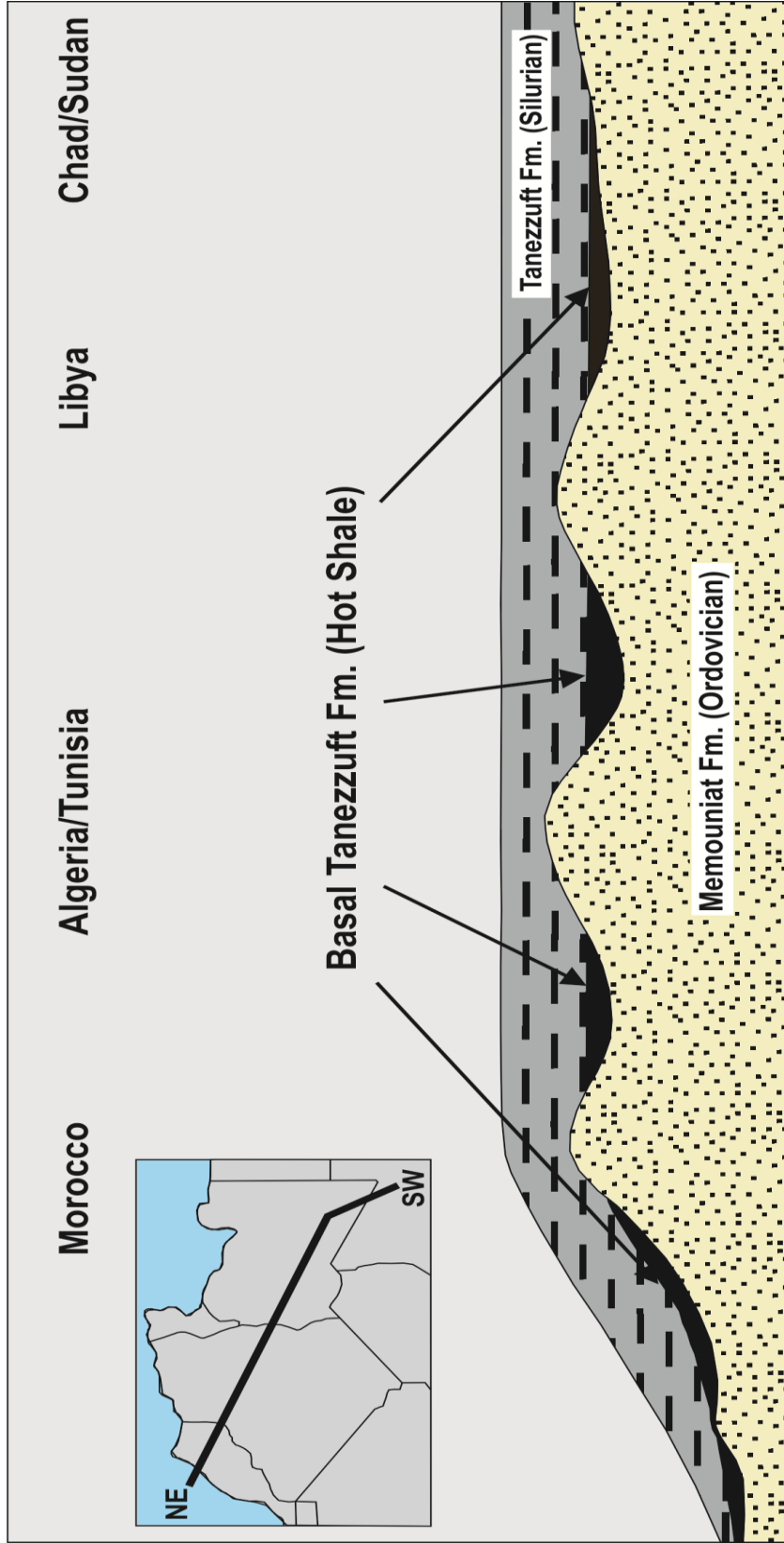


Figure 50: Relative thickness variation of the Early Silurian aged Basal Tanezzuft Formation due to paleodepressions attributed with ice activity. (Lüning et al., 1999).

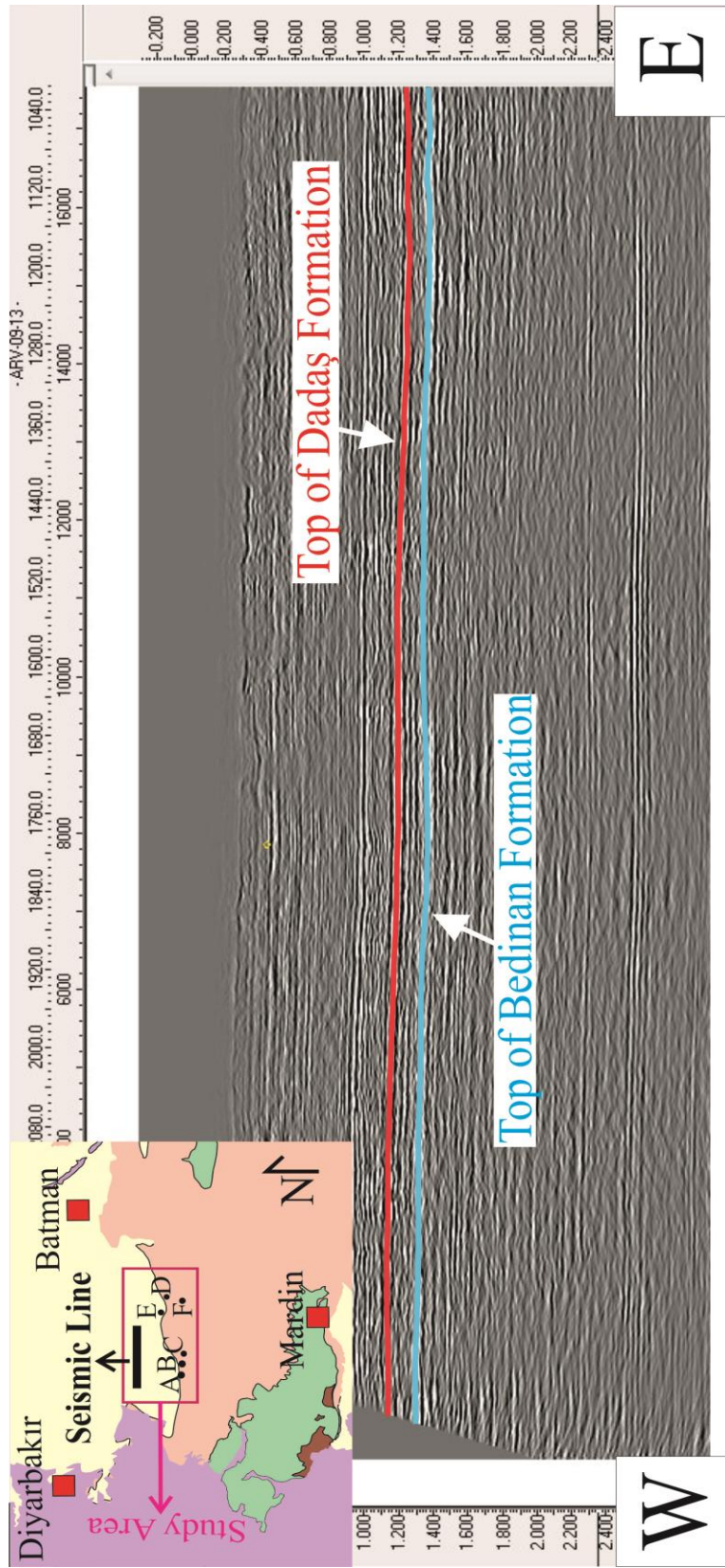


Figure 51: E-W seismic line across the northern side of the study area. Parallel seismic reflections of the Silurian organic rich Dadaş Formation and the Bedinan Formation clastic levels denotes subaerial exposure and glacial activity. The seismic data is obtained from Çalık Petrol database.

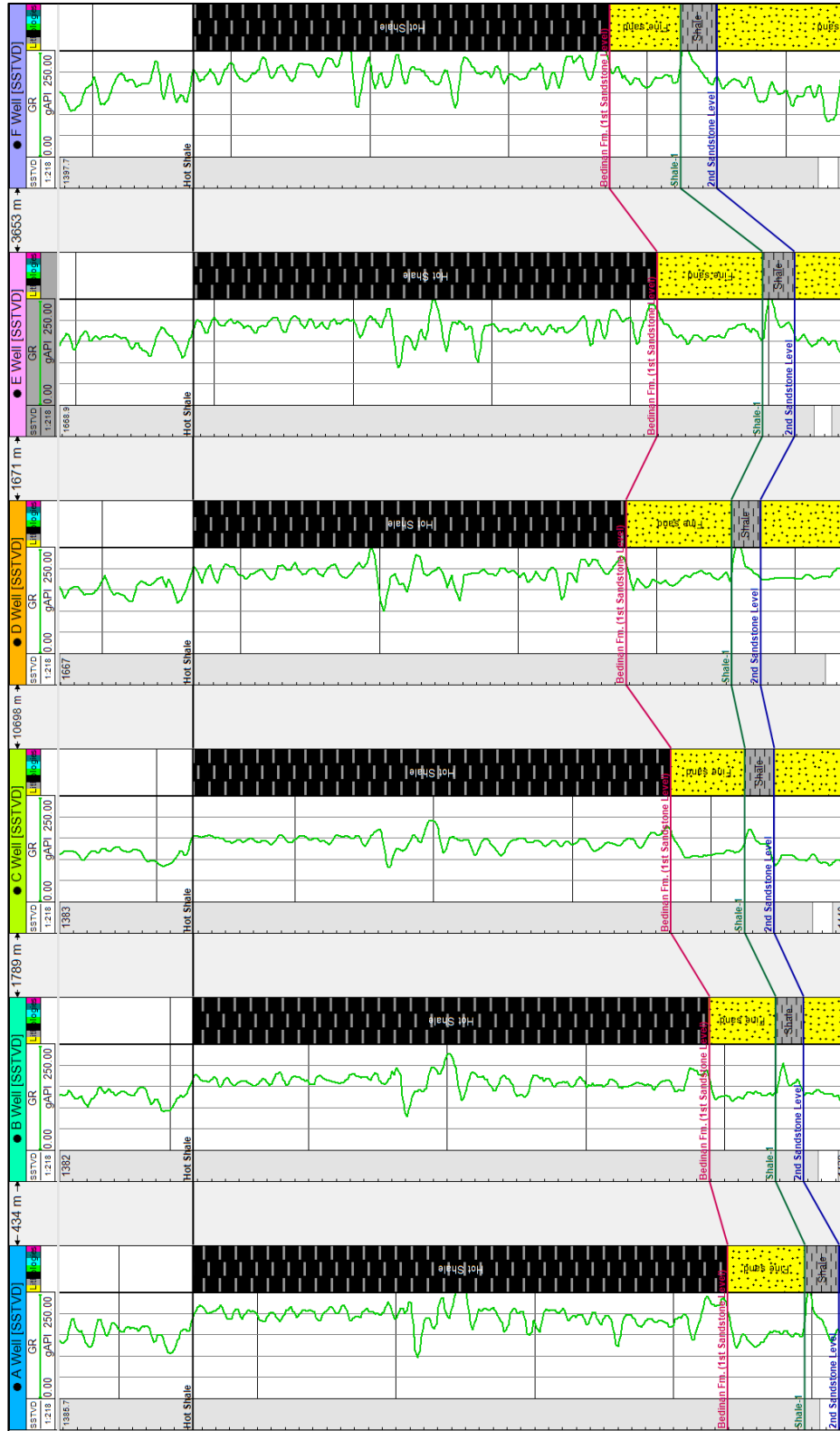


Figure 52: The correlation of the “Hot Shale” level of the Silurian aged Dadaş Formation in the studied wells (A, B, C, D, E and F). Each minor tick in SSTVD column corresponds to 1 meter. The wireline log data from Çalık Petrol database.

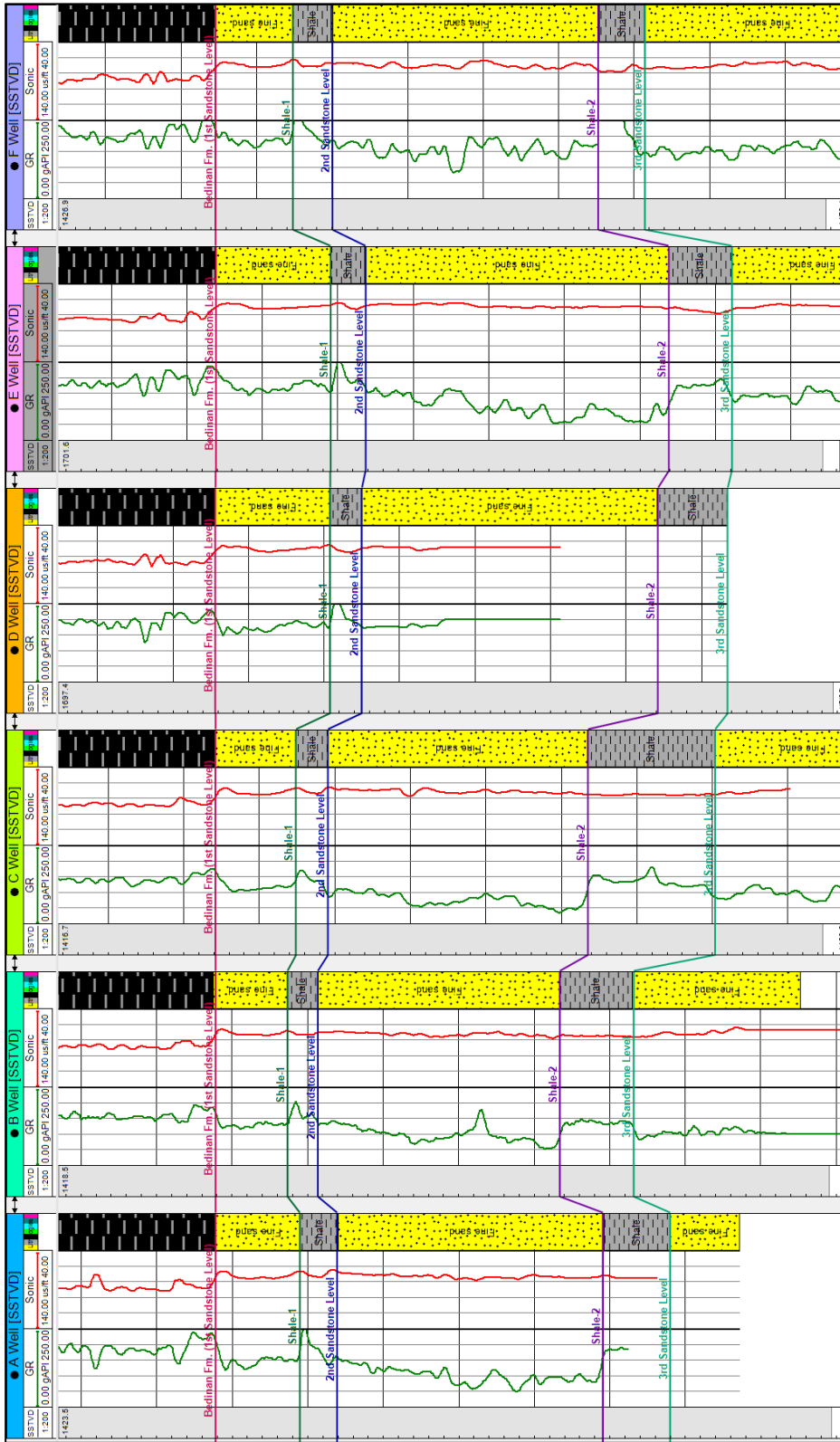


Figure 53: The uppermost Bedkhan Formation 1st and 2nd sandstone reservoir levels are correlable which is justified by GR and Sonic wireline log readings. This fact denies the ice activity on the levels of interest. Scale: each minor tick space in MD column= 1 m. The well logs data is obtained from Çalık Petrol database.

CHAPTER 6

RESERVOIR HETEROGENEITY

The relative variation in porosity, permeability and capillary pressure rates infers to reservoir heterogeneity and exerted great control on planning and determining well stimulation methods to increase hydrocarbon production rate, flow rate and recovery (Worden and Morad, 2000; Worden and Barclay, 2003; Ajdukiewicz and Lander, 2010; Morad et al., 2010; Al-Laboun et al., 2014, Worden et al., 2018). The scale and extent of reservoir heterogeneity (Figure 54) are hosted in many questions and has still subjected to debate.

Because of the fact that porosity and permeability are the key parameters for petroleum reservoirs to recover hydrocarbon, comprehensive and rasterized 3D modeling of reservoir rocks has become a prominent way to perform commercial evaluations.

The recent hydrocarbon discoveries executed in the Ordovician aged Bedinan Formation sandstone levels reveal that the lower Paleozoic petroleum system provides an economic profit opportunity for the petroleum companies. The number of wells penetrated through the Bedinan Formation sandstone reservoir levels allowed geologists to evaluate reservoir quality. The differences in flow rates, volumetric estimations, porosity, permeability, water saturation and formation pressure observed (Table 10,11,12; Figures 55, 56, 57, 58, 59) in Bedinan Formation by A, B, C, D, E and F wells are the most important parameters that push to work on reservoir heterogeneity in detail.

Reservoir quality is characterised as a function of (i) depositional facies (sorting, grain size, grain morphology, sand/mud ratio, provenance, sedimentary structures) (ii) diagenesis (compaction, dissolution, cementation, development of clay coating

minerals) (iii) structural features (fault, fracturing e.t.) (Worden and Morad, 2000; Worden and Barclay, 2003; Ajdukiewicz and Lander, 2010; Morad et al., 2010; Al-Laboun et al., 2014). Although depositional facies and compaction exerted a strong control on reservoir quality of the Bedinan Formation sandstone levels, in this study, reservoir heterogeneity is linked to eodiagenetic (early diagenetic) and dominantly mesodiagenetic (late diagenetic) clay coating minerals, quartz overgrowth and carbonate (calcite and dolomite) cement. The detailed study is carried out on eodiagenetic and mostly mesodiagenetic factors and discussed in detail in next diagenesis chapter.

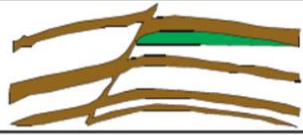
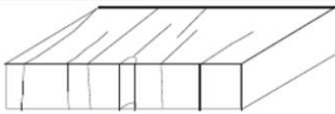
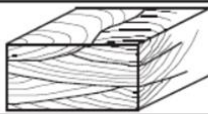
Scale	Reservoir heterogeneity types	
Giga (>300 m)	Sealing to nonsealing faults	
	Fracturing	
Mega (10–100 m)	Genetic unit boundaries	
	Permeability zonation within genetic units	
Macro (in meters)	Baffles within genetic units	
	Sedimentary structures	
Micro (µm)	Microscopic heterogeneity	

Figure 54: Micrometers to hundreds of meters scaled reservoir heterogeneity types with various extend constitutes as a function of depositional facies and diagenetic evaluation (Morad et al., 2010).

Table 10: Vertical and horizontal porosity variation in the 1st and 2nd sandstone levels penetrated in A, B, C, D, E and F wells.

The Studied Levels	A Well		B Well		C Well		D Well		E Well		F Well		
	Depth (m)	Por. (%)	Depth (m)	Por. (%)	Depth (m)	Por. (%)	Depth (m)	Por. (%)	Depth (m)	Por. (%)	Depth (m)	Por. (%)	
1st sandstone level	1	13,33	1	14,27	1	7,49	1	5	1	3,66	1	7,99	
	2	18,72	2	17,46	2	15,59	2	9	2	11,82	2	11,84	
	3	11,43	3	14,13	3	15,02	3	14	3	13,62	3	14,51	
	4	17,96	4	16,60	4	16,21	4	14	4	14,14	4	19,35	
	5	11,64	5	1,63	5	9,83	5	12	5	13,01	5	9,42	
Shale-1	6	0,3	6	2,74	6	0,21	6	13	6	12,87	6	5,45	
	7	1,16	7	12,26	7	1,09	7	6	7	1,24	7	3,8	
2nd sandstone level	8	5,47	8	13,88	8	4,15	8	3	8	3,52	8	7,65	
	9	13,03	9	9,68	9	8,02	9	1	9	4,82	9	13,87	
	10	15,9	10	17,48	10	12,74	10	-	10	7,85	10	19,02	
	11	14,02	11	14,71	11	11,62	11	-	11	9,97	11	12,89	
	12	13,65	12	11,02	12	9,8	12	-	12	9,58	12	11,01	
	13	11,16	13	18,55	13	18,55	13	-	13	7,69	13	15,52	
	14	13,98	14	19,71	14	14,76	14	-	14	5,15	14	14,82	
	15	21,51	15	17,61	15	16,24	15	-	15	9,56	15	21,05	
	16	22,28	16	9,85	16	16,89	16	-	16	13,49	16	4,38	
	17	15,69	17	17,15	17	14,52	17	-	17	12,02	17	4,62	
	18	17,37	18	14,63	18	10,42	18	-	18	13,71	18	14,79	
	19	15,97	19	16,6	19	15,67	19	-	19	14,19	19	18,39	
	20	11,29	20	14,16	20	13,52	20	-	20	13,09	20	20,6	
	21	-	21	-	21	14,66	21	-	21	13,13	21	18,87	
	22	-	-	22	15,46	22	15,46	22	-	22	13,51	22	9,75
	23	-	-	23	15,48	23	15,48	23	-	23	12,87	23	13,08
24	-	-	24	16,45	24	16,45	24	-	24	12,61	24	12,61	
25	-	-	25	-	25	-	25	-	25	12,61	25	12,61	
26	-	-	26	-	26	-	26	-	26	12,74	26	12,74	
27	-	-	27	-	27	-	27	-	27	13,61	27	13,61	
28	-	-	28	-	28	-	28	-	28	13,75	28	13,75	

Explanations:	Por. : Effective Porosity
Assumption:	Depth of the Top of Bedinan Formation: 0 m

Table 11: Vertical and horizontal permeability variation in the 1st and 2nd sandstone levels penetrated in A, B, C, D, E and F wells.

The Studied Levels	A Well		B Well		C Well		D Well		E Well		F Well	
	Depth (m)	Perm. (mD)	Depth (m)	Perm. (mD)	Depth (m)	Perm. (mD)	Depth (m)	Perm. (mD)	Depth (m)	Perm. (mD)	Depth (m)	Perm. (mD)
1st sandstone level	1	0,7622	1	0,4726	1	0,0034	1	0,001	1	0,001	1	0,0744
	2	4,4282	2	1,6191	2	0,3783	2	0,1	2	0,3750	2	1,2572
	3	0,1772	3	0,2567	3	0,1081	3	0,9	3	0,7361	3	5,5413
	4	2,2612	4	0,5591	4	0,2911	4	0,9	4	0,911	4	15,0921
	5	0,2695	5	0,0001	5	0,01	5	0,2	5	0,4633	5	0,3405
Shale-1	6	0,001	6	0,0001	6	0,0001	6	0,08	6	0,9671	6	0,0193
	7	0,001	7	0,0847	7	0,0001	7	0,001	7	0,0001	7	0,0009
2nd sandstone level	8	0,001	8	0,0077	8	0,0001	8	0,0001	8	0,0001	8	0,0339
	9	0,0142	9	0,0002	9	0,0009	9	0,0001	9	0,0001	9	0,7881
	10	0,1728	10	0,1327	10	0,0578	10	-	10	0,0099	10	6,5733
	11	0,0023	11	0,0267	11	0,0299	11	-	11	0,094	11	1,442
	12	0,0015	12	0,0031	12	0,0043	12	-	12	0,0432	12	0,226
	13	0,001	13	0,2704	13	2,3725	13	-	13	0,0001	13	3,0037
	14	0,0412	14	0,4045	14	0,4215	14	-	14	0,0001	14	1,432
	15	2,9606	15	0,1887	15	0,6939	15	-	15	0,0325	15	24,1898
	16	5,6799	16	0,0001	16	0,6459	16	-	16	0,5357	16	0,0517
	17	0,3002	17	0,157	17	0,0842	17	-	17	0,228	17	0,0181
	18	0,3354	18	0,0478	18	0,0098	18	-	18	0,2212	18	3,3135
	19	0,5767	19	0,1243	19	0,5491	19	-	19	0,6406	19	8,2856
	20	0,0056	20	0,0365	20	0,0895	20	-	20	0,2442	20	12,5599
	21	-	21	-	21	0,3003	21	-	21	1,2698	21	9,3471
	22	-	22	-	22	0,7659	22	-	22	1,0776	22	0,5478
	23	-	23	-	23	1,3328	23	-	23	0,3484	23	1,8527
	24	-	24	-	24	1,8531	24	-	24	0,2239	24	-
25	-	25	-	25	-	25	-	25	0,3363	25	-	
26	-	26	-	26	-	26	-	26	0,6458	26	-	
27	-	27	-	27	-	27	-	27	1,2354	27	-	
28	-	28	-	28	-	28	-	28	0,4268	28	-	
Explanations:	Perm. : Permeability											
Assumption:	Depth of the Top of Bedinan Formation: 0 m											

Table 12: Vertical and horizontal water saturation variation in the 1st and 2nd sandstone reservoir levels penetrated in A, B, C, D, E and F wells.

The Studied Levels	A Well		B Well		C Well		D Well		E Well		F Well	
	Depth (m)	Sw (%)	Depth (m)	Sw (%)	Depth (m)	Sw (%)	Depth (m)	Sw (%)	Depth (m)	Sw (%)	Depth (m)	Sw (%)
1st sandstone level	1	33,64	1	42,55	1	70,69	1	98	1	98	1	36,92
	2	29,4	2	37,46	2	49,7	2	90	2	70,32	2	23,81
	3	43,67	3	49,64	3	63,23	3	70	3	68,87	3	18,4
	4	34,91	4	47,96	4	63,45	4	70	4	58,57	4	19,41
	5	39,48	5	100	5	70,7	5	90	5	58,98	5	27,55
Shale-1	6	100	6	74,37	6	100	6	93	6	62,8	6	34,79
	7	100	7	56,3	7	100	7	95	7	100	7	54,48
2nd sandstone level	8	98	8	96,9	8	100	8	100	8	100	8	44,28
	9	78,09	9	100	9	89,72	9	100	9	100	9	36,12
	10	60,32	10	86,79	10	92,54	10	-	10	64,44	10	26,08
	11	91,16	11	94,12	11	93,22	11	-	11	67,56	11	25,7
	12	92,23	12	100	12	93,1	12	-	12	78,59	12	38,92
	13	97,12	13	90,25	13	87,81	13	-	13	92,45	13	25,79
	14	70,64	14	84,12	14	95,82	14	-	14	90,28	14	31,83
	15	56,89	15	89,2	15	100	15	-	15	95,09	15	18,38
	16	65,7	16	1000	16	100	16	-	16	100	16	17,43
	17	75,44	17	100	17	100	17	-	17	91,65	17	76,06
	18	91,58	18	100	18	100	18	-	18	100	18	33,38
	19	100	19	100	19	99,56	19	-	19	100	19	34,77
	20	95,83	20	100	20	100	20	-	20	100	20	31,54
	21	-	21	-	21	100	21	-	21	100	21	35,76
	22	-	22	-	22	100	22	-	22	100	22	47,94
	23	-	23	-	23	100	23	-	23	100	23	36,66
	24	-	24	-	24	100	24	-	24	100	24	-
25	-	25	-	25	-	25	-	25	100	25	-	
26	-	26	-	26	-	26	-	26	100	26	-	
27	-	27	-	27	-	27	-	27	100	27	-	
28	-	28	-	28	-	28	-	28	100	28	-	

Explanations: Sw : Water Saturation

Assumption: Depth of the Top of Bedinan Formation: 0 m

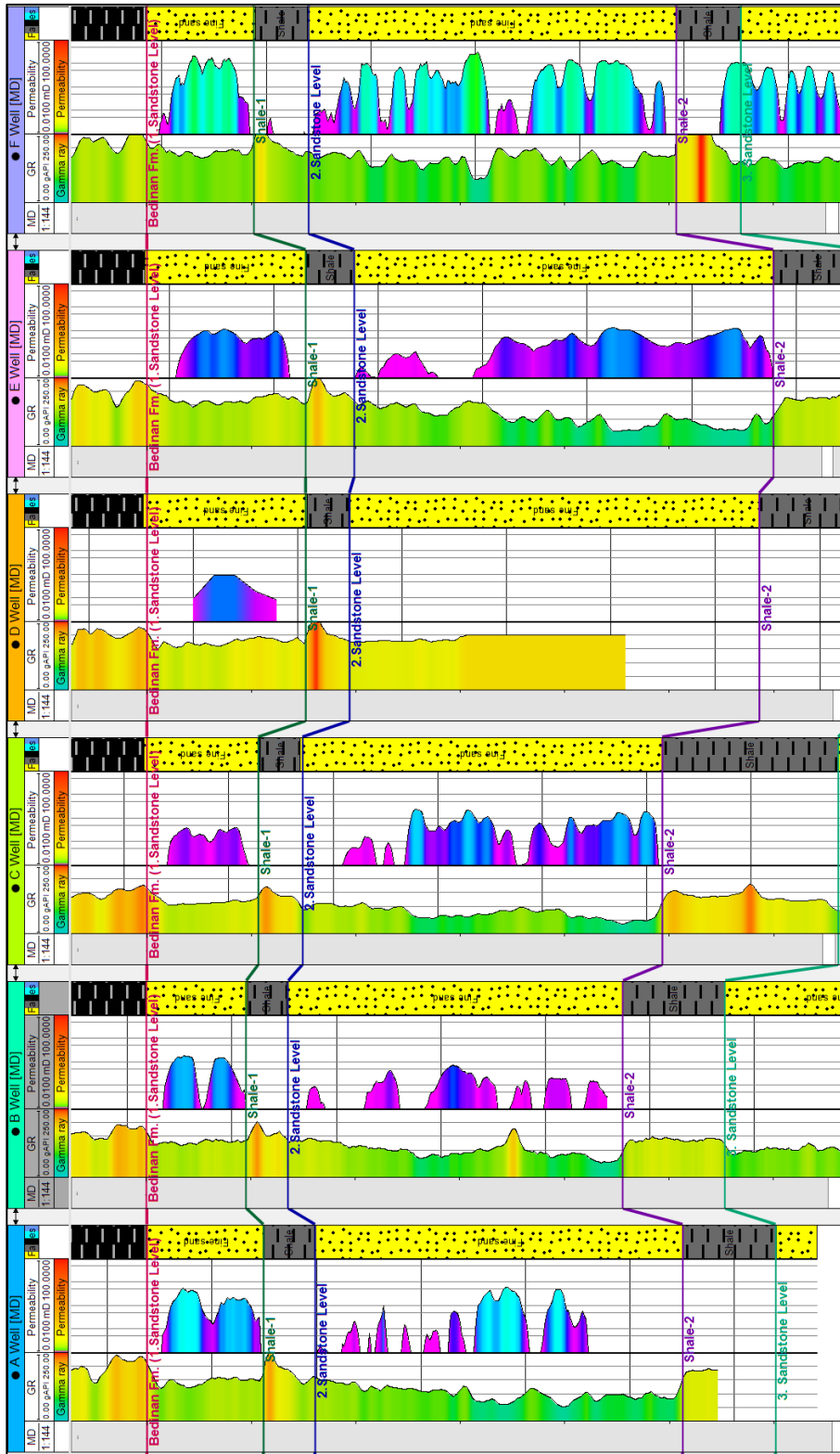


Figure 55: Vertical and horizontal permeability variation and correlation through the 1st and the 2nd sandstone levels of the uppermost Bedinan Formation in A, B, C, D, E and F wells (permeability log in logarithmic scale, minor ticks in MD corresponds to 5 meters). Distance between the wells: no scale.

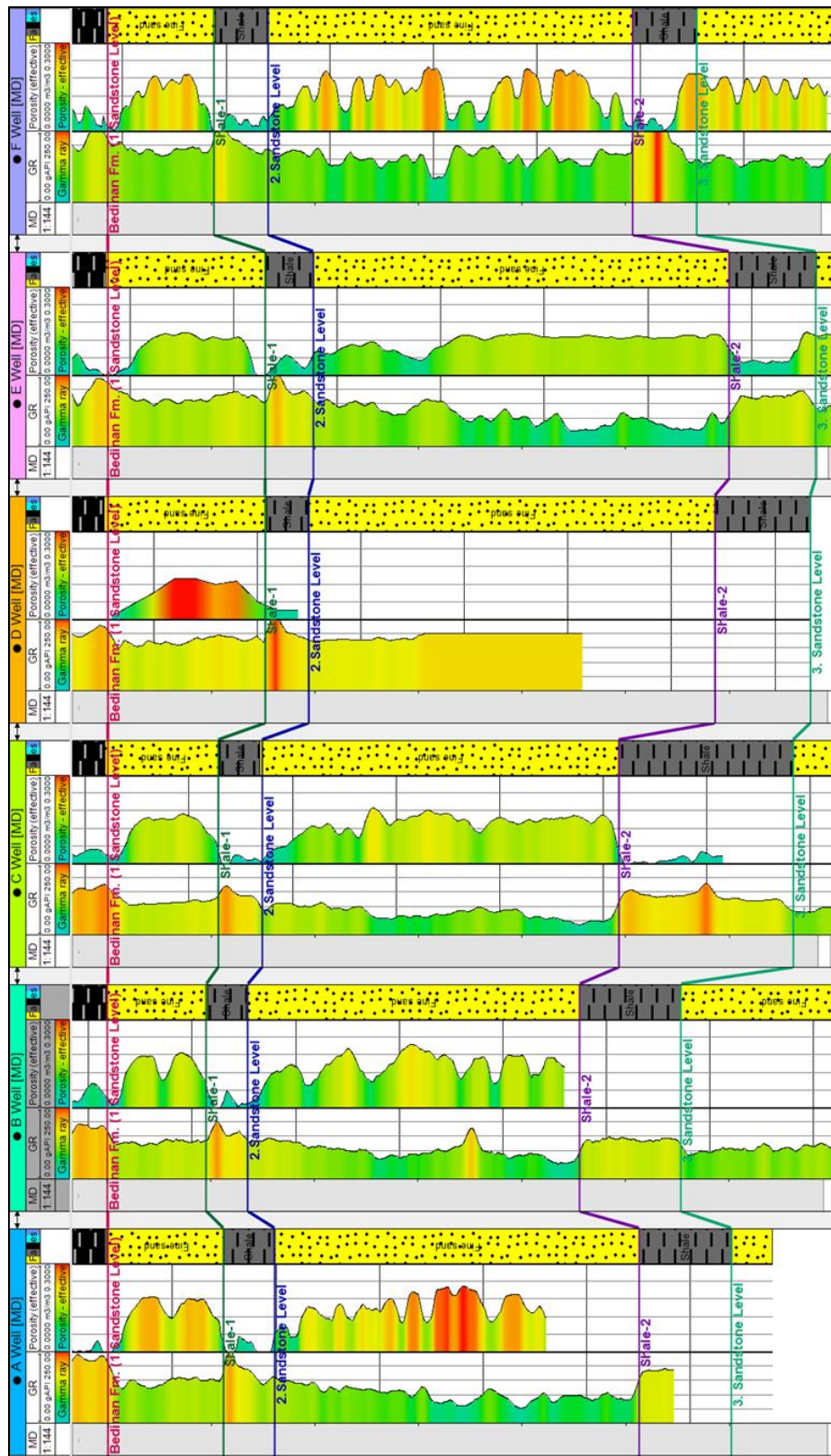


Figure 56: Vertical and horizontal porosity variation and correlation through the 1st and the 2nd sandstone levels of the uppermost Bedinan Formation in A, B, C, D, E and F wells (minor ticks in MD column corresponds to 5 meters). Distance between the wells: no scale. The wireline log data from Çalık Petrol database.

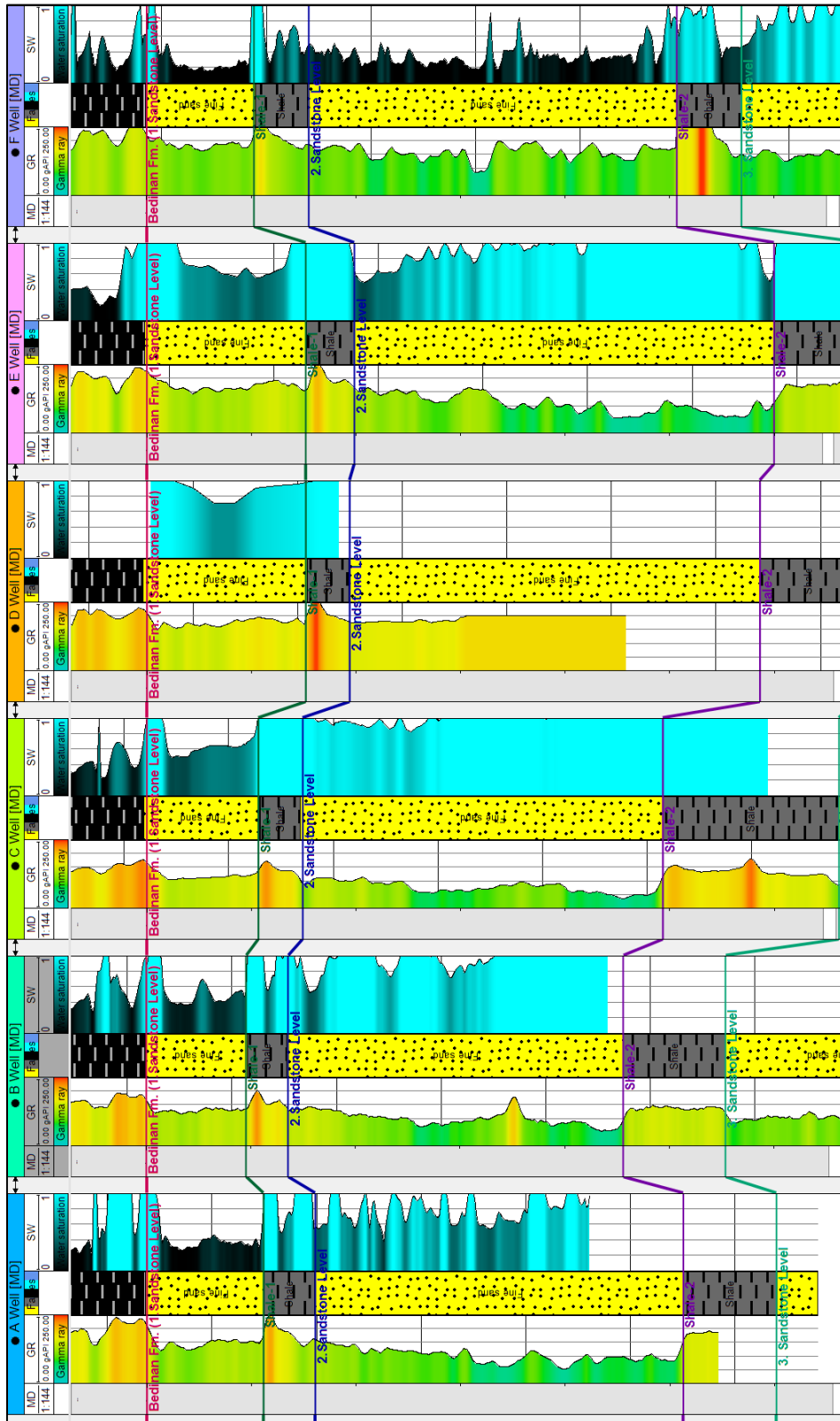


Figure 57: Vertical and horizontal water saturation variation and correlation through the 1st and the 2nd sandstone levels of the uppermost Bedinan Formation in A, B, C, D, E and F wells (minor ticks in MD column corresponds to 5 meters). Distance between the wells: no scale. The wireline log data from Çalık Petrol database.

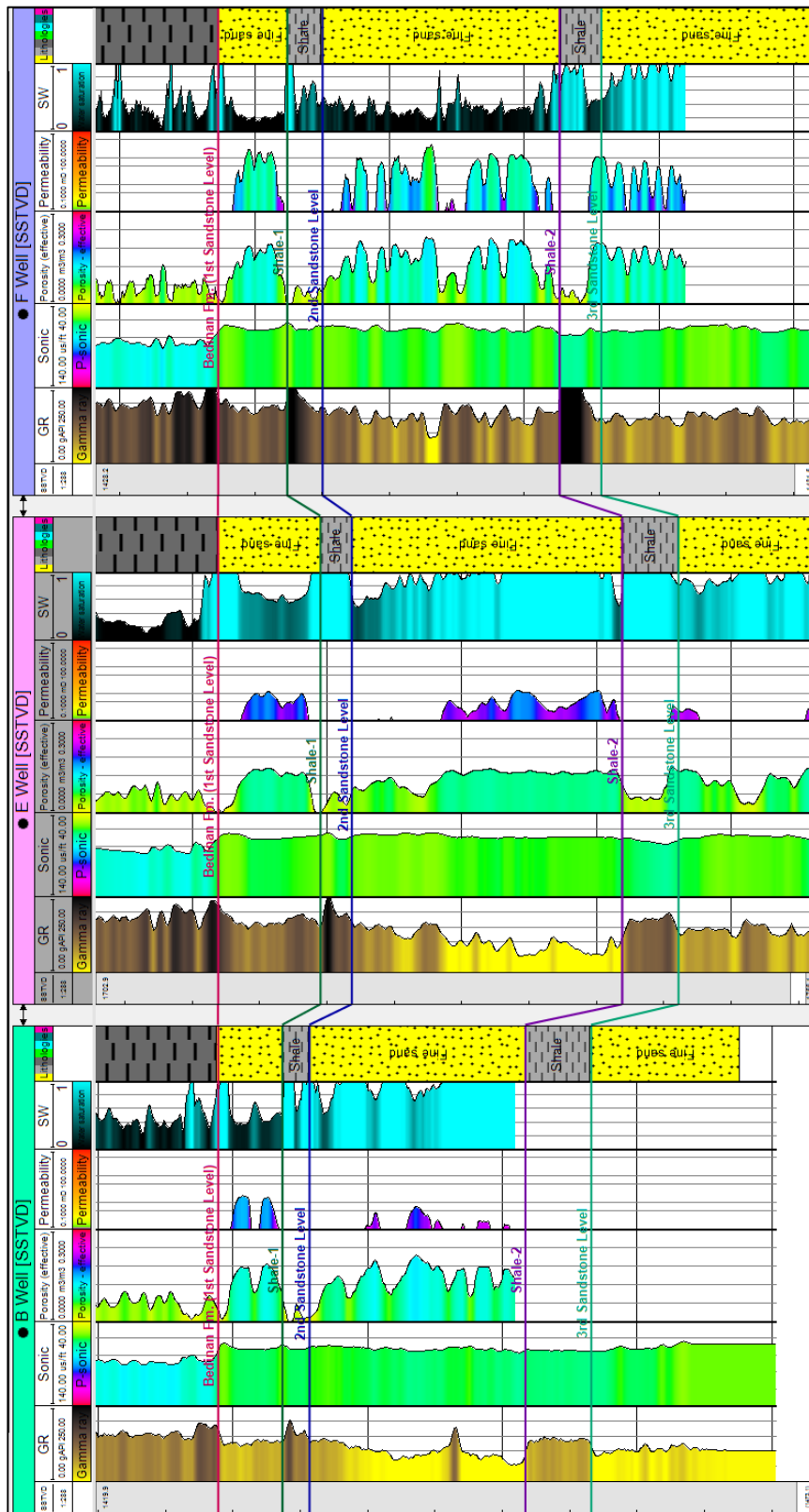


Figure 58: Vertical and horizontal porosity, permeability and water saturation variation and correlation through the 1st and the 2nd sandstone levels of the uppermost Bedinan Formation in B, E and F wells located in different prospects (minor ticks in SSTDV column corresponds to 5 meters). Distance between the wells: no scale. The wireline log data from Çalık Petrol database.

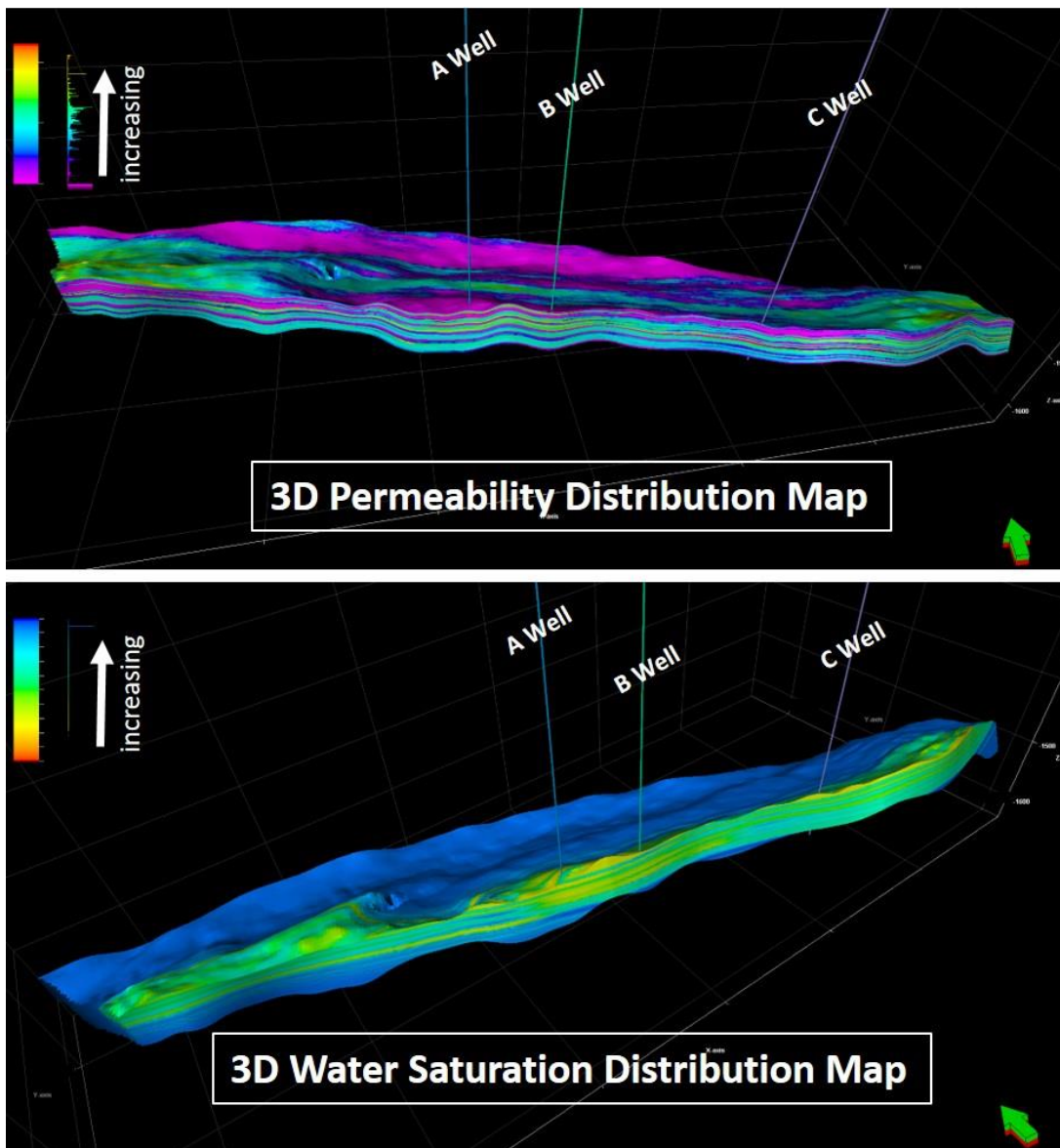


Figure 59: 3D property (permeability, water saturation) modelling of the trapped area where A, B, C wells drilled.

6.1. Statistical Measurements for Reservoir Heterogeneity

A variety of researches have been performed to understand the concept of heterogeneity as a scale-dependent descriptor. Several geostatistical techniques have been identified to quantify heterogeneity of reservoir rocks through heterogeneity measures. In this study, the coefficient of variation, one of the geostatistical methods, was used to describe the heterogeneity in the studied sandstone levels.

6.1.1. Coefficient of Variation

The coefficient of variation (CV) is one of the methods to measure the heterogeneity of the reservoir levels. CV is a measure of standard deviation relative to the mean value and formulated as below (Fitch et al., 2015; El-Deek et al., 2017);

$$CV = \frac{\sigma}{\mu}$$

σ : standard deviation

μ : mean of permeability values

The CV values of permeability distribution in reservoir rock is less than 0.5 in a homogenous medium, between 0.5 and 1.0 in a heterogenous medium and higher than 1.0 in a very heterogenous medium (Lake and Jensen, 1991; Fitch et al., 2015; El-Deek et al., 2017).

The CV values of 2.2805 (Figure 60, Table 13) measured for the studied sandstone levels (penetrated in A, B, C, D, E and F wells) indicate very heterogenous permeability distribution.

Additionally, the CV values of permeability distribution was evaluated in each well to determine the scale of heterogeneity. According to the measurements, the CV values of 1.5968 (A well), 1.6914 (B well), 1.2197 (C well), 1.6756 (D well), 1.2197 (E well) and 1.3069 (F well) indicate very heterogenous medium and heterogeneity in meter scale.

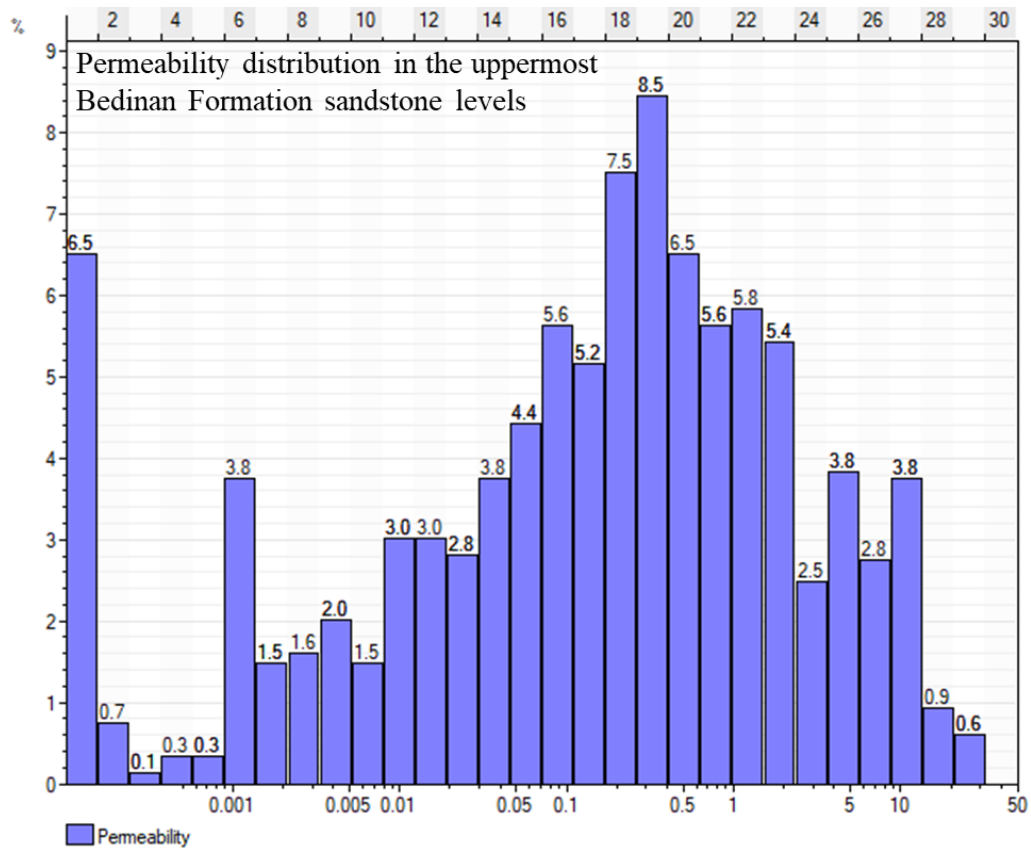


Figure 60: Permeability distribution in the uppermost Bedinan Formation penetrated in A, B, C, D, E and F wells (x axis: permeability, y axis: percentage of permeability distribution).

Table 13: Statistical measurements for the heterogeneity index of the studied sandstone levels.

Statistics for Permeability (A, B, C, D, E, F Wells)			
Axis	Min	Max	Delta
Permeability	0,0001 mD	31,8408 mD	31,8407 mD
Number of defined values:	1475		
Mean:	1,468965		
Standard deviation :	3,3501		
Variance:	11,2232		
CV (Coefficient of Variation):	2,2805		
Heterogeneity:	Very heterogeneous		

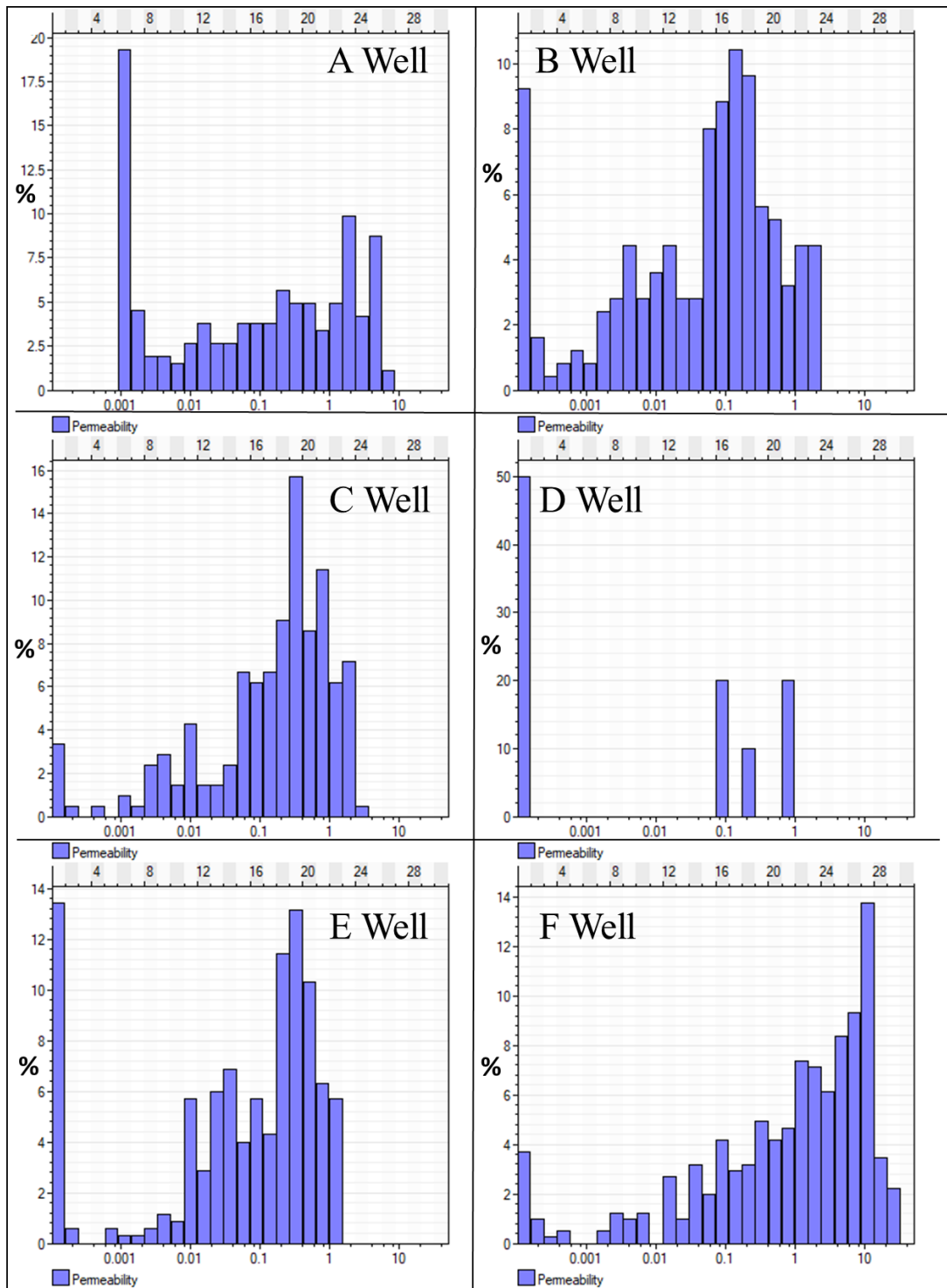


Figure 61: Permeability distribution in the uppermost Bedinan Formation in each well (x axis: permeability, y axis: percentage of permeability distribution).

Table 14: Statistical measurements for the heterogeneity index of the sandstone levels penetrated in each studied well.

Statistics for Permeability (A Well)				Statistics for Permeability (B Well)			
Axis	Min	Max	Delta	Axis	Min	Max	Delta
Permeability	0,001 mD	6,0119 mD	6,0109 mD	Permeability	0,0001 mD	1,8013 mD	1,8012 mD
Number of defined values:	264			Number of defined values:	249		
Mean:	0,9157			Mean:	0,2489		
Standard deviation :	1,4622			Standard deviation :	0,4210		
Variance:	2,138			Variance:	0,1772		
CV (Coefficient of Variation):	1,5968			CV (Coefficient of Variation):	1,6914		
Heterogeneity:	Very heterogeneous			Heterogeneity:	Very heterogeneous		

Statistics for Permeability (C Well)				Statistics for Permeability (D Well)			
Axis	Min	Max	Delta	Axis	Min	Max	Delta
Permeability	0,0001 mD	2,3725 mD	2,3724 mD	Permeability	0,0001 mD	0,9 mD	0,8999 mD
Number of defined values:	210			Number of defined values:	10		
Mean:	0,4477			Mean:	0,2180		
Standard deviation :	0,5461			Standard deviation :	0,3653		
Variance:	0,2982			Variance:	0,1335		
CV (Coefficient of Variation):	1,2197			CV (Coefficient of Variation):	1,6756		
Heterogeneity:	Very heterogeneous			Heterogeneity:	Very heterogeneous		

Statistics for Permeability (E Well)				Statistics for Permeability (F Well)			
Axis	Min	Max	Delta	Axis	Min	Max	Delta
Permeability	0,0001 mD	1,3575 mD	1,3574 mD	Permeability	0,0001 mD	31,8408 mD	31,8407 mD
Number of defined values:	350			Number of defined values:	407		
Mean:	0,2497			Mean:	4,1217		
Standard deviation :	0,3120			Standard deviation :	5,3869		
Variance:	0,0973			Variance:	29,0183		
CV (Coefficient of Variation):	1,2197			CV (Coefficient of Variation):	1,3069		
Heterogeneity:	Very heterogeneous			Heterogeneity:	Very heterogeneous		

CHAPTER 7

CLAY TYPING BASED ON PETROPHYSICAL METHODS

The physical separation of the different clay minerals has many difficulties due to the overlapping range of properties like density (Table 15) (Totten et al., 2002). XRD (X-ray Diffraction) and SEM (Scanning Electron Microscopy) are the most comprehensive methods to understand the clay coating minerals and their morphology. Besides these methods, enhanced well logging technology enables the collection of geological data as in the collection of geophysical and geochemical data. In this chapter, the clay coating mineral and their type is discussed by the use of petrophysical methods.

Table 15: Density range of clay minerals (Tottens et al., 2002).

Clay mineral group	Density range (g/cc)
Smectites	2.0 - 2.6
Illites	2.6 - 2.9
Kaolinites	2.61 - 2.68
Chlorites	2.6 - 3.3
Muscovites	2.77 - 2.88

Spectral gamma-ray (SGR) logs being well established tool, enables the differentiation of three radioactive elements (potassium ‘K’, thorium ‘Th’ and uranium ‘U’) sourced from the corresponding strata. Not only SGR high-resolution log data but also photoelectric factor (Pefz) log serve as proxies for determining the type of clay content in the sandstone levels of interest (Schlumberger, 2009; Nabawy and Sharawy, 2015; Klaja and Dudek, 2016). In the present study, Thorium (ppm) –

Potassium (%) and Pefz – Potassium (%) cross plots proposed by Schlumberger (2009) are used to designate the type of clay in the studied sandstone levels. Besides, the sandstone levels (1st and 2nd sandstone levels of uppermost Bedinan Formation) in D well have high clay content and high water saturation, enhanced SGR readings are selected to identify clay mineral associations as a reference. The numerical values of Thorium (ppm), Potassium (%), Pefz wireline log data of D well for the sandstone level of interest are plotted on Potassium (%) – Thorium (ppm) (Figure 62) and Potassium (%) - Pefz charts (Figure 63). Although XRD and SEM give a more accurate result for relative proportion of clay mineral association, petrophysical logging interpretation is also widely used as an aid to determining the discrimination of clay minerals. Additionally, the depositional environment, the provenance, the paleogeography of the studied intervals during the time of deposition may be used as auxiliary data to reach decisive result in terms of clay type of matrix. Collation of Tho/K – Tho/U ratio plot (Figure 64) is an additional indicator of the clay type as well as depositional environment prevailed during deposition of the sandstone levels of interest. Plotting the numerical concentration value of radioactive elements (thorium (ppm), potassium (%), uranium (ppm)) on the cross plot indicate that the clay coating minerals forming the matrix of the 1st and 2nd sandstone levels of uppermost Bedinan Formation are in turn illite and mixed clay layer. Additionally, mostly shallow marine environmental conditions were predominant in accordance with Tho/U ratio plots. However, uranium is exclusively concentrated in organic matter content of shale or carbonates, not directly linked to the clay contamination (Klaja and Dudek, 2016), so Tho/U ratio can skew the depositional environment interpretation of the studied intervals. Thus, Tho/U ratio plot cannot be a unique tool to determine depositional environment except organic rich rocks. The three cross plots (Thorium (ppm) - Potassium (%), Thorium (ppm) - Pefz, Thorium (ppm)&Potassium (%) – Thorium (ppm)&Uranium (ppm)) ensure that, the clay mineral associations in the sandstone levels of uppermost Bedinan Formation of interest is in order of abundance by illite and mixed clay layer.

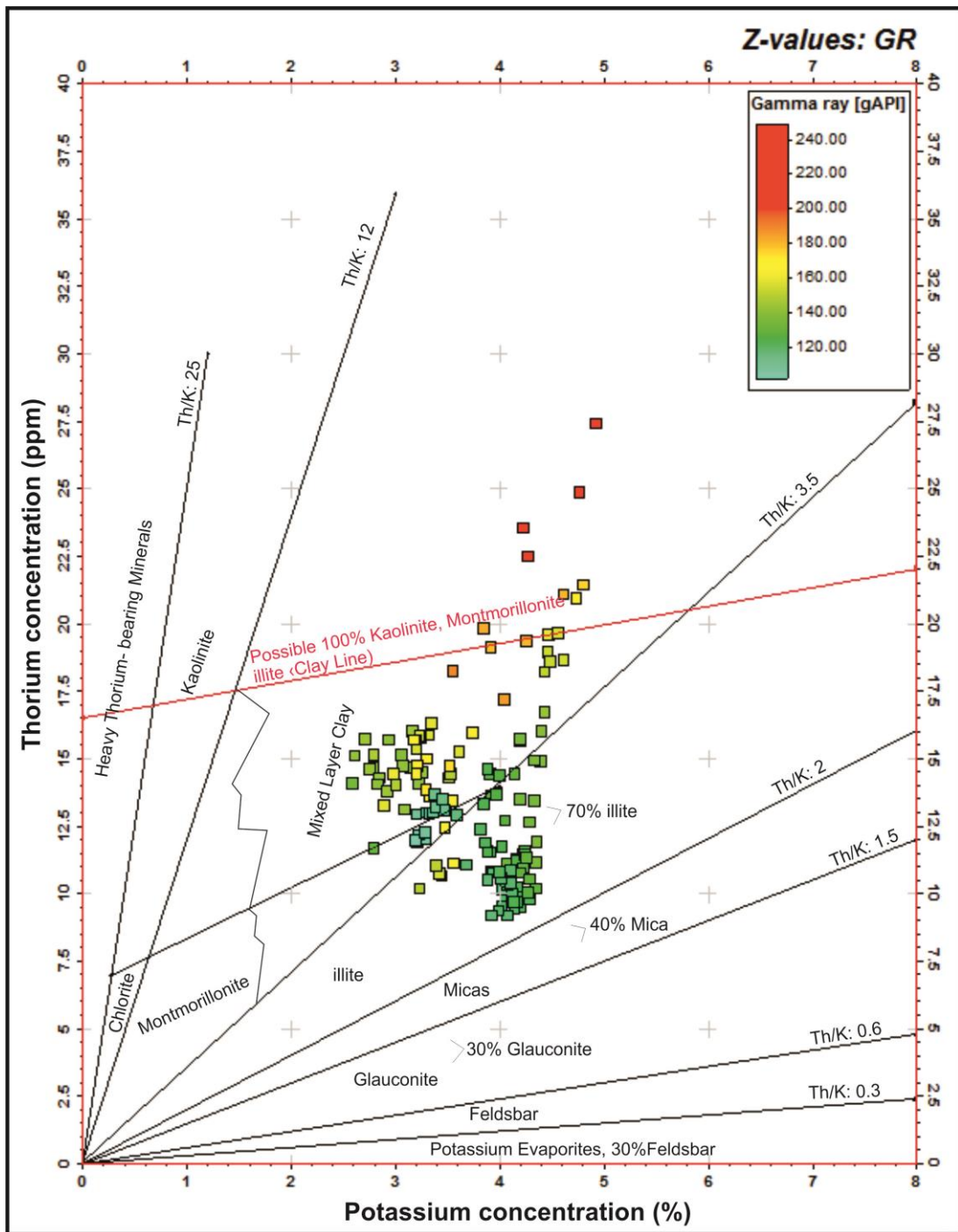


Figure 62: Types of the clay coating minerals forming matrix of the sandstone levels of the uppermost Bedinan Formation based on Thorium and Potassium concentration cross plot for D well.

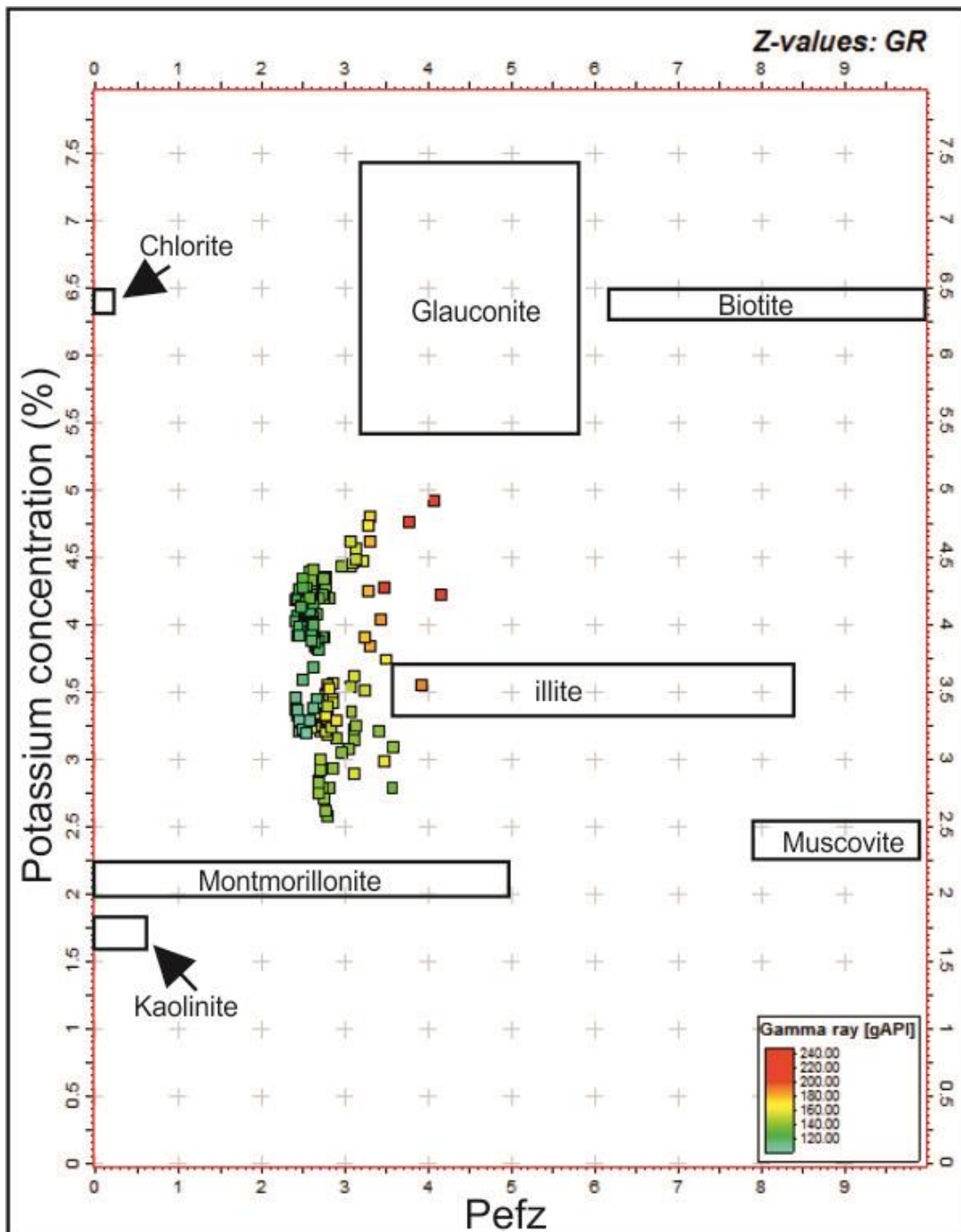


Figure 63: Type of the clay coating minerals forming matrix of the sandstone levels of the uppermost Bedinan Formation based on Potassium concentration and Photoelectric factor cross plot for D well.

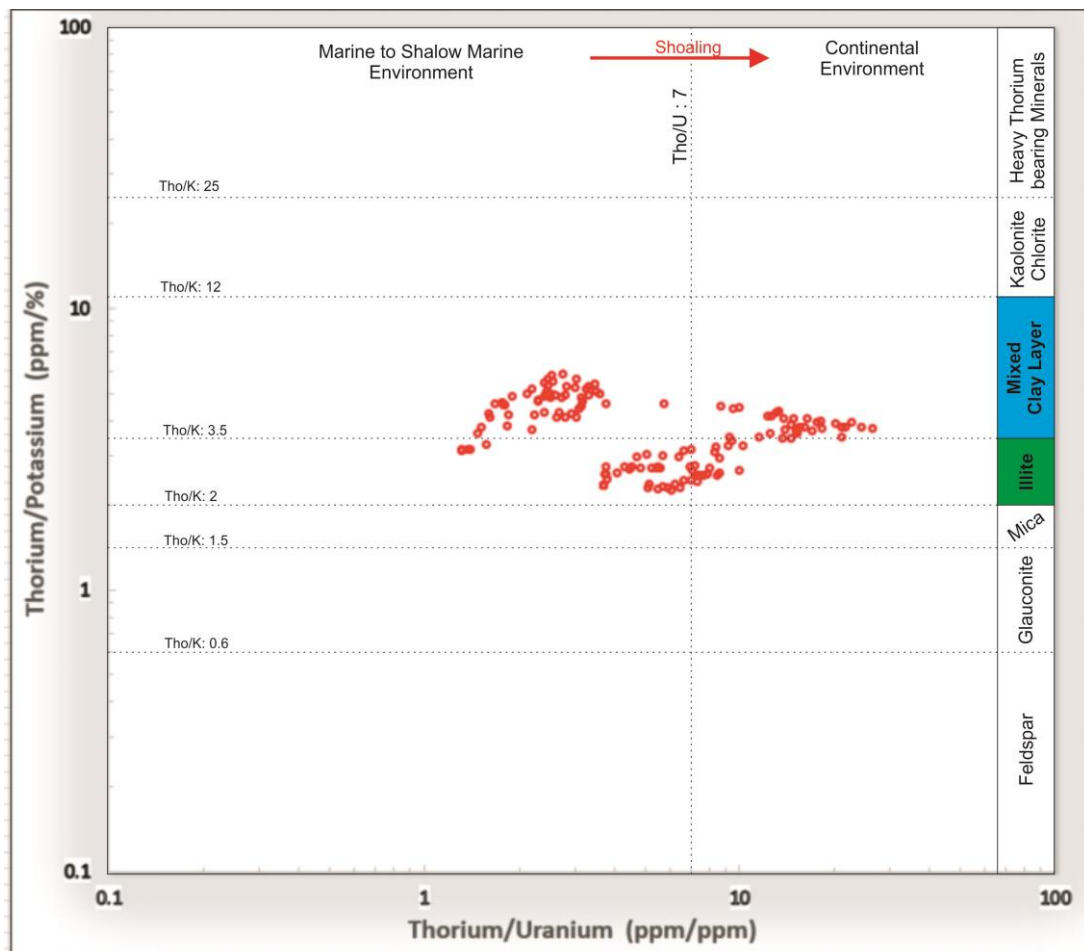


Figure 64: Besides depositional environment, Thorium/Potassium & Thorium/Uranium cross plot is useful tool to determine type of clay and used for determination of the clay coating minerals occupying matrix of the uppermost Bedinan Formation sandstone levels (D well).

CHAPTER 8

X-RAY DIFFRACTION BULK POWDER ANALYSIS

X-ray diffraction (XRD) is one of the most useful analytical method to identify crystalline materials (Moore and Reynolds, 1997; Chipera and Bish, 2013; Zhou et al., 2018). This method was applied to the 4 core samples collected from the studied levels in A (1st sandstone level), B (1st and 2nd sandstone levels) and F (1st sandstone level) wells. The framework minerals identified in the XRD analysis are in order of abundance by quartz. The analysis performed on the core sample resulted in that the studied samples are formed of quartz, feldspar (plagioclase and K-feldspar), dolomite and clay minerals (Table 16) (Figure 65, 66, 67, 68, 69, 70, 71, 72).

Table 16: The framework minerals in accordance with X-ray diffraction bulk powder analysis.

Well	Level	XRD (bulk powder mineral association) (%)					
		Quartz	Plagioclase	K-Feldpar	Dolomite	Calcite	Total Clay
A	2nd sandstone	82.6	6.00	6.9	2.6	-	1.9
B	1st sandstone	69.9	11.2	13.3	3.3	-	2.4
B	2nd sandstone	63.8	11	15	5.6	-	4.6
F	1st sandstone	83.1	2.4	10.6	2.7	-	1.1

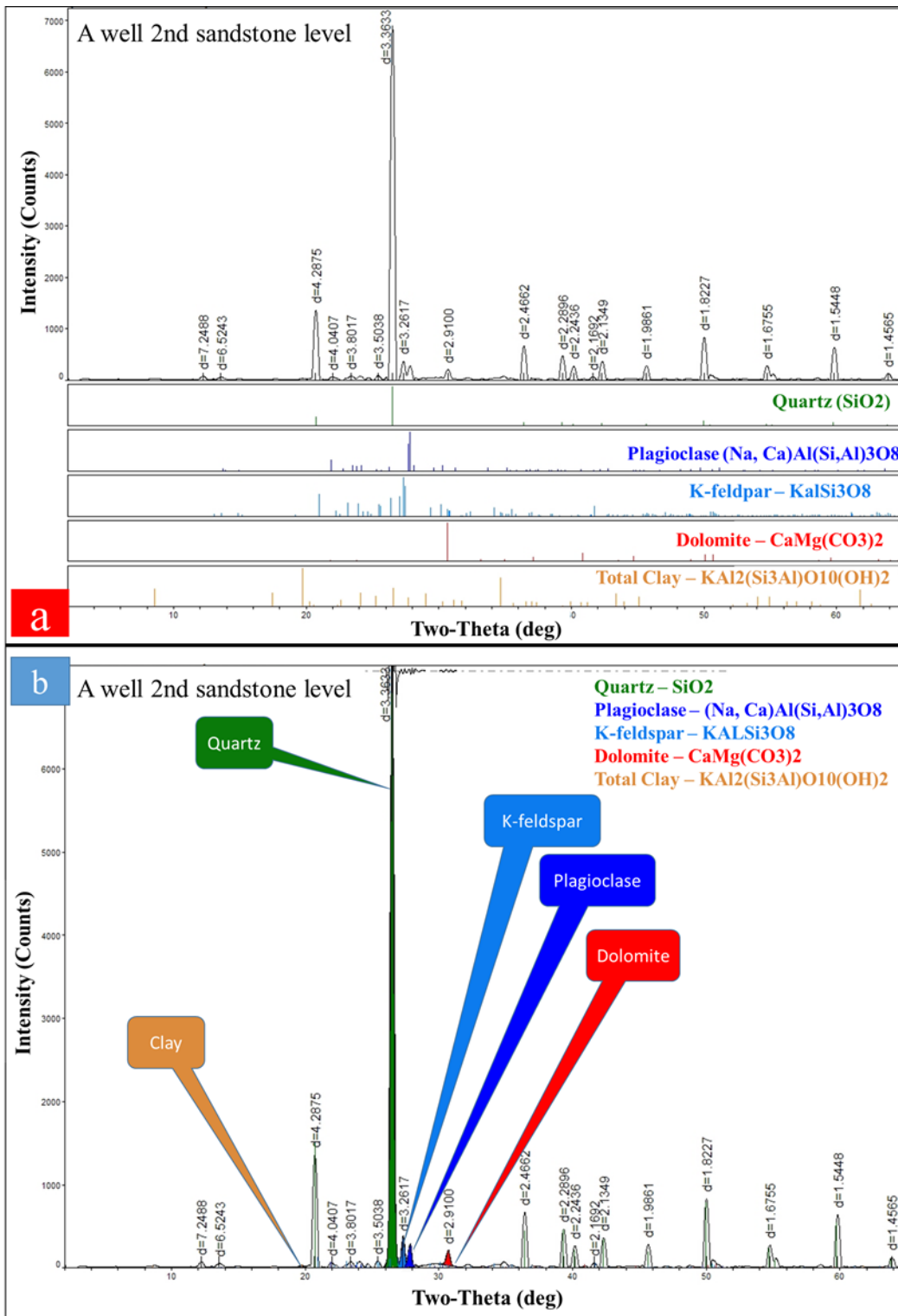


Figure 65: The raw (a) and interpreted (b) bulk powder XRD diffractograms of the sample of the 2nd sandstone level (A well).

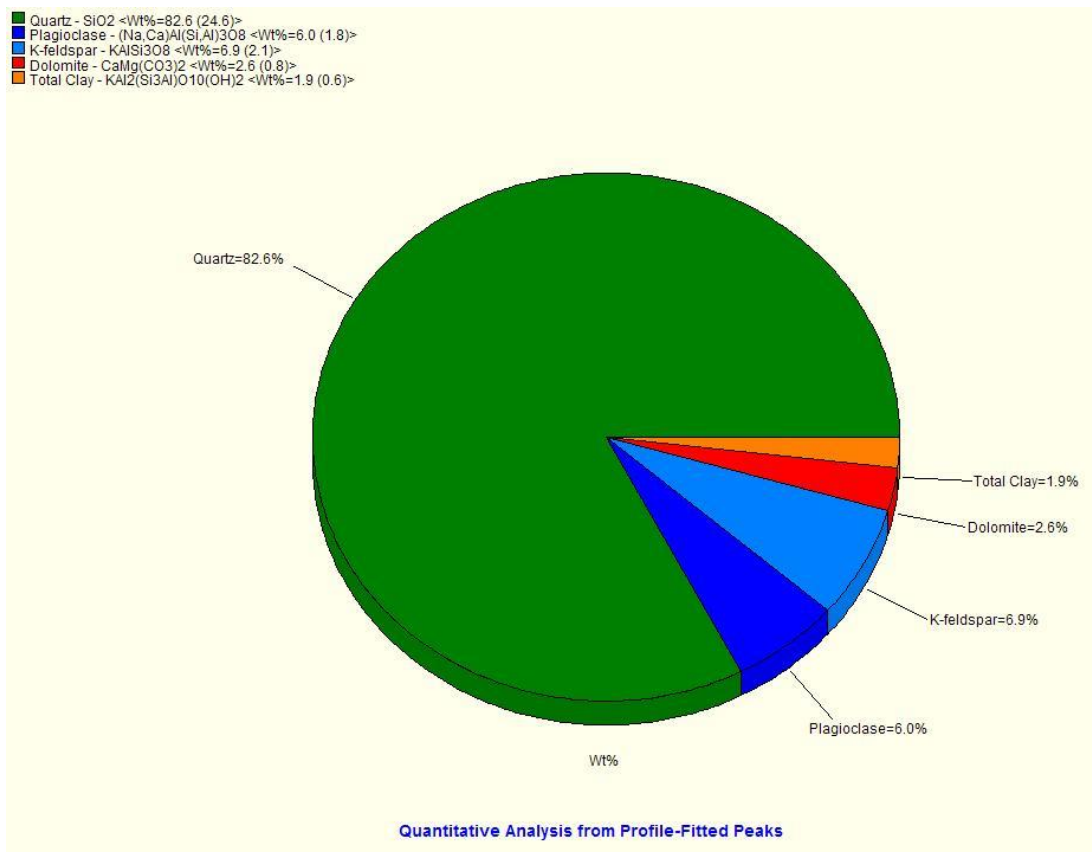


Figure 66: The pie diagram of mineral abundance of the sample (the 2nd sandstone level, A well).

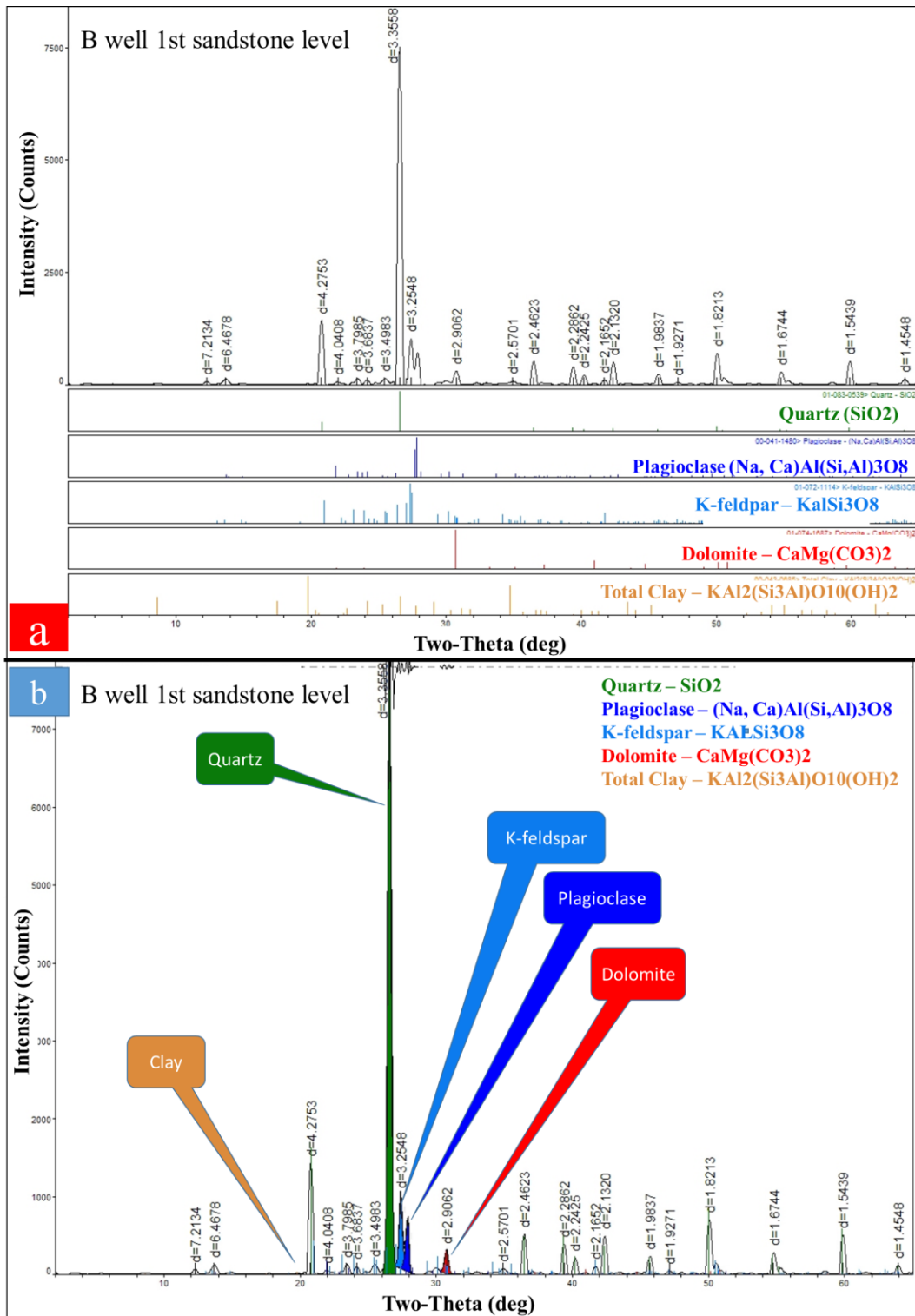


Figure 67: The raw (a) and interpreted (b) bulk powder XRD diffractograms of the sample of 1st sandstone level (B well).

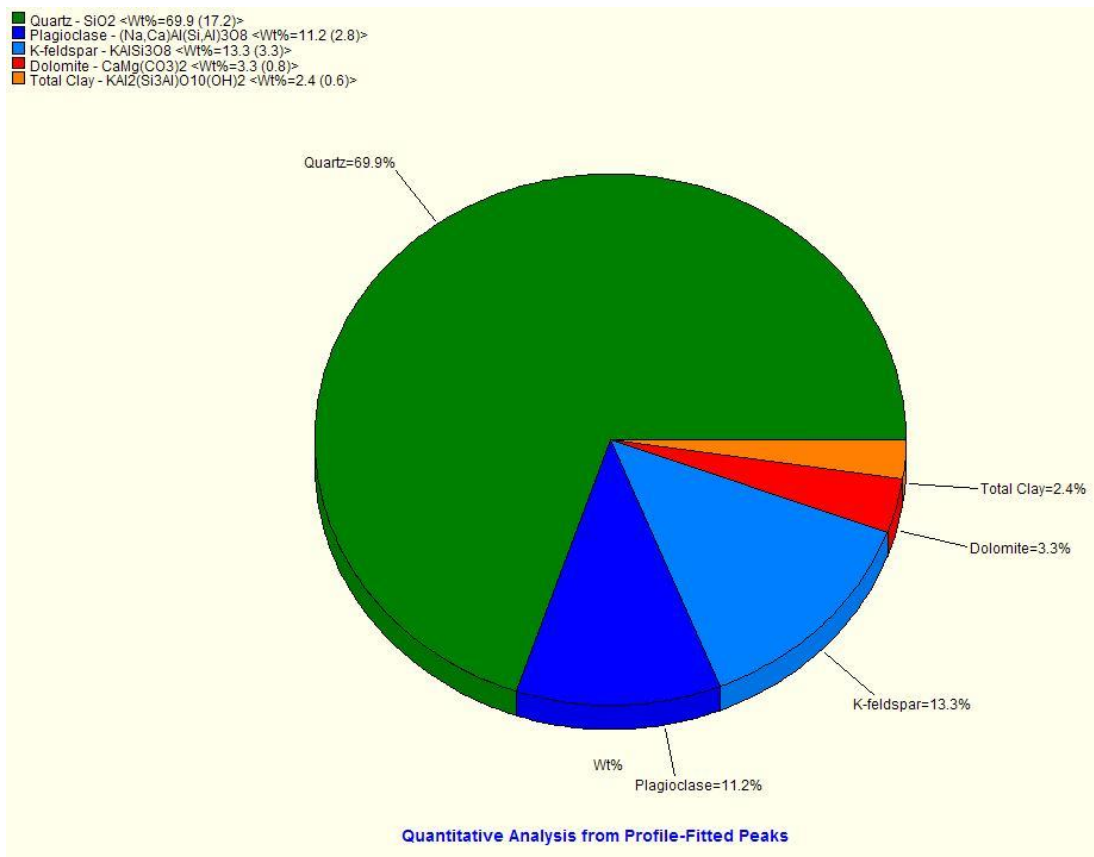


Figure 68: The pie diagram of the mineral abundance of the sample (the 1st sandstone level, B well).

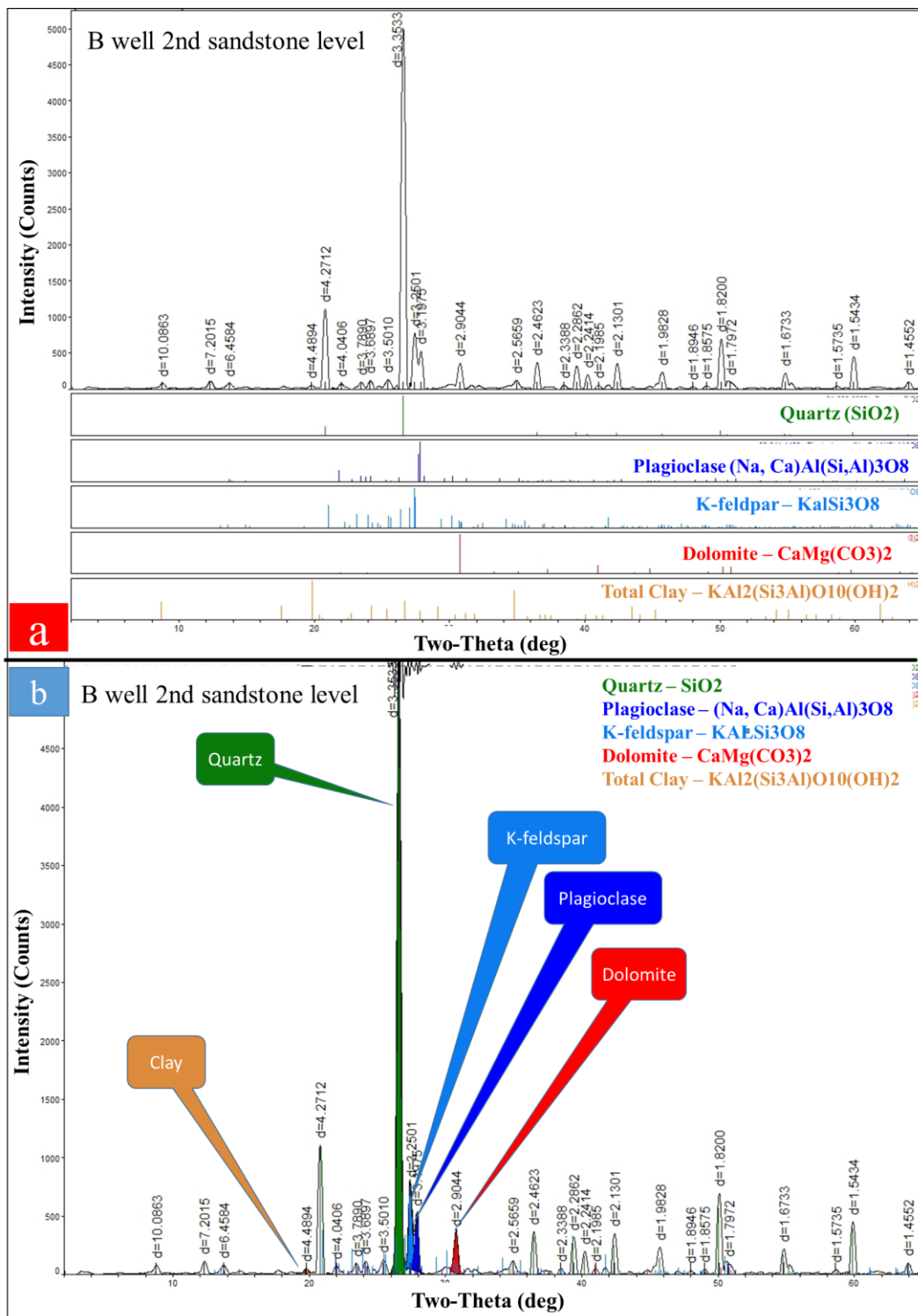


Figure 69: The raw (a) and interpreted (b) bulk powder XRD diffractograms of the sample of 2nd sandstone level (B well).

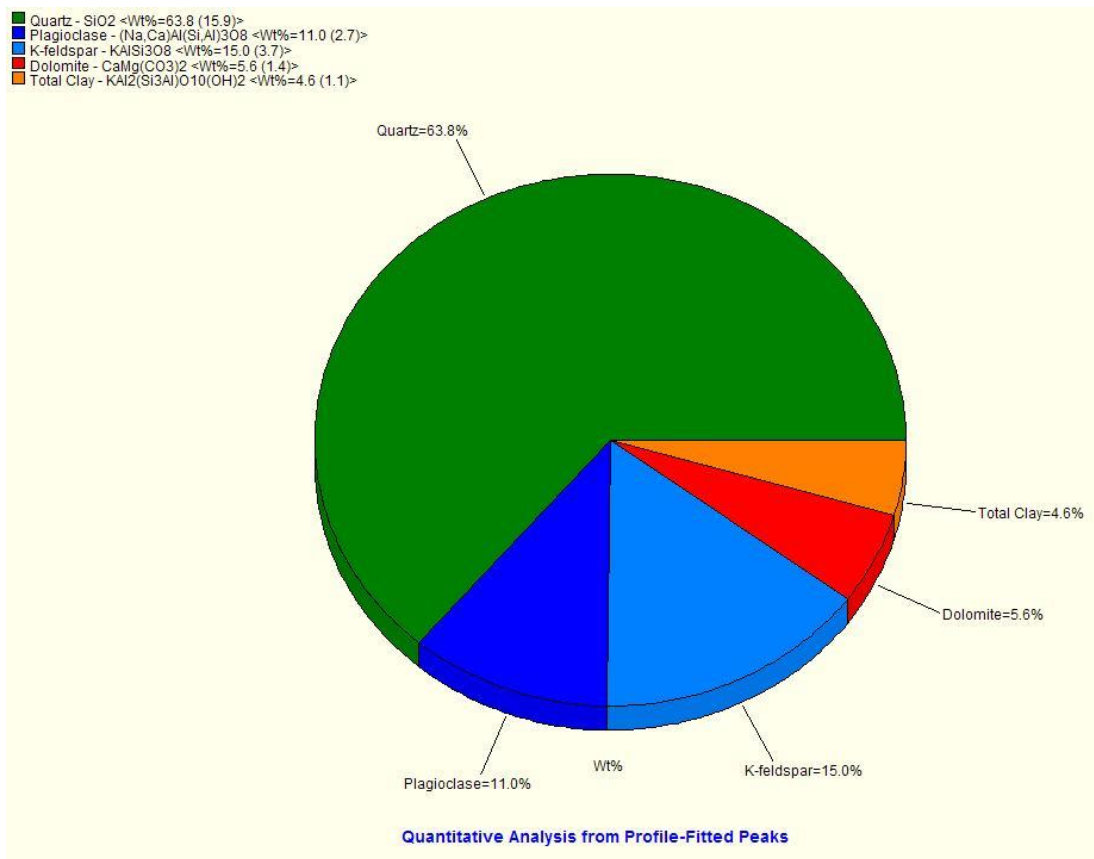


Figure 70: The pie diagram of the mineral abundance of the sample (the 2nd sandstone level, B well).

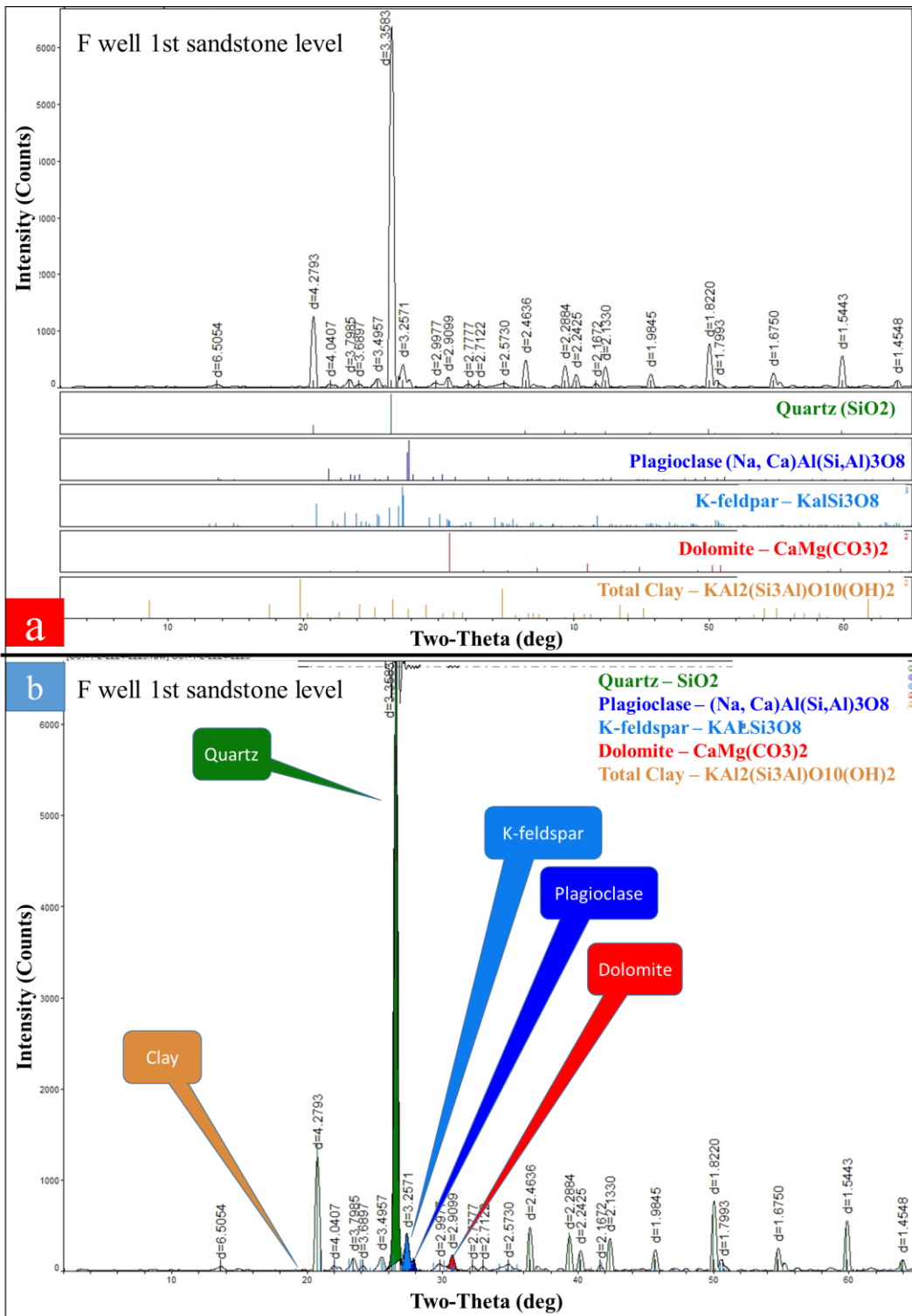


Figure 71: The raw (a) and interpreted (b) bulk powder XRD diffractograms of the sample of the 1st sandstone level (F well).

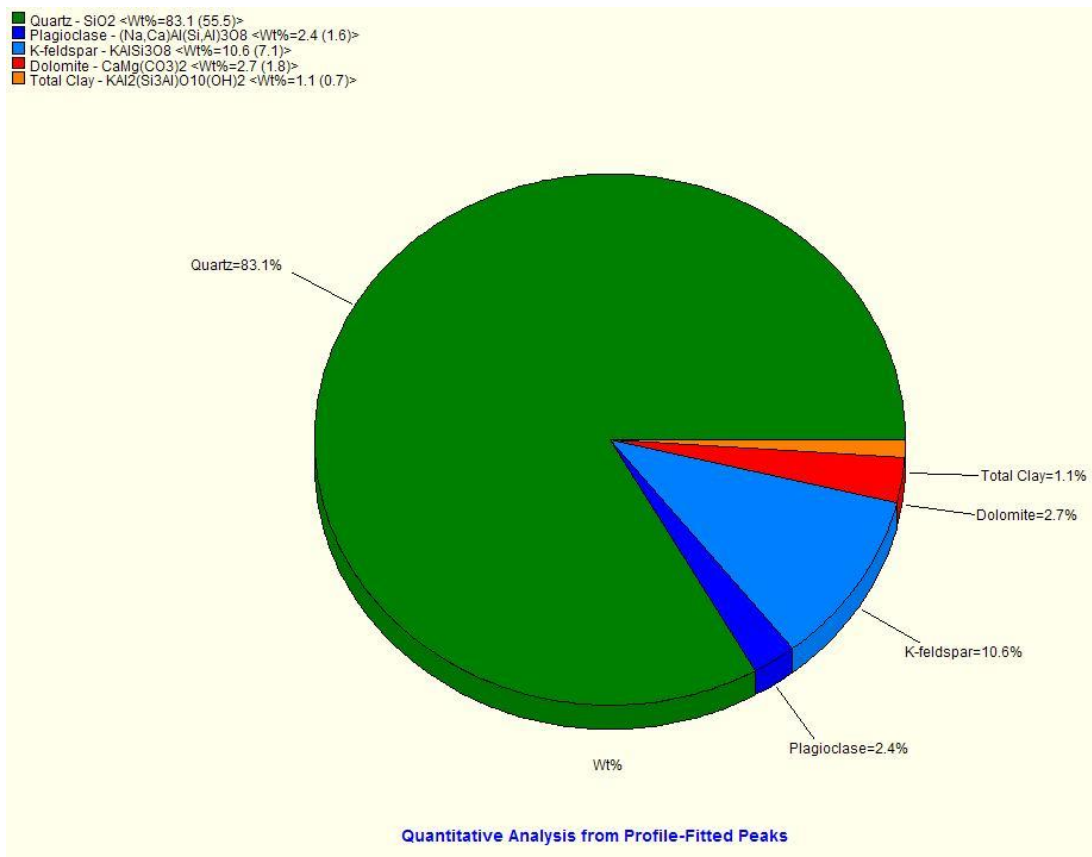


Figure 72: The pie diagram of the mineral abundance of the sample (the 1st sandstone level, F well).

8.1. Clay Typing based on XRD Analysis

XRD analysis is useful in mineral identification, as well as clay typing. The type of clay minerals in the matrix was evaluated with their distinctive diffraction patterns. In accordance with the XRD analysis results of the clay-bearing level, the main clay minerals in the studied levels are illite, kaolinite and illite-smectite (montmorillonite) mixed clay layer (Figure 73, 74, 75).

Although kaolinite and chlorite give almost same peak at the same position around 12.2° (Chen, 1977; Moore and Reynolds, 1997) and it needs XRD clay mineral analyses to differentiate kaolinite and chlorite, the depositional environment (acidic

pore water) and the source rock (igneous) of the studied levels prove the presence of kaolinite rather than chlorite (discussed in detail in the diagenesis chapter).

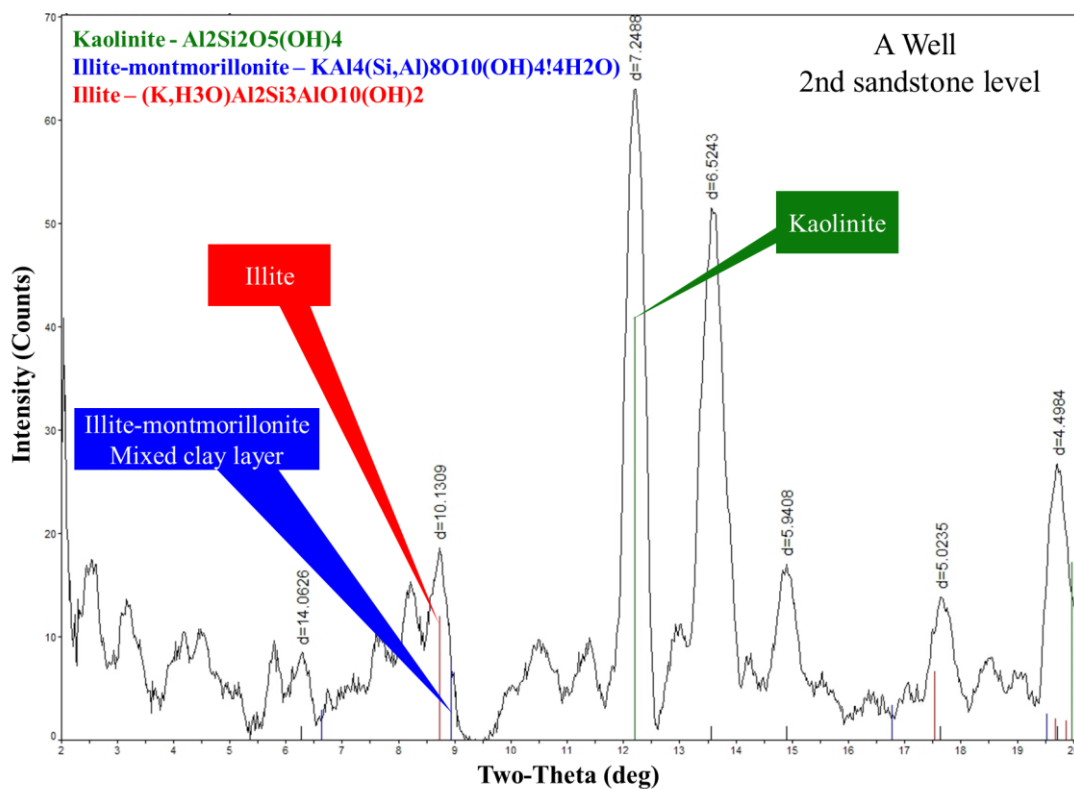


Figure 73: The interpreted clay mineral XRD diffractograms of the sample of the 2nd sandstone level (A well).

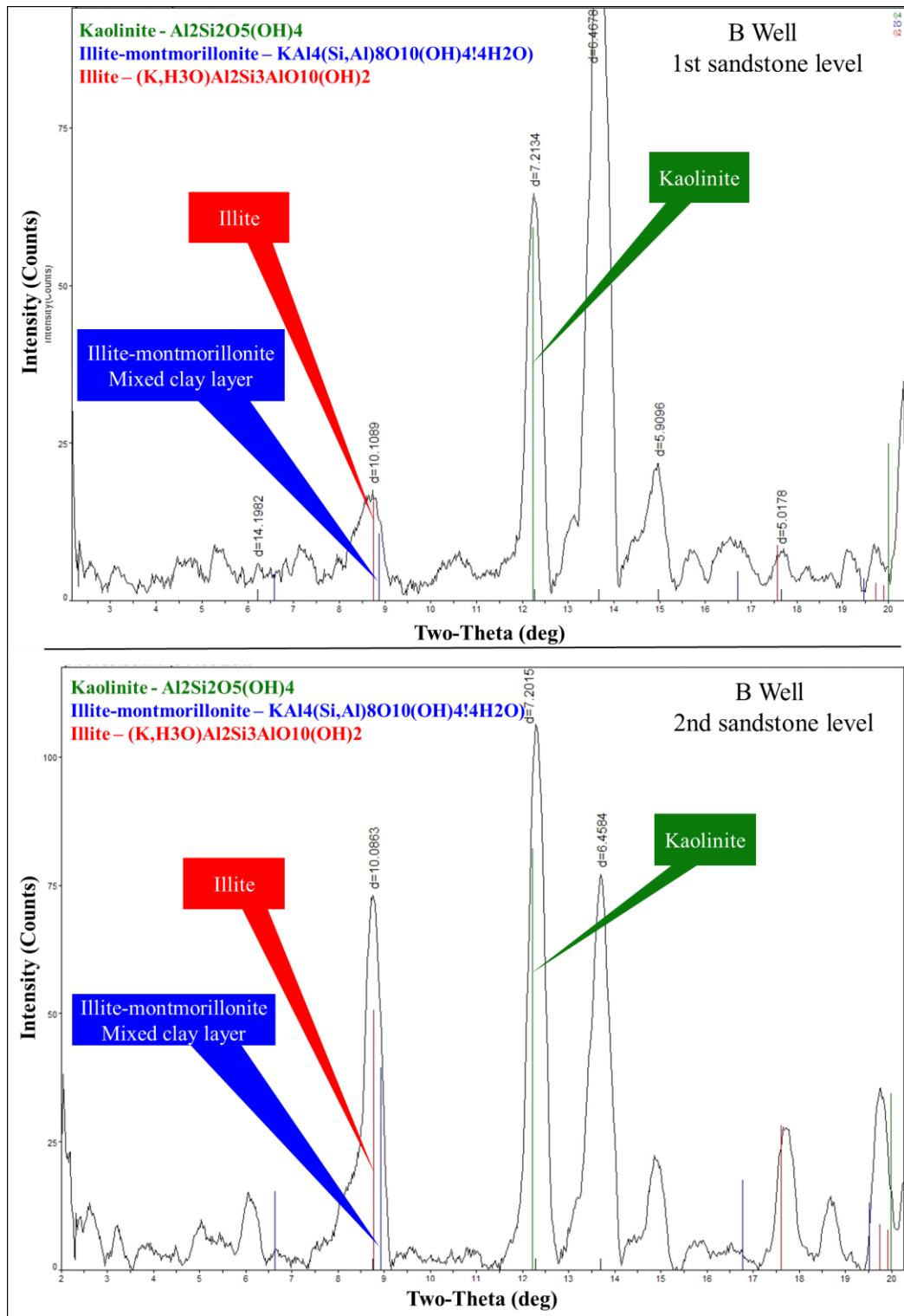


Figure 74: The interpreted clay mineral XRD diffractograms of the samples of the 1st and 2nd sandstone levels (B well).

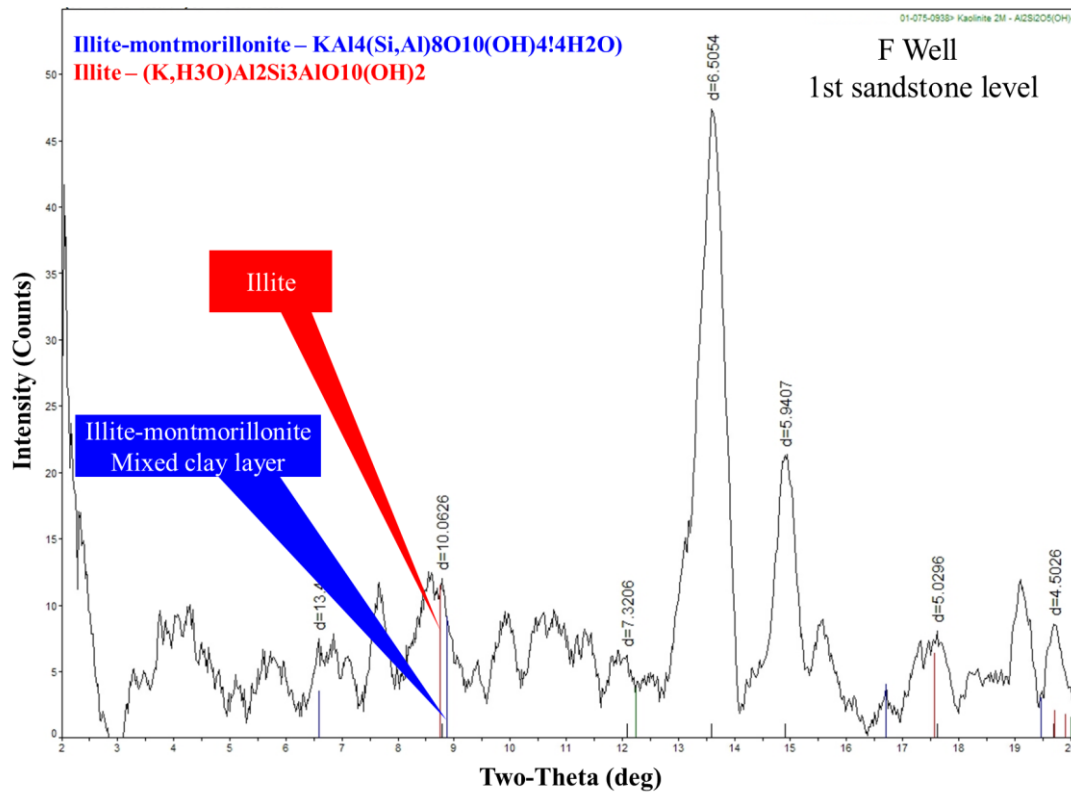


Figure 75: The interpreted clay mineral XRD diffractograms of the sample of the 1st sandstone level (F well).

8.2. Comparison of Petrophysical and XRD Methods for Clay Typing

The clay coating minerals in the studying sandstone levels were identified by the use of the well logs and XRD analysis as of illite-mixed clay layer, illite-kolinite-illite/smectite(montmorillonite) mixed clay layer respectively.

In accordance with petrophysical analysis for the clay typing, the presence of illite minerals was proven; however, the mineral association of mixed clay layer remains uncertain.

The XRD analysis resulted in that the studied sandstone levels includes illite, kaolinite and illite-montmorillonite(smectite) mixed clay layer. The clay typing based on XRD analysis gave more precise results to understand the clay mineral association in the

studied levels. Moreover, the results of the XRD analyses is proven and supported by the depositional environment and the provenance of the studied levels, and discussed in more detail in diagenesis chapter.

CHAPTER 9

DIAGENESIS

The Ordovician aged Bedinan Formation sandstone levels have become one of the most prolific reservoir levels since recent hydrocarbon discoveries; nevertheless, despite its importance as a reservoir, a few published data exist exclusively upon the reservoir quality with diagenesis. In this chapter, diagenetic evaluation of the levels of interest will be dealt to examine physical and chemical change, and their effect on the reservoir quality of the uppermost Bedinan Formation sandstone levels penetrated in petroleum exploration and production wells from the study area which is situated in southern Diyarbakır Basin, SE Turkey.

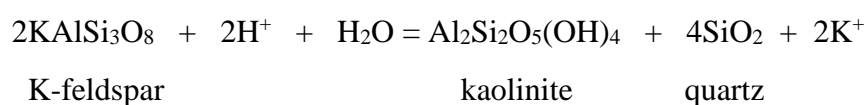
Diagenesis which is the physical and chemical processes being effective from the start of deposition to metamorphism exerts great effort on not only heterogeneity of the reservoir rocks but also rest of the rock type (Worden and Morad, 2000; Morad et al., 2010). During this period of the interval, the factors enhancing or deteriorating porosity and permeability play an important role for hydrocarbon recovery in the Petroleum Industry. The principle diagenetic cement and minerals appeared in the intervals of interest are clay coating minerals, quartz overgrowth and patchy-shaped calcite and dolomite cement. This study covers predominantly clay coating minerals, quartz and carbonate cementation relied on late diagenesis (mesodiagenesis) and their effect on reservoir quality. The observations on the cutting samples and cores taken from the wells (A, B, C, D, E and F) in the study area exhibit that the effect of distinctive clay matrix variation in the uppermost Bedinan Formation sandstone levels on reservoir quality is incontrovertible. In support of this view, the hydrocarbon production performance of the wells with high clay content in the sandstone levels of uppermost Bedinan Formation is dramatically lower in comparison with the well with

low or free of clay content in the sandstone levels of interest. Revealing the type of clay and other factors like quartz and carbonate cementation deteriorating the reservoir quality has become vital to carry out convenient well stimulation methods with the object of increase in hydrocarbon production.

9.1. Clay Coating Mineral Associations and Their Origin

The petrophysical and especially XRD analyses indicate that the clay coating minerals in the studied levels are illite, kaolinite and illite-smectite (montmorillonite) mixed clay layer.

Kaolinite is the second most abundant clay mineral after illite in the sandstone levels of uppermost Bedinan Formation sandstone levels. In support of this view, the Bedinan Formation deposited in the environment far from equator in southern high latitudes with low-ph condition (acidic) during the Ordovician period (Lüning et al., 1999; Ghienne et al., 2007; Monod et al., 2003; Herrmann et al., 2004; Haq and Al-Qahtani, 2005; Tetiker et al., 2015; Haq and Schutter, 2008; Munnecke et al., 2010; Torsvik and Cocks, 2013; Masri, 2017). Acidic formation water induces the alteration of feldspar to kaolinite (Hurst and Irwin, 1982; Worden and Morad, 2000; Rahman and McCann, 2011; Morad et al., 2010). The transition reaction is formulated as below;



The acidic waters may have been migrated from mature (Tmax: 438 - 445 °C) organic rich overlying Dadaş Formation ‘Hot Shale’ level via feldspar alteration during the stage of mesodiagenesis. Besides the eodiagenetic and mesodiagenetic impacts on the transformation reaction (the transformation reaction from feldspar to kaolinite),

kaolinite exclusively piles rather in shallow marine environment where the uppermost Bedinan Formation deposited in correspondance of higher density (Table 15) in comparison with smectite (Totten et al., 2002; McKinley et al., 2003).

Wettability is another useful tool to estimate not only relative proportion of kaolinite but also the other clay coating minerals' proportions in the matrix. Wettability is a qualitative term and it is described as the ability of rock enables oil to contact with grain surface. The remaining or irreducible water saturation is high in water-wet reservoirs compared with oil-wet reservoirs. While the sandstones with kaolinite above oil-water contact are oil-wet with low irreducible water saturation, the ones with illite above oil-water contact are water-wet having high irreducible water saturation (Worden and Morad, 2000). Based on petrophysical interpretations to evaluate reservoir quality (porosity, permeability) and fluid (hydrocarbon and water) saturation of the uppermost Bedinan Formation in A, B, C, D, E and F wells, the irreducible water saturation in the sandstone levels of interest is observed to reach 70% despite above oil-water contact. Thus the sandstone reservoir levels of uppermost Bedinan Formation can be interpreted as water-wet and consisting of more illite than kaolinite.

The third most abundant clay mineral in the sandstone level is smectite (montmorillonite). The lesser dense clay coating mineral, smectite can form via coupling of the depositional and diagenetic factor. The reworking of weathering product of surficial soil, volcanic or volcanoclastic material and authigenic eodiagenetic processes are three main origins for the formation of smectite (McKinley et al., 2003). Smectite clay minerals are particularly formed as a product of igneous and metamorphic source rocks as well as, basaltic volcanics and volcanoclastics and metabasites. While the weathering of igneous or metamorphic originated plagioclase and alkali feldspars yield dioctahedral smectite (montmorillonite), the weathering of Fe-Mg rich minerals such as biotite and pyroxene in mafic rich basaltic volcanics and volcanoclastics and metabasites exclusively produce trioctahedral smectite (Chang et al., 1986; McKinley et al., 2003). The smectite minerals are quite a lot in aeolian, fluvial, lacustrine and turbidite sandstone and preferentially arid climatic conditions

where chemical weathering is minimized; additionally, in marine environment, suspended smectite minerals standing water column can migrate towards deeper marine due to its lower density (Table 13) in comparison with the rest of other clay minerals (McKinley et al., 2003; Morad et al., 2010). Because of the fact that the igneous source rock constituted kitchen area for the uppermost Bedinan Formation sandstone levels of interest as mentioned under the provenance chapter, the weathering product, dioctahedral smectite clay minerals can be expected as a participant of the clay matrix of the studied sandstone levels.

However, the lower dense smectite clay mineral standing in the water column can mostly be carried further into deep marine and left behind the fractional amount of the clay. Conceivably, in the light of information that the depositional environment and the provenance of the levels of interest are in turn shallow marine and igneous rock, dioctahedral smectite clay minerals may exclusively constitute the fractional percentage of clay coating minerals occupying the matrix of the sandstone levels of uppermost Bedinan Formation.

The origin of the most abundant clay mineral in the sandstone levels of interest, illite can be both detrital and diagenetic (Burst, 1969). The fact that the presence of illite in the matrix of studied sandstone levels can directly be attributed to depositional environment or distance of transport related with the density of detrital illite; however, more comprehensive investigation is needed to elucidate the impact of mesodiagenetic reactions for illite formation.

Temperature, potassium availability and acidity of the formation water are the main factors for transformation reaction of clay coating minerals and K-feldspar to reach equilibrium. Temperature increment can be induced through contact metamorphism, hydrothermal activity and burial diagenesis (Hower et al., 1976; Burtner and Warner, 1986; Morad et al., 2000; Totten et al., 2002; Al-Ramadan et al., 2004; Rahman and McCann, 2010; Morad et al., 2010; Credoz et al., 2011; Al-Ramadan, 2014, Wazir et al., 2014; Al-Ramadan et al., 2017; Worden et al., 2018). In this chapter, burial

diagenesis is committed as the controlling mechanism for the change in the relative proportion of clay coating minerals due to the absence of contact metamorphism and hydrothermal activity in the Bedinan Formation in the study area. Burial diagenesis so-called mesodiagenesis infers to the condition with a temperature greater than 50-60 °C and the depth deeper than 2.000 m. The empirical studies exhibit that, mesodiagenetic illite formation from smectite, kaolinite and K-feldspar occurs at the temperature of 50-95 °C with increasing illite proportion as a consequence of progressive temperature increment. The reaction can also perform at lower temperature over long period of time in old rocks (Hower et al., 1976; Martin-Martin et al., 2006; Al-Ramadan, 2014; Worden et al., 2018) as expected in the Ordovician aged Bedinan Formation. In support of this view, the studies carried out upon Oligocene-Miocene clastic sediments rich in clay minerals of Gulf Coast of the United States from the depth of 1.250-5.500 m exhibit that while calcite, kaolinite, smectite, potassium feldspar decrease in ratio with between 2.000-3.700 m and remain constant in deeper depth , illite/smectite, silica ratio and chlorite increase (Figure 77) via progressive temperature increment with depth (Hower et al., 1976).

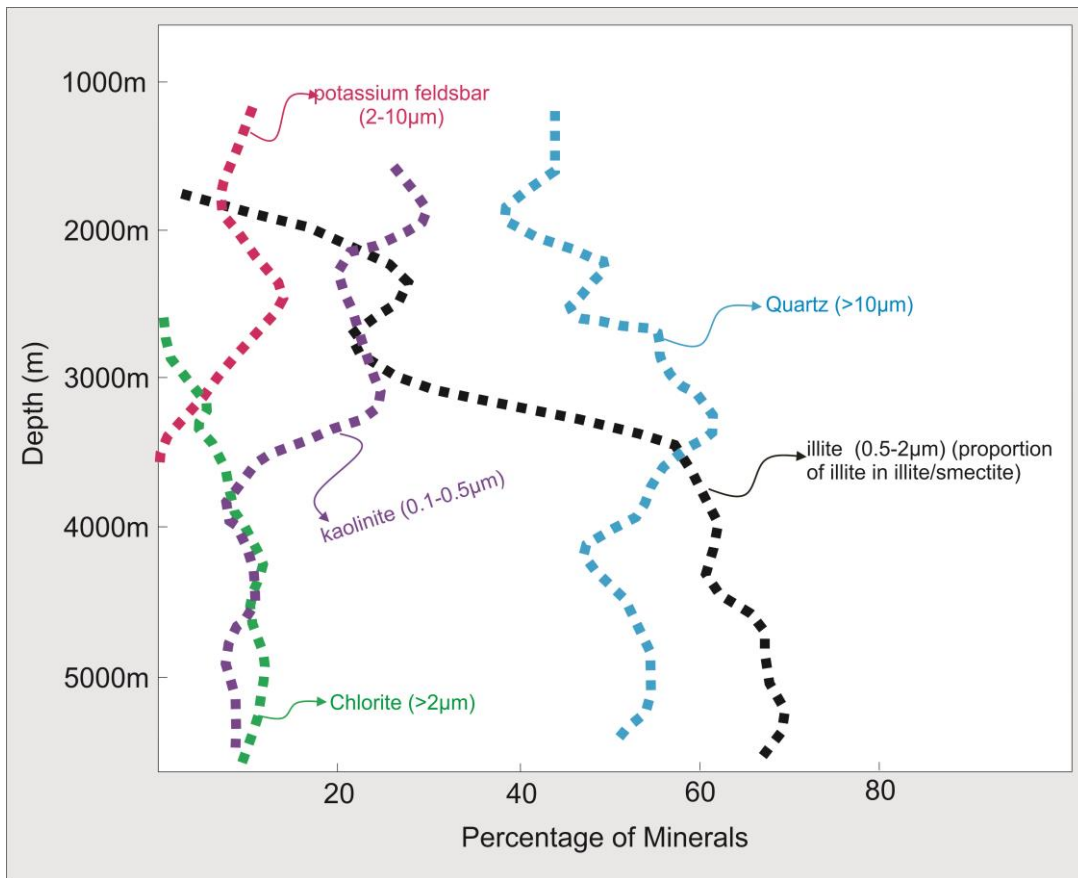
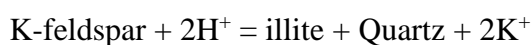
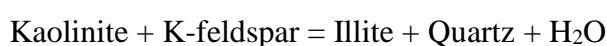
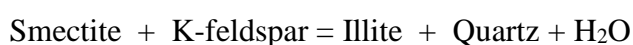


Figure 76: Depth depended variation of relative ratio and amount of illite/smectite, quartz, kaolinite, chlorite and potassium feldspar through progressive temperature increment, modified from Hower et al., (1976).

Apart from the temperature increment, the availability of potassium derived from dissolution of K-feldspar plays a vital role for illitization reactions. Feldspars are sourced from igneous and metamorphic rocks and formed under the elevated temperature (>300 °C). By considering the feldspar generation conditions, feldspars are out of equilibrium under diagenetic pressure, temperature and pore fluid chemistry and thus conceivably exert to reach equilibrium state through alteration (i.e., dissolution, replacement by clay minerals and albitization). Alteration of K-feldspars results in liberation of potassium as well as sodium and calcium (Worden and Morad, 2000). The coupling of high temperature and the available potassium ions derived

from K-feldspar and diffused to formation water provides convenient conditions for illitization.

The illitization chemical reaction formula at the expense of infiltrated clays (smectite, kaolinite) and K-feldspar via progressively increasing temperature is envisaged (Hower et al., 1976; Lahann, 1980; Fisher and Land, 1987; Worden and Morad, 2000; Worden and Barclay, 2003; Mantovani et al., 2010; Al-Ramadan, 2014) and simplified as;



The illitization reactions are also controlled by the type of formation fluid and permeability. For instance, the oil saturated sandstone levels with high permeability are generally rich in potassium ions compared to water saturated zone due to slow movement of the ions in oil zone and potassium escape from water zone to oil zone (Worden and Barclay, 2003); for this reason, the further illitization reaction can be expected more in the zone having high oil saturation with high permeability. In the light of the mentioned information, mesodiagenetic illite can be expected in the sandstone levels of uppermost Bedinan Formation due to the fact that average depth of top of Bedinan Formation in study area is approximately 2.400 m which is deeper

than 2000 m, and the formation is old enough for illitization reaction even in lower temperature, and the level of interest are observed as oil saturated in the studied wells. Although the depth and age of the Bedinan Formation are enough to elucidate the possible mesodiagenetic illite formation in the sandstone levels of interest, there are some more tangible methods like illite crystallinity (IC) and maturity level of adjacent rock sequence to evaluate the diagenetic stage of the sandstone levels of uppermost Bedinan Formation.

Illite crystallinity (IC) method is one of the most useful measurements to identify diagenetic stages by using the full width at half maximum of the first illite diffraction peak (Kübler and Jaboyedoff, 2000). Besides the IC method, the maturity level of the adjacent rock and the ages of the studied levels can give a clue for the stage of diagenesis (Smart, 1985; Al-Ramadan, 2014; Worden et al., 2018). The common coincidence between hydrocarbon generation and mesodiagenetic clay transformation like smectite to illite (Figure 78) enable that hydrocarbon generation can be used to infer diagenetic stage of the rock accompanying by diagenetic clay formation (Smart, 1985; Kübler and Jaboyedoff, 2000; Jiang, 2012; Al-Ramadan, 2014; Worden et al., 2018). The fact that organic rich 'Hot Shale' level of the Silurian Dadaş Formation overlying the Ordovician aged Bedinan Formation reached the thermal maturity for oil generation in the study area in accordance with pyrolysis analysis results (Tmax: 438-445 °C) implemented upon the full-diameter cores and the cutting samples of 'Hot Shale' level from A, D and E wells, is a guide to estimate the uppermost Bedinan Formation as mesodiagenetic stage. In addition to common occurrence time for both the maturation of adjacent organic rich source rock and illitization, acidic pore water migrated from the source rock during maturation stage increases the illitization rate (Kübler and Jaboyedoff, 2000; Worden and Morad 2000; Creoz et al., 2011; Jiang, 2012).

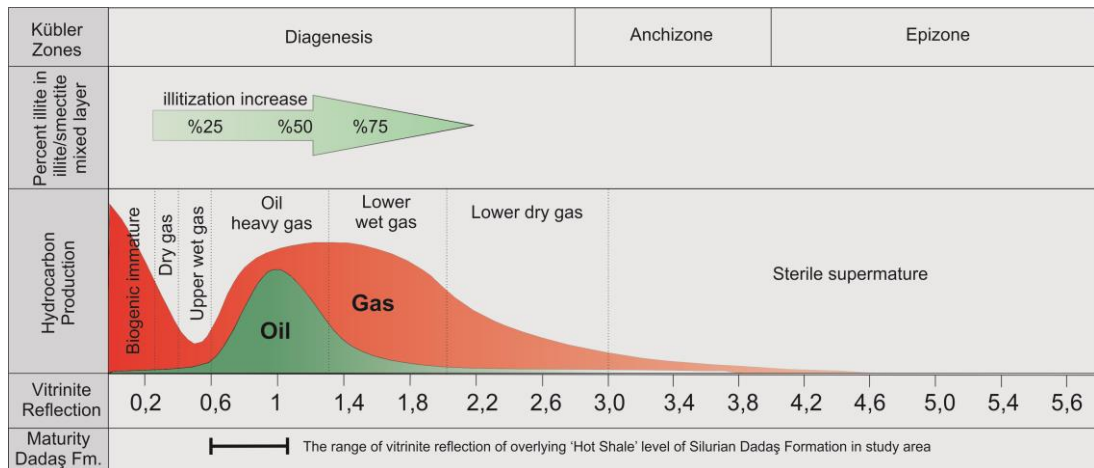


Figure 77: Hydrocarbon generation, diagenesis, source rock maturity (vitrinite reflectance) and relative ratio of mixed-layer illite/smectite relationship. Figure and data summarized from Kübler and Jaboyedoff (2000), Jiang (2012).

9.1.1. Regional Correlation

SEM and XRD laboratory studies on the exposed age equivalent of uppermost Bedinan Formation designated as Halevikdere Formation in uplifted Mardin-Derik-Kızıltepe area exhibit that the most common clay coating minerals take place in siltstone levels of interest are illite, kaolinite, mixed layered illite-smectite (Figure 78) (Tetiker et al., 2015). Illite crystallinity measurement was carried out upon the surface samples of Halevikdere Formation including a considerable amount of illite. As a result of the measurement, Halevikdere Formation is in low diagenetic stage (Tetiker et al., 2015). The Late Ordovician aged Sarıyardere Formation including the alternation of shale, siltstone and sandstone lithologies, represented in Antalya Unit of the Tauride belt, southwestern Turkey consists of phyllosilicate minerals in order of abundance by mixed layer illite-smectite, illite, kaolinite and chlorite (Bozkaya et al., 2010). Illite crystallinity measurement performed on the samples of the Late Ordovician aged Sarıyardere Formation indicates that the Sarıyardere Formation clastic levels are in late diagenetic to immediately in the transition to metamorphic grades (Bozkaya et al., 2010) designated as anchimetamorphic or anchizone (Kübler

and Jaboyedoff, 2000). Clay minerals analogy with the exposed Halevikdere Formation which were studied in Mardin-Derik-Kızıltepe area may be conceivable due to closeness to the study area.

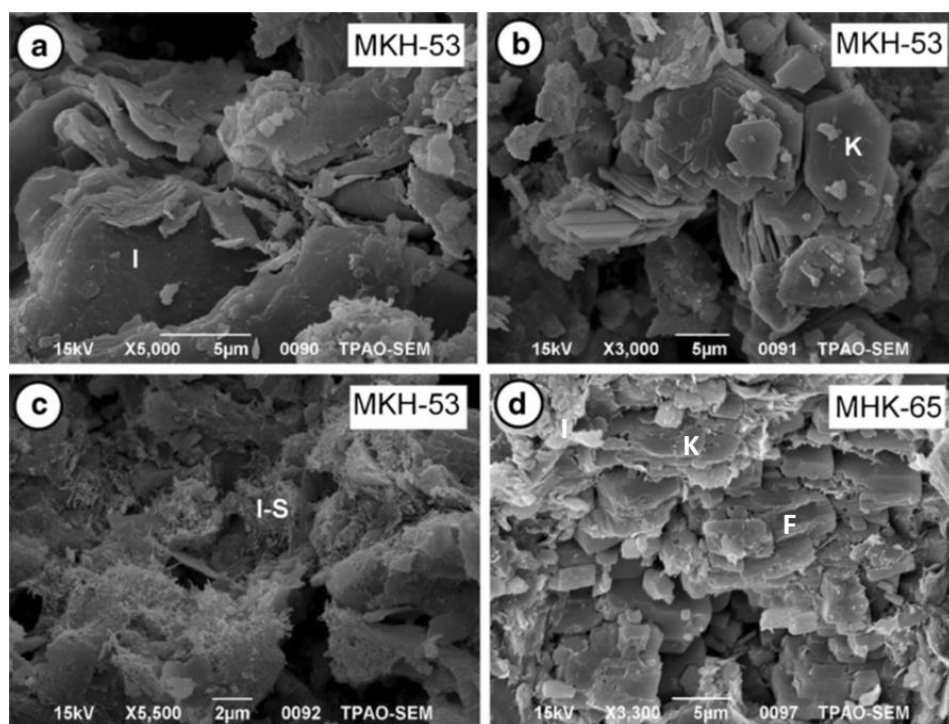


Figure 78: SEM image of the most common clay coating minerals of the siltstone levels of the Halevikdere Formation exposed in Mardin-Derik-Kızıltepe area. a: illite (I) plates. b: Kaolinite (K) minerals. c: Mixed layer illite-smectite (I-S). d: illite, kaolinite and euhedral feldspars (Tetiker et al., 2015).

9.2. Diagenetic Quartz Cementation

The microscopic investigations upon the thin sections of the studied cores and cutting samples of the sandstone levels of uppermost Bedinan Formation exhibit that syntaxial quartz overgrowth (Figure 79) is developed around tightly packed detrital quartz grain and indicate mesodiagenetic origin (Worden and Morad, 2000; Rahman and McCann, 2011). Although the quartz overgrowth constitutes a relatively fractional portion of

the studied sandstone levels even almost absent in clay rich levels as it is observed in B well, the presence of it serves as an aid to understand the diagenetic stage, reservoir quality, and to develop enhanced well stimulation methods. The quartz overgrowths around quartz grains are observed on the thin sections of the studied intervals. This quartz cement may have been generated from different sources. The main known source of the silica are internally, pressure solution at grain contact and in stylolites, dissolution of feldspars, illitization of some clay coating minerals (i.e., smectite), dissolution of biogenic silica, and externally silica migrated from adjacent mudrock.

The one of the sources of the silica which is observed on the thin sections is pressure solution developed at grain contacts (Figures 80, 81). The silica derived from pressure solution at elevated depth accompanying progressively increasing lithostatic pressure and temperature can induce quartz overgrowth around clean quartz grains in sandstone beds or in adjacent one (Worden and Morad, 2000; Morad et al., 2010).



Figure 79: Photomicrograph of the quartz overgrowth developed around tightly packed fine grained quartz of the 1st sandstone level (Core-2) of the uppermost Bedinan Formation in F well.

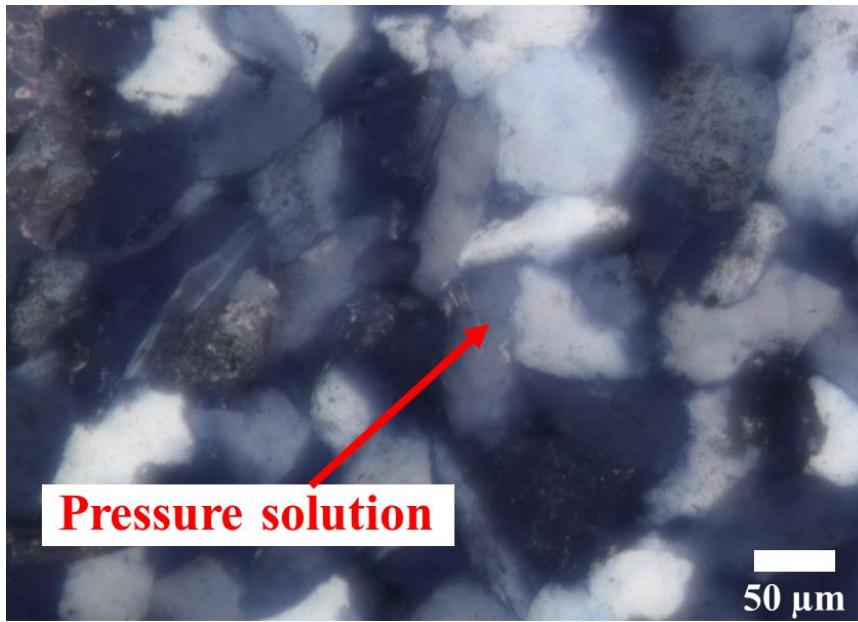


Figure 80: Photomicrograph of solution of fine grained quartz edges (F well, the 1st sandstone level, the core-2) by compaction related pressure solution.

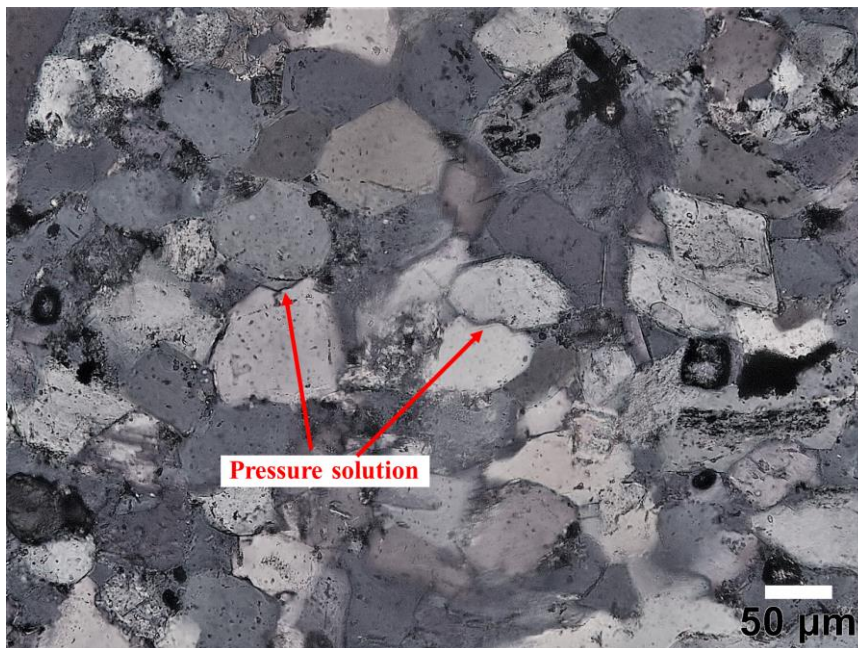


Figure 81: The contact of the grains has subjected to dissolution leading to the penetration one grain by another (F well, 1st sandstone level, Core-2).

In accordance with empirical studies, it is reported that fine grained quartz tend to have more pressure dissolution in comparison with coarse grained one (Worden and Morad 2000). Thus, it can be envisaged that the very fine to fine grained quartz minerals in the studied sandstone levels of Bedinan Formation may have subjected to more pressure solution as a consequence of compaction.

Another source of quartz for cementation in the sandstone levels of interest is most likely the transition reaction of smectite and kaolinite to illite during mesodiagenesis. In support of this view, smectite incorporates high Si/Al ratio, hence the alteration reaction with progressively increasing temperature during burial releases silica and water to reach equilibrium (Hower et al., 1976; Lahann, 1980; Worden and Morad, 2000; Worden et al., 2003; Al-Ramadan, 2014). The silica liberated and diffused to formation water via the transition reaction may be formed in-situ or from adjacent shale dominated Dadaş Formation during mesodiagenesis.

The quartz cement around quartz grains of the uppermost Bedinan Formation is mostly yielded by dissolution of feldspar. As noted before, the feldspars form at elevated temperature ($>300\text{ }^{\circ}\text{C}$) and try to reach an equilibrium state in diagenetic stage through alteration. The expense of feldspars with high Si/Al ratio (~ 3) results in liberation of silica and formation of clay coating minerals (Si/Al ratio is around 1 for illite and kaolinite) (Worden and Morad, 2000).

Apart from the known source noted before, it is important to accentuate that type of rock is also a determinant and controlling factor in relative amount of quartz cement; in other words, silica availability and silica cementation in the rock may be correlated with the type of sandstone (Figure 82) (Worden and Morad, 2000). The subarkose to quartz arenitic sandstone levels of uppermost Bedinan Formation has the favourable framework in terms of silica availability.

As a consequence, the main sources of silica cement observed around quartz grains of the sandstone level of interest are intergranular pressure solution, dissolution of feldspar and transition reaction of smectite and kaolinite to illite. While the source of

silica is clear, the precipitation process of quartz in porous media is still open to debate. The laboratory studies and the observations indicate that the most influential agent for quartz precipitation is temperature with low pH values (Hower et al., 1976, Fisher and Land, 1987; Walderhaug, 2000; Worden and Morad, 2000; Totten et al., 2002; Morad et al., 2010; Rahman and McCann, 2011; Al-Ramadan, 2014; Anovitz et al., 2015; Worden et al., 2018). The common remark for quartz precipitation is that the convenient temperature for the piling of silica around quartz grains is as low as 40-60 °C at over a longer period of time ; however, the precipitation also occurs at higher temperature over a shorter time span (Hower et al., 1976, Worden and Morad, 2000; Anovitz et al., 2015) The temperature increment attributed with burial diagenesis is the most effective factor for quartz precipitation around fine grained quartz grains in the sandstone levels of uppermost Bedinan Formation. While the factors like temperature induce quartz cementation; the presence of clay coating mineral, oil emplacement and overpressure on sandstone inhibit the adsorption of silica around quartz grains (Worden and Morad, 2000). Based on the well side observation and studies on the thin sections, quartz overgrowth relatively low in clay rich sandstone levels. The quartz overgrowth is relatively high in the almost clay free sandstone levels of the uppermost Bedinan Formation in F well, whereas the clay rich the sandstone equivalent levels in B well is almost quartz cement free in accordance with the thin section analysis. Because of the fact that the sandstone levels of Bedinan Formation in A, B, C, D, E, F wells are oil saturated and the Bedinan Formation underwent high pressure (pressure solution along quartz grains contact is the indicator of high pressure load) due to over-loading of overlying rock sequences, the quartz cementation may be envisaged to be inhibited due to the reasons listed above.

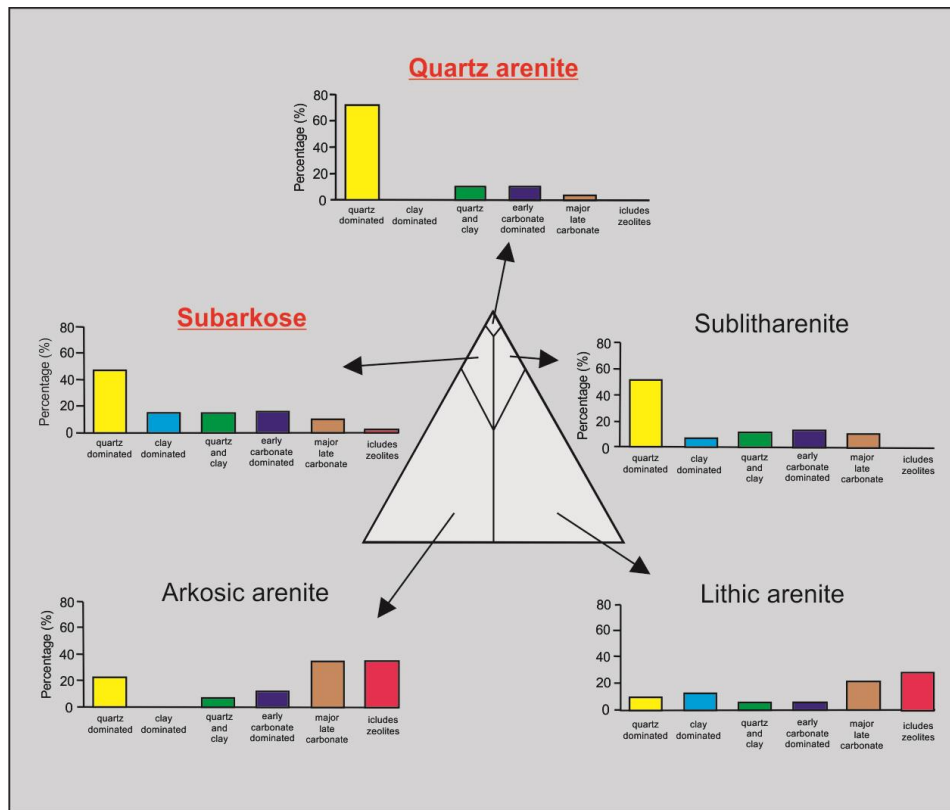


Figure 82: Relative variation of the quartz cement and rest of other cements in accordance with the type of rock. Based on QFL (Quartz-Feldspar-Lithic fragment) relative ratio, the uppermost Bedinan Formation sandstone levels are subarkose to quartz arenite (Worden and Morad, 2000).

9.3. Diagenetic Carbonate Cementation

The Gazzi-Dickinson method of point counting is used on the thin sections to measure the percentage of carbonate cement, and to identify the type of carbonate cements (calcite, dolomite) in the studied intervals. The percentage of isolated (patchy-shaped) pore filling carbonate cements (calcite and dolomite) in the studied sandstone levels (Figure 83) ranges between 4,93-9,25% (0,35-0,95% calcite, 4-8,9% dolomite) in the studied the 1st and the 2nd sandstone levels of uppermost Bedinan Formation. These isolated (patchy-shaped) carbonate cement in the studied sandstone levels can be associated with the dissolution of the plagioclase and K-feldspars which may create

secondary moldic porosity. The formation fluid becomes rich in calcium (Ca), potassium (K) and sodium (Na) as a consequence of dissolution reaction of feldspars (Worden and Morad, 2000; Rahman and McCann, 2011).

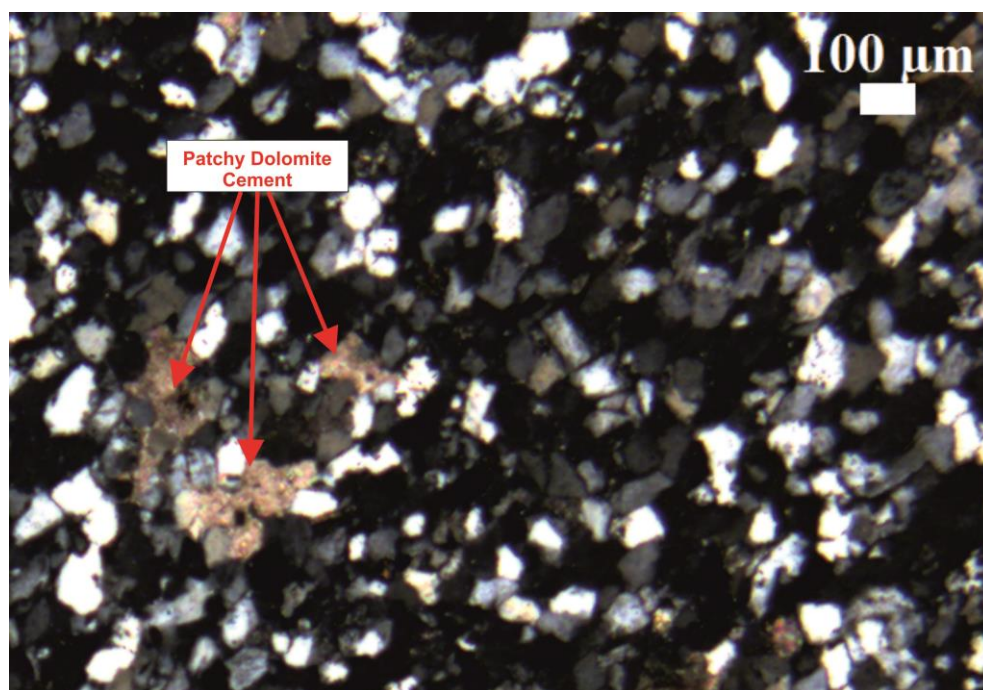
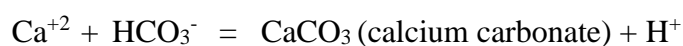


Figure 83: The photomicrography of isolated (patchy-shaped)dolomite cement in the 1st sandstone level of the uppermost Bedinan Formation (core-2) in F well.

During diagenesis, the calcium ions liberated by the dissolution reaction of feldspars react with the dissolved bicarbonates (HCO_3^-) which are freely circulating in the formation water (Worden and Morad, 2000) which resulted in the formation of calcium carbonate. This reaction is formulated (Worden and Morad, 2000) as below;



However, the most abundant carbonate cement mineral in the studied interval is dolomite (4-8,9%) rather than calcite (0,35-0,95%). It can be conceivably interpreted that during diagenesis, calcite cements of the studied intervals may have transformed

to dolomite by reacting with aluminum (Al) derived from the decomposition of K-feldspar and micas, or magnesium (Mg) derived from the transition reaction from smectite to illite (Hower et al., 1976; Boles and Franks, 1979; Lahann, 1980; Al-Ramadan, 2014).

As a consequence of burial diagenesis, it seems that quartz and feldspar minerals are partially replaced by calcite minerals. The melting of the minerals induced the development of dissolution porosity in the studied interval. Although no stylolite development was observed between the grains, chemical and physical compaction between the grains resulted in pressure solution between the grains.

9.4. The Impact of Diagenesis on the Reservoir Quality

In accordance with initial assessment, the coupling of production performance and well side (A, B, C, D, E, F wells) observations reveal that the main factors which have taken place as controlling factor for reservoir volume, flow rate and recovery of hydrocarbon are variations of clay coating minerals in the 1st and the 2nd sandstone levels of uppermost Bedinan Formation in the studied wells (A, B, C, D, E and F).

However, XRD bulk powder analysis, petrophysical and microscopic studies reveal that the factors deteriorating the reservoir quality and resulted in the heterogeneity of the studied reservoir levels in terms of porosity and permeability, are not only clay coating mineral but also quartz overgrowth around tightly packed quartz grains and carbonate cement in the studied intervals. The most abundant clay minerals in the sandstone reservoir levels of Bedinan Formation as already mentioned are illite, kaolinite and mixed clay layer (illite-smectite). Experimental studies exhibit that the clay coating minerals are the most prominent factor enhancing or deteriorating reservoir quality in terms of porosity, permeability and hydrocarbon recovery. While kaolinite enhances the reservoir quality by the formation of intracrystal and moldic porosity, illite and illite-smectite (montmorillonite) mixed clay layer have a negative effect on reservoir quality (Figure 84) (Al-Ramadan, 2006; Morad et al., 2010; Liu et

al., 2016). In support of this view, the clay rich sandstone levels of the Bedinan Formation in the studied wells (C, D and E) has low hydrocarbon production performance attributed to low reservoir quality, conversely the clay free sandstone levels in the wells (A, B, F wells) have considerable amount of production performance due to good reservoir quality. The most abundant illite clay coating minerals in the studied sandstone levels of interest have positive effect on porosity preservation by precluding quartz overgrowth; however, illite occludes pore throats partially to completely, hence deteriorate permeability and precludes fluid flow (Worden and Barclay, 2003; Al-Ramadan, 2006; Morad et al., 2010). The negative effects of illite on reservoir properties elucidate why the sandstone levels with the considerable amount of illite rich clay matrix in the wells so called C, D and E have low hydrocarbon production performance as a consequence of low permeability. The studies carried out on Ordos Basin's tight Chang 7 sandstone reservoir levels reveal that the influence of illite-smectite on the reservoir is almost same with illite (Liu et al., 2017). As already mentioned, illite mineral precludes quartz overgrowth, which forms during mesodiagenesis, hence preserves porosity (Morad et al., 2010). In support of this view, the thin section analysis under the microscope for the reservoir levels of interest reveal that quartz overgrowth is most abundant in clay free sandstone levels (e.g., the 1st and the 2nd sandstone levels in F well). Although quartz overgrowth results in porosity and permeability deteriorating in reservoir levels (Walderhaug, 2000; Worden and Morad, 2000; Morad et al., 2010), its negative effect on the reservoir quality of the levels of interest in A, B and F well is negligible in comparison with illite according to production performance and petrophysical interpretations.

The diagenetic pore filling carbonate cementation in the studied sandstone levels induces to the deterioration of porosity and permeability which precludes the fluid flow (Morad et al., 2010). However, the percentage of the carbonate cement in the studied sandstone intervals is almost same in the A, B and F wells according to the thin section analysis results. Therefore, the effect of the carbonate cement on reservoir

quality (porosity and permeability) of the studied interval can be interpreted as low in comparison with the clay coating minerals.

The negative effect of illite on reservoir and recovery of hydrocarbon is not limited with permeability. Illitization transition reactions from smectite and kaolinite induce the release of considerable amount of water as accentuated in the reactions formula (Hower et al., 1976; Lahann, 1980; McKinley et al., 2003; Al-Ramadan, 2014). The water released from the transition reactions causes hydrocarbon to move in pore spaces or inhibit the emplacement of oil. The reactions related water release and water wet behaviour of illite prove that high water saturation even in the zone above oil-water contact in uppermost Bedinan Formation sandstone levels penetrated in the studied wells were induced by the transition reaction between clay coating minerals or particularly illitization reaction. For instance, despite the fact that A, B and C wells were drilled on the same structure and the formation are reached at the shallower depth in C well than A and B wells, water saturation is higher at the sandstone levels of interest in C well than as A and B wells. The fact of low permeability, high water saturation at the sandstone levels of interest penetrated in C well explain the negative effect of illite on reservoir quality and hydrocarbon recovery.

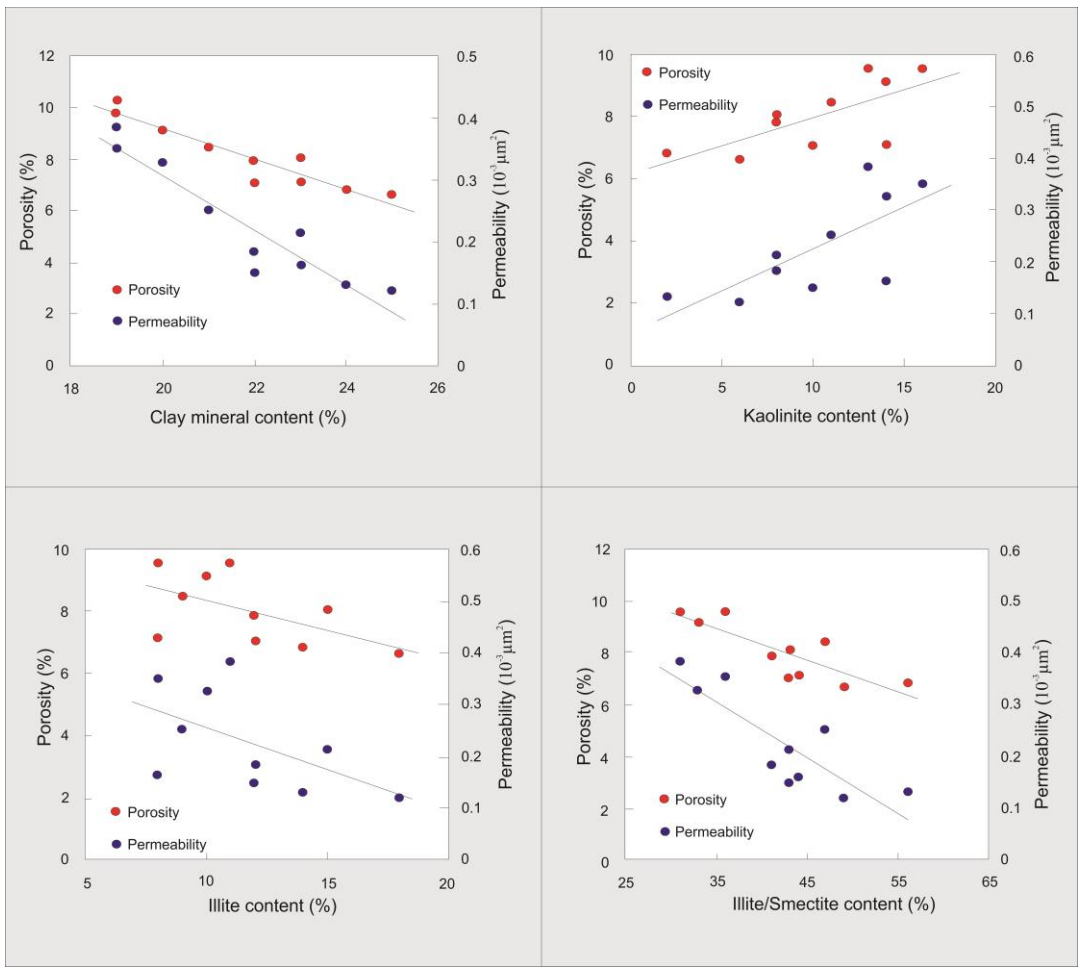


Figure 84: The experimental study through the impact of clay coating minerals on porosity and permeability of the Chang 7 sandstone reservoir levels (Ordos Basin) (Liu et al., 2016).

CHAPTER 8

DISCUSSION

According to the seismic line interpretations, the wireline log correlations, the well side observations and sedimentary records in the Late Ordovician units of the study area; the uppermost Bedinan Formation deposited in ice distal glaciomarine environments, and does not have any imprint of glaciogenic sedimentary features and ice related structures.

Sedimentological investigations are carried out to understand vertical and horizontal facies variation through the sandstone levels. The Gazzi-Dickinson method of point counting was the method that used to elucidate the type of sandstone, the tectonic setting where the sands are eroded and transferred to the depositional area. The relative abundance of quartz (Q), feldspar (F) and lithic fragment (L) indicates that the studied sandstone levels are subarkose to quartz arenitic with variable clay matrix (< %15), and derived from stable craton. Additionally, the quartz crystal orientation and crystal boundaries of the polycrystalline quartz served as a proxy for estimation of the source rock of the studied sandstone levels. In accordance with the point counting measurement, roundly 85 percent monocrystalline quartz and 15 percent percent polycrystalline quartz with straight boundary were counted which indicates that igneous rock constitutes the source rock of the studied sandstone levels.

The porosity of bulk volume of the studied sandstone body is interrogated via the point counting and the petrophysical interpretations. Furthermore, X-ray computed tomography imagin technique is used to determine 3D volume and diameter of each pore. While the porosity (intergranular and minor amount of dissolution porosity) of the sandstone levels is measured as between 16-19% according to the point counting method, the petrophysical interpretations carried out by Nutech Energy Company

indicate that the porosity (effective porosity) in the studied intervals ranges between 11-21%. The volume and maximum diameter values of pore spaces of the selected cube are in turn 0,001-0,04 mm³ and 0,095-1,023 mm according to x-ray computed tomography measurements. The porosity of the randomly selected interval of the 1st sandstone level (F well) measured by X-ray CT is 1.2 %.

Comprehensive depositional environment interpretation for the 1st and 2nd sandstone levels were examined in support of sedimentary structures, ripple mark geometry together with corresponding Gamma Ray reading changes in trend. Based on the results of the assessment, the 1st and 2nd sandstone levels were deposited between the lower shoreface and upper shoreface; whereas the shale dominant interlayers (lying between 1st and 2nd sandstone levels and beneath the 2nd sandstone level) were accumulated between offshore and offshore transition zone.

Hydrocarbon production performance (daily production rates) variation observed in A, B, C, D, E and F wells from uppermost Bedinan Formation and 3D petrophysical modelings (permeability and water saturation distribution maps by using Petrel E&P Software platform, version 2016.3 of Schlumberger company) is the indicator of reservoir heterogeneity inferred to variation in porosity, permeability and capillary pressure. Additionally, permeability distribution in the studied levels having the CV values (coefficient of variation) of 2.2805 indicates very heterogeneous permeability distribution. Although reservoir quality is characterized as a function of depositional facies (sorting, grain size, grain morphology, sand/mud ratio, provenance), diagenesis (compaction, dissolution, cementation, development of clay coating minerals) and structural features (fault, fracturing e.t.); in this thesis, eodiagenetic and mostly mesodiagenetic clay coating minerals, quartz and carbonate cements were investigated for the reservoir quality characterization.

Enhanced spectral gamma ray which enables the differentiation of three radioactive elements (thorium, potassium and uranium) and Photoelectric Factor log readings were plotted to ternary diagrams proposed by Schlumberger (2009) to identify clay

minerals association in the matrix. Based on the cross plots (thorium-potassium, potassium-Pefz and thorium/potassium-thorium/uranium), the clay mineral association in matrix of 1st and 2nd sandstone levels is in order of abundance by illite and mixed clay layer. Clay typing performed by XRD analysis resulted in that the clay coating minerals occupying the matrix of the studied levels are illite, kaolinite and illite-smectite(montmorillonite) mixed clay layer. While the some clays in the matrix were formed during early diagenesis because of their heavier density and acidity relative to the water, most of them such as illite were transformed during mesodiagenesis stage from less stable minerals like smectites, feldspars or kaolinites through progressive temperature increment with depth and available potassium ions in formation water.

Another mesodiagenetic originated product is quartz overgrowth developed around tightly packed detrital quartz grains of the sandstone levels of interest. While pressure solution, transformation reactions between clay minerals, dissolution of feldspars constitute the main source of silica, temperature increment attributed with burial diagenesis is the main reason for induced quartz precipitation or quartz overgrowth in the levels of interest. The 1st and 2nd sandstone levels having high clay content and low production rate observed in B, C and D wells include almost no quartz cement because of the fact that clay content especially illite inhibits quartz cementation.

Transition reactions between clay coating minerals, particularly illitization reactions during burial diagenesis cause releasing of the considerable amount of water which preclude oil emplacement or movement of hydrocarbon.

With regard to the integrity of the data of well side observation, production performance, XRD analysis, petrophysical interpretation and sedimentological analyses reveal that the main factor exerted great control on reservoir quality is clay coating minerals. Especially existence of illite and illite-smectite mixed clay layer the studied levels induce deterioration of reservoir quality in terms of permeability, flow rate, recovery of hydrocarbon and reservoir volume.

CHAPTER 9

CONCLUSION

The results of the study are listed below:

1. The studied sandstone levels of the uppermost Bedinan Formation can be classified as subarkose-quartzarenite.
2. The framework grains of the sandstone interval are derived from the stable craton. Additionally, igneous rock constitutes the source for the sandstones of the studied interval.
3. While the studied 1th and 2nd sandstone levels are deposited between wave-dominated lower shoreface to upper shoreface environment, the shale dominant interlayers (shale-1 and shale-2) are piled in offshore transition-offshore environment.
4. The uppermost Bedinan Formation is deposited in ice-distal glaciomarine environment; therefore, the reservoir heterogeneity in the uppermost Bedinan Formation can not be attributed with Hirnantian glacial activity.
5. The porosity (total) of the studied sandstone levels ranges between 16-19% according to Gazzi-Dickinson method of point counting carried out on the thin sections of the sandstone levels. Furthermore, the effective porosity of the interval ranges between 11-21% in accordance with the petrophysical log interpretation.

6. The maximum diameter and the volume of each pore are in turn 0.095-1,023 mm and 0,001-0,04 mm³ according to X-ray computed tomography measurements. The porosity of the randomly drawn square on the studied core is 1,2 %. The dominantly intergranular porosity with relatively minor amount of dissolution porosity is observed not only in the thin section analyses but also in X-ray computed tomography analysis.
7. The studied sandstone intervals show reservoir heterogeneity in terms of porosity, permeability and capillary pressure in vertical and horizontal direction, which leads to the fact that while commercial oil production has been performed from the uppermost Bedinan Formation sandstone levels in some wells, the others could not produce or produce oil in very low daily rates.
8. Permeability distribution in the sandstone levels having CV (coefficient of variation) value of 2.2805 indicates very heterogeneous permeability distributions.
9. The main factors affecting to the reservoir heterogeneity in the sandstone levels are; diagenetic clay coating minerals in matrix, syntaxial quartz overgrowth and carbonate (calcite and dolomite) cement.
10. The clay coating minerals forming the matrix of the studied sandstone level are illite, kaolinite and mixed clay layer (illite - smectite) determined by the use of XRD bulk powder analysis, petrophysical wireline log interpretations, the provenance and the depositional environment of the level of interest.
11. The studied intervals of the uppermost Bedinan Formation show evidence of the effects of mesodiagenetic environment.

12. Temperature and potassium availability with burial depth in the studied intervals are the key factors that control the illitization.
13. The illitization of smectite and kaolinite induces the release of considerable amount of water, which leads to petroleum migration and/or the inhibition of petroleum emplacement. Therefore, the intervals (e.g. the 1st sandstone level in C well) above oil-water contact have high water saturation.
14. Although the syntaxial quartz overgrowth and carbonate cements cause to reservoir deterioration in the studied interval, the main factor causing reservoir deterioration of the studied intervals is the mesodiagenetic clay coating minerals, especially the presence of illite and illite-smectite mixed clay layer.

REFERENCES

- Adams, A. E., Mackenzie, W., & Guilford, C. (1984). *Atlas of Sedimentary Rocks under the Microscope*. Beccles and London: Longman Group UK Ltd.
- Ajdukiewicz, J. M., & Lander, R. H. (2010). Sandstone Reservoir Quality Prediction: The State of the Art. *AAPG Bulletin*, 1083-1091.
- Akin, S., & Kovscek, A. R. (2014). Computed Tomography in Petroleum Engineering Research. *The Geological Society of London*, 23-38. doi:10.1144/GSL.SP.2003.215.01.03
- Ala, M. A., & Moss, B. (1979). Comparative Petroleum Geology of Southeast Turkey and Northeast Syria. *Journal of Petroleum Geology*, 3-27.
- Al-Laboun, A., Al-Quraishi, A., Zaman, H., & Benaafi, M. (2014). Reservoir Characterization of the Burqan Formation Sandstone from Midyan Basin, Northwestern Saudi Arabia. *Turkish Journal of Earth Science*, 204-214.
- Al-Ramadan, K. (2006). Impact of Diagenetic Alterations on Reservoir Quality and Heterogeneity of Paralic and Shallow Marine Sandstones. *Acta Universitatis Upsaliensis Uppsala*.

Al-Ramadan, K. (2014). Illitization of Smectite in Sandstones: The Permian Unayzah Reservoir, Saudi Arabia. *Arab. J. Sci. Eng.*, 407-412.

Al-Ramadan, K. A., Hussain, M., Imam, B., & Saner, S. (2004). Lithologic Characteristics and Diagenesis of the Devonian Jauf Sandstone at Ghawar Field, Eastern Saudi Arabia. *Marine and Petroleum Geology*, 1221-1234.

Al-Ramadan, K., Franks, S., Al-Shammari, S., Rees, A., Koeshidayatullah, A., & Abu-Khamsin, S. (2017). Depositional and Diagenetic Barriers, Baffles and Conduits: Permian-Carboniferous Unayzah Reservoir, Nuayyim Field, Central Saudi Arabia. *Journal of Petroleum Geology*, 85-103.

Alsharhan, A., & Nairn, A. (1997). *Sedimentary Basins and Petroleum Geology of the Middle East*. Amsterdam: Elsevier.

Amaco. (1985), Turkey ESRI report no. ET 85/1 Geological Studies in SE Turkey (Pervari-Beytüşşebap, Hazro, Mardin): TPAO Arama Grubu, Rapor no. 2115, 214 s.

Anovitz, L. M., Cole, D. R., Jackson, A. J., Rother, G., Littrell, K., Allard, L. F., . . . Wesolowski, D. J. (2015). Effect of Quartz Overgrowth Precipitation on the 1 Multiscale Porosity of Sandstone: A (U)SANS and Imaging Analysis. *Geochimica et Cosmochimica Acta*.
doi:<http://dx.doi.org/10.1016/j.gca.2015.01.028>.

- Araç, M., & Öncü, H. (1990). Sedimentology of the Garzan Formation in the Oyuktaş-Bada Fields of District X, SE Turkey. 8th Petroleum Congress of Turkey (s. 297-304). Ankara: Turkish Association of Petroleum Geologists.
- Aydemir, A. (2012). Comparison of Mississippian Barnett Shale, Northern-Central Texas, USA and Silurian Dadas Formation in Southeast Turkey. *Journal of Petroleum Science and Engineering*, 81-93.
- Blakslee, G., Sturz, C. and Hansen, M., (1960) Regional Geological Compilation report of Southeast Turkey and Adjacent Areas (Tidewater Oil Company Report): Petrol İşleri Genel Müdürlüğü, 116p.
- Blumenthal. (1947). Geologische der Taurusketten im Hinterland van Seydişehir und Beyşehir: MTA Ser. D., no. 2.
- Boggs, S. (2010). Principles of Sedimentology and Stratigraphy. (P. Lynch, Dü.) New Jersey, United States of America: Pearson Education.
- Boles, J. R., & Franks , S. (1979). Clay Diagenesis in Wilcox Sandstones of Southwest Texas: Implications of Smectite Diagenesis on Sandstone Cementation. *Journal of Sedimentary Petrology*, 55-70.
- Bolgi, T. (1961). V. Petrol Bölgesi Seksiyon Ölçmeleri AR/TPO/261 nolu Saha ile Reşan-Dodan Arası Batısındaki Sahanın Strüktürel Etüdlere: TPAO Arama Grubu, Rapor no. 162, 52 s.

Boulila, S., Laskar, J., Haq, B., Galbrun, B., & Hara, N. (2018). Long-Term Cyclicities in Phanerozoic Sea-Level Sedimentary Record and Their Potential Drivers. *Global and Planetary Change*. doi:10.1016/j.gloplacha.2018.03.004

Bozdogan, N., Göncüoğlu, M., & Kozlu, H. (1996). Lower Paleozoic Stratigraphy of Southeastern Turkey. *Serie Correlacion Geologica*, 47-57.

Bozdoğan, N., & Erten, T. (1990). The Age and Effects of the Mardin High, SE Anatolia. 8 th Petroleum Congress of Turkey (s. 207-227). Ankara: Turkish Association of Petroleum Geologists Uctea Chamber of Petroleum Engineers.

Bozdoğan, N., & Ertuğ, K. (1995). Geological Evolution and Paleogeography of the Southeast Anatolia in the Paleozoic. Early Paleozoic Evolution in NW Gondwana (s. 39-49). Ankara: Turkish Association of Petroleum Geologist.

Bozdoğan, N., Bayçelebi, O., & Willink, R. (1987). Güneydoğu Anadolu Hazro Bölgesinde (X. Bölge Kuzeyi) Paleozoyik Stratigrafisi ve Petrol Üretkenliği. 7th Biannual Petroleum Congress of Turkey. Ankara: TAPG.

Bozdoğan, N., Gürgey, A., Aköz, Ö., & Erenler, M. (1996). Chronostratigraphy and Paleogeographic Evolution of the Sayındere, Kastel and Karadut Formations at North of Diyarbakir Region (SE Anatolia). 11 th Petroleum Congress of Turkey. Ankara: Turkish Association of Petroleum Engineers.

- Bozdoğan, N., Karabulut, A., Erten, T., İztan, H., Çubukçu, A., & Korucu, M. (1994). Stratigraphy and Petroleum Potential of the Paleozoic Units in Diyarbakır Area, SE Turkey. 10th Petroleum Congress of Turkey. Ankara: Turkish Association of Petroleum Geologists.
- Bozkaya, Ö., & Yalçın, H. (2010). Geochemistry of Mixed-Layer Illite-Smectites from an Extensional Basin, Antalya Unit, Southwestern Turkey. *Clays and Clay Minerals*, 644-666.
- Bozkaya, Ö., Yalçın, H., & Kozlu, H. (2011). Clay Mineralogy of the Paleozoic-Lower Mesozoic Sedimentary Sequence from the Northern Part of the Arabian Platform, Hazro (Diyarbakir, Southeast Anatolia). *Geologica Carpathica*, 489-500. doi:0.2478/v10096-011-0035-6
- Burst, J. F. (1969). Diagenesis of Gulf Coast Clayey Sediments and Its Possible Relation to Petroleum Migration. *AAPG Bulletin*, 73-93.
- Burtner, R. L., & Warner, M. (1986). Relationship Between Illite/Smectite Diagenesis and Hydrocarbon Generation in Lower Cretaceous Mowry and Skull Creek Shales of the Northern Rocky Mountain Area. *Clays and Clay Minerals*, 390-402. doi:10.1346/CCMN.1986.0340406
- Cater, J., & Gillcrist, J. (1994). Karstic Reservoir of the Mid-Cretaceous Mardin Group, SE Turkey: Tectonic and Eustatic Controls on their Genesis, Distribution and Preservation. *Journal of Petroleum Geology*, 253-278.

Chang, H. K. (1986). Comparisons between the Diagenesis of Dioctahedral and Trioctahedral Smectite, Brazilian Offshore Basins. *Clays and Clay Minerals*, 407-423.

Charvin, K., Hampson, G., Gallagher, K., Storms, J., & Labourdette, R. (2011). Characterization of Controls on High-Resolution Stratigraphic Architecture in Wave-Dominated Shoreface-Shelf Parasequences Using Inverse Numerical Modeling. *Journal of Sedimentary Research*, 562-578.

Chen, P., (1977). Table of key lines in X-ray powder diffraction patterns of minerals in clays and associated rocks: Indiana Geological Survey Occasional Paper 21, 67 p., 1 table, 21 app.

Chipera, S. J., & Bish, D. L. (2013). Fitting Full X-Ray Diffraction Patterns for Quantitative Analysis: A Method for Readily Quantifying Crystalline and Disordered Phases. *Advance in Material Physics and Chemicals*, 47-53.

Cobb, R. E. (1957 a). Reconnaissance of the Derik Area Southeast Turkey Columnar Section Sadan-Sosink-Paleozoic: TPAO Arama Grubu, Arşiv no. 567.

Cobb, R. E. (1957 c). Columnar section Bedinan-Kanisorik-Paleozoic: TPAO Arama Grubu, Arşiv no. 576.

- Coşkun, B. (1996). Tectonic Controls on the Evolution of Porosity in the Cretaceous Mardin Group Carbonates, Adıyaman Oilfields, SE Turkey. *Journal of Petroleum Geology*, 445-460.
- Craigie, N. W., Rees, A., MacPherson, K., & Berman, S. (2016). Chemostratigraphy of the Ordovician Sarah Formation, North West Saudi Arabia: An Integrated Approach to Reservoir Correlation. *Marine and Petroleum Geology*, 1056-1080.
- Creodoz, A., Bildstein, O., Jullien, M., Raynal, J., Trotignon, L., & Pokrovsky, O. (2011). Mixed-Layer Illite–Smectite Reactivity in Acidified Solutions: Implications for Clayey Caprock Stability in CO₂ Geological Storage. *Applied Clay Science*, 402-408.
- Çoruh, T., Yakar, H., & Ediger, V. (1997). Güneydoğu Anadolu Bölgesi Otokton İstifinin Biyostratigrafi Atlası. Ankara: Türkiye Petrolleri A.O. Araştırma Merkezi Grubu Başkanlığı.
- Dean, W. T. (1967). The Correlation and Trilobite Fauna of the Bedinan Formation (Ordovician) in South-Eastern Turkey. *Bulletin of the British Museum*, 81-123.
- Dean, W. T. (1975). Cambrian and Ordovician Correlation and Trilobite Distribution in Turkey. *Fossils and Strata*.

Dean, W. T. (1979a). Report on the Cambro-Ordovician Stratigraphy and Faunals of the Derik-Mardin Region, S. E. Turkey: TPAO Arama Grubu, Rapor no. 1453, 3 s.

Dean, W. T. (1979b). Report on the Cambro-Ordovician Stratigraphy and Faunals of the Hakkari Region, S. E. Turkey: TPAO Arama Grubu, Rapor no. 1453, 13 s.

Dean, W. T., Martin, F., Monod, O. (1993). Report on Field Programme with TPAO in Northern and Southern Turkey, 1990-1992: TPAO Arama Grubu, Rapor no. 3272, 64 s.

Dean, W. T., Monod, O., Günay, O. (1981) Correlation of Cambrian Rocks in Southeastern Turkey: Petroleum Administration Publication, Bulletin no. 25, p. 269-291.

Dean, W. T. & Monod, O. (1985). A New Interpretation of Ordovician Stratigraphy in the Bahçe Area, Northern Amanos Mountains, South Central Turkey: Geology Magazine, vol. 122, no.1, p. 15-25.

Delabroye, A., & Vecoli, M. (2010). The End-Ordovician Glaciation and the Hirnantian Stage: A Global Review and Questions about Late Ordovician Event Stratigraphy. *Earth-Science Reviews*, 269-282.

- Demirel, I. H., & Guneri, S. (2000). Cretaceous Carbonates in the Adiyaman Region, SE Turkey: An Assessment of Burial History and Source-Rock Potential. *Journal of Petroleum Geology*, 91-106.
- Demirtaşlı, E. (1974). İran, Pakistan ve Türkiye'deki Alt Paleozoyik Yaşlı Kayaların Stratigrafik Korrelasyonu. Ankara: Maden Tetkik ve Arama Enstitüsü.
- Dickinson, W. R. (1970). Interpreting Detrital Modes of Graywacke and Arkose. *Journal of Sedimentary Petrology*, 695-707.
- Dickinson, W. R. (1985). Interpreting Provenance Relations from Detrital Modes of Sandstones. Provenance of Arenites, 333-361.
- Dickinson, W. R., & Suczek, C. (1979). Plate Tectonics and Sandstone Compositions. *AAPG Bulletin*, 2164-2182.
- Dietrich, P., Ghienne, J.-F., Lajeunesse, P., Normandeau, A., Deschamps, R., & Razin, P. (2018). Deglacial Sequences and Glacio-Isostatic Adjustment: Quaternary Compared with Ordovician Glaciations. The Geological Society of London.
- Duran, O., Şemşir, D., Sezgin, İ., & Perinçek, D. (1988). Stratigraphy and Sedimentology of the Midyat and Silvan Groups and Their Hydrocarbon Potentials, Southeast Turkey. *TAPG Bulletin*, 99-126.

Durkee, E. F. (1961). Proposed Stratigraphic Nomenclature, District VI, Southeast Turkey: Petroleum Administration Publication, Bulletin no. 6, p. 38-46

El-Deek, I., Abdullatif, O., Korvin, G. (2017). Heterogeneity Analysis of Reservoir Porosity and Permeability in the Late Ordovician Galcio-fluvial Sarah Formation Paleovalleys, Central Saudi Arabia. *Arabian Journal of Geoscience*, DOI: 10.1007/s12517-017-3146-2.

Ettensohn, F. R. (2010). Origin of Late Ordovician (mid-Mohawkian) Temperate-Water Conditions on Southeastern Laurentia: Glacial or Tectonic? *The Geological Society of America*, 163-175.

Fisher, R., & Land, L. (1987). Diagenetic History of Eocene Wilcox Sandstones, South-Central Texas. *Geochimica et Cosmochimica Acta*, 3073-3074.

Fitch, P. J. R., Lovell, M. A., Davies, S. J., Pritchard, T., Harvey, P. K. (2015). An Integrated and quantitative Approach to Petrophysical Heterogeneity. *Marine and Petroleum Geology*, 82-96.

Ghienne, J.-F., Le Heron, D., Moreau, J., Denis, M., & Deynoux, M. (2007). The Late Ordovician Glacial Sedimentary System of the North Gondwana Platform. *International Association of Sedimentologists*.

- Ghienne, J.-F., Monod, O., Kozlu, H., & Dean, W. (2010). Cambrian–Ordovician Depositional Sequences in the Middle East: A Perspective from Turkey. *Earth-Science Reviews*, 101-146.
- Goncuoglu, M. C., & Kozlu, H. (2000). Early Paleozoic Evolution of the NW Gondwanaland: Data from Southern Turkey and Surrounding Regions. *Gondwana Research*, 315-324.
- Gossage, D. W. (1956). Compiled Progress Report on the Geology of Part of Petroleum District VI, Southeast Turkey: N. V. Turkse Shell, Report no. GRT. 2,22p
- Guiraud, R., Bosworth, W., Thierry, J., & Delplanque, A. (2005). Phanerozoic Geological Evolution of Northern and Central Africa: An Overview. *Journal of African Earth Science*, 83-143.
- Gürsu, S., Möller, A., Usta, D., Köksal, S., Ateş, Ş., Sunkari, E., & Göncüoğlu, M. (2017). Laser Ablation Inductively Coupled Plasma Mass Spectrometry U-Pb Dating of Detrital and Magmatic Zircons of Glacial Diamictites and Pebbles in Late Ordovician Sediments of the Taurides and Southeast Anatolian Autochthon Belt, Turkey: Indications for Their. *The Journal of Geology*.
- Güven, A., Dinçer, A., Tuna, M., & Çoruh, T. (1991). Stratigraphic Evolution of the Campanian-Paleocene Autochthonous Succession of the Southeast Anatolia. *Ozan Sungurlu Symposium Proceedings* (s. 238-261). Ankara: TPAO.

Haq, B. U., & Al-Qahtani, A. (2005). Phanerozoic Cycles of Sea-Level Change on the Arabian Platform. *GeoArabia*.

Haq, B. U., & Schutter, S. (2008). A Chronology of Paleozoic Sea-Level Changes. *Science*. doi:10.1126/science.1161648

Handfield, R. W., Bryant, G. F., Keskin, C. (1959). Measured Section, Korudağ (American Overseas Petroleum): TPAO Arama Grubu, Arşiv no. 523.

Herrmann, A. D., Haupt, B., Patzkowsky, M., Seidov, D., & Slingerland, R. (2004). Response of Late Ordovician Paleooceanography to Changes in Sea Level, Continental Drift, and Atmospheric pCO₂: Potential Causes for Long-Term Cooling and Glaciation. *Palaeogeography, Palaeoclimatology, Palaeoecology*, 385-401.

Howell, J. (2005). Sedimentary Environments | Shoreline and Shoreface Deposits. *Encyclopedia of Geology*, 570-579.

Hower, J., Eslinger, E. V., Hower, M. E., & Perry, E. A. (1976). Mechanism of Burial Metamorphism of Argillaceous Sediment: 1. Mineralogical and Chemical Evidence. *Geological Society of America Bulletin*, 725-737.

Hurst, A., & Irwin, H. (1982). Geological Modelling of Clay Diagenesis. *Clay Minerals*, 5-22.

Ingersoll, R. V. (1984). The Effect of Grain Size on Detrital Modes: A Test of the Gazzi-Dickinson Point-Counting Method. *Journal of Sedimentary Petrology*, 103-116.

Jiang, S. (2012). Clay Minerals from the Perspective of Oil and Gas Exploration. M. Valaskova, *Clay Minerals in Nature* (s. Chapter 2).

Karabulut, A., Köylüoğlu, M., & Sayılı, A. (1992). Evaluation of the Reservoirs in Mardin Group and Karaboğaz Formation in the Platform Region Petroleum District X, S.E. Anatolia, Türkiye. 9th Petroleum Congress and Exhibition of Türkiye (s. 471-477). Ankara: Turkish Association of Petroleum Geologist.

Kellogg, H. E. (1960a). Stratigraphic Report, Hazro Area, Petroleum District V, SE Turkey (American Overseas Petroleum (AMOSEAS) Report): Report no : 1,42 s (unpublished). Ankara.

Kellogg, H. E. (1960b). Stratigraphic Report, Bitlis-Siirt Area, Petroleum District V, Southeast Turkey (American Overseas Petroleum (AMOSEAS) Report) : Report no: 2,25 s (unpublished). Ankara

Kellogg, H. E. (1960c). Stratigraphic Report, Derik-Mardin Area, Petroleum District V, Southeast Turkey (American Overseas Petroleum (AMOSEAS) Report) Report no: 1367 (unpublished). Ankara.

Kellogg, H. E. (1961). Regional Stratigraphy and Petroleum Possibilities of Southeast Turkey (American Overseas Petroleum (AMOSEAS) Report): Petrol İşleri Genel Müdürlüğü Teknik Arşivi, Kutu no. 201, Rapor no. 1, 29 s. (TPAO Arama Grubu, Rapor no. 767)

Koaster, E. A. (1963). Petroleum Geology of District V, Turkey with Special Reference to License no. 649 of Aladdin Middle East Ltd. (AME Report): Petrol İşleri Genel Müdürlüğü Teknik Arşivi, Kutu no. 125, Rapor no. 4,22 s.

Klaja, J., & Dudek, L. (2016). Geological interpretation of spectral gamma ray (SGR) logging in selected boreholes. Oil and Gas Institute – National Research Institute. doi:10.18668/NG2016.01.01

Konert, G., Afifi, A., & Al-Hajri, S. (2001). Paleozoic Stratigraphy and Hydrocarbon Habitat of the Arabian Plate. *GeoArabia*.

Köylüoğlu, M. (1986). Güneydoğu Anadolu Otokton Birimlerinin Kronostratigrafi, Mikrofasiyes ve Mikrofosilleri. TPAO Araştırma Merkezi, Eğitim Yayınları.

Köylüoğlu, M. (1988). The Paleontology and Stratigraphy of the Beloka Formation in Which Kasrık and Şemikan Phosphate Deposits are Found, Mardin-Mazıdağı, Southeast Turkey. *TAPG Bulletin*, 141-151.

Krausert, R. & Temple, P. (1957). Derik Section (Esso Standart (Turkey) Inc.): TPAO Arama Grubu, Arşiv no. 920.

- Kübler, B., & Jaboyedoff, M. (2000). Illite Crystallinity. *Sciences de la Terre et des planètes*, 75-89.
- Laboun, A. A. (2010). Paleozoic Tectono-Stratigraphic Framework of the Arabian Peninsula. *Journal of King Saud University*, 41-50.
- Lahann, R. W. (1980). Smectite Diagenesis and Sandstone Cement: The Effect of Reaction Temperature. *Journal of Sedimentary Petrology*, 755-760.
- Lake, L., & Jensen, J. (1991). A review of heterogeneity measures used in reservoir characterization. *In Situ* 15(4):409–440.
- Le Hérisse, A., Molyneux, S. G., & Miller, M. A. (2015). Late Ordovician to Early Silurian Acritarchs from the Qusaiba-1 Shallow Core Hole, Central Saudi Arabia. *Review of Palaeobotany and Palynology*, 22-59.
- Le Heron, D. P., & Howard, J. (2010). Evidence for Late Ordovician Glaciation of Al Kufrah Basin, Libya. *Journal of African Earth Sciences*, 354-364.
- Le Heron, D. P., Craig, J., Sutcliffe, O. E., & Whittington, R. (2006). Late Ordovician Glaciogenic Reservoir Heterogeneity: An Example from the Murzuq Basin, Libya. *Marine and Petroleum Geology*, 655-677.

- Lefebvre, V., Servais, T., François, L., & Averbuch, O. (2010). Did a Katian Large Igneous Province Trigger the Late Ordovician Glaciation? A Hypothesis Tested with a Carbon Cycle Model. *Palaeogeography, Palaeoclimatology, Palaeoecology*, 310-319. doi:10.1016/j.palaeo.2010.04.010
- Liu, G., Li, S., Gu, D., Lu, Y., & Asamoah, E. (2016). Experimental Study of Petrophysical Properties of a Tight Formation by Considering the Clay Minerals and Flow Sensitivities. *Earth Sciences Research Journal*. doi:10.15446/esrj.v20n2.54508
- Lüning, S., Craig, J., Fitches, B., Mayouf, J., Busrewil, A., El Dieb, M., . . . McIlroy, D. (1999). Re-Evaluation of the Petroleum Potential of the Kufra Basin (SE Libya\ NE Chad) does the Source Rock Barrier Fall? *Marine and Petroleum Geology*, 693-718.
- Lüning, S., Craig, J., Loydell, D., Storch, P., & Fitches, B. (2000). Lower Silurian 'hot shales' in North Africa and Arabia: Regional Distribution and Depositional Model. *Earth-Science Reviews*, 121-200.
- Mantovani, M., Escudero, A., & Becerro, A. (2010). Effect of Pressure on Kaolinite Illitization. *Applied Clay Science*, 342-347.
- Martini, I. P., French, H. M., & Alberti, A. P. (2011). Ice-Marginal and Periglacial Processes and Sediments: An Introduction. *Geological Society*, 1-13. doi:10.1144/SP354.1

- Martín-Martín, J., Gómez-Gras, D., Sanfeliu, T., Permanyer, A., Núñez, J. A., & Parcerisa, D. (2006). Conditions of Kaolin Illitization in the Permo-Triassic Sandstones from the SE Iberian Ranges, Spain. *Journal of Geochemical Exploration* 89, 263-266.
- Mason, S. L. (1930). Geology of Prospective Oil Territory in Republic of Turkey: AAPG Bulletin, vol. 14, no. 6, p. 687-707.
- Masri, A. (2017). Late Ordovician Glacial and Glacio-Fluvial Paleovalley Architecture and Sedimentation in Southeast Jordan and Northwest Saudi Arabia. *Arab J Geosci.* doi:10.1007/s12517-017-3081-2
- Maxson, J. H. (1936). Geology and Petroleum Possibilities, and Mineral Resources of Southeastern Turkey: MTA Derleme no. 680, 80 s.
- Maxson, J. H. (1937). Reconnaissance Geology, Oil Possibilities, and Mineral Resources of Southeastern Turkey: MTA Derleme no. 680, 80 s.
- McKinley, J., Worden, R., & Ruffell, A. (2003). Smectite in Sandstones: A Review of the Controls on Occurrence and Behaviour during Diagenesis. *Int. Assoc. Sedimentol. Spec. Publ.*, 109-128.
- Mees, F., Rudy, S., Geet, M., & Jacobs, P. (2003). Applications of X-Ray Computed Tomography in the Geosciences. Geological Society of London.

- Monod, O., Kozlu, H., Ghienne, J.-F., Dean, W., Günay, Y., Le Hérissé, A., Robardet, M. (2003). Late Ordovician Glaciation in Southern Turkey. *Terra Nova*, 249-257.
- Monod, O., and Dean, W. T. (1980). TPAO 1980 Field Season Report: TPAO Arama Grubu, Rapor no. 1875, 29 s.
- Morad, S., Al-Ramadan, K., Ketzer, J., & De Ros, L. (2010). The Impact of Diagenesis on the Heterogeneity of Sandstone Reservoirs: A Review of the Role of Depositional Facies and Sequence Stratigraphy. *AAPG Bulletin*, 1267-1309.
- Moore, J. C., & Reynolds, D. M. (1997). *X-Ray Diffraction and the Identification and Analysis of Clay Minerals*, 2nd ed. Xviii 378pp. Oxford, New York: Oxford University Press, doi: 10.1017/S0016756898501501.
- Morsilli, M., & Pomar, L. (2012). Internal Waves vs. Surface Storm Waves: A Review on the Origin of Hummocky Cross-Stratification. *Terra Nova*, 273-282.
- Moses, H. F. (1934). *Geological Report on the Mardin-Cizre Region, Southeast Turkey*: MTA Derleme no. 212, 17 s.
- Munnecke, A., Calner, M., Harper, D., & Servais, T. (2010). Ordovician and Silurian Sea–Water Chemistry, Sea Level, and Climate: A synopsis. *Palaeogeography, Palaeoclimatology, Palaeoecology*, 389-413.

- Nabawy, B. S., & Sharawy, M. (2015). Hydrocarbon Potential, Structural Setting and Depositional Environments of Hammam Faraun Member of the Belayim Formation, Southern Gulf of Suez, Egypt. *Journal of African Earth Sciences*, 93-110. doi:<http://dx.doi.org/10.1016/j.jafrearsci.2015.09.010>
- Nardin, E., Godd ris, Y., Donnadi u, Y., Hir, G., Blakey, R., Puc at, E., & Aretz, M. (2011). Modeling the Early Paleozoic Long-Term Climatic Trend. *Geological Society of America Bulletin*. doi:10.1130/B30364.1
- Nazik, A., T rkmen,  ., Aksoy, E., Orhan, H., Ko  Tařın, C., Ognjanova-Rumenova, N., & řeker, E. (2013). New Paleontological and Sedimentological Data Related to Closure of Neotethys at the Southeastern Anatolia (Adiyaman). *TAPG Bulletin*, 29-53.
- N. V. Turkse Shell. (1966). The Kevan Anticline, a Complex Foothills Structure in Northeastern District VI: Petroleum Administration Publication, Bulletin no. 11, p. 61-63.
- Oktay, B., & Wellman, C. (2019). Palynological Analysis of Upper Ordovician to Lower Silurian Sediments from the Diyarbakir Basin, Southeastern Turkey. *Review of Palaeobotany and Palynology*, 28-46.
-  zt rk, S. S., Demirel,  ., & G nay, Y. (2016). Petroleum Source Rock Potential of the Silurian Dadař Shales in the Hazro and Korudaę regions of Southeast Anatolia, Turkey. *Marine and Petroleum Geology*.

- Paris, F., Herisse, A. L., Monod, O., Kozlu, H., Ghienne, J. F., Dean, W. T., . . . Gunay, Y. (2007). Ordovician Chitinozoans and Acritarchs from Southern and Southeastern Turkey. *Revue de Micropaleontologic*, 81-107.
- Pemberton, S. G., MacEachern, J., Dashtgard, S., Bann, K., Gingras, M., & Zonneveld, J.-P. (2012). Shorefaces Developments in Sedimentology (s. 563-603).
- Perinçek, D. (1978). V-VI-IX. Bölge (Güneydoğu Anadolu Otokton-Allokton Birimler) Jeoloji Sembolleri: TPAO Arama Grubu, Arşiv no. 6657.
- Perinçek, D. (1980). Sedimentation on the Arabian Shelf Under the Control of Tectonic Activity in Taurid Belt. Fifth Petroleum Congress of Turkey, (s. 77-93). Ankara.
- Perinçek, D. (1990). Stratigraphy of the Hakkari Province, Southeast Turkey. *TAPG Bulletin*, 21-68.
- Perinçek, D., Duran, O., Bozdoğan, N., & Çoruh, T. (1991). Stratigraphy and Paleogeographical Evolution of the Autochthonous Sedimentary Rocks in the SE Turkey. *Ozan Sungurlu Symposium proceedings*, (s. 274-305). Ankara.
- Pettijohn, F. J. (1957). *Sedimentary Rocks*. New York: Harper and Brothers.
doi:10.1017/S0016756800070254

- Pettijohn, F. J. (1975). *Sedimentary Rocks*. New York: Harper and Row Publishers.
- Pohl, A., Donnadieu, Y., Hir, G., Buoncristiani, J.-F., & Vennin, E. (2014). Effect of the Ordovician Paleogeography on the (in)stability of the Climate. *Climate of the Past*.
- Rahman, M. J., & McCann, T. (2011). Diagenetic History of the Surma Group Sandstones (Miocene) in the Surma Basin, Bangladesh. *Journal of Asian Earth Sciences*.
- Rigo de Righi, M., & Cortesini, A. (1964). Gravity Tectonics in Foothills Structure Belt of Southeast Turkey: *AAPG Bulletin*, no. 48, p. 1911-1937.
- Reineck, H. E. (1980). Tidal Flats. *Recognition of Ancient Sedimentary Environments* (s. 430-456).
- Saberi, M. H., Rabbani, A., & Ghavidel-syooki, M. (2016). Hydrocarbon Potential and Palynological Study of the Latest Ordovician - Earliest Silurian Source Rock (Sarchahan Formation) in the Zagros Mountains, Southern Iran. *Marine and Petroleum Geology*, 12-25.
- Schlumberger. (2009). *Log Interpretation Charts*. Sugar Land, Texas: Schlumberger.

Schmidt, G. C. (1961). Stratigraphy and Petroleum Possibilities of Central District VI, Turkey: Petrol İşleri Genel Müdürlüğü Teknik Arşivi, Kutu no. 332, Rapor no.4, 43s. (TPAO Arama Grubu, Rapor no. 767).

Schmidt, G. C. (1964). Proposed Rock Unit Nomenclature Petroleum District V, SE-Turkey (Autochthonous terrain) (Mobil Exploration Mediterranean Inc.) (unpublished). Ankara.

Schmidt, G. C. (1966). Stratigraphy of Lower Paleozoic Rock Units of Petroleum District V-Turkey: Petroleum Administration Publication, Bulletin no. 11, p. 73-90.

Schmidt, K. (1935). First Report over Geological and Paleontological: MTA Derleme no. 1532, 11 s.

Scotese, C. (2014). Atlas of Silurian and Middle-Late Ordovician Paleogeographic Maps (Mollweide Projection), Maps 73 – 80, Volumes 5, The Early Paleozoic, Paleomap Atlas for ArcGIS, Paleomap Project. Evanston, IL.

Scotese, C. (2015). Phanerozoic Temperature Curve. Evanston, IL.

Sharland, P. R., Archer, R., Casey, D. M., Davies, R. B., Hall, S. H., Heward, A. P., . . . Simmons, M. D. (2001). Arabian Plate Sequence Stratigraphy. *GeoArabia*, 199-214.

- Siddiqui, N. A., EL-Ghali, M., & bin Abd Rahman, A. (2013). Depositional Environment of Shallow-Marine Sandstones from Outcrop Gamma-Ray Logs, Belait Formation, Meragang Beach, Brunei Darussalam. *Research Journal of Environmental and Earth Sciences*, 305-324.
- Siddiqui, N. A., Rahman, A., Sum, C., Yusoff, W., & bin Ismail, M. (2017). Shallow-Marine Sandstone Reservoirs, Depositional Environments, Stratigraphic Characteristics and Facies Model: A Review. *Journal of Applied Sciences*, 212-237.
- Smart, G. (1985). The Progressive Illitization of Interstratified Illite-Smectite from Carboniferous Sediments of Northern England and Its Relationship to Organic Maturity Indicators. *Clay Minerals*, 455-466.
- Stemans, P., Herisse, A., & Bozdogan, N. (1996). Ordovician and Silurian Cryptospores and Miospores from Southeastern Turkey. *Review of Palaeobotany and Palynology*, 35-76.
- Stratum. (1963). General Geological Report on the Petroleum District V with reference to the areas AR/A.M.E./648, 649, AR/C.M.E./657, 660, AR/P.E.R/650, 659 (Aladdin Middle East Ltd. Report): Petrol İşleri Genel Müdürlüğü Teknik Arşivi, Kutu no. 125, Rapor no. 7, 19 s.
- Şengündüz, N., & Soylu, C. (1990). Sedimentology and Organic Geochemistry of Sphaeroidal-Rich Horizon of the Derdere Formation. 8th Petroleum Congress of Turkey (s. 50-61). Ankara: Turkish Association of Petroleum Geologist.

- Tanner, W. F. (1967). Ripple Mark Indices and Their Uses. *Sedimentology*, 89-104.
- Tardu, T., Akçay, Y., & Iş, L. (1990). Seismic Stratigraphic Analysis of Some Selected Lithostratigraphic Units Southeastern Anatolia. 8th Petroleum Congress of Turkey (s. 240-259). Ankara: Turkish Association of Petroleum Geologist and Uctea Chamber of Petroleum Engineers.
- Tardu, T., Başkurt, T., Güven, A., Us, E., Dinçer, A., Tuna, M., & Tezcan, Ü. (1987). Structural and Stratigraphic Aspects of Akçakale Graben and Its HC Potential. 7th Biannual Petroleum Congress of Turkey. Ankara.
- Taşman, C. E. (1930). Mardin ve Siirt Vilayetindeki bazı Aksamının Jeoloji ve Petrol İhtimalatı Hakkında Rapor: MTA Derleme no. 215, 21 s.
- Taud, H., Martinez-Angeles, R., Parrot, J., & Hernandez-Escobedo, L. (2005). Porosity Estimation Method by X-ray Computed Tomography. *Journal of Petroleum Science and Engineering*, 209-217.
- Ten Dam, A. (1953). Detailed Report on the Geology of the Deeper part of the Raman No. 16 well: MTA Derleme no. 2109, 30 s.
- Ten Dam, A. (1954). Preliminary Report on the İspandika Section: MTA Derleme no. 2211, 17 s.

- Tetiker, S., Yalçın, H., & Bozkaya, Ö. (2015). Evidence of the diagenetic history of Sediment Composition in Precambrian-Early Paleozoic Rocks: A Systematic Study from the Southeast Anatolian Autochthon, Mardin (Derik-Kızıltepe), Turkey. *Arabian Journal of Geoscience*, 11261-11278.
- Topdemir, S. A. (1992). Diagenesis of the Hazro Formation Kayayolu-2 and Hazro South-2 Wells, Southeast Turkey. 9th Petroleum Congress and Exhibition of Türkiye (s. 413-423). Ankara: Turkish Association of Petroleum Geologist.
- Torsvik, T. H., & Cocks, L. (2013). Gondwana from Top to Base in Space and Time. *Gondwana Research*, 999-1030.
- Totten, M. W., Hanan, M. A., Knight, D., & Borges, J. (2002). Characteristics of Mixed-Layer Smectite/Illite Density Separates during Burial Diagenesis. *American Mineralogist*, 1571-1579.
- Turkish Petroleum Company, (1966). Regional Sections Southeast Turkey: Petroleum Administration, Bulletin no. 11, p. 55-57
- Tuna, D. (1973). VI. Bölge Litostratigrafi Birimleri Adlamasının Açıklayıcı Raporu. Ankara: Türkiye Petrolleri Anonim Ortaklığı.
- Turner, B. R., Makhlof, I., & Armstrong, H. (2005). Late Ordovician (Ashgillian) Glacial Deposits in Southern Jordan. *Sedimentary Geology*, 73-91.

- Vakarelov, B. K., Ainsworth, R., & MacEachern, J. (2012). Recognition of Wave-Dominated, Tide-Influenced Shoreline Systems in the Rock Record: Variations from a Microtidal Shoreline Model. *Sedimentary Geology*, 23-41.
- Walderhaug, O. L. (2000). Modelling Quartz Cementation and Porosity in Reservoir Sandstones: Examples from the Norwegian Continental Shelf. *Spec. Publs int. Ass. Sediment*, 39-49.
- Wazir, I., Pagel, M., Tournier, F., Portier, E., & Renac, C. (2014). Role of Compressive Tectonics on Gas Charging into the Ordovician Sandstone Reservoirs in the Sbaa Basin, Algeria: Constrained by Fluid Inclusions and Mineralogical Data. *Geofluids*, 106-126.
- Wetzel, R. (1959). In *Lexique Stratigraphic International*, Vol. III, Asie, fasc. 10 a. Iraq: Centre Nat. Recn, Scien. Paris
- Wilson, H. H. & Krummenacher, R. (1959). Geology and Oil Prospects of the Gaziantep Region, Southeast Turkey (N. V. Turkse Shell Report): Petrol İşleri Genel Müdürlüğü Teknik Arşivi, Kutu no. 351, Rapor no. 2, 53 s (TPAO Arama Grubu, Rapor no. 839)
- Worden, R. H., & Barclay, S. (2003). The Effect of Oil Emplacement on Diagenetic Clay Mineralogy: the Upper Jurassic Magnus Sandstone Member, North Sea. *Int. Assoc. Sedimentol. Spec. Publ.*, 453-469.

Worden, R. H., & Morad, S. (2000). Quartz Cementation in Oil Field Sandstones: A Review of the Key Controversies. *Spec. Publs int. Ass. Sediment.*, 1-20.

Worden, R. H., Armitage, P. J., Butcher, A. R., Churchill, J. M., Csoma, A. E., Hollis, C., Lander, R., Omma, J. E. (2018). *Petroleum Reservoir Quality Prediction: Overview and Contrasting Approaches from Sandstone and Carbonate Communities*. The Geological Society of London.

Yılmaz, E., & Duran, O. (1997). Güneydoğu Anadolu Bölgesi Otokton ve Allohton Birimler Stratigrafi Adlama Sözlüğü " Lexicon". Ankara: TPAO.

Zhou, X., Liu, D., Bu, H., Deng, L., Liu, H., Yuan, P., Du, P., Song, H. (2018). XRD-based quantitative analysis of clay minerals using reference intensity ratios, mineral intensity factors, Rietveld, and full pattern summation methods: A critical review. *Solid Earth Science*, 1-14.

Zieba, K. J., & Grøver, A. (2016). Isostatic Response to Glacial Erosion, Deposition and Ice Loading. Impact on Hydrocarbon Traps of the Southwestern Barents Sea. *Marine and Petroleum Geology*, 168-183. doi:<http://dx.doi.org/10.1016/j.marpetgeo.2016.09.009>

